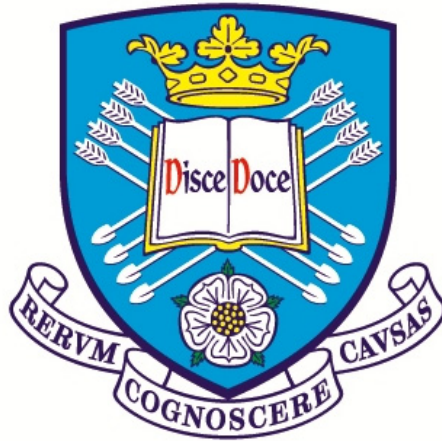


**The Effect OF Wetting and Drying Cycles  
and Carbonation on Thaumaside Formation**



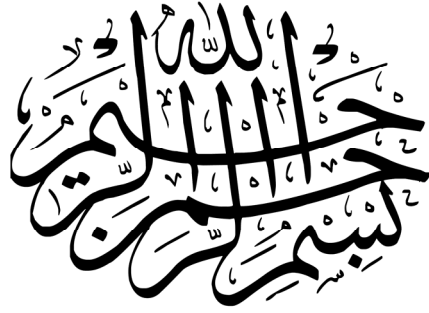
A thesis submitted for the degree of Doctor of Philosophy in  
the Faculty of Engineering of the University of Sheffield

By  
Jumma Musbah Abualgasem

DEPARTMENT OF CIVIL AND STRUCTURAL ENGINEERING  
THE UNIVERSITY OF SHEFFIELD

May 2014





اقْرَأْ بِاسْمِ رَبِّكَ الَّذِي خَلَقَ (1) خَلَقَ الْإِنْسَانَ مِنْ عَلَقٍ (2) اقْرَأْ وَرَبُّكَ الْأَكْرَمُ  
(3) الَّذِي عَلَّمَ بِالْقَلَمِ (4) عَلَّمَ الْإِنْسَانَ مَا لَمْ يَعْلَمْ (5)

سورة العلق

The Holy Quran: Chapter 96



---

*To:*

*My family*

*For their love, prayers, patience  
and so much faith in me*

*To my country,*

*Libya,*

*hoping for a better future.*

# **Declaration**

I, Jumma Musbah Abualgasem, confirm that the work presented in this thesis is my own.

Where information has been derived from other sources, I confirm that this has been indicated in the thesis.

## Abstract

Thaumasite form of sulfate attack is having great attention since its discovering in series of foundations supporting motorway bridges in the UK in the late nineties of the last century. This is mainly due to its destructive effect on concrete structures, and the lack of information about its formation mechanisms. This research conducted a study on the effect of wetting and drying, carbonation and the effect of water to cement ratio on the thaumasite formation, and whether these effects are linked with other parameters such as cement type and sulfate concentration or not. 10 different mixes were produced based on four binder types in this study namely 100% CEM I, 90% CEM I + 10% Limestone filler, 50% CEM I + 50% PFA and 30% CEM I + 70% GGBS. A series of mortar samples of two types were prepared 50 mm cubes and 40 × 40 × 160 mm prisms. The samples were kept in three different solutions contain BRE DS3, DS4 based on magnesium sulfate  $MgSO_4 \cdot 7H_2O$  in addition to deionised water. Two different temperatures 5°C and 20°C were also used to confirm the formation of thaumasite at ambient temperatures (20°C) and to accelerate its formation at 5°C. The effect of wetting and drying cycles on thaumasite formation was studied and compared with samples immersed continuously in the same solutions for 12 months.

Powder-sulfate interaction and its effect on thaumasite formation was studied by grinding mortar samples to a fine powder, thus eliminating the permeability effect and enabling physical factors that affect the rate at which solutions can be transferred through the mortar to be separated from chemical factors that affect the rate at which the chemical reactions take place.

Visual observations, mass and length changes were used to assess the mortar deterioration, along with X-ray diffraction, infra-red spectroscopy and SEM that were used to determine the mineralogy of deterioration products.

For the cyclic wetting and drying exposure regime the results showed that wetting and drying cycles significantly delayed thaumasite formation compared with control specimens.

For powder samples, it is found that thaumasite is readily formed in these powders after 3 months of exposure to sulfate solutions including GGBS and PFA samples, on the other hand cubes and prisms, exposed to the same solutions for 24 months showed no signs of deterioration.

Thermodynamic modelling was used to predict the deterioration products for powders samples and good agreement between predicted and observed results was found.

Keywords: Thaumasite, wetting drying sulfate attack, carbonation.

# Acknowledgements

Firstly, I would like express my sincere thanks my supervisors Dr **John Cripps** and Dr. **Cyril Lynsdale** for being a source of constant guidance and advice throughout the period of this research. Without their help this work would not have finished.

Secondly, I would like to acknowledge the financial support for this work which was provided via a scholarship from the Ministry of Higher Education, Libya.

Thanks also go to the staff of heavy structures laboratory at the University of Sheffield for their technical help, friendship and providing me an effective working environment.

**Farhat Abubaker** and **Ashraf Abdulkader** deserve a big thank you for their priceless friendship, support and valuable discussions.

Thanks should also go to **Abdlaziz Elarabi**, **Husni Amer** and **Mohamed Zambri** for the wonderful moment we shared in Sheffield.

I would like also to thank Dr. Barbara Lothenbach from EMPA Switzerland, for their help and advice regarding thermodynamic modeling.

I would also like to thank the Geotechnical research group at the University of Sheffield for having me with them in their room.

Finally, a big thank you goes to my wife, my parents, relatives and friends in Libya and the UK for their unlimited support and encouragement throughout this work and during the Libyan uprising events in 2011.

# Contents

<b>Contents</b> .....	<b>vi</b>
<b>List of Tables</b> .....	<b>xi</b>
<b>List of Figures</b> .....	<b>xii</b>
<b>List of Abbreviations and Nomenclature</b> .....	<b>xxi</b>
<b>1. Introduction</b> .....	<b>1</b>
1.1 Background.....	1
1.2 Objectives of the study .....	4
1.3 Structure of the thesis.....	4
<b>2. Literature review</b> .....	<b>6</b>
2.1 Introduction .....	6
2.2 Conventional sulfate attack .....	7
2.3 Thaumasite form of sulfate attack TSA .....	9
2.4 Formation of thaumasite .....	12
2.5 Effect of wetting and drying cycles on durability of concrete. ....	14
2.6 Effect carbonation and early air curing on sulfate attack. ....	16
2.7 Factors affecting thaumasite formation .....	17
2.7.1 Role of Cement type.....	17
2.7.2 Role of Temperature .....	23
2.7.3 Role Sulfate concentration.....	25
2.7.4 Role of pH .....	25
2.8 Identification of thaumasite .....	27
2.9 Thermodynamic modelling.....	28

<b>3. Experimental Programme .....</b>	<b>30</b>
3.1 Introduction .....	30
3.2 Materials .....	30
3.2.1 Cement (CEMI) .....	30
3.2.2 Limestone filler .....	31
3.2.3 Ground Granulated Blastfurnace Slag (GGBS).....	31
3.2.4 Pulverized Fly Ash (PFA) .....	31
3.2.5 Aggregate.....	31
3.2.6 Water .....	31
3.2.7 Exposure solutions .....	33
3.3 Mortars Mixing and Casting.....	34
3.4 Curing: .....	35
3.4.1 Initial curing.....	35
3.4.2 Long term exposure to sulfate environment .....	35
3.5 Sampling and Testing: .....	36
3.5.1 pH Measures .....	36
3.5.2 Visual observations .....	36
3.5.3 Length and mass change .....	37
3.5.4 X-ray Diffraction (XRD).....	38
3.5.5 Fourier Transform Infrared Spectroscopy (FTIR) .....	39
3.5.6 Scanning Electron Microscopy (SEM).....	39
3.5.7 Carbonation depth measurement.....	40
3.5.8 Thermodynamic modelling.....	40
<b>4. Effect of wetting and drying cycles.....</b>	<b>42</b>
4.1 Introduction .....	42

4.2	Visual observation assessment .....	43
4.3	Patterns of attack .....	49
4.4	Mass Changes .....	49
4.5	Length Change .....	56
4.6	X-Ray Diffraction.....	63
4.7	Fourier Transform Infrared Spectroscopy (FTIR) .....	74
4.8	PH measurements .....	83
4.9	Microstructure of thaumasite and other deterioration products. ....	90
4.10	Summary .....	96
<b>5.</b>	<b>Effect of Carbonation.....</b>	<b>100</b>
5.1	Introduction .....	100
5.2	Carbonation depth .....	100
5.3	pH measurements .....	102
5.4	XRD analysis.....	103
5.5	Fourier Transform Infrared Spectroscopy (FTIR) .....	106
5.6	SEM analysis .....	109
5.7	Summary .....	114
<b>6.</b>	<b>Effect of water to cement ratio .....</b>	<b>115</b>
6.1	Introduction .....	115
6.2	Visual observation assessment.....	116
6.2.1	CEMI cement samples .....	116
6.2.2	LFC cement samples .....	118
6.2.3	Visual observations of FAC cement samples .....	120
6.2.4	Visual observations of SLC cement samples .....	121
6.2.5	Visual observations (overall comparison) .....	123

6.3	Mass Changes .....	123
6.3.1	CEMI cement samples .....	123
6.3.2	LFC cement samples.....	125
6.3.3	Mass changes for FAC cement samples.....	127
6.3.4	Mass changes for SLC cement samples.....	129
6.3.5	Overall comparison of mass changes .....	131
6.4	Length change .....	132
6.4.1	CEMI cement samples .....	132
6.4.2	LFC cement samples.....	134
6.4.3	FAC cement samples .....	136
6.4.4	SLC cement samples.....	138
6.4.5	Length change (overall comparison) .....	139
6.5	X-Ray Diffraction .....	141
6.5.1	XRD for CEMI cement samples .....	141
6.5.2	XRD for LFC cement samples .....	145
6.5.3	XRD for FAC cement samples .....	149
6.5.4	XRD for SLC cement samples .....	153
6.6	Fourier Transform Infrared Spectroscopy (FTIR) .....	156
6.6.1	FTIR for CEMI cement samples.....	157
6.6.2	FTIR for LFC cement samples .....	160
6.6.3	FTIR for FAC cement samples .....	162
6.6.4	FTIR for SLC cement samples .....	164
6.7	Microstructure of deterioration products. ....	166
6.7.1	CEMI cement samples .....	166
6.7.2	SEM for LFC cement samples .....	168

6.7.3	FAC cement samples .....	171
6.7.4	SEM for SLC cement samples .....	173
6.8	Thermodynamic modelling.....	175
6.8.1	CEMI cement samples .....	175
6.8.2	LFC cement samples .....	177
6.8.3	FAC cement samples .....	178
6.8.4	SLC cement samples .....	179
6.8.5	Thermodynamic modelling (overall quantitative comparison) 182	
6.9	Summary .....	184
<b>7.</b>	<b>Overall Discussions.....</b>	<b>188</b>
7.1	Introduction .....	188
7.2	The effect of wetting and drying cycles on the formation of thaumasite in cement mortars.....	189
7.3	The effect of water to cement ratio on thaumasite formation in cement mortars .....	194
<b>8.</b>	<b>Overall conclusions and recommendations .....</b>	<b>198</b>
8.1	Overall conclusions .....	198
8.2	Implementations for engineering .....	201
8.3	Recommendation for further study .....	202
	<b>References .....</b>	<b>204</b>
	<b>Appendix A.....</b>	<b>212</b>
	<b>Appendix B.....</b>	<b>214</b>

## **List of Tables**

Table 3.1 Chemical and mineralogical composition of Cement, LF, PFA and GGBS .....	32
Table 3.2 Chemical compositions and Physical properties of sand .....	32
Table 3.3 Mortar Mixes and Materials .....	34
Table 4.1 Coding system for used cements.....	42
Table 4.2 Summary of the degree of deterioration based on visual observation and mass loss .....	56
Table 4.3 Relative intensities of phase assemblage as identified by XRD analysis .....	73
Table 6.1 Coding system for used cements.....	116
Table 6.2 Summary of the intensity of the attack based on mass loss for different samples. ....	132
Table 6.3 Summary of Length change results for the most deteriorated samples .....	140

## List of Figures

Figure 2.1 Limestone mortar prime after 18 months of exposure to sulfate solution. ....	10
Figure 2.2 View of cubes with and without limestone filler.....	20
Figure 3.1 Sieve analysis of sand.....	33
Figure 3.2 Thaumasite started to form at edges of limestone cement samples in DS4 at 5 °C after 84 days.....	37
Figure 3.3 Length change measurement .....	38
Figure 4.1 Mortar cubes in DS4 sulfate solution at 5 °C after 24 months. ....	44
Figure 4.2 Mortar cubes in DS3 sulfate solution at 5 °C after 24 months. ....	45
Figure 4.3 The outer layer of specimens is un-attacked with the deterioration is progressing underneath it. ....	46
Figure 4.4 Mortar cubes in DS3 sulfate solution at 20 °C after 24 months.....	47
Figure 4.5 Mortar cubes in DS4 sulfate solution at 20 °C after 24 months.....	48
Figure 4.6 Deterioration Patterns a) cracks started to appear around the edges, b) cracks then filled with white substance (thaumasite), c) Spall off the corners and edges, d) deterioration of the sample .....	49
Figure 4.7 Mass change for samples in DS3 solution at 5C. (continuous immersion) .....	50
Figure 4.8 Mass change for samples in DS4 solution at 5 °C (continuous immersion) .....	51
Figure 4.9 Mass change for samples in DS3 solution at 20 °C. (continuous immersion).....	52
Figure 4.10 Mass change for samples in DS4 solution at 20 °C. (Continuous immersion) .....	52

Figure 4.11 Mass change for samples in DS3 solution at 5 °C. (Wetting & drying).....	53
Figure 4.12 Mass change for samples in DS4 solution at 5 °C. (Wetting & drying).....	54
Figure 4.13 Mass change for samples in DS3 solution at 20 °C. (Wetting & drying) .....	54
Figure 4.14 Mass change for samples in DS4 solution at 20 °C. (Wetting & drying) .....	55
Figure 4.15 Length change for samples in DS3 solution at 5 °C. (Continuous immersion) .....	57
Figure 4.16 Length change for samples in DS4 solution at 5 °C. (Continuous immersion) .....	58
Figure 4.17 Length change for samples in DS3 solution at 20 °C. (Continuous immersion) .....	59
Figure 4.18 Length change for samples in DS4 solution at 20 °C. (Continuous immersion) .....	59
Figure 4.19 Length change for samples in DS3 solution at 5 °C. (Wetting & drying) .....	60
Figure 4.20 Length change for samples in DS4 solution at 5 °C. (Wetting & drying) .....	61
Figure 4.21 Length change for samples in DS3 solution at 20 °C. (Wetting & drying).....	62
Figure 4.22 Length change for samples in DS4 solution at 20 °C. (Wetting & drying).....	62
Figure 4.23 XRD patterns for samples in DS3 solutions at 5 °C (continuous immersion) .....	64
Figure 4.24 XRD patterns for samples in DS3 solutions at 5 °C (continuous immersion) .....	64
Figure 4.25 XRD patterns for samples in DS4 solutions at 5 °C (12 months).....	66

Figure 4.26 XRD patterns for samples in DS4 solutions at 5 °C (continuous immersion).....	67
Figure 4.27 XRD patterns for samples in DS4 solutions at 5 °C(wetting and drying).....	68
Figure 4.28 XRD patterns for samples in DS3 solutions at 20 °C (continuous immersion).....	69
Figure 4.29 XRD patterns for samples in DS3 solutions at 20 °C (wetting and drying).....	70
Figure 4.30 XRD patterns for samples in DS4 solutions at 20 °C (continuous immersion).....	71
Figure 4.31 XRD patterns for samples in DS4 solutions at 20 °C (wetting and drying).....	72
Figure 4.32 IR spectra for samples in DS3 solutions at 5 °C (continuous immersion) .....	75
Figure 4.33 IR spectra for samples in DS3 solutions at 5 °C (Wetting and drying cycles) .....	76
Figure 4.34 IR spectra for samples in DS4 solutions at 5 °C (continuous immersion) .....	77
Figure 4.35 IR spectra for samples in DS4 solutions at 5 °C (Wetting and drying cycles) .....	78
Figure 4.36 IR spectra for samples in DS3 solutions at 20 °C (continuous immersion) .....	80
Figure 4.37 IR spectra for samples in DS3 solutions at 20 °C (Wetting and drying cycles).....	81
Figure 4.38 IR spectra for samples in DS4 solutions at 20 °C (continuous immersion) .....	82
Figure 4.39 IR spectra for samples in DS4 solutions at 20 °C (Wetting and drying cycles).....	82
Figure 4.40 pH values for samples in DS3 solutions at 5 °C (continuous immersion) .....	83

Figure 4.41 pH values for samples in DS3 solutions at 5 °C (wetting and drying cycles).....	85
Figure 4.42 pH values for samples in DS4 solutions at 5 °C (continuous immersion) .....	86
Figure 4.43 pH values for samples in DS4 solutions at 5 °C (wetting and drying cycles).....	87
Figure 4.44 pH values for samples in DS3 solutions at 20 °C (continuous immersion) .....	88
Figure 4.45 pH values for samples in DS3 solutions at 20 °C (wetting and drying cycles).....	88
Figure 4.46 pH values for samples in DS4 solutions at 20 °C (continuous immersion) .....	89
Figure 4.47 pH values for samples in DS4 solutions at 20 °C (wetting and drying cycles).....	90
Figure 4.48 BSE of CEM I sample in DS4 at 5 °C in continuous immersion .....	91
Figure 4.49 EDX microanalysis for spot A in Figure 4.48 showing thaumasite elements .....	91
Figure 4.50 Magnified BSE image for thaumasite crystals in CEM I sample.....	92
Figure 4.51 Magnified BSE image for spot B in Figure 4.48 .....	93
Figure 4.52 EDX microanalysis for spot A in Figure 4.48 showing CSH gel .....	93
Figure 4.53 BSE of LFC sample in DS4 at 5 °C in continuous immersion .....	94
Figure 4.54 Magnified BSE image for spot A in Figure 4.53.....	95
Figure 4.55 EDX microanalysis for spot A in Figure 4.53 showing thaumasite elements .....	95
Figure 5.1 Carbonation results for different samples.....	101
Figure 5.2 carbonation depth for different samples .....	101
Figure 5.3 pH values of carbonated and non-carbonated samples.....	103

Figure 5.4 XRD patterns for core samples in DS4 at 5 °C .....	104
Figure 5.5 XRD patterns for surface samples in DS4 at 5 °C.....	105
Figure 5.6 FTIR spectra for core samples in DS4 at 5 °C SiO <sub>6</sub> indicating Thaumasite, AlO <sub>6</sub> indicating Ettringite .....	107
Figure 5.7 FTIR spectra for surface samples in DS4 at 5 °C (SiO <sub>6</sub> indicating Thaumasite, AlO <sub>6</sub> indicating Ettringite) .....	108
Figure 5.8 the outer layer used for SEM analysis.....	109
Figure 5.9 BSE of CEM I+ 10%LF sample in DS4 at 5 °C in under wetting and drying system.....	110
Figure 5.10 EDX microanalysis for zone 1 in Figure 5.9 showing thaumasite.....	110
Figure 5.11 EDX microanalysis for zone 2 in Figure 5.9 showing thaumasite Ettringite solid solution.....	111
Figure 5.12 EDX microanalysis for zone 3 in Figure 5.9 showing Calcium silicate hydrate.....	112
Figure 5.13 EDX microanalysis for zone 4 in Figure 5.9 showing magnesium silicate hydrate .....	113
Figure 5.14 EDX microanalysis for zone 5 in Figure 5.9 showing calcium carbonate .....	113
Figure 6.1 Visual appearance of CEMI samples of various mixes under different exposure conditions and temperatures after 24 months.....	117
Figure 6.2 Visual appearance of LFC samples of various mixes under different exposure conditions and temperatures after 24 months.....	119
Figure 6.3 Visual appearance of FAC samples of various mixes under different exposure conditions and temperatures after 24 months.....	121
Figure 6.4 Visual appearance of SLC samples of various mixes under different exposure conditions and temperatures after 24 months.....	122
Figure 6.5 Mass change for CEMI samples in sulfate solutions at 5 °C . .....	124
Figure 6.6 Mass change for CEMI samples in sulfate solutions at 20 °C . .....	125

Figure 6.7 Mass change for LFC samples in sulfate solutions at 5 °C .	126
Figure 6.8 Mass change for LFC samples in sulfate solutions at 20 °C .	127
Figure 6.9 Mass change for FAC samples in sulfate solutions at 5 °C.	128
Figure 6.10 Mass change for FAC samples in sulfate solutions at 20 °C.	129
Figure 6.11 Mass change for SLC samples in sulfate solutions at 5 °C.	130
Figure 6.12 Mass change for SLC samples in sulfate solutions at 20 °C.	130
Figure 6.13 Length change for CEMI samples in sulfate solutions at 5 °C	133
Figure 6.14 Length change for CEMI samples in sulfate solutions at 20 °C	134
Figure 6.15 Length change for LFC samples in sulfate solutions at 5 °C	135
Figure 6.16 Length change for LFC samples in sulfate solutions at 20 °C	136
Figure 6.17 Length change for FAC samples in sulfate solutions at 5 °C	137
Figure 6.18 Length change for FAC samples in sulfate solutions at 20 °C	137
Figure 6.19 Length change for SLC samples in sulfate solutions at 5 °C	138
Figure 6.20 Length change for SLC samples in sulfate solutions at 20 °C	139
Figure 6.21 XRD patterns for CEMI solid samples at 5 °C.....	142
Figure 6.22 XRD patterns for CEMI Powder samples at 5 °C.....	143
Figure 6.23 XRD patterns for CEMI solid samples at 20 °C.....	144
Figure 6.24 XRD patterns for CEMI Powder samples at 20 °C.....	145

Figure 6.25 XRD patterns for LFC solid samples at 5 °C .....	146
Figure 6.26 XRD patterns for LFC powder samples at 5 °C .....	147
Figure 6.27 XRD patterns for LFC solid samples at 20 °C .....	148
Figure 6.28 XRD patterns for LFC powder samples at 20 °C .....	149
Figure 6.29 XRD patterns for FAC solid samples at 5 °C .....	150
Figure 6.30 XRD patterns for FAC powder samples at 5 °C .....	151
Figure 6.31 XRD patterns for FAC solid samples at 20 °C .....	152
Figure 6.32 XRD patterns for FAC powder samples at 20 °C .....	153
Figure 6.33 XRD patterns for SLC solid samples at 5 °C .....	154
Figure 6.34 XRD patterns for SLC powder samples at 5 °C .....	155
Figure 6.35 XRD patterns for SLC solid samples at 20 °C .....	155
Figure 6.36 XRD patterns for SLC powder samples at 20 °C .....	156
Figure 6.37 IR spectra for CEMI samples in DS4 solutions at 5 °C .....	158
Figure 6.38 IR spectra for CEMI samples in DS4 solutions at 20 °C .....	159
Figure 6.39 IR spectra for LFC samples in DS4 solutions at 5 °C .....	160
Figure 6.40 IR spectra for LFC samples in DS4 solutions at 20 °C .....	162
Figure 6.41 IR spectra for FAC samples in DS4 solutions at 5 °C .....	163
Figure 6.42 IR spectra for FAC samples in DS4 solutions at 20 °C .....	164
Figure 6.43 IR spectra for SLC samples in DS4 solutions at 5 °C .....	165
Figure 6.44 IR spectra for SLC samples in DS4 solutions at 20 °C .....	166
Figure 6.45 BSE of CEMI-45 sample at 20 °C .....	167
Figure 6.46 Magnified image for spot A in Figure 6.45 a) microstructure of the matrix. b) EDX microanalysis showing thaumasite\ettringite solid solution .....	167
Figure 6.47 a) BS image and b) EDX analysis for ettringite formed in air void .....	168
Figure 6.48 BSE of LFC-45 sample at 20 °C .....	169
Figure 6.49 Magnified image for spot A in Figure 6.48 and micro EDX analysis .....	169
Figure 6.50 A needle like thaumasite crystals filling the cracks in LFC-45 sample .....	170

Figure 6.51 EDX microanalysis for spot B in Figure 6.48 showing ettringite elements in additions to small Si peak .....	170
Figure 6.52 BSE of FAC-65 sample at 5 °C .....	171
Figure 6.53 Magnified image and EDX analysis for thaumasite ettringite solid solution in FAC-65 sample at 5 °C.....	172
Figure 6.54 Magnified image and EDX analysis for gypsum phase in FAC-65 sample at 5 °C .....	172
Figure 6.55 BSE of SLC-65 sample at 5 °C .....	173
Figure 6.56 EDX microanalysis for spot A in Figure 6.55 showing thaumasite elements .....	173
Figure 6.57 EDX microanalysis for spot B in Figure 5.55 showing thaumasite ettringite solid solution elements .....	174
Figure 6.58 Magnified image and EDX analysis for gypsum phase in SLC-65 sample at 5 °C.....	175
Figure 6.59 Phase assemblage for CEMI in DS3 at 5 °C .....	176
Figure 6.60 Phase assemblage for CEMI in DS4 at 5 °C .....	176
Figure 6.61 Phase assemblage for LFC in DS3 at 5 °C.....	177
Figure 6.62 Phase assemblage for LFC in DS4 at 5 °C.....	178
Figure 6.63 Phase assemblages for FAC in DS3 at 5 °C.....	179
Figure 6.64 Phase assemblages for FAC in DS4 at 5 °C.....	179
Figure 6.65 Phase assemblages for SLC in DS3 at 5 °C.....	180
Figure 6.66 Phase assemblage for SLC in DS4 at 5 °C .....	181
Figure 6.67 Volume of resulted phases for different cements in DS3 ..	183
Figure 6.68 Volume of resulted phases for different cements in DS4 ..	183
Figure 7.1 Proposed phases in the carbonated layer based on SEM analysis .....	193
Figure 7.2 Relationship between onset of attack and w/c ratio .....	195
Figure 7.3 Relationship between mass change and different w/c ratios .....	196
Figure 7.4 Relationship between length change and different w/c ratios .....	196

Figure A.1 Length change for samples in water at 5 °C. (Continuous immersion) .....	212
Figure A.2 Length change for samples in water at 20 °C. (Continuous immersion) .....	212
Figure A.3 Length change for samples in water at 20 °C. (wetting and drying).....	213
Figure B.1 Phase assemblage for CEMI (w/c=0.45) .....	214
Figure B.2 Phase assemblage for LFC (w/c=0.45) .....	214
Figure B.3 Phase assemblage for FAC (w/c=0.45) .....	215
Figure B.4 Phase assemblage for SLC (w/c=0.45) .....	215
Figure B.5 Phase assemblage for CEMI (w/c=0.55) .....	216
Figure B.6 Phase assemblage for LFC (w/c=0.55) .....	216
Figure B.7 Phase assemblage for FAC (w/c=0.55) .....	217
Figure B.8 Phase assemblage for SLC (w/c=0.55) .....	217

# List of Abbreviations and Nomenclature

## Abbreviations

BRE	Building Research Establishment
BSE	Backscattered electron
CEM I	Cement type 1 according to 197
EDX	Energy-dispersive X-ray analysis
FTIR	Fourier Transform Infrared
GGBS	Ground Granulated Blastfurnace Slag
LSF	Limestone Filler
OPC	Ordinary Portland cement
PFA	Pulverized Fly Ash
pH	Potential hydrogenii
SEM	Scanning electron microscopy
TEG	Thaumasite Expert Group
TF	Thaumasite formation
TGA	Thermogravimetric analysis
TSA	Thaumasite form of sulfate attack
w/c	Water to cement ratio
XRD	X-ray diffraction
XRF	X-Ray Fluorescence
CSH	Calcium Silicate Hydrate
MSH	Magnesium Silicate Hydrate

## Nomenclature

Cement notation	Chemical formula	Mineral Name
C2S	$2\text{CaO} \cdot \text{SiO}_2$	Dicalcium silicate
C3A	$3\text{CaO} \cdot \text{Al}_2\text{O}_3$	Tricalcium aluminate
C3A.3CŠ.H32	$3(\text{CaO}) \cdot (\text{Al}_2\text{O}_3) \cdot 3(\text{CaSO}_4) \cdot 32\text{H}_2\text{O}$	Ettringite
C3S	$3\text{CaO} \cdot \text{SiO}_2$	Tricalcium silicate
C3SČŠH15	$\text{CaSiO}_3 \cdot \text{CaCO}_3 \cdot \text{CaSO}_4 \cdot 15\text{H}_2\text{O}$	Thaumasite
C4AF	$4\text{CaO} \cdot \text{Al}_2\text{O}_3 \cdot \text{Fe}_2\text{O}_3$	Tetracalcium aluminoferrite
CČ	$\text{CaCO}_3$	Calcite
CH	$\text{Ca}(\text{OH})_2$	Calcium hydroxide (Portlandite)
C-S-H	$(\text{C}_3\text{S}_2\text{H}_3) \cdot 3\text{CaO} \cdot 2\text{SiO}_2 \cdot 3\text{H}_2\text{O}$	Calcium silicate hydrate
CsH <sub>2</sub>	$\text{CaSO}_4 \cdot 2\text{H}_2\text{O}$	Gypsum
MH	$\text{Mg}(\text{OH})_2$	Brucite



# 1

## Introduction

### 1.1 Background

Conventional type of sulfate attack which is usually attributed to gypsum  $\text{CaSO}_4 \cdot 2\text{H}_2\text{O}$  and ettringite  $(\text{CaO})_3(\text{Al}_2\text{O}_3)(\text{CaSO}_4)_3 \cdot 32\text{H}_2\text{O}$  is very well known and well documented. However another destructive kind of attack was discovered in 1998 causing massive deterioration to concrete foundations (of about 30 years old) supporting bridges along M5 motorway in the UK. This new type is known as Thaumasite type of Sulfate Attack (TSA). Since then, thaumasite  $(\text{CaSiO}_3 \cdot \text{CaSO}_4 \cdot \text{CaCO}_3 \cdot 15\text{H}_2\text{O})$  is having great attention due to its severity compared with the commonly known sulfate attack types. It attacks calcium silicate hydrate the binding gel of the hydrated cement paste and converts it into mushy materials and causing loss of integrity and strength. The UK government formed what is known as Thaumasite Expert Group (TEG) to study the reasons behind this phenomenon and to suggest the proper ways to deal with it. This group presented its first report and pointed out the causes and parameters either needed to form or those can involve later to motivate it (Thaumasite Expert Group 1999).

The report summarised the causes risks, diagnosis, remedial works and guidance on new construction after the field investigation to the affected areas. It was pointed out that limestone used in concrete either as an additive or as aggregate is implicated in most recorded thaumasite cases. In addition to carbonate sources, the report also concluded that low temperature, source of silicate, source of sulfate and access of water or humidity are necessary to form thaumasite. Two reviews were also published one and three years after the first report. Almost all the published literature after that agreed with the report and its recommendations with regard to the risk factors leading to thaumasite and the proper ways to reduce the risk of thaumasite occurrence. The role of limestone and temperature in thaumasite formation has received the attention of researchers. The relation between limestone, either as a cement replacement material or as aggregate, is well established although the mechanism of thaumasite formation is not yet fully known. These recommendations were used as a base for Building Research Establishment (BRE) to publish a Special Digest (BRE SD1 2001) as a guidance for concrete placed in aggressive ground conditions in order for concrete to resist chemical attack, the soils and ground water are classified according to their sulfate content into 5 levels DS1 to DS5 where DS5 most aggressive environment, which contains more than 6000 *mg/l* of SO<sub>4</sub>. In parallel with this digest an amendment took place for British standards (BS) BS5328 and BS882 where BN 206-1 and BS 8500 were replaced to take into consideration concrete resistance to thaumasite attack (Nixon et al. 2003). Attempts to prevent the thaumasite attack were made via various ways; including using cement with low C<sub>3</sub>A which is usually used in high sulfate environments and using SRPC cement but none of them showed any better in their resistance to thaumasite than normal OPC (now replaced by CEM I). However, cements made with PFA tend to delay the thaumasite formation and those made with GGBS showed good performance against TSA.

Being the exterior part of the structures, concrete is more vulnerable to frequent exposure to sun, rain, wind, and sulfate that comes from ground water or soil. Combinations of some of these types happen in frequent cycles for example freezing and thawing and wetting and drying which can reduce the service life of structures. A study conducted by (Moukwa 1990) concluded that deeper penetration of aggressive ions is resulted from wetting and drying cycles.

Wetting and drying cycles are known to be classified as an aggressive environments since the movement of sulfate ions and its accumulation in concrete pores (Hong and Hooton 1999).

Although the large numbers of publications about thaumasite, there is no published research with regard of the formation of thaumasite under wetting and drying cycles, and weather it accelerate it or mitigate it. Such conditions are most likely to affect buried concrete structures as a consequence of seasonal changes in groundwater levels or the infiltration of precipitation from the ground surface, where structures are situated in the unsaturated zone above the water table. Another aspect is the physical properties such as powder-sulfate interaction and its effect on thaumasite formation and whether or not it is responsible for the resistance of concrete to thaumasite type of sulfate attack TSA. This was studied by grinding mortar samples to a fine powder, thus eliminating the permeability effect and enabling physical factors that affect the rate at which solutions can be transferred through the mortar to be separated from chemical factors that affect the rate at which the chemical reactions take place. In addition, the relative resistance of GGBS and PFA cements to TSA in aggressive ground conditions is confirmed but the reasons behind this resistance are still undiscovered. Moreover, the temperature effect on formation of thaumasite is also a matter of debate and it its role was also studied.

Thermodynamic modelling based on Gibbs Energy Minimisation was used as useful application to calculate the phase assemblage for the reaction and deterioration products and as a quantitative tool to confirm the results obtained experimentally.

## **1.2 Objectives of the study**

The main aims of this research are 1) to investigate the effect of wetting and drying regime on the thaumasite type of sulfate attack. 2) To investigate the effect of carbonation and carbonated layer on the thaumasite formation. And 3) to investigate the effect of water to cement ratio on the formation of thaumasite in cement mortars. To meet these aims the following objectives were investigated:

- To study the behaviour of different cement types especially GGBS and PFA in wetting and drying environments with regard to thaumasite formation (TF).
- The effect of temperature on thaumasite formation.
- The effect of sulfate concentration on thaumasite type of sulfate attack.
- Using thermodynamic modelling as a tool to calculate the reaction and deterioration products and compare it with experimental results from XRD, FTIR and SEM.

## **1.3 Structure of the thesis**

The thesis consists of eight chapters as follow:

Chapter 1 introduces the problem of sulfate attack and thaumasite type of sulfate attack.

Chapter 2 presents a literature survey about sulfate attack in general and about thaumasite type of sulfate attack and the factors affecting its formations and the possible ways of avoiding it.

Chapter 3 describes the materials and the experimental procedures followed to characterize and understand the aims of the study.

Chapter 4 presents the results of the effect of the wetting and drying cycles on the formation of thaumasite in cement mortars.

Chapter 5 shows the results of the effect of carbonation and carbonated layer on thaumasite formation.

Chapter 6 reports the results about the effect of water to cement ratio on thaumasite formation in cement mortars and the possibility of thaumasite formation in powders made from grinding cement mortar samples and eliminating the permeability effect.

Chapter 7 deals with the overall discussions of the results presented in Chapters 4, 5 and 6.

Chapter 8 summarises the findings of the research and the recommendations for future work.

# 2

## Literature review

### 2.1 Introduction

With the rapid developments of modern societies, the demand on concrete has also rapidly increased, since it is the largest used construction material. This increment has brought more concrete problems with it. Sulfate attack is one of the problems that have been always linked to the durability of concrete structures causing cracks, expansion and severe deterioration to buildings. Classical sulfate attack which is resulted from ettringite and gypsum formation is well known and well documented, but another kind of attack known as thaumasite type of sulfate attack (TSA), although is not new, is having great attention in the past two decades after its discovering in foundations supporting motorway bridges in the UK in 1998. Thaumasite is well known as a natural mineral. It was first discovered to cause deterioration to concrete structures in the USA in 1965 (Crammond 2003). Thaumasite is favoured to form in low temperatures around 5°C and requires sources of carbonate, and humidity or water (Bensted 1999).

Over recent years, a severe damage to concrete structures caused by the thaumasite formation has been considered as an important aspect, and due to this the UK government had formed a group of specialists to study

this phenomenon. Furthermore, thaumasite cases were reported in many countries, mainly those with cold climate all over the world (Thaumasite Expert Group 1999).

Being the exterior part of the structures, concrete is more vulnerable to frequent exposure to sun, rain, wind, and sulfate that comes from ground water or soil. Combinations of some of these types happen in frequent cycles for example freezing and thawing and wetting and drying which can reduce the service life of structures. A study conducted by Moukwa (1990) concluded that deeper penetration of aggressive ions is resulted from wetting and drying cycles.

Wetting and drying cycles are known to be classified as an aggressive environments since the movement of sulfate ions and its accumulation in concrete pores (Hong and Hooton 1999).

With respect to conventional sulfate attack, using low  $C_3A$  cement used to protect concrete against attack, this is no longer correct with respect to thaumasite type of sulphate attack (TSA) because thaumasite does not involve aluminium (Blanco-Varela et al. 2006, Brown and Hooton 2002, Nobst and Stark 2003). Designing high quality concrete with low water to cement ratio and using blended cement especially GGBS seems to grant the concrete the required resistance to this type of attack. However the reason behind why these cements are performed well in thaumasite environments is not yet known and whether it is linked to physical properties or chemical reactions is in place of debate.

## **2.2 Conventional sulfate attack**

Sulfate attack can be defined as a result of chemical reactions between hydration products of cement, mainly the cement paste and sulfate ions. This happens when concrete is being exposed to sulfate environments and in presence of moisture or water. Sulfate attack is attributed mainly

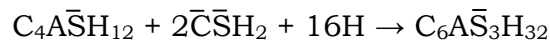
to one of two mechanisms, namely formation of ettringite and formation of gypsum, both of these types result in expansion, cracks and loss of strength for concrete (Jan Skalny et al. 2003).

The attack results from sulfate can occur in one of two forms; EXTERNAL which is more common to happen due to the presence of sulfate ions in external sources such as soil and ground water then it penetrate into concrete. The second is INTERNAL and that comes from incorporated sourced used at mixing stage of preparing concrete, for example sulfates present in aggregate (Jan Skalny et al. 2003).

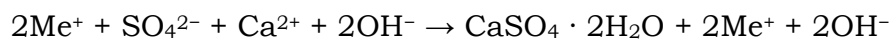
Ettringite is formed during the hydration of Portland cement and calcium silicate bearing phases according to the following equation:



If substantial amounts of ettringite are formed, an expansion is occurred. More expansion is expected to happen when the ettringite is formed from monosulfate:



Gypsum is formed as a result of the reaction between sulfate ions and calcium hydroxide from the paste:



Sulfate attack is responsible for deteriorating the cement matrix due to the chemical changes that occur to cement hydration products when exposed to sulfate solutions: The term “conventional” is used here to distinguish between the attack caused by previous known sulfate types

(ettringite and gypsum) rather than thaumasite (Torres 2004). In general, some hydration products of cement are not stable in sulfate solutions. Indeed, it was found that high magnesium concentration altered the results of chloride diffusion in mortars in the diffusion cell test by blocking the surface through the formation of brucite.

### **2.3 Thaumasite form of sulfate attack TSA**

Thaumasite ( $\text{CaSiO}_3, \text{CaSO}_4, \text{CaCO}_3 \cdot 15\text{H}_2\text{O}$ ) is a calcium silicate carbonate sulfate hydrate that can be formed during the degradation process of cementitious materials with ettringite, gypsum or on its own. It is a result of the combination between carbonation and sulfate attack, and occurs in concrete structures and in masonry walls. Thaumasite formation causes damage to cementitious materials by decomposing the C-S-H phase. (Ramachandran et al. 2002, Sabbioni et al. 1999, Hooton and Thomas 2002, Crammond 2002).

In severe cases of thaumasite attack (TSA), the binding phase C-S-H is entirely converted to thaumasite and the cement paste is turned into mushy materials (Crammond et al. 2003).

Figure 2.1 shows a mortar prism that suffered from severe thaumasite sulfate attack during this study.



**Figure 2.1 Limestone mortar prime after 18 months of exposure to sulfate solution.**

However, Collepari (1999) mentioned similarities in the effect of thaumasite and ettringite formation where they both lead to expansion, cracking, spalling, loss of strength and adhesion of cementitious materials, but ettringite formation is associated primarily with expansion, cracking and spalling, while the damaging resulting from thaumasite formation is much more severe, transforming hardened concretes or mortars in a pulpy mass with a complete loss of strength and integrity.

Although there is no alumina in the structure of thaumasite, it is believed that the presence of ettringite is a necessary precursor, and hence the similarity in their crystal structure, Ettringite is possibly acting as a nucleating agent (Newman and Choo 2003).

Macphee and Diamond (2003) emphasised that the deterioration resulted from TSA can be much more severe than that caused by conventional forms of sulfate attack (attributed to gypsum and ettringite formation) as it attacks and deteriorates the calcium silicate hydrate (C-S-H), which

gives the integrity to the cement matrix, rather than calcium aluminate hydrate which is the attractive phase of conventional sulfate attack and it can continue to form as long as the needed sources of carbonate and sulfate are available. There is no relation between the thaumasite and alumina content of cement (Crammond 2002).

With respect to TSA, it was initially thought that using sulfate-resistant Portland cement (SRPC), which contains low  $C_3A$  content may inhibit the thaumasite formation process, as it does in case of conventional sulfate attack. However, Report of the Thaumasite Expert Group (1999) reported that, concrete with high quality, made with sulfate resistant Portland cement can still suffer from severe thaumasite sulfate attack, as calcium silicate phases are in the system and thus not resistant to TSA (Sims and Huntley 2004).

Blanco-Varela et al. (2006) presents a review of research made by different authors regarding thaumasite attack in concretes and mortars made with sulfate-resistant Portland cements containing low and high percentages of  $C_3A$ , and there is an agreement that TSA also forms in specimens made with ordinary cements, however, the rate of formation is slower than in samples with sulfate-resistant cements. This is due to classical sulfate attack usually in the form of ettringite using aluminium provided by the cement which is limited in quantity in normal cements. The study observed that the cement content of  $C_3A$  affects the type and the formation process of deteriorating salt produced, according to and their results and observation, they confirmed that magnesium sulfate is less aggressive than gypsum and more thaumasite tend to form in low  $C_3A$  cement specimens. Consequently, although the use of sulfate-resisting Portland cement in normal sulfate environments provides some protection to concrete against deterioration, this type of cement does not give any particular resistance against thaumasite attack. On the other hand, Crammond (2002) showed that, in order for ettringite or gypsum to

form, carbonate ions are not necessary to be present but they are required for thaumasite formation. The carbon dioxide dissolved in water can serve as a source of carbonate or it can be provided from limestone incorporated in the materials themselves as filler or aggregate. Thus, if a cementitious material containing limestone comes into contact with sulfated medium; that means the required parameters for thaumasite formation are present, and the speed of the reaction increases considerably at cold temperatures preferably below 15°C.

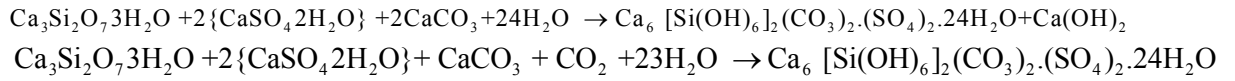
## 2.4 Formation of thaumasite

In order for thaumasite to form there are few conditions that should be met and these are (Bensted 1999):

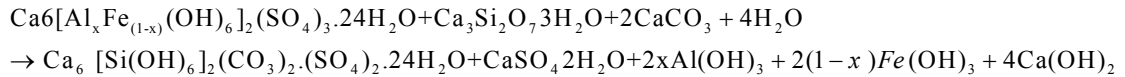
- A source of calcium silicate, for example calcium, calcium oxide or calcium hydroxide plus silica, tricalcium silicate  $C_3S$ , decalcium silicate  $C_2S$  preferably  $\beta$ -form. This can be provided by the calcium silicate hydrate CSH the binding gel of the hydrated cement itself.
- A source of sulfate, such as calcium sulfate, gypsum  $CaSO_4 \cdot 2H_2O$  or anhydrite ( $CaSO_4$ ). This can be provided from sulfate bearing soil or groundwater.
- A source of calcium carbonate which can be in the form of calcium carbonate calcite  $CaCO_3$ . And this comes from different sources like carbonate aggregates and limestone filler or even from the atmospheric carbon dioxide  $CO_2$ .
- Excess of water or humidity.
- Low temperature below 15°C.

Bensted (2003) mentioned two proposal routes for the formation of thaumasite:

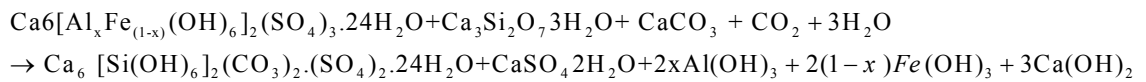
**First** is the **Direct route** in which C-S-H gel reacts with carbonates ions



**Second** is the **Woodfordite route** in which C-S-H gel reacts with carbonate in ettringite



Or



The reaction in both routes is very slow and it may take a few months for thaumasite to develop. In both routes calcium hydroxide formed in the reaction will not stay as an end product since it will serve as a reactant with carbon dioxide or  $\text{CO}_3$  to form calcite which will react again to form more thaumasite.

In comparison, between the two routes the XRD results showed that the woodfordite route is relatively quicker. This is mainly attributed to the presence of aluminate. Thaumasite formed from direct route affect  $\text{C}_3\text{S}$ ,  $\text{C}_2\text{S}$  phases while Thaumasite formed from woodfordite route affect  $\text{C}_3\text{S}$ ,  $\text{C}_2\text{S}$ ,  $\text{C}_3\text{A}$ ,  $\text{C}_4\text{AF}$  phases. However these two routes are closed to each other (Bensted 2003).

Crammond (2002) mentioned what is called thaumasite formation TF, and this in situations where thaumasite can be identified or formed in cracks and air voids without associating with any visual deterioration to the mortar or concrete.

## **2.5 Effect of wetting and drying cycles on durability of concrete.**

Wetting and drying cycles are known to be classified as an aggressive environments since the movement of sulfate ions and its accumulation in concrete pores (Hong and Hooton 1999). Same study showed that exposing to wetting and drying cycles led to increase the chloride penetration into concrete samples. Yigiter et al. (2007) tested concrete samples made from Portland cement slag cement under cyclic wetting and drying exposure to sea water and found that both compressive and tensile strength decreased for PC but not for slag cement. Sahmaran et al.(2007) studied the possibility of plain and blended cements to resist sulfate attacks under wetting-drying cycles and cooling-heating environments, it was concluded that for ordinary Portland cement (OPC) the rate of deterioration increased for samples subjected to wetting-drying cycles compared to those been continuously in sulfate solutions, sulphate resisting Portland cement (SRPC) showed performance better than (OPC) to sulfate but it is not guaranteed high sulfate resistance, blended cements made with class F fly ash and natural pozolana were also highly affected by cyclic exposure regime. Aye et al. (2010) used hardness test to evaluate the performance of Portland cement OPC and high alumina cement (HAC) mortars to sulfate attack under wetting-drying cycles. Their observation showed that complete damage of PC mortar resulted from crystallization of salts and formation of gypsum, while the insignificance damage of HAC mortar was linked to physical crystallization of salt. Results of study conducted by Wang et al. (2006) showed severe damage confirmed by strength and mass losses of concrete samples exposed to  $\text{CaCl}_2$  solution under wetting-drying and freeze-thaw conditions. In a research by Escadeillas et al. (2007) it was summarized that wetting-drying cycles are not mandatory for delayed

ettringite formation DEF to occur, however, their contribution may be limited to slightly accelerate the reaction.

Exposing to magnesium sulfate solution at 60 °C with wetting– drying cycles can be considered an accelerated method for sulfate attack (Hekal et al. 2002).

A rapid failure by mechanisms such as sodium sulfate crystallisation can be caused from localised extraordinary high concentrations of sulfate due to Wetting-drying cycling (Novak and Colville 1989). In the UK and according to Plowman and Cabrera (1996) It is generally observed that for exposure to sea water, intertidal, splash, and spray zones are the most aggressive.

Formation and crystallization of sodium sulfate salts under wetting and drying cycles was a major mechanism of distress in concrete in the exposure conditions (Stark, 2002).

However, there is no published research found with regard to the effect of wetting-drying cycles on thaumasite formation. Even for the sulfate attack measures the work done was carried out at room temperature or higher, neglecting the low temperatures which are motivating thaumasite formation. It was also noted that using the accelerated drying measures such as heating which is not in accordance with what is happening in the reality where wetting and drying usually occurs at similar temperatures.

In this study the performance of plain and blended cements under cyclic wetting and drying environments is investigated.

## **2.6 Effect carbonation and early air curing on sulfate attack.**

The effect of carbonation layer in concrete on its resistance to sulfate attack was studied in a research by Osborne (1990), where he tested samples made from Portland cement and blended with blastfurnace slags and stored in Magnesium sulfate for 5 years. It was concluded in his research that the formation of carbonated layer near the surface extremely enhanced the resistance of concrete to sulfate attack.

In another study, Mangat and el-Khatib (1992) studied the influence of initial curing on the resistance of blended cement concrete to sulfate attack. They used ordinary Portland cement which partially replaced with PFA and GGBS, they concluded that; the presence of a carbonated layer on the concrete surface is generally accompanied by superior sulfate resistance; they also found that the early dry out of concrete during early curing and carbonation led to more resistance to sulfate attack. They linked this resistance to the reduction in  $\text{Ca(OH)}_2$  content in the surface layers which leads to smaller volumes of the expansive reaction products with sulfate ions.

The mechanical properties were significantly improved and binding capacity was increased for concretes cured in a carbon dioxide environment when compared to samples cured in nitrogen or normal atmospheric conditions (Lange et al. 1997).

Higgins and Crammond (2003) reported that, the early air cured GGBS concretes performed extremely well after 6 years of exposure to strong sulfate solutions.

## **2.7 Factors affecting thaumasite formation**

### **2.7.1 Role of Cement type**

#### *2.7.1.1 Effect of Limestone*

Limestone aggregates are commonly used in the UK and elsewhere for long time. Indeed, in recent years the cement standards BS EN 197-1:2000 (2011) allow incorporation of up to 5% limestone to be used as a clinker replacement. This is mainly because of its environment friendly role and the improvements that given to the concrete in terms of durability. A greater increase of strength obtained with addition of very fine limestone powder than is found with the addition of natural Pozzolana or slag. Evidently, there is a physical effect brought by the addition of a powder which gives a greater denseness to the mortar (Poitevin 1999).

Results reported by Gaze and Crammond (2000) showed that the durability of non-calcite containing mortars is found to be slightly less than those containing calcite, particularly in weak magnesium sulfate solution. This was explained as the impermeability of added-calcite mortars is improved rather than any chemical resistance to sulfate attack.

In Norway, Justnes (2003) tested mortars made with 20% limestone filler and kept in 5% sodium sulfate solution at 5°C. After 10 months of exposure the results showed extensive presence of thaumasite, the samples also suffered from mass loss and expansion.

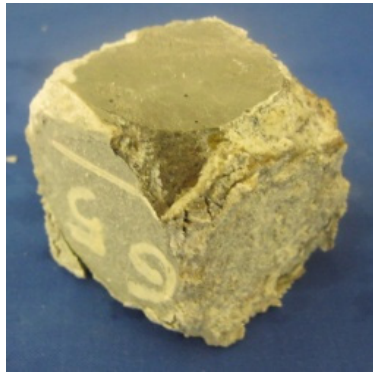
Kakali et al. (2003) employed limestone cement containing 15% and 30% limestone with siliceous and calcareous sand immersed in 1.8% MgSO<sub>4</sub> solution and studied their durability, they concluded that, at low temperature, mortars made with limestone, either sand or as main cementitious constituent, are attacked by thaumasite. The rate of the

attack was greater, as the level of limestone content was higher. In a study incorporating the substitution of 15% weight of cement by finely ground limestone by Zelic et al. (2000), it was shown that using limestone has significantly increased the porosity, while such an addition with up to 8% silica fume can reduce the porosity. However, the amount of limestone used is affected by the silica fume content in the mix. Replacing Portland cement with more than 8% silica fume resulted in calcium hydroxide being available for limestone reaction as active participant. Thus, in these conditions, limestone acts as filler. Accordingly, the improved performance of combined cementitious systems containing Portland cement, GGBS, silica fume and limestone in sulfate solution, Zelic et al. (1999) implies that the effects of combination of limestone and Pozzolana might be a considerable improvement in the durability of concrete against thaumasite type of sulfate attack. However, Bensted (1999) noted that; in hardened cements, mortars and concretes limestone is not chemically dormant, but can react, if the conditions to produce thaumasite are met. In another research project by Hartshorn et al. (2002) to investigate mortar samples made from Portland cement with different percentage of limestone additions. The results showed a readily thaumasite formation in cements containing 35% limestone mortars after 126 days immersion in magnesium sulfate solution. Thaumasite, gypsum and brucite were identified in the surface layer of mortars. The SEM images revealed that thaumasite was responsible for the deterioration caused to the concrete. However, the intensity of the attack was greater at 5°C compared to samples kept at 20°C, although some thaumasite was observed at higher temperature. Same author (Hartshorn et al. (2001) stated that only small quantities of thaumasite were identified in the 5% limestone filler samples in the first 12 months, and no significant changes were recorded to the engineering properties of concrete. Moreover, the danger of thaumasite sulfate attack might

increase due to long-term carbonation of the Portlandite (Hartshorn et al. 2002).

The buried columns supported several bridges along the M5 motorway in the UK were attacked and expansive thaumasite was identified. As limestone fine and coarse aggregates were employed for these structures, it was thought the carbonate ions were supplied by the aggregates, particularly their fines. However, Hooton and Thomas (2002) reported that 20 years of field experience in Europe and Canada with up to 5% limestone filler used in Portland cement, no cases of TSA have been reported. These propose permitting use of up to 5% limestone in Portland cements. Also, Higgins and Crammond (2003) reported the beneficial effect of presence of carbonate in mixes containing 70% GGBS and 30% Portland cement as this enhanced the resistance of concrete to conventional sulfate attack. On the contrary, Hartshorn et al. (1999) and Torres et al. (2003) confirmed TSA in samples with only 5% limestone. The thaumasite formation in cements containing limestone filler immersed in sulfate solution at 20°C was reported by Irassar et al. (2005). They stated that OPC and high-C<sub>3</sub>S SRPC containing 20% limestone filler were susceptible to sulfate attack proposing that, this attack is first led to the formation of ettringite, then formation of gypsum and finally thaumasite formation where ettringite formed during the first stage of attack is decomposed.

Figure 2.2 below shows 2 years old deteriorated samples with different limestone content where the deterioration increases with increasing the limestone level, these samples were stored in DS4 sulfate solutions based on MgSO<sub>4</sub> at 5 °C ( from this study).



CEMI



CEMI + 10% Limestone filler

**Figure 2.2 View of cubes with and without limestone filler**

However, a study by Pajares et al. (2003) explained that a decomposing of ettringite starts to happen when it incorporates increasing amounts of carbonate in its structure.

The limestone was added to CEM I in this study with percentage of 10% by weight in order to accelerate the thaumasite formation process, as it can be clearly seen from the literature that limestone cement is more likely to suffer from thaumasite sulfate attack once the other conditions are met.

### **2.7.1.2 Ground Granulated Blast furnace Slag (GGBS)**

Many research articles have dealt with the effect of GGBS as a cement replacement on the thaumasite formation. Among these studies Higgins and Crammond (2003) who tested concrete made with 70% GGBS and two aggregate types in four different sulfate solutions at 5 and 20°C. They reported that concretes made with normal aggregates performed extremely well against thaumasite sulfate attack and showed no signs of deterioration in all solutions. On the other hand, concrete made with poor quality carbonate aggregate did not perform well at either temperature. Bellmann and Stark (2007) stated that using high amounts

of GGBS and fly ash in cements will lower the calcium / silica ratio and reduce the susceptibility to TSA.

In another study Tsivilis et al. (2003) reported that an incorporation of 50% GGBS led to an improvement of the resistance of limestone cements to sulfate attack. They also reported that if concrete is exposed to sulfates before the start of the pozzolanic reaction, the effective resistance to sulfate attack will be reduced, which is a consequence of the slow increase in pozzolanic bonding. Hill et al. (2003) investigated the effect of GGBS on thaumasite formation in concrete cubes exposed to several sulfate solutions for 5 months. The results showed that no thaumasite was formed in any of the solutions used, which indicates the resistance of GGBS cements to thaumasite formation within that timescale. Incorporation of GGBS and metakaoline by Skaropoulou et al. (2009) substantially to improve resistance to TSA . Barnett et al. (2002a) concluded that combining blast furnace slag with OPC retards or possibly stops the formation of thaumasite. In studies in which OPC cements were partly replaced with Metakaolin (MK) and GGBS and specimens were immersed in sulfate solutions at 5°C for 280 days, Smallwood et al. (2003) concluded that samples containing 14% MK, 21% MK and 80 % GGBS showed no signs of deterioration due to sulfate attack and the expansions of these concretes were negligible.

It is widely agreed in the literature that durability of cements blended with GGBS is improved in terms of the resistance of concrete to TSA. However, reasons why does the GGBS containing cement is resisting thaumasite attack are not yet understood, and whether the resistance belongs to chemical or physical factors are not yet confirmed. In this research by using 70% GGBS as a replacement and this study exposes ground GGBS mortar samples to sulfate solution thus eliminating the effect of the pore structure and permeability on thaumasite development and compares this to the performance of solid specimens. Moreover the

performance of such blended cement in environments such as wetting and drying cycles is investigated.

### **2.7.1.3 Pulverized Fuel Ash (PFA)**

Thomas and Matthews (2004) Examined concrete samples which were exposed to marine environment for 10 years and they were containing 30% and 50% fly ash. The results showed no signs of thaumasite formation although the presence of sulfate and carbonate in the surface 5 mm layer of concrete. They also noticed a significant reduction of the levels of chloride in the concretes made with PFA compared to the normal PC concrete with (0% PFA), the reductions become greater as the level of PFA content increased. There was no explanation given for these results.

A study conducted by Nobst and Stark (2003) on three types of fly ash with different amount of aluminium oxide on ground cement pastes mixed with gypsum and calcite and conclude that: at low temperatures, the addition of lignite coal fly ash (FA3) seems to increase the amount of thaumasite formed corresponding to the increase in  $\text{Al}_2\text{O}_3$  content. At the same time the pozzolanic reaction of the lignite coal fly ash is more effective at low temperatures as compared to that of the hard fly ashes (FA1 and FA2), whose reactions are better at room temperature as this favours ettringite formation. As a part of a long term durability investigation of PFA concrete in sulfate solutions, Hill et al. (2003) observed that PFA concrete was attacked but instead of thaumasite, ettringite was formed. In another study by Tsivilis et al. (2003) on the effect of using mineral admixtures to prevent thaumasite formation, it was concluded that using fly ash can retard thaumasite formation in samples immersed in 1.8%  $\text{MgSO}_4$  at 5°C. On the other hand, Mulenga et al. (2003) reported the formation of thaumasite in mortars made with fly ash within 84 days of immersion in sulfate solutions. However the

quantity of formed thaumasite depends on the type of cement used. A comprehensive project carried out by BRE between 2000 and 2003 and studied the OPC and SRPC blended with different levels of PFA and GGBS, concluded that the higher the level of PFA the better the thaumasite resistance of concrete where concretes containing 45% PFA performed better than those with 30% fly ash in term of their resistance to thaumasite sulfate attack (Crammond 2002). Torii et al. (1995) studied concrete samples made with cement blended with 50% PFA and immersed in 10% Na<sub>2</sub>SO<sub>4</sub> for two years and found that the 50% replacement of fly ash improved the resistance against sulfate attack.

As it can be noticed from the literature there are no many published papers used PFA in percentages more than 40% although it is agreed that the higher the PFA content in cement the better resistance to sulfate attack is gained. 50% PFA is added to CEM I cement to study its performance under continuous and wetting and drying exposure conditions.

### **2.7.2 Role of Temperature**

There is general attitude that temperatures lower than 15 °C preferably between 0-10°C are favour for thaumasite formation, this is confirmed by many researchers in literature (Thaumasite Expert Group 1999, Bensted 1988, Halliwell and Crammond 1999, Barker and Hobbs 1999, Martinez-Ramirez et al. 2011)

Although initially it was believed that a temperature below 5 °C was essential for thaumasite formation, investigations by Diamond (2003) in some parts of California showed evidence of formation of thaumasite from of sulfate attack even in warm climates.

Another study reported by Santhanam et al. (2003) succeeded to produce thaumasite from samples stored at 25 °C and concluded that

the thaumasite formation does not have to be limited to low temperatures.

Moreover, in their research Hartshorn et al. (2002) reported that some thaumasite was formed at room temperature about 20 °C , although the extent of thaumasite sulfate attack was greater at 5°C than at 20 °C.

Pipilikaki et al. (2008) studied the effect of temperature on thaumasite formation; their specimens were immersed in Na<sub>2</sub>SO<sub>4</sub> at 5°C, 10°C, and 20°C for one year after which the results showed sever damage to samples kept at 5°C while less damage recorded on samples stored at 10°C while the samples left at 20°C remained intact and no thaumasite detected after one year on immersion.

Lixiong et al. (2005) indicated that it is easier for thaumasite to form at lower temperatures 3-10 °C.

Bensted (1988) argues that the low temperature will increase the co-ordination number to allow formation of Si(OH)<sub>6</sub>. However this does not mean the formation of thaumasite at higher temperatures is prevented.

The TEG report (1999) proposes that using heating equipments inside buildings may improve their foundation's resistance against TSA.

Bensted (1999) has suggested that the stability of thaumasite is higher at lower temperature due to the adoption of octahedral co-ordination available in thaumasite by silicon is more easily at lower temperatures. But once it is formed it can remain stable up to high temperature approximately 110°C.

As it can be noted from the literature, the formation of thaumasite at higher temperatures is a matter of debate. In this research the effect of temperature is investigated where samples will be kept at low 5°C and room temperature around 20°C.

### **2.7.3 Role Sulfate concentration**

Lee et al. (2005) employed different levels of Metakaolin in solution with different  $\text{MgSO}_4$  concentrations and demonstrated that, the increment in sulfate concentration led to more deterioration to concrete samples. This is mainly associated with the formation of gypsum as a result of magnesium sulfate attack. It was also found that a larger expansion resulted from increasing the concentration of magnesium sulfate solution from 0.42% to 1.27%, while sulfate concentration increment to 4.24% did not have any significant effect on length change. In a research done by Juel et al. (2003) where thermodynamic modelling was used to predict the thaumasite stability, the presented experimental results were well agreed with the model which predicts that possibility of thaumasite to form only in Portland cements where sulfate levels are high enough to form gypsum at ambient temperature.

In another two studies done by Bellmann (2004a), (2004b) it was shown that the formation of thaumasite could be from gypsum, calcite, portlandite, C-S-H and water. The precipitation of thaumasite was calculated to be possible at low sulfate concentrations of 1,5g  $\text{SO}_4$  /l in solution which is in agreement with the observations of Mulenga et al. (2003) who showed that even at low sulfate concentrations ( $\leq 3\text{g SO}_4$ ) in solution thaumasite formation is possible.

Although, a lot of research has been done recently, it has not been definitively established to what extent sulfate concentration influence the formation of thaumasite.

In this study BER DS3 and DS4 sulfates were used to measure the extent of thaumasite formed.

### **2.7.4 Role of pH**

Several studies have investigated the stability of thaumasite at different pH levels, Jallad et al. (2003) tested 10 natural thaumasite samples

weighing 1g each and immersed them in three different groups of solutions varying in their pH from 6 to 13 for 30 days against decomposition and reaction with ions existing in the solutions. The study concluded that the pH of the surrounding environment has affected the stability of thaumasite, where at pH value of 6.00 the observations showed decomposition of thaumasite, while at pH levels of 9.00 and 10.00, SEM results showed no sign of thaumasite; instead; calcium carbonate was present. At pH level of 11.00, XRD analysis showed presence of thaumasite and traces of calcite. Same study reported that at relatively higher values of pH 12.45 and 13.00 the thaumasite was stable.

Another study by Gaze and Crammond (2000) found that thaumasite did not form in environments with pH level below 10.5 where C-S-H become unstable. On the other hand thaumasite readily formed in pH level of 13 and once it is formed it remains stable in pH levels as low as 7.0.

Hobbs and Taylor (2000) reported that the probabilities of thaumasite formation is higher in environments with pH higher than 12.5, and decreases at pH lower than 8.0. In addition, for this formation to take place an amount of gypsum is needed, as well as for ettringite formation.

In a separate study on the effect of carbonate sources other than aggregate and filler on thaumasite formation carried by Collett et al. (2004) pointed out that a reason for this pH threshold can be that the carbonate species in solution, such as  $CO_2$  and  $HCO_3$  which take part in the reaction mechanism of thaumasite formation, are in equilibrium at the pH of 10.33. Moreover when the temperature drops from 25°C to 5°C, this equilibrium is around pH of 10.55. Furthermore Slater et al. (2003) stated that the pH level of ground water which was about 8.0-8.6 has

increased to values of about 10.5-11.33 towards the thaumasite affected concrete-soil interface.

In the presence of magnesium sulfate the lower concentration of sulfate leads to a higher pH value as there is insufficient sulfate to react with lime. In exposed concrete samples carbonation can result in decreased pH and therefore more C-S-H disintegration. The conditions for thaumasite formation were found to be similar to those for ettringite. The results from mortar samples cured in exposed diluted magnesium sulfate solution showed long-term contact between thaumasite and a lower pH solution, so, in this respect, thaumasite appeared to be more stable than ettringite (Gaze and Crammond 2000). Moreover, Zhou et al. (2006) concluded that the formation of thaumasite is not promoted in acid medium. Although concrete exposed to acid conditions was deteriorated, the mechanism was not thaumasite formation as observed in alkaline mediums.

## **2.8 Identification of thaumasite**

The formation of TSA transforms the cement paste matrix in a white mush composed of thaumasite, which loosely holds the surrounding aggregate particles together. In addition, the thaumasite fills the cracks and white haloes of thaumasite occurring around aggregates. It can also occur in a non-destructive way, as mentioned before, by Crammond (2002) as thaumasite formation TF.

On the other hand, according to Collepardi (1999): the crystallographic structure of ettringite and thaumasite is very similar, in spite of the difference between their chemical compositions.

Due to this similarity there are considerable number of cases of sulfate attack that were associated with ettringite but were in fact result of thaumasite formation (Crammond 2002). Due to improvements in

diagnostic techniques the differentiation between the two minerals becomes easier and that is probably why there is an increase in the reported thaumasite attack cases. The main difference between the two is that in TSA calcium silicate hydrate is the main target of the reactions instead of calcium aluminates hydrate (Lothenbach and Winnefeld 2006). Consequently, the X-Ray diffraction patterns for these two composites are very similar since the similarity in their unit cells and low-angle, high-intensity reflections (Skibsted et al. 2003). Indeed this technique is the very common way for detection of thaumasite.

Thermal analysis and infrared spectroscopy also provide the identification of thaumasite with possibility of confusion with Ettringite (Bensted and Satya Prakash 1976), (Skibsted et al. 2003). Raman spectroscopy is possible to be used for this propose, as low-vacuum scanning electron microscopy (SEM) which requires several steps of preparation of the samples before the investigation (Yang and Buenfeld 2000, Sahu et al. 2002).

### **2.9 Thermodynamic modelling**

A thermodynamic model was developed by Juel et al. (2003) to predict the assemblage of hydration products for cement blended with limestone filler and exposed to magnesium sulfate solutions. The model predicted that the stability of thaumasite is low in the presence of AFm phases and it is only possible to form under conditions where gypsum would be favour to form at higher temperatures. This prediction was confirmed by XRD analysis results.

Lothenbach and Winnefeld (2006) applied thermodynamic modelling to calculate the hydration products and pore solutions of Portland cement. The predicted phases compared well with experimental results obtained from XRD and TGA analyses.

In another study by Lothenbach et al. (2008), they used thermodynamic modelling to study the effect of temperature on the hydration of OPC. A good agreement between calculated and observed results was achieved for temperatures up to 20 °C but not at 50 °C where the modelling predicted the conversion of ettringite to monosulfate.

Lothenbach and Gruskovnjak (2007) modelled the hydration of alkali activated slag and found that same phase were identified in modelled data and from XRD and TGA analyses.

Schmidt et al. (2008) studied the conditions of thaumasite formation under thermodynamic equilibrium with regard to temperature and C<sub>3</sub>A content in cement. They found that thaumasite is favoured to form at low temperature 8 °C with no obvious link to C<sub>3</sub>A content in the used cement.

Kunther et al. (2013) conducted an experimental and thermodynamic study on the effect of bicarbonate on the deterioration of cement mortars exposed to sulfate solutions. They pointed out the role of bicarbonate on the deterioration process, where ettringite becomes unstable in the presence of bicarbonate ions. The thermodynamic predictions were in agreement with observed results.

# 3

## **Experimental Programme**

### **3.1 Introduction**

For the purpose of achieving the aims of this research, an experimental programme has been designed, and required parameters have been chosen. Based on literature; sources of carbonates, silicates, sulfates were provided in addition to low temperature and excess of water. This section will cover the Materials used and the experimental work that was carried out in order to achieve the objectives set for this research.

### **3.2 Materials**

The following materials were used all over the study:

#### **3.2.1 Cement (CEMI)**

In this research, cement type CEM I-52.5, complying with the requirement of BS EN 197-1:2011 (2011) was used. The chemical and mineralogical compositions and physical properties of the cement as obtained from XRF analysis are shown in Table 3.1. Bogue equations were used to calculate the mineralogical composition of the cement. CEM I was chosen for this study as a main binder since it is the most common used cement in construction projects nowadays.

#### **3.2.2 Limestone filler**

Limestone was used as filler and 10% by mass was added to CEM I. The addition of limestone was used as a way of acceleration of thaumasite attack since the limestone blended cements are known to be the most susceptible cements to TSA. The necessary analysis procedure was made to ensure it comply with the specifications BS EN 197-1:2011 (2011) The chemical compositions of the limestone as gained from XRF analysis are shown in Table 3.1

#### **3.2.3 Ground Granulated Blastfurnace Slag (GGBS)**

The ground granulated blast-furnace slag (GGBS) conforming to BS EN 15167-1:2006 was used as additive materials replacing CEM I with 70% by mass. The chemical composition of the used GGBS as obtained from for XRF analysis techniques are presented in Table 3.1

#### **3.2.4 Pulverized Fly Ash (PFA)**

The pulverised fly ash (PFA) complying with BS EN 450 -1 and of class S was used as additive materials replacing CEMI with 50% by mass. The chemical compositions of the used PFA as determined from for XRF analysis are presented in Table 3.1.

#### **3.2.5 Aggregate**

Medium graded natural sand passing from 5 mm sieve complying with BS EN 12620:2002+A1:2008 was used in the mortar mixes. The chemical compositions and the physical properties of the used Sand as provided by the supplier are presented in Table 3.2 the sieve analysis results are presented in Figure 3.1

#### **3.2.6 Water**

Normal tap water available in the laboratory was used for the mixing of mortars.

**Table 3.1 Chemical and mineralogical composition of Cement, LF, PFA and GGBS**

Oxide/Phases (Mass, %)	Material			
	CEM I	Limestone	PFA	GGBS
SiO <sub>2</sub>	19.85	0.63	50.83	35.58
CaO	64.61	55.2	2.56	40.66
Al <sub>2</sub> O <sub>3</sub>	4.67	0.28	24.95	12.82
Fe <sub>2</sub> O <sub>3</sub>	2.74	0.15	9.78	0.45
Na <sub>2</sub> O	0.23	< 0.003	0.92	0.32
K <sub>2</sub> O	0.449	0.054	3.539	0.629
MgO	1.09	0.47	1.72	7.52
LOI	3.015	42.89	0.436	2.384
SO <sub>3</sub>	2.52	< 0.002	3.44	0.94
C <sub>3</sub> S	68.28			
C <sub>2</sub> S	5.4			
C <sub>3</sub> A	7.74			
C <sub>4</sub> AF	8.34			

**Table 3.2 Chemical compositions and Physical properties of sand**

**A- Chemical analysis**

Element	%
Silica SiO <sub>2</sub>	94.8
Aluminium Al <sub>2</sub> O <sub>3</sub>	2.9
Calcium CaO	< 0.1
Calcium carbonate CaCO <sub>3</sub>	0.1
Iron Fe <sub>2</sub> O <sub>3</sub>	0.8
Magnesium MgO	0.2
Magnesium carbonate MgCO <sub>3</sub>	0.4
Manganese MnO	< 0.1
Potassium K <sub>2</sub> O	0.9
Sodium Na <sub>2</sub> O	0.1

**B- Physical Properties**

Property	Value
Aggregate Abrasion Value	4.1
Aggregate Crushing Value	12
Aggregate Impact Value	19
Magnesium sulfate Soundness	88
Relative density ( Oven dry) O.D	2.82
Relative density S.S.D	2.63
Water Absorption by weight %	0.5

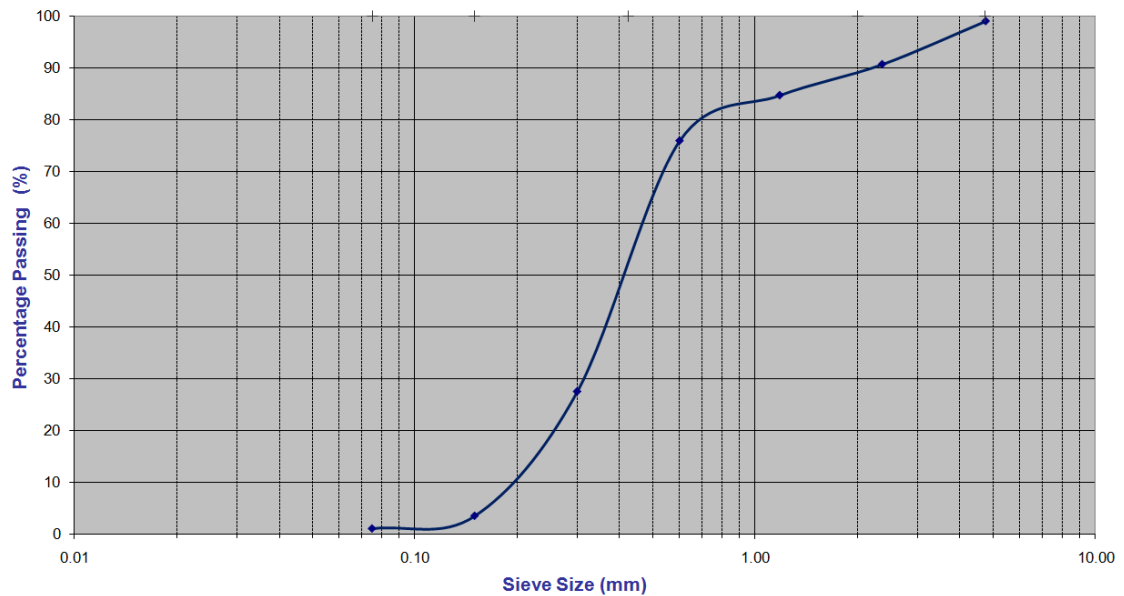


Figure 3.1 Sieve analysis of sand

### 3.2.7 Exposure solutions

Through the study, two different sulfate solutions based on (BRE DS3 and DS4) in addition to deionised water as a control solution were used. The solutions were made by diluting Magnesium sulfate ( $\text{MgSO}_4 \cdot 10\text{H}_2\text{O}$ ) in the deionised water. For Class 3 (DS3) sulfate 7.69 grams of  $\text{MgSO}_4 \cdot 10\text{H}_2\text{O}$  per litre which is equivalent to  $3\text{gm/l}$  of  $\text{SO}_4^{-2}$  and for Class 4 (DS4) sulfate 15.38 grams of  $\text{MgSO}_4 \cdot 10\text{H}_2\text{O}$  per litre which is equivalent to  $6\text{gm/l}$  of  $\text{SO}_4^{-2}$  (BRE SD1 2001). The volume of the solution to the mortar samples was 4:1 (Schmidt et al. 2009). The solutions are renewed every three months up to 6 months, after which, some samples showed severe deterioration and it was decided not to remove them from the solutions. The upper limit concentration of sulfate for BRE DS-3 and DS-4 were used in order to investigate the maximum damage caused by sulfates on concrete samples.

Magnesium sulfates were chosen for this study because it is far more aggressive to concrete than other sulfates since, in addition to attacking the aluminates, they attack and decalcify the CSH matrix, forming gypsum, brucite, and hydrous silica. This results in loss of strength and softening of the affected areas (Hooton and Thomas 2002).

### 3.3 Mortars Mixing and Casting

A series of mortar cubes ( $50 \times 50 \times 50 \text{ mm}$ ) and prisms ( $40 \times 40 \times 160 \text{ mm}$ ) were produced for 10 different mixes depending on cement type, water to cement ratio and binder replacement level. Table 3.3 shows the mixes proportions. Binder to sand ratio was kept at 1:2.5 for all mixes. . This mix was chosen to provide a mortar of low density, which would serve to reduce the time required for the testing. Each mix was cast in one batch, where cement and sand were first dry mixed for about one minute then the water was added gradually and mixed for another two minutes to achieve the desired consistency. Pre-oiled Metal moulds were used and mortars were casted into two layers on a vibrating table for good compaction. After casting, moulds were covered with polyethylene sheet and left in the lab for 24 hours before demolding.

**Table 3.3 Mortar Mixes and Materials**

Mix No.	Cement type	w/b	Mix proportion Kg/m <sup>3</sup>					
			CEM I	LF	PFA	GGBS	Water	Sand
Mix 1	100% CEM I	0.45	380	-	-	-	171	950
Mix 2	100% CEM I	0.55	380	-	-	-	209	950
Mix 3	100% CEM I	0.65	380	-	-	-	247	950
Mix 4	90%CEM I+10%LF	0.45	342	38	-	-	171	950
Mix 5	90%CEM I+10%LF	0.55	342	38	-	-	209	950
Mix 6	90%CEM I+10%LF	0.65	342	38	-	-	247	950
Mix 9	50%CEM I+50%PFA	0.55	190	-	190	-	209	950
Mix 10	50%CEM I+50%PFA	0.65	190	-	190	-	247	950
Mix 13	30%CEM I+70%GGBS	0.55	114	-	-	266	209	950
Mix 14	30%CEM I+70%GGBS	0.65	114	-	-	266	247	950

### **3.4 Curing:**

#### **3.4.1 Initial curing**

Specimens were kept in the laboratory at about 20°C for 24 hrs after casting; afterwards they were de-moulded and then placed in water at 20±2°C for 6 days before being moved out of water and cured in air at 20±2°C for 21 days. This regime was used to simulate field conditions (Tsvilis et al. 2003, Torres 2004). After these 28 days the samples were transferred to water and sulfates containers to expose to desired solutions.

#### **3.4.2 Long term exposure to sulfate environment**

According to the objectives of this research; the long term exposure programme was divided into three categories:

##### ***Category 1: Samples for studying the effect of wetting and drying cycles:***

These samples were first kept in solutions for 10 days and then were taken out of solutions to be dried for 20 days (1 month cycle). This cycle was repeated for one year. The time of drying cycle is longer because samples need more time to dry than wetting time (Neville 2002). The 5°C samples were kept in fridge at desired temperature, while the 20°C samples were kept over shelves in the laboratory.

##### ***Category 2: Samples for studying the effect of water to cement ratio and blended cement levels:***

These samples are kept in solutions all times in two temperatures 5 and 20°C some of these samples are also used as comparable samples with the wetting and drying samples.

***Category 3: Samples for studying the powder-sulfate interaction on thaumasite formation:***

These samples are made from grinding the mortar cubes after compressive strength test to produce powders passing from sieve size 212 $\mu$ m. The powder samples were placed in glass bottles and solutions were added to them with the same liquid to solid ratio as for the other samples (the cubes and prisms). 5°C samples were kept in fridge, and the 20°C samples were kept over shelves in the laboratory.

**3.5 Sampling and Testing:**

**3.5.1 pH Measures**

The pH of solutions in each individual container is being measured using appropriate pH measuring meter (Hanna HI8424) every two weeks starting from the day before moving samples to the containers for up to 60 days and then for every 28 days. The pH meter is calibrated regularly, and to avoid the contamination between solutions the electrode is washed and dried between uses.

**3.5.2 Visual observations**

Different views of every individual sample were taken using good camera immediately after demolding and before immersing in solutions in order to use them in the comparison process after attack takes place. These photos are taken in a designated photography box to achieve high resolution photos. Moreover, Visual observations of mortar samples in solutions are carried out regularly. Changes in samples such as colour, cracks, spalling off, deteriorated corners or edges, precipitation of any materials on top and sides of samples are recorded and a good quality digital camera in addition to digital mobile microscope with magnification factor of 400 is used to take photos. Figure 3.2 shows some samples of

CEMI+10% LF samples immersed in DS4 solutions after around 3 months.

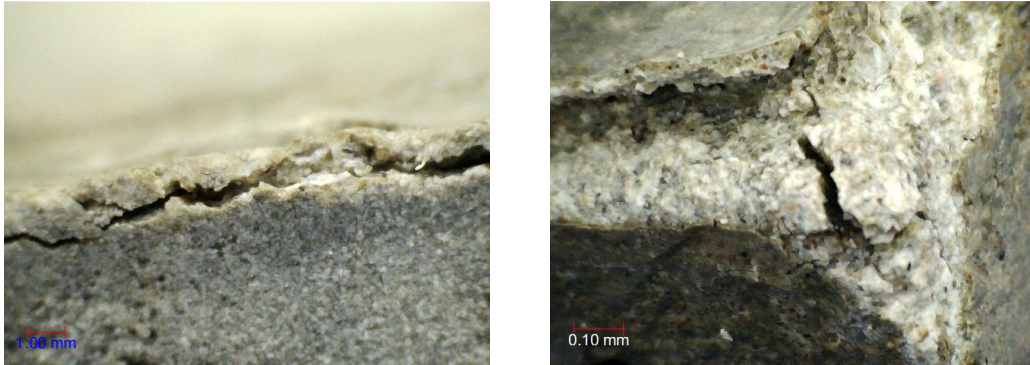


**Figure 3.2 Thaumasite started to form at edges of limestone cement samples in DS4 at 5 °C after 84 days**

#### **3.5.3 Length and mass change**

It is well known that thaumasite is causing loss of integrity of concretes and mortars by converting them to mushy materials (Crammond et al. 2003). Those can be easily separated from the sample core, and as one way of assessing the attack severity, change of weight of the samples was recorded to compare it with the initial (control) weight which has been already measured before and after placing the samples in the solutions. Length change measure of mortar prisms was performed according to BS 812-123:1999 it was carried out once a month, a stainless steel pre-inserted studs were used to measure the change in length in the prisms and compared with standard calibration bar Figure 3.3, this way is used as a quantifying measure with regard to conventional sulfate attack (ettringite). The mass change was determined with precision of 0.01g and the length change with precision of 0.001mm.



**Figure 3.3 Length change measurement**

#### **3.5.4 X-ray Diffraction (XRD)**

Samples for XRD were taken from mortars, and then they were air dried at room temperature to avoid any change in crystallization of deteriorated materials. After which they were ground using a mortar and pestle to pass a 63  $\mu\text{m}$  sieve. The powders obtained were kept in sealed jars in a fridge at about 5  $^{\circ}\text{C}$  before X-ray diffraction analysis. XRD analysis of these samples was carried out on a Phillips PW1830 XRD diffractometer using  $\text{CuK}\alpha$  radiation, 40 kV and 30  $\mu\text{A}$ . The analyses were run between 5 to 55 degrees  $2\theta$  at speed of  $2^{\circ}/\text{min}$  and step size of 0.02. And the results are analysed using Powder Diffraction Files (PDF) data base and WinX<sup>po</sup>e software to identify the crystalline phases. This test was carried out every three months for the powder samples and where the visual observations show significant changes in the surfaces of samples. To minimize the crystal orientation, the powders were back-filled in an aluminium holder. For powder samples, the solutions are filtered using filter paper and then they were left to dry at room

temperature for 24 hours, after that they were further ground to pass 63  $\mu\text{m}$  sieve and same procedure as above were followed.

#### **3.5.5 Fourier Transform Infrared Spectroscopy (FTIR)**

Thaumasite and ettringite are very similar in their microstructure (Barnett et al. 2002, Barnett et al. 2003, Zhou et al. 2006). In order to distinguish between the two the FTIR technique is used to follow XRD results to refer the deterioration either to thaumasite or ettringite. IR tests were run on same samples used for XRD.

Discs of 12 *mm* (diameter) were prepared by mixing 2 *mg* of the sample powder with 198 *mg* of potassium bromide (KBr) to produce homogenous mixture. The mixed powders were compressed in an appropriate die, under vacuum, for 1 minute at 1 *ton* and further 1 minute at 10 *tons*. Afterwards, the pressure is slowly released to avoid breaking the discs.

A Perkin-Elmer Spectrum 200 FTIR spectrometer chamber was used for scanning of samples. The scan was performed in the Mid-infrared (MIR) range of 7800-370  $\text{cm}^{-1}$ , and resolution of  $\pm 4 \text{ cm}^{-1}$ . Spectrum for Windows software suite was used to analyse the spectra.

#### **3.5.6 Scanning Electron Microscopy (SEM)**

Based on XRD and FTIR results, selected samples were chosen to be analysed by SEM technique. Deteriorated materials collected from samples then dried in desiccators at room temperature, and then they were mounted with cold epoxy resin under vacuum and left for 24 hours to harden. The samples then were de-moulded and manually ground using four different sand papers 200, 400, 800 and 1200. The samples were polished using diamond discs for up to 0.25 micron after which, they were immersed in acetone in an ultrasonic bath for 5 minutes to clean their surface. The samples then coated with carbon layer to enhance the EDX scan. The samples were analysed by taking

Backscattered Images BSI using Camscan Mk 2 SEM/Link (BSI/15kv). Selected points were analysed using Energy Dispersive Spectroscopy EDX (X-ray microanalysis) in order to identify elements available in each phase.

#### **3.5.7 Carbonation depth measurement**

The depth of carbonation layer was measured by using phenolphthalein test, where desired samples were broken to two halves and immediately spread with phenolphthalein solution on the surface.

#### **3.5.8 Thermodynamic modelling**

The use of thermodynamic modelling in cement hydration is a useful way to describe the equations and the relationship between the composition of the cement raw materials and the resulted reaction products based on thermodynamic equilibrium. A comprehensive database is essential for the thermodynamic modelling to produce reliable results.

A good example for the modelling in cement science is Bogue equations (around 90 years ago) for calculating the cement oxides based on a fully equilibrium system, this approach is still widely used with some modification (Matschei 2007).

Thermodynamic modelling is a flexible and easy way which allows fast changes of parameters and input data such as cement composition, temperature and the concentration of sulfate solutions to predict reaction products (Lothenbach et al. 2010).

Geochemical modelling software code GEMS (<http://gems.web.psi.ch>) was used for the thermodynamic calculations (Kulik et al. 2013, Wagner et al. 2012). It was equipped with PSI GEMS and CEMDATA14 database (Lothenbach et al. 2008).

It was assumed that the system is under full equilibrium conditions. The degree of reactivity of slag and fly ash was assumed to be 50% after few runs of different reactivity percentages showed no much difference in the resulted phase assemblage.

The simulation of sulfate attack in the thermodynamic calculations was performed by increasing the quantities of sulfate solutions to the hydrated cement. The model provides an easy and fast way to calculate the phase assemblage; however, it does not consider any kind of time scale or kinetics calculations. In a study by Lothenbach et al. (2010) found good agreement between results obtained from this approach and other predicted by transport modelling.

The compositions of used cements given in Table 3.1 (cement oxides) were used as an input data for the thermodynamic modelling calculations in addition to water and  $\text{MgSO}_4$  solutions.

The stable phases (volumes) in the system were plotted as a function of the ratio of Magnesium sulfate  $\text{MgSO}_4$  solution to the volume of hydrated cement. The obtained results were compared with the experimental results.

# 4

## Effect of wetting and drying cycles

### 4.1 Introduction

This chapter presents the results of studying of the effect of wetting and drying cycles on the formation of thaumasite for four different cements (CEM I, 90% CEM I+10%LF, 50% CEM I +50%PFA and 30% CEM I + 70%GGBS) at different temperatures and different sulfate concentration solutions. The mixing and samples preparation are explained in details in Chapter 3 together with testing programme. Table 4.1 shows the codes for these cements. The results reported for 24 months exposure unless otherwise stated.

**Table 4.1 Coding system for used cements**

Cement used	Codes
100% CEM I	CEMI
90% CEM I + 10% Limestone filler	LFC
50% CEM I + 50% Fly Ash	FAC
30% CEM I + 70% GGBS	SLC

## **4.2 Visual observation assessment**

Samples were regularly examined in order to monitor any visible signs of deterioration such as discolouration, cracks, spalling and expansion or other kinds of damage.

Figure 4.1 and 4.2 show the appearance of the different samples after 24 months of exposure to DS3 and DS4 solutions respectively at 5°C. The first signs of deterioration were observed after around 84 days, when the continuously immersed LFC samples exposed to DS4 sulfate solutions started to show some cracking around the corners and along the edges. These cracks soon expanded and became filled with white soft materials.

CEMI samples immersed in DS4 started to deteriorate after about 100 days of exposure, while PFA and GGBS blended cement showed no signs of deterioration at this time. With the passage of time the severity of the attack become more and the attacked samples started to lose their integrity and become mushy, outer layers started to spall off and deposit in the container and it was easy to detach deteriorated materials from the surface of the samples.

As it can be seen in Figure 4.1, samples containing limestone filler showed more deterioration compared to samples with plain cement and those of PFA and GGBS blended cements.

The samples that were subjected to wetting and drying showed no signs of deterioration until around 250 days, where, again the Limestone samples exposed to DS4 sulfate solutions started to show the same signs of attack as described for continuous immersion. The blended PFA and GGBS cements again showed no signs of attack at this stage and remained intact.

#### 4. Effect of wetting and drying cycles on thaumasite formation

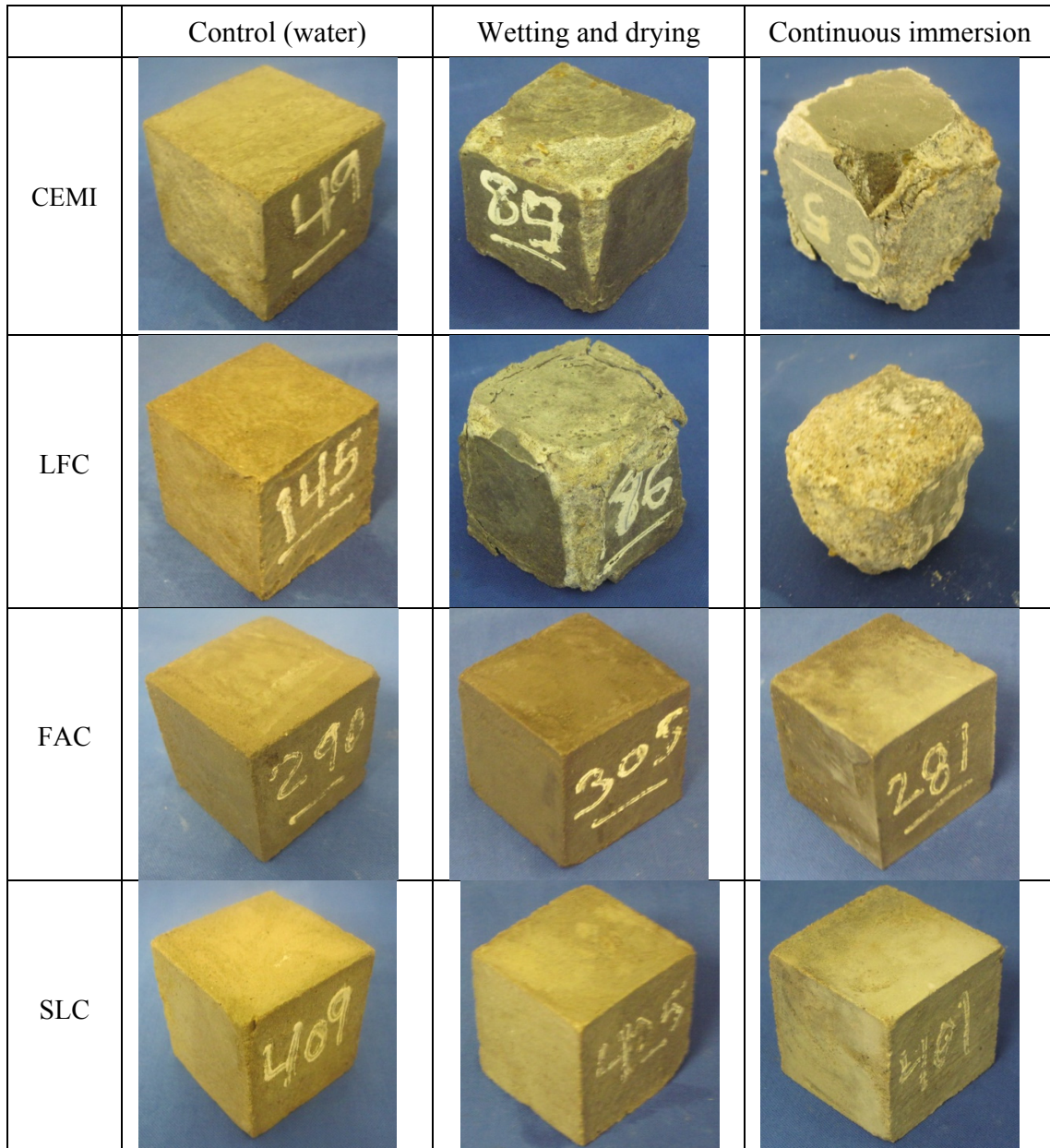


**Figure 4.1 Mortar cubes in DS4 sulfate solution at 5 °C after 24 months.**

As shown in Figure 4.2 exposure to DS3 experienced the same patterns of deterioration as for DS4 for all cement types and solutions but in longer periods of time - and attack was less severe.

4. Effect of wetting and drying cycles on thaumasite formation

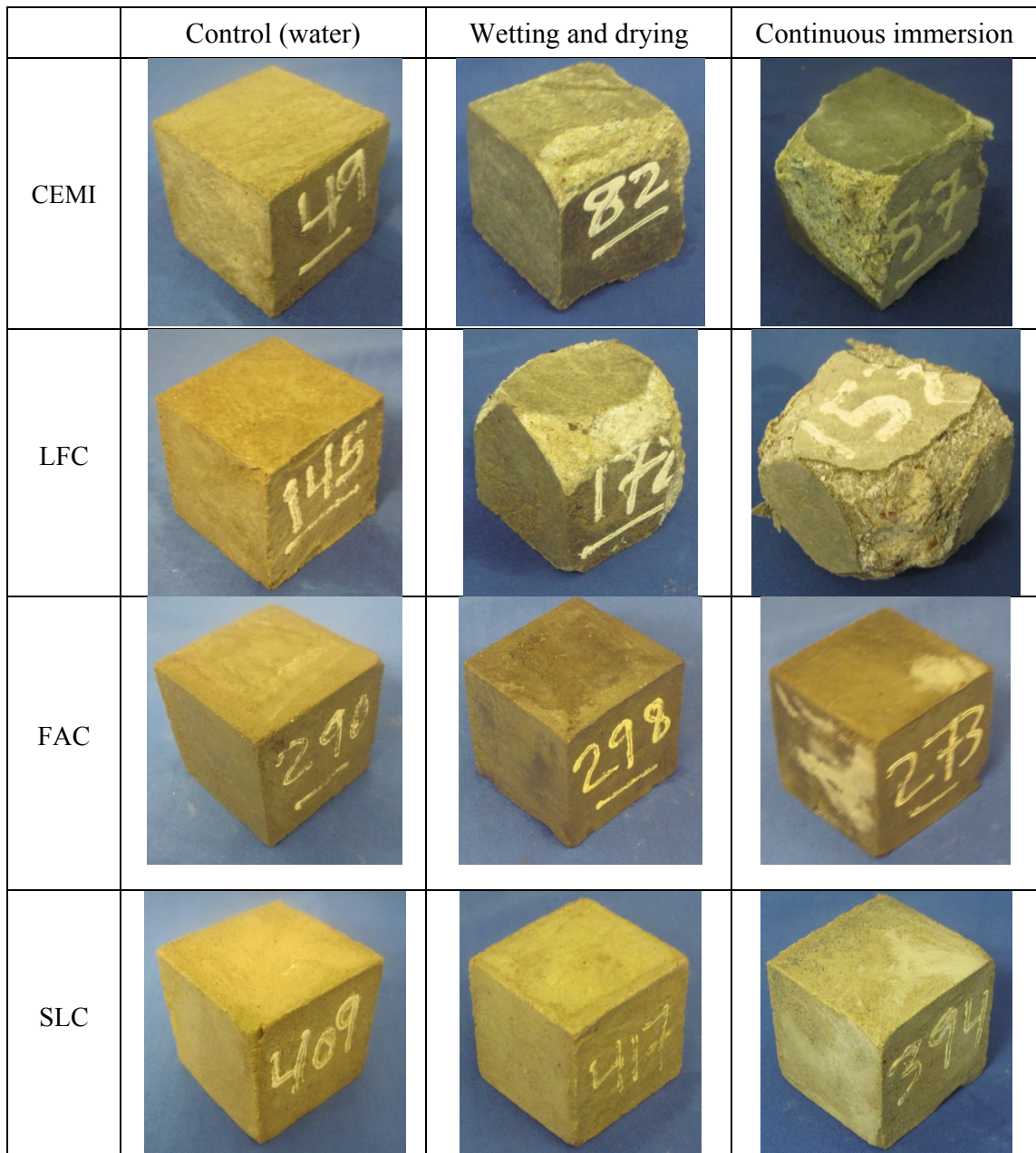


Figure 4.2 Mortar cubes in DS3 sulfate solution at 5 °C after 24 months.

It is worth mentioning here that the outer layer of the specimens on the faces of the cubes did not exhibit attack and remained intact with the deterioration was occurring a few *mm*s beneath, as shown in Figure 4.3.



**Figure 4.3 The outer layer of specimens is un-attacked with the deterioration is progressing underneath it.**

At 20°C, as can be seen in Figure 4.4, all samples of different cement types performed well and remain intact after 2 years of immersion in DS3 sulfate solutions under wetting and drying cycles. However CEMI samples started to show cracks alongside the edges filled with white substances indicating thaumasite type of sulfate attack as it was confirmed by XRD and FTIR test. The other three cements performed well under continuous immersion in sulfate solutions of class 3 (DS3) and no signs of deterioration were detectable.

Samples exposed to DS4 solutions are illustrated in Figure 4.5 where it can be seen that only continuously immersed CEM I and LFC samples suffered deterioration.

This was more serious for the CEM I samples which started to lose their integrity and became spalled, while LFC samples displayed only minor cracking along edges and without any spalling. Samples made from FLC and SLC cement showed no signs of attack, which was the case in all samples that underwent cyclic wetting and drying in this solution.

4. Effect of wetting and drying cycles on thaumasite formation

	Control (water)	Wetting and drying	Continuous immersion
CEMI			
LFC			
FAC			
SLC			

Figure 4.4 Mortar cubes in DS3 sulfate solution at 20 °C after 24 months.

4. Effect of wetting and drying cycles on thaumasite formation

	Control (water)	Wetting and drying	Continuous immersion
CEMI			
LFC			
FAC			
SLC			

Figure 4.5 Mortar cubes in DS4 sulfate solution at 20 °C after 24 months.

### 4.3 Patterns of attack

Almost all deteriorated samples showed the same patterns of attack. As Figure 4.6 shows this started as a fine crack along the edges and around the corners of the cube, which then became filled with white materials. The attack then progressed under the outer surface layer which resulted in it becoming detached from the sample. At this stage the specimen would start to lose its integrity and become mushy and friable.

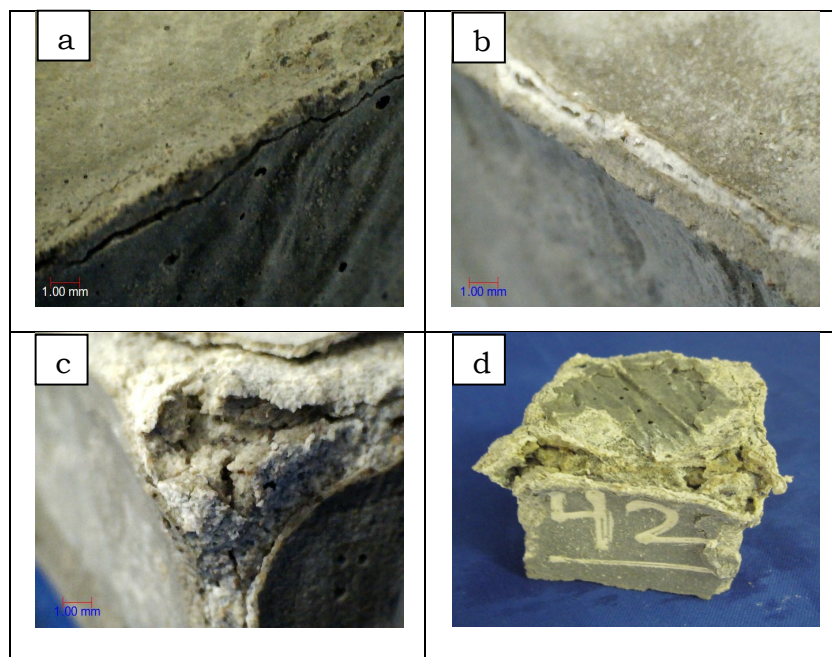


**Figure 4.6 Deterioration Patterns a) cracks started to appear around the edges, b) cracks then filled with white substance (thaumasite), c) Spall off the corners and edges, d) deterioration of the sample**

### 4.4 Mass Changes

The change in mass of the cubes was determined at intervals throughout the tests and the results for the various mixes are shown in Figure 4.7 to Figure 4.14 .

#### 4. Effect of wetting and drying cycles on thaumasite formation

It can be observed in Figures 4.7 and 4.8 that during the first 200 days at 5 °C, all samples showed slight increases in their mass that is apparently due to uptake of solutions and formation of hydration products which fills the voids and pores. It seems that weight gain increased after the samples started to show evidence of deterioration and the opening of the cracks allowed more solution to enter the unaltered mortar and cause expansion. At a later stage of deterioration loss of mass was observed as material was lost as a consequence of spalling. Samples made with FLC and SLC continued gradually to gain mass and ended up with an increase of their mass of about 1.5% in both sulfate solutions. Samples made with both CEMI and LFC showed significant mass loss at the end of the exposure.

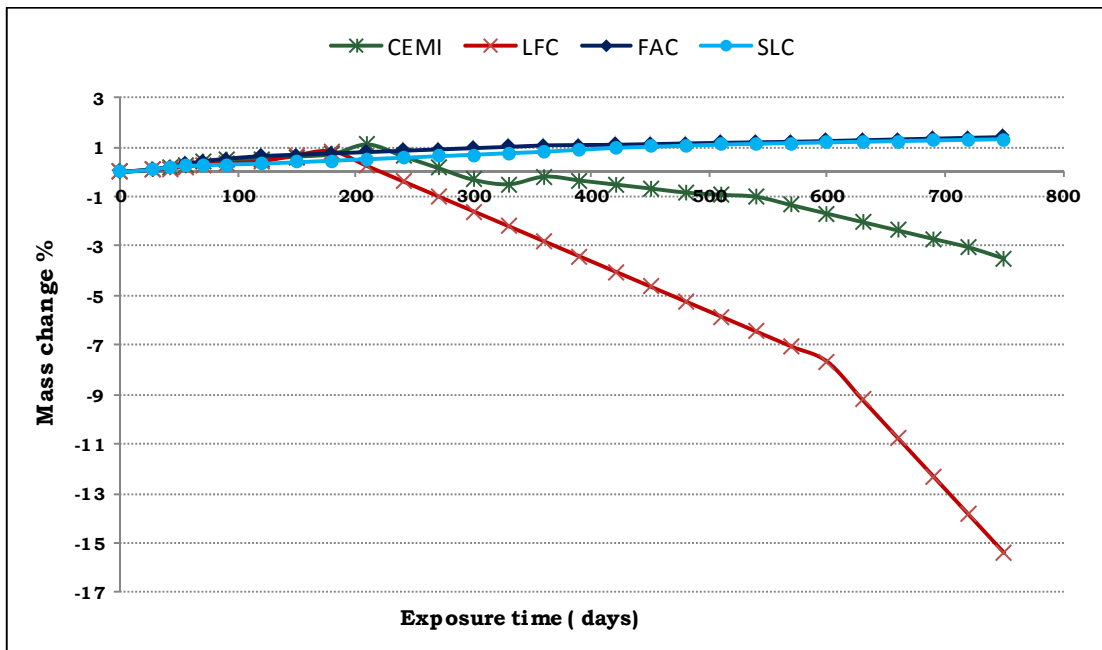


**Figure 4.7 Mass change for samples in DS3 solution at 5C. (continuous immersion)**

The LFC samples showed higher mass loss than the CEMI samples which lost about 15 and 26 % of their mass in DS3 and DS4 solutions,

#### 4. Effect of wetting and drying cycles on thaumasite formation

respectively. Samples made with plain CEMI lost between about 3 and 9% of their original mass in same sulfate solutions.

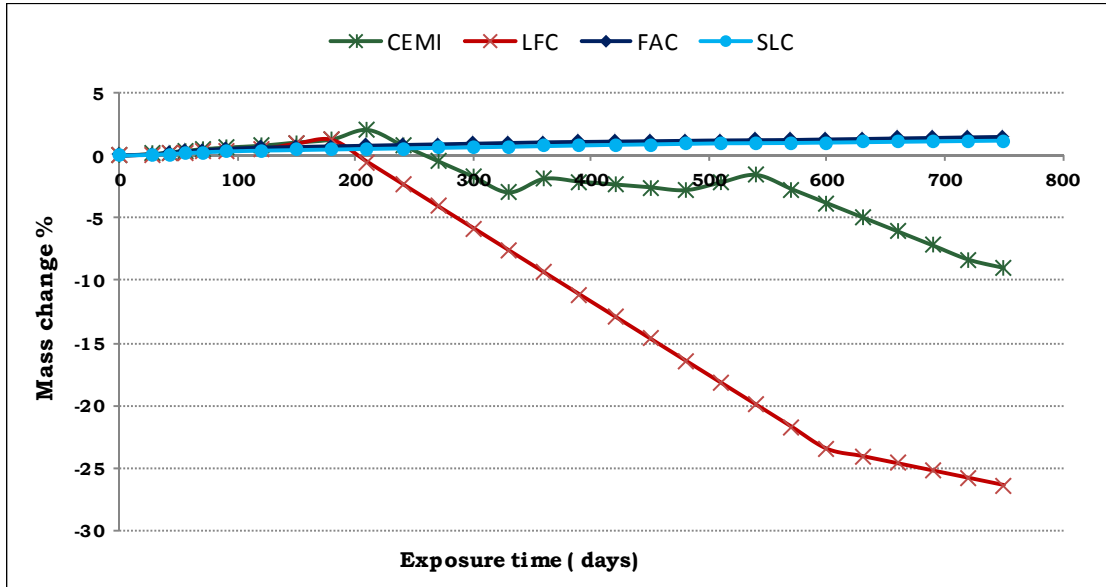


**Figure 4.8 Mass change for samples in DS4 solution at 5 °C (continuous immersion)**

At 20 °C, all samples showed gradual increase in mass in both sulfate solutions, as Figure 4.9 and Figure 4.10 show. Apart from CEMI samples, which started to show cracks in the samples immersed in DS3, the samples did not display visible deterioration. The cracking of CEMI samples in DS3 solution seen in Figure 4.4 did not result in mass loss at this stage, whereas CEMI samples immersed in DS4 suffered a slight mass loss but this was not significant and in fact it was much smaller than the gain during their exposure. Although LFC samples in DS4 solution suffered minor cracking, they did not experience any mass loss. Throughout the tests SLC samples exposed to DS3 solutions showed the highest mass gain of about 1.1 % while CEMI samples showed the smallest, with less than 0.8 %.

#### 4. Effect of wetting and drying cycles on thaumasite formation

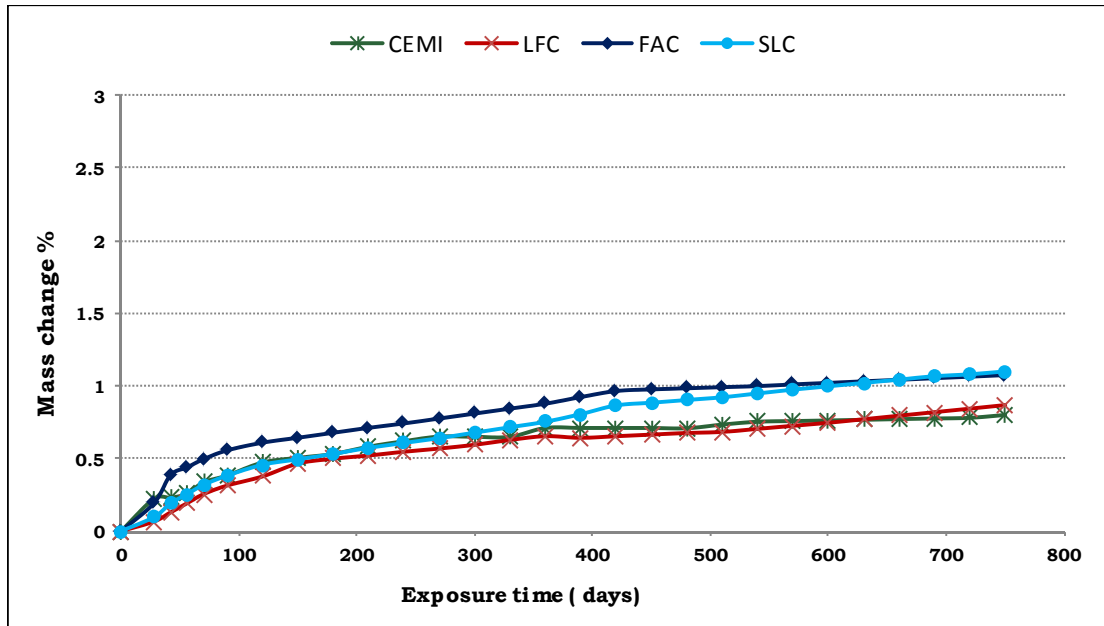


Figure 4.9 Mass change for samples in DS3 solution at 20 °C. (continuous immersion)

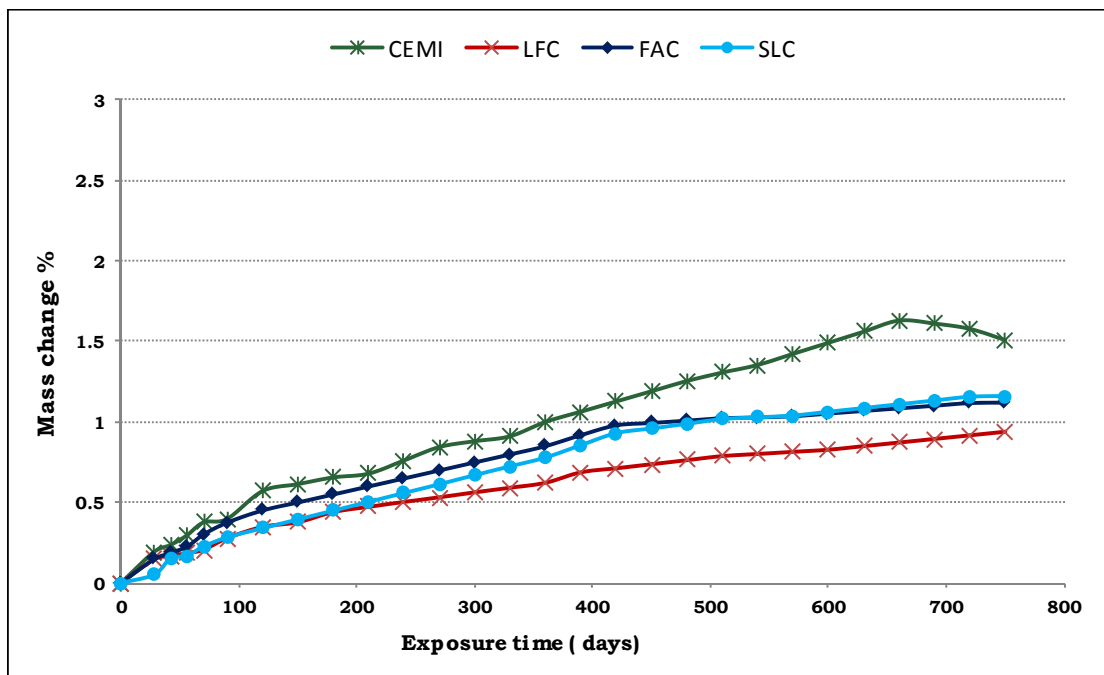


Figure 4.10 Mass change for samples in DS4 solution at 20 °C. (Continuous immersion)

#### 4. Effect of wetting and drying cycles on thaumasite formation

For the samples exposed to DS4 solutions, CEMI showed the highest mass gain at more than 1.6 % before some loss of mass and resulted in an overall increase of around 1.5 % of their original mass. LFC samples showed increase in mass very similar to samples in DS3 solutions with gain of mass of around 1.1%.

Cyclic wetting and drying caused a slightly different pattern of mass change as presented in Figure 4.11 to Figure 4.14. As it can be seen, the trend for all samples is a similar gradual mass gain during the exposure time. FAC samples showed the highest variation in mass change due to the different in the moisture content as a result of wetting and drying cycles, while the SLC samples showed the lowest change.

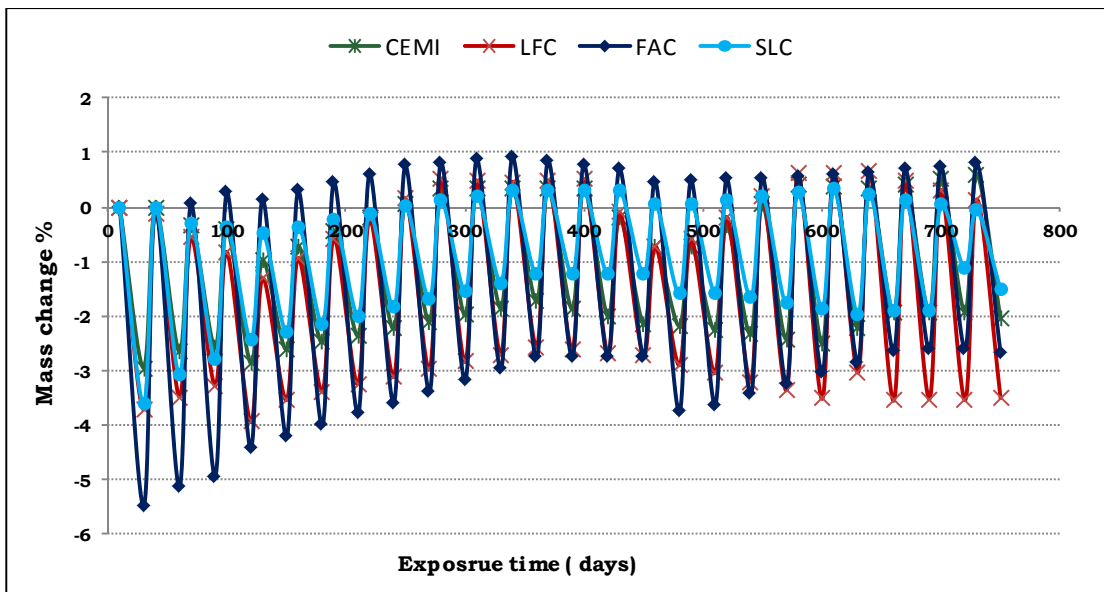


Figure 4.11 Mass change for samples in DS3 solution at 5 °C. (Wetting & drying)

For samples CEMI and LFC at 5 °C, the latter showed the greatest mass loss of 3.5 and 6.0 % in DS3 and DS4 respectively. CEMI samples lost around 1.6 and 2.5% respectively in the same solutions.

#### 4. Effect of wetting and drying cycles on thaumasite formation

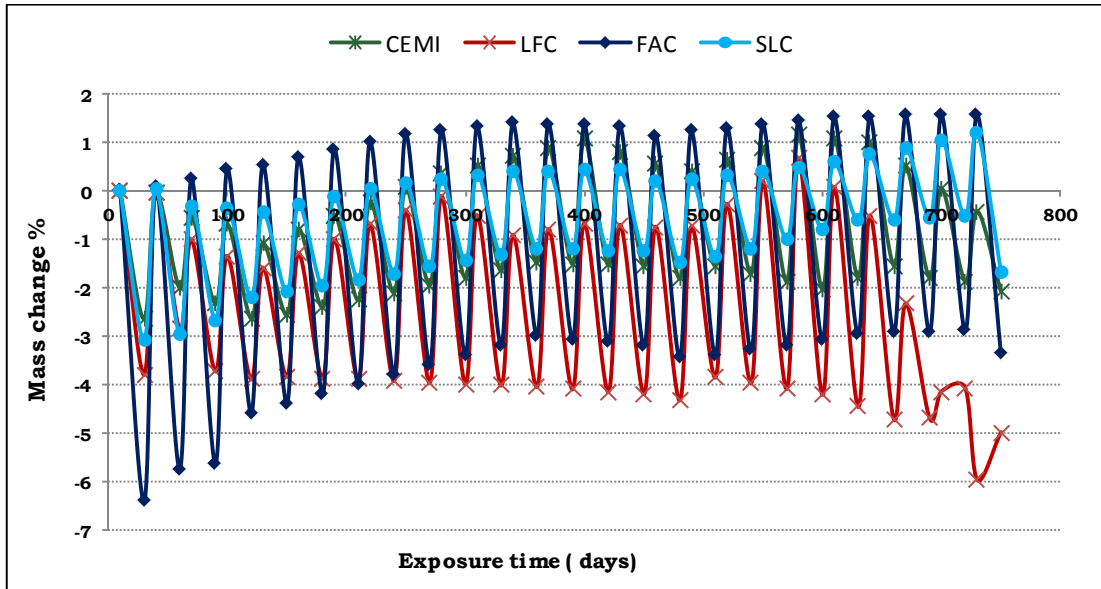


Figure 4.12 Mass change for samples in DS4 solution at 5 °C. (Wetting & drying)

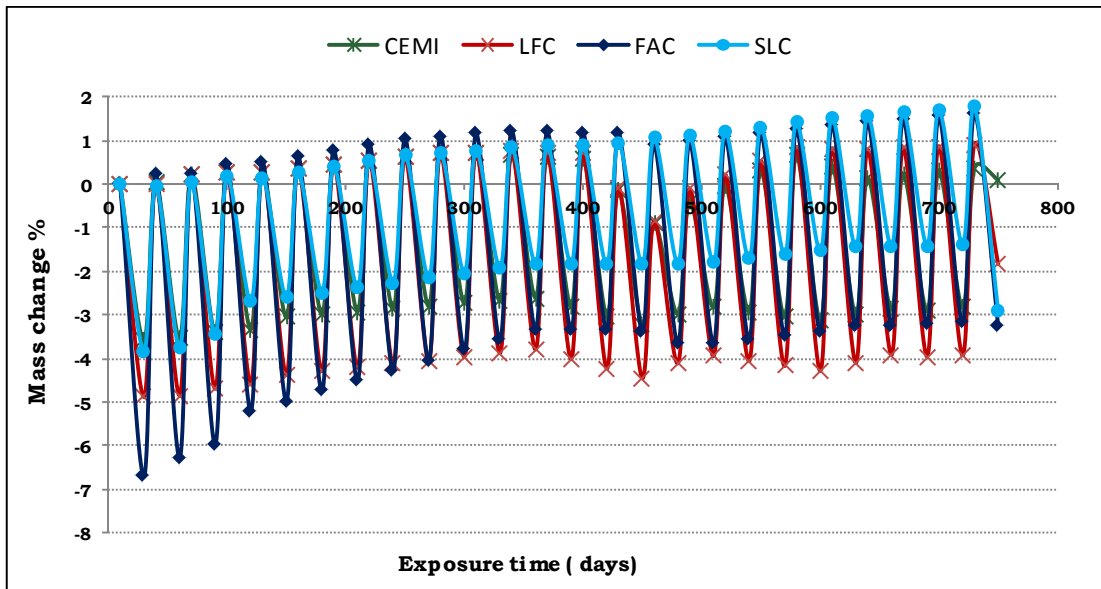


Figure 4.13 Mass change for samples in DS3 solution at 20 °C. (Wetting & drying)

#### 4. Effect of wetting and drying cycles on thaumasite formation

As was noticed with continuous immersion; the severity of the attack and hence the mass loss increased with the presence of limestone filler, for higher sulfate concentration and lower temperature. The trends for the samples kept at 20 °C in wetting and drying curing regime were similar to those observed for continuous immersion at same temperature, where again here FAC cements showed the highest variation in mass due change in moisture content.

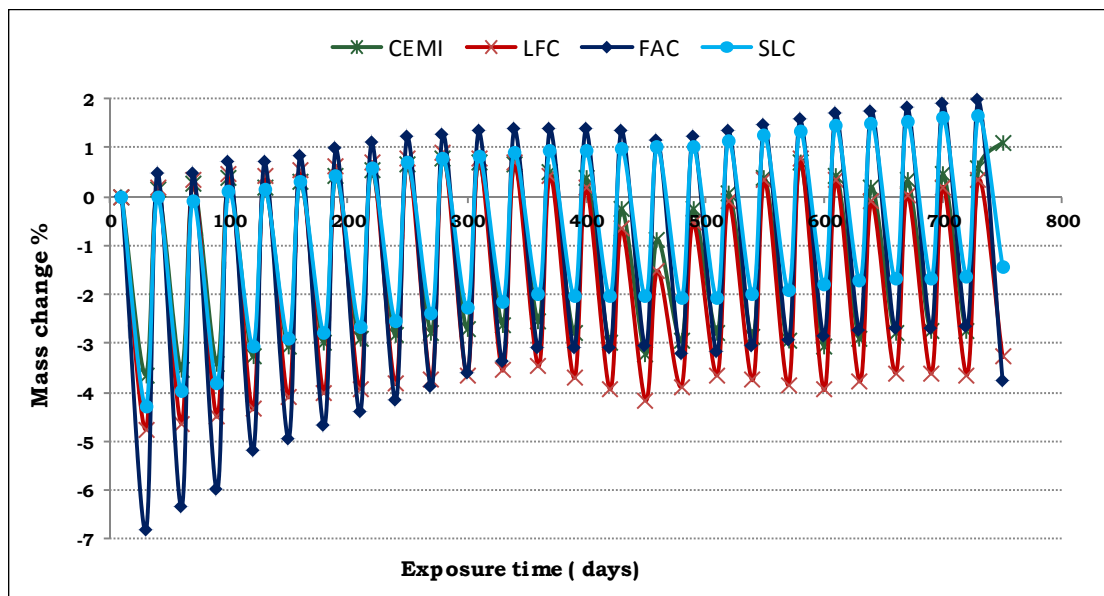


Figure 4.14 Mass change for samples in DS4 solution at 20 °C. (Wetting & drying)

The visual observation and the mass change performances of these cements are summarised in Table 4.2 in order of decreasing vulnerability to attack. Only samples that suffered some signs of deterioration are included in this list. As the table shows, samples that continuously immersed in sulfate solutions have suffered more deterioration compared to samples exposed to wetting and drying cycles. In each exposure regime it can be clearly seen that samples made with LFC and kept at 5 °C and DS4 were the least to resist the attack, followed with samples

#### 4. Effect of wetting and drying cycles on thaumasite formation

---

exposed to DS3 from same cement and then CEMI samples. Continuous immersion samples stored in sulfate solutions at 20 °C performed better than samples exposed to frequent wetting and drying cycles at 5 °C.

**Table 4.2 Summary of the degree of deterioration based on visual observation and mass loss**

order	Cement type	Exposure condition	solution	temperature
1	LFC	Continuous immersion	DS4	5 °C
2	LFC	Continuous immersion	DS3	5 °C
3	CEMI	Continuous immersion	DS4	5 °C
4	CEMI	Continuous immersion	DS3	5 °C
5	LFC	Wetting and drying cycles	DS4	5 °C
6	LFC	Wetting and drying cycles	DS3	5 °C
7	CEMI	Wetting and drying cycles	DS4	5 °C
8	CEMI	Wetting and drying cycles	DS3	5 °C
9	CEMI	Continuous immersion	DS4	20 °C
10	CEMI	Continuous immersion	DS3	20 °C
11	LFC	Continuous immersion	DS4	20 °C

#### 4.5 Length Change

The length of all samples was measured and the change in length was plotted against time of exposure. Samples kept in water showed that the change in length in all samples was well below the standards (ASTM C1012: 2010) which sets a limit of 0.1 %. The results for these samples are presented in Appendix A.

Figure 4.15 and Figure 4.16 show the change in length for samples exposed to DS3 and DS4 respectively at 5 °C. As it was observed for the continuous immersion samples the change in length in both exposure solutions was proportional to the visually observed deterioration rate

#### 4. Effect of wetting and drying cycles on thaumasite formation

where, LFC samples showed the greatest expansion followed by CEMI, while FLC and SLC blended cements showed no expansion at all, but instead underwent a little shrinkage. Length change values were higher for samples kept in DS4 than those in DS3 solution.

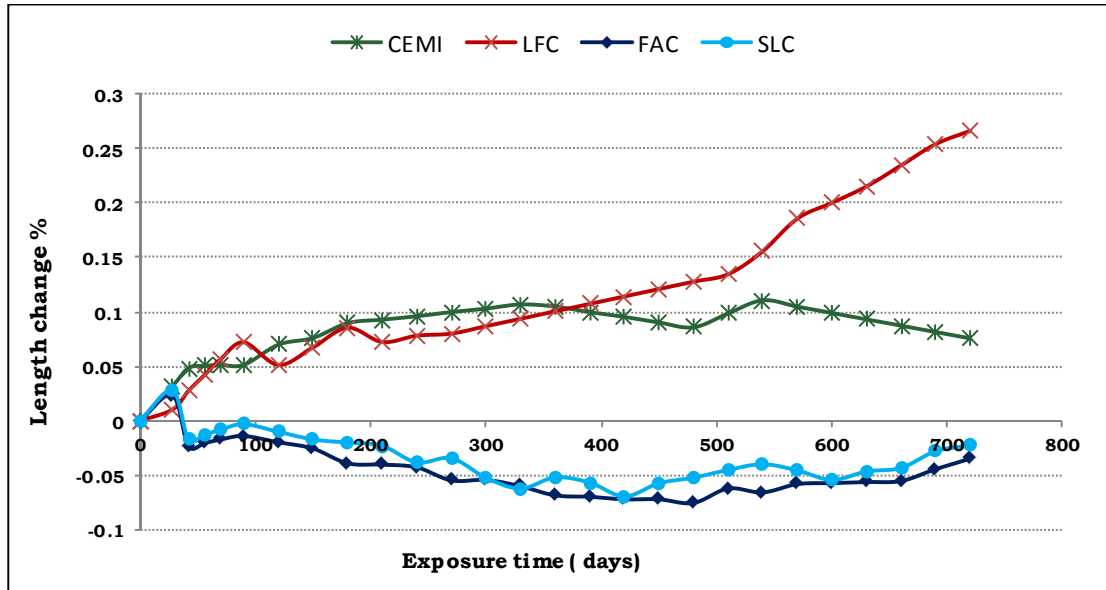


**Figure 4.15 Length change for samples in DS3 solution at 5 °C. (Continuous immersion)**

Looking to these graphs it can be noticed that once samples became cracked, no significant change in length occurred – any change and was below the 0.1% limit.

#### 4. Effect of wetting and drying cycles on thaumasite formation

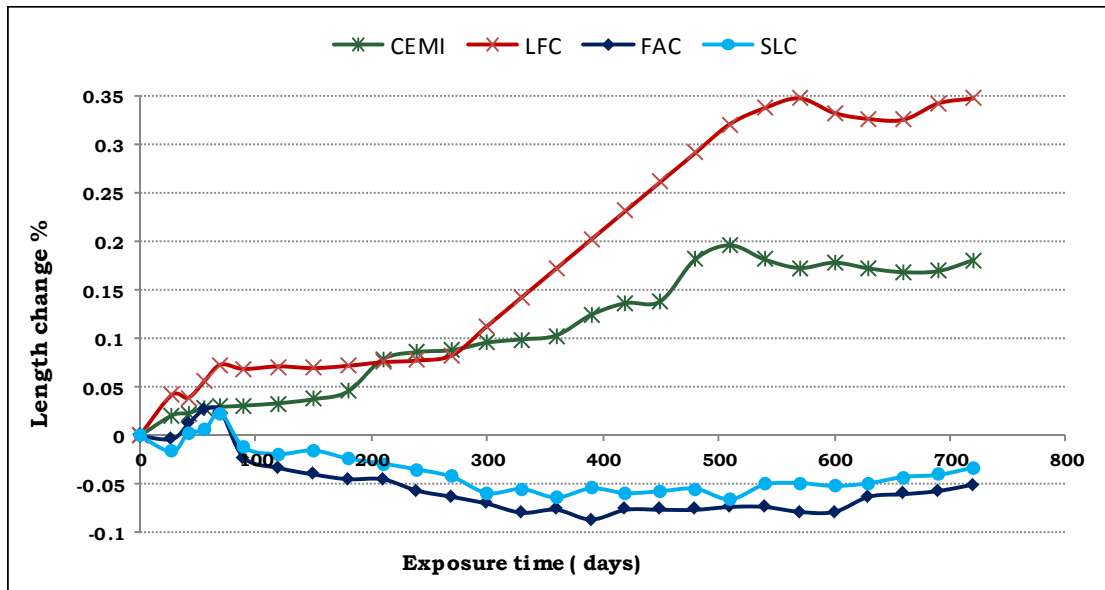


**Figure 4.16 Length change for samples in DS4 solution at 5 °C. (Continuous immersion)**

On the other hand severe attack resulted in significant expansion. LFC showed final expansion values of 0.26% and 0.35% in DS3 and DS4 respectively while CEM I showed 0.08% and 0.18 % in the same solutions. It can be also seen that the FLC and SLC cements performed in a similar way in both sulfate solutions.

Data for 20 °C are presented in Figure 4.17 Figure 4.18 which show that CEMI samples expanded the most, whereas the other three binders showed no expansion. This demonstrates the superior performance at higher temperatures of blended cements over plain cement (CEMI) in resisting classical sulfate attack. Similar trends were observed for samples exposed to DS4 with higher expansion values. Indeed, the observed expansion values were higher at DS4 than at DS3 and they were higher at 5 °C than at 20 °C.

#### 4. Effect of wetting and drying cycles on thaumasite formation

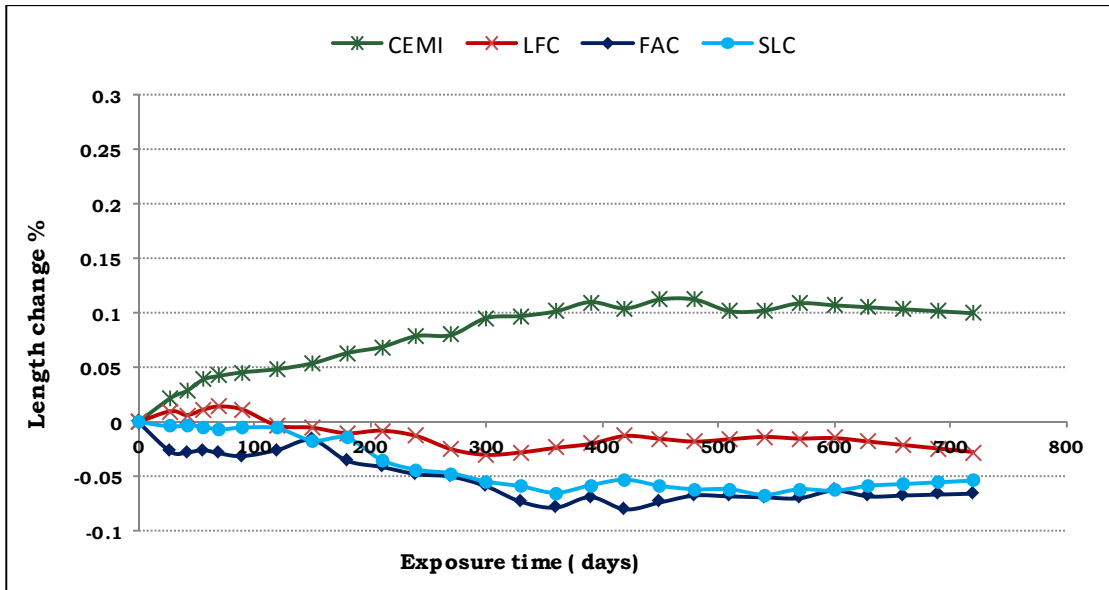


Figure 4.17 Length change for samples in DS3 solution at 20 °C. (Continuous immersion)

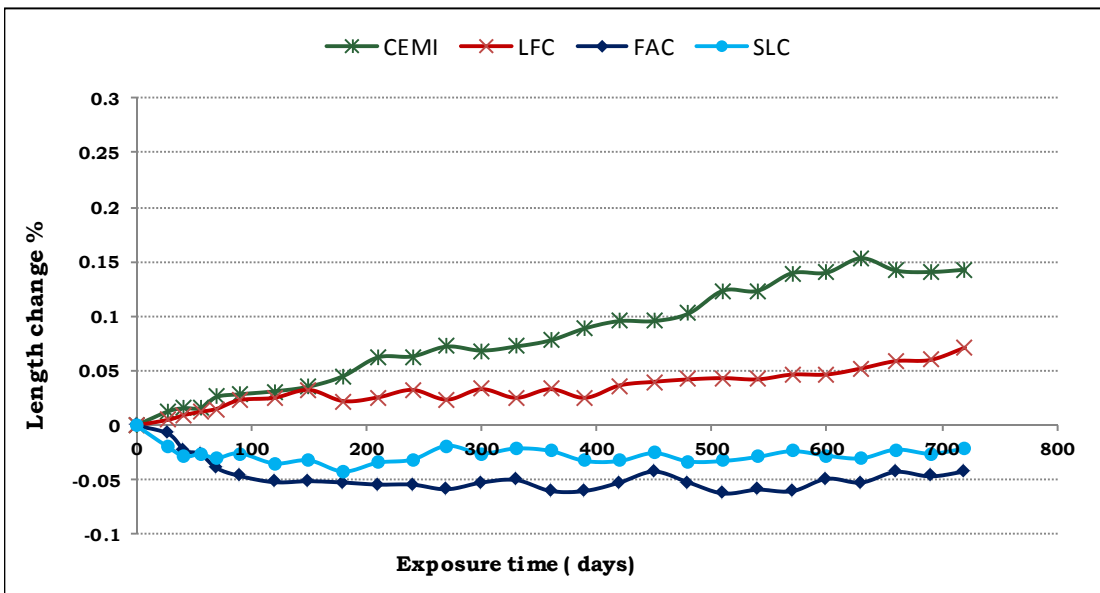


Figure 4.18 Length change for samples in DS4 solution at 20 °C. (Continuous immersion)

#### 4. Effect of wetting and drying cycles on thaumasite formation

Cyclic wetting and drying caused a smaller change in length than continuous immersion. Figure 4.19 to Figure 4.22 show the results of mass change measurements for wetting and drying samples in different solutions and temperatures. LFC samples showed the highest expansion values of about 0.1% and 0.13% in DS3 and DS4 correspondingly, while 0.06% and 0.09% were recorded for CEM I samples in the same solutions. It was noted that despite the formation of the thaumasite and mass loss in these samples, the corresponding over-all length change was not significant with expansion values well below the standard limit of 0.1%. Only LFC samples, after 600 days of exposure expanded more than this. As these graphs show that the cyclic wetting and drying caused a very obvious change in length in the LFC samples compared to CEMI samples.

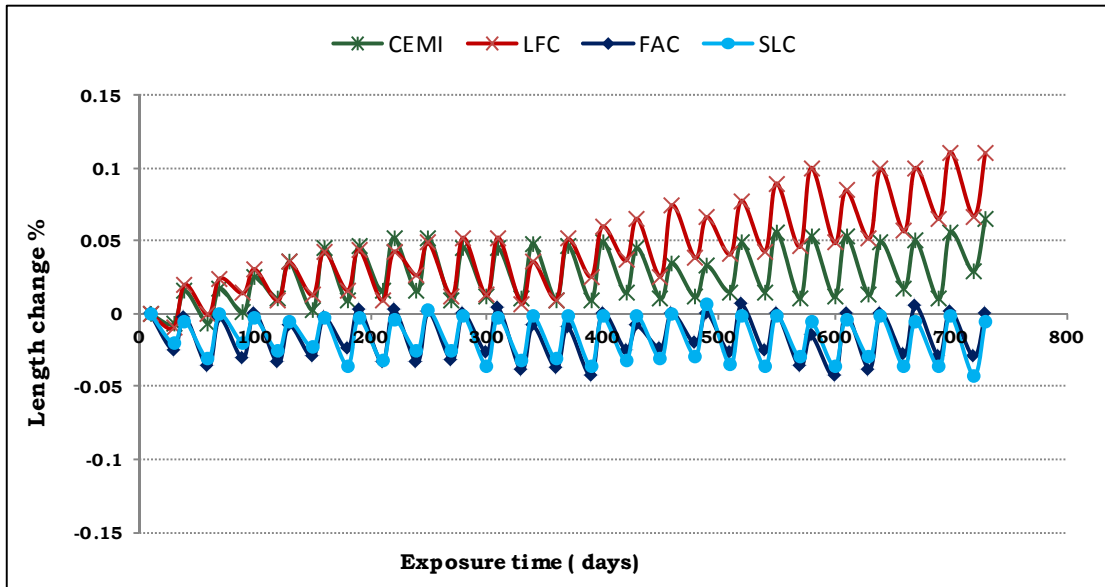
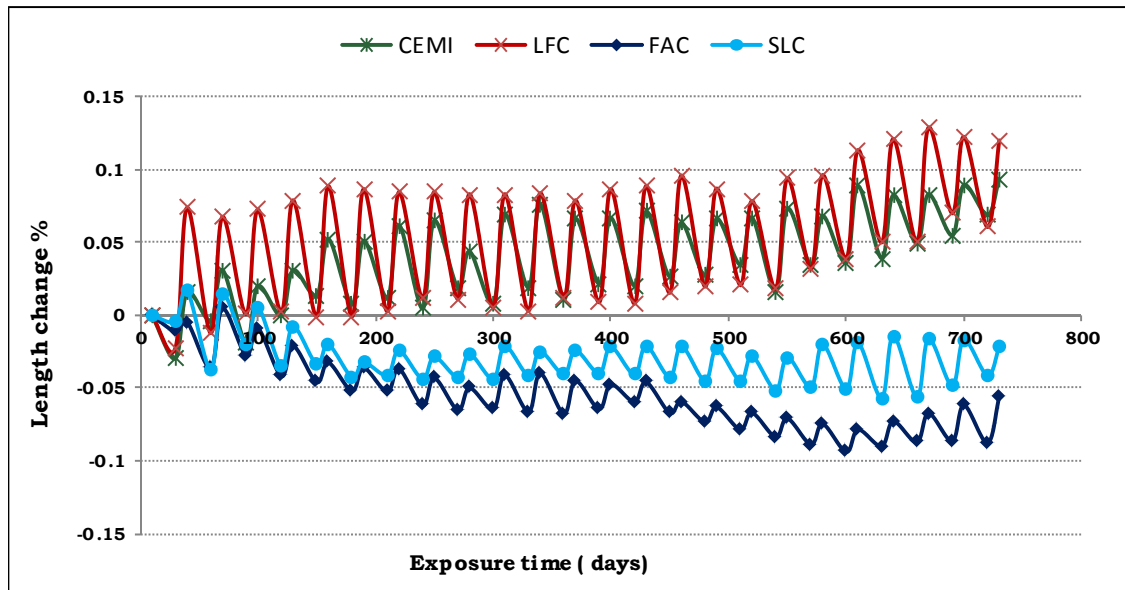


Figure 4.19 Length change for samples in DS3 solution at 5 °C. (Wetting & drying)

#### 4. Effect of wetting and drying cycles on thaumasite formation



**Figure 4.20 Length change for samples in DS4 solution at 5 °C. (Wetting & drying)**

The FAC and SLC blended cements did not show any expansion after 24 months of exposure in either sulfate solution.

None of the samples exposed to sulfate solutions and wetting and drying cycles at 20 °C showed any signs of attack. Accordingly, none of these samples showed change in length but CEM I samples did show slight expansion in both sulfate solutions, which suggests that CEMI samples may be the first samples to show evidence of attack.

#### 4. Effect of wetting and drying cycles on thaumasite formation

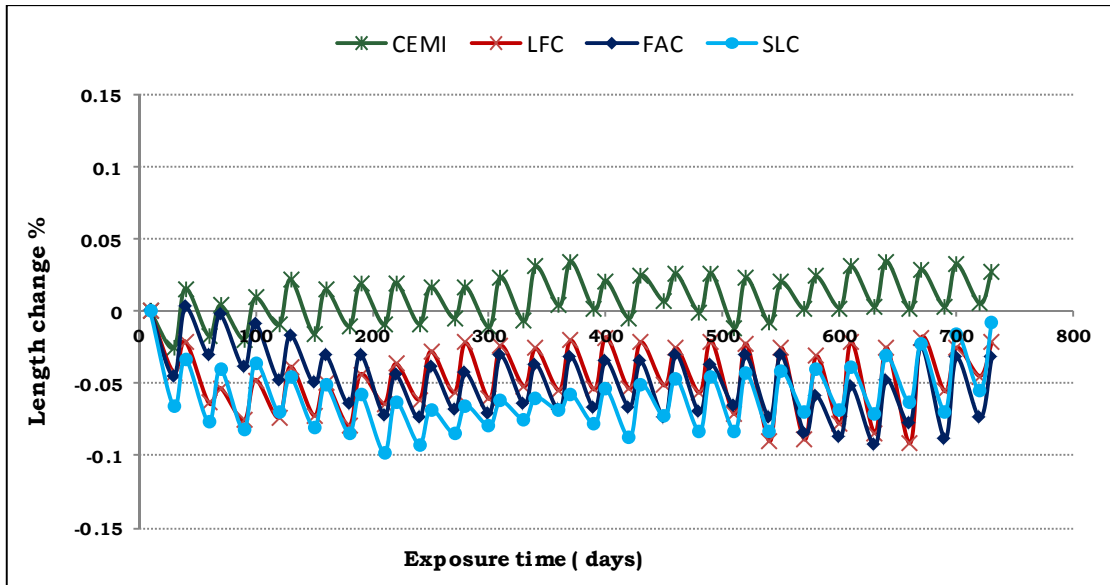


Figure 4.21 Length change for samples in DS3 solution at 20 °C. (Wetting & drying)

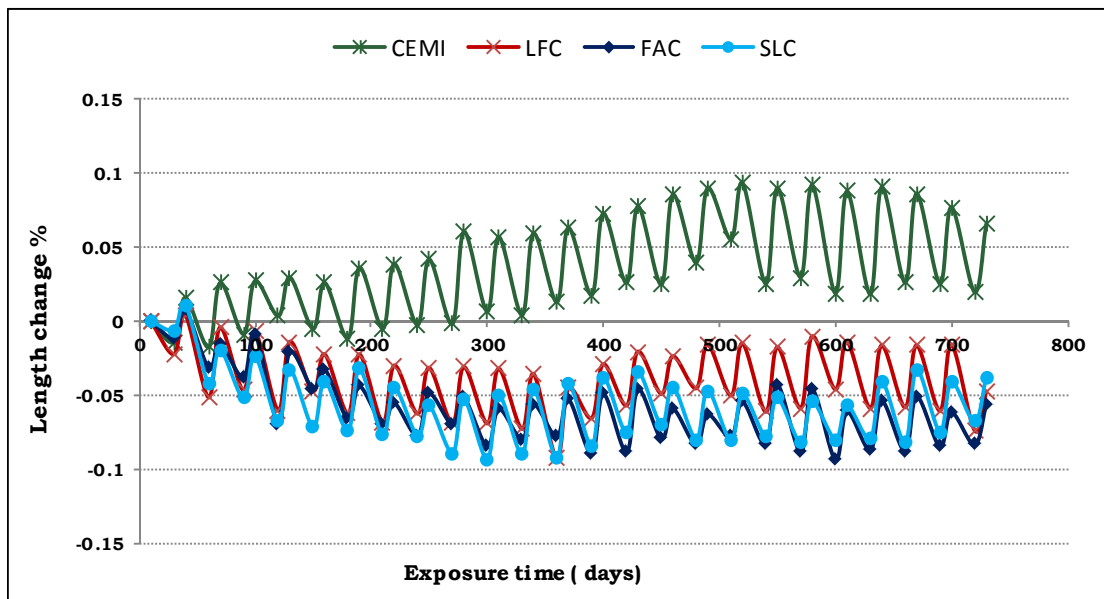


Figure 4.22 Length change for samples in DS4 solution at 20 °C. (Wetting & drying)

#### **4.6 X-Ray Diffraction**

The results presented in this section are for the deteriorated products collected from damaged samples after 24 months of exposure. In cases where samples did not show any cracks or signs of deterioration, fractured pieces (about 1 *mm* thick) were taken from the surface of the samples and then dried, ground and analysed. All the results are summarised in Table 4.3. Figure 4.23 and Figure 4.24 show the different X-ray patterns for samples immersed in DS3 at 5 °C continuously and under wetting and drying cycles respectively. As these indicate, the mineralogical compositions are similar for all binders.

The intensive peaks observed at  $2\theta$  of (9.2, 16, 23.5 and 28) are attributed to thaumasite, ettringite has very similar peaks at (9.08 and 15.8  $2\theta$ ) as their crystal structures are very similar and it is not easy to distinguish between them. However these peaks are stronger in case of samples immersed continuously in sulfate solutions compared to those observed in samples subjected to wetting and drying cycles indicating more thaumasite/thaumasite ettringite solid solution formation in the former samples and reflecting the higher damage rate as observed visually.

#### 4. Effect of wetting and drying cycles on thaumasite formation

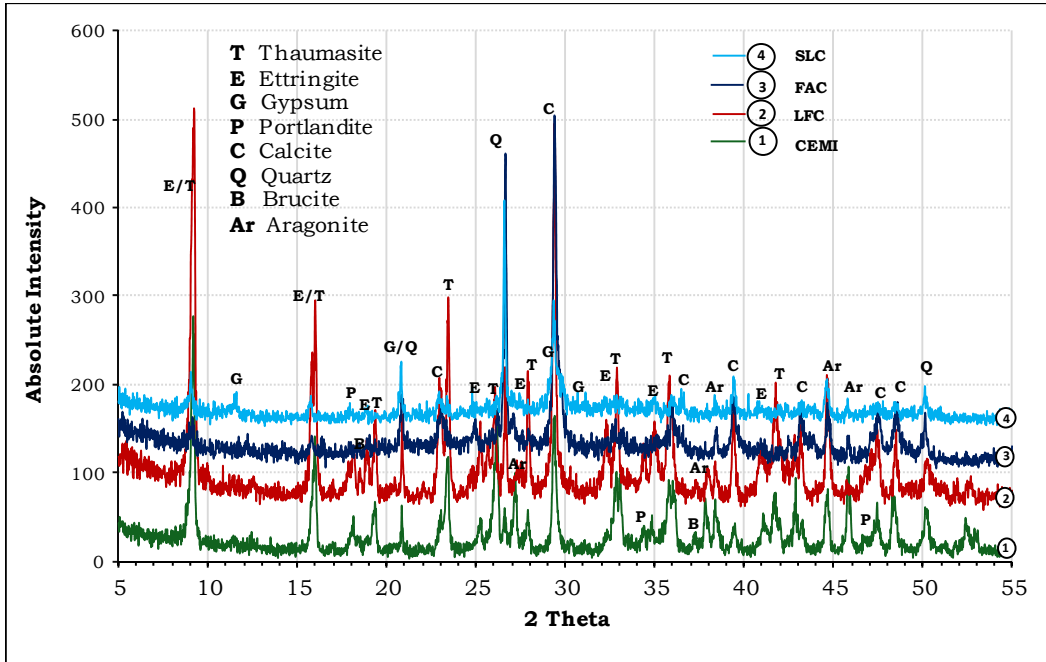


Figure 4.23 XRD patterns for samples in DS3 solutions at 5 °C (continuous immersion)

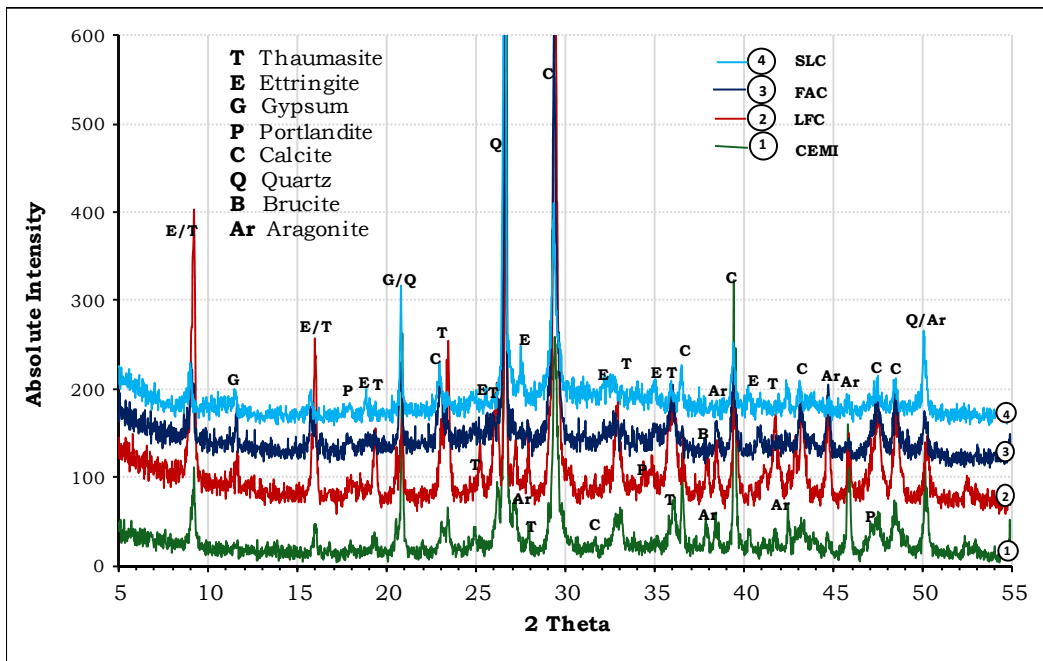


Figure 4.24 XRD patterns for samples in DS3 solutions at 5 °C (continuous immersion)

#### 4. Effect of wetting and drying cycles on thaumasite formation

---

Peaks assigned to gypsum at (11.59 2 $\theta$ ) were very small and they were absent from all samples but SLC samples in the continuous immersion regime, however, they were more obvious in samples subjected to wetting and drying cycles and again they were absent from CEMI samples. Interestingly, comparing these XRD results with those at 12 months age in Figure 4.25, the intense gypsum peaks in both samples at that time can be clearly seen, which may indicate that gypsum was formed earlier in these samples and then served as a source of sulfate to form more thaumasite. The relatively weak portlandite peaks at (18.11 2 $\theta$ ), especially in the wetting and drying samples may indicate the consumption of portlandite in the formation of other products such as calcite rather than thaumasite. Calcite peaks mainly at (29.50 and 39.40 2 $\theta$ ) can be seen in all samples in both regimes and it is not surprising that these peaks are more intense in LFC samples which incorporate more limestone in them. Indeed, it is not surprising also that these peaks are more intense in the cyclic wetting and drying samples where there is potential for the formation of carbonates as a result of the carbonation process.

#### 4. Effect of wetting and drying cycles on thaumasite formation

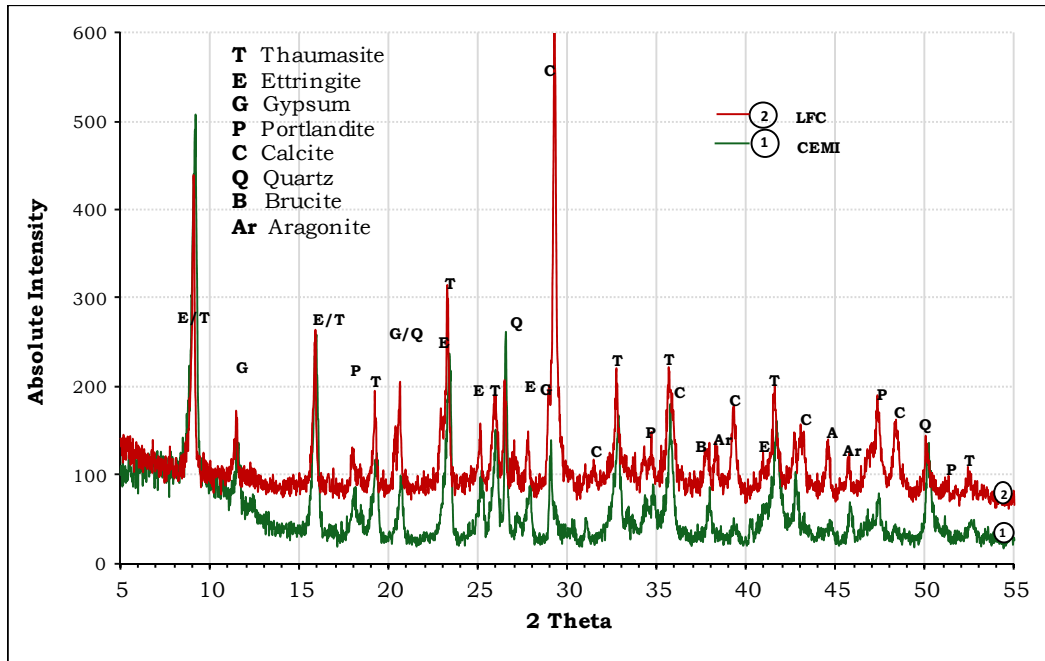


**Figure 4.25 XRD patterns for samples in DS4 solutions at 5 °C (12 months)**

Aragonite peaks at (27.22, 33.13, 36.18 and 45.86 2 $\theta$ ) and quartz peaks at (20.85, 26.63 and 50.11 2 $\theta$ ) are also observed in all samples. The case of quartz, these peaks are stronger in the samples that resisted deterioration because these samples were still sound and sand particles were included in the crushed samples, while in the deteriorated samples sand grains were easily removed before crushing. Small peaks assigned to brucite Mg(OH)<sub>2</sub> at (18.50, 37.98 and 50.88 2 $\theta$ ) were detected in all samples.

Figure 4.26 and Figure 4.27 show the different X-ray patterns for samples immersed in DS4 at 5 °C continuously and under wetting and drying cycles respectively. As it can be noted, the patterns are similar to those of samples kept in DS3 solutions, except that the intensities for thaumasite or thaumasite containing phases are slightly stronger in both exposure regimes, suggesting that higher sulfate concentrations have led

#### 4. Effect of wetting and drying cycles on thaumasite formation

to more thaumasite formation. Gypsum peaks are also stronger in higher concentration sulfate solutions and they are higher in samples subjected to wetting and drying cycles. This is probably as a result of portlandite reacting with sulfate to form gypsum.

However, these peaks can be observed in all samples except for LFC in continuous immersion, which is the most deteriorated sample. Calcite, aragonite, portlandite, quartz and brucite peaks can be identified in higher quantities to samples in DS3 solution.

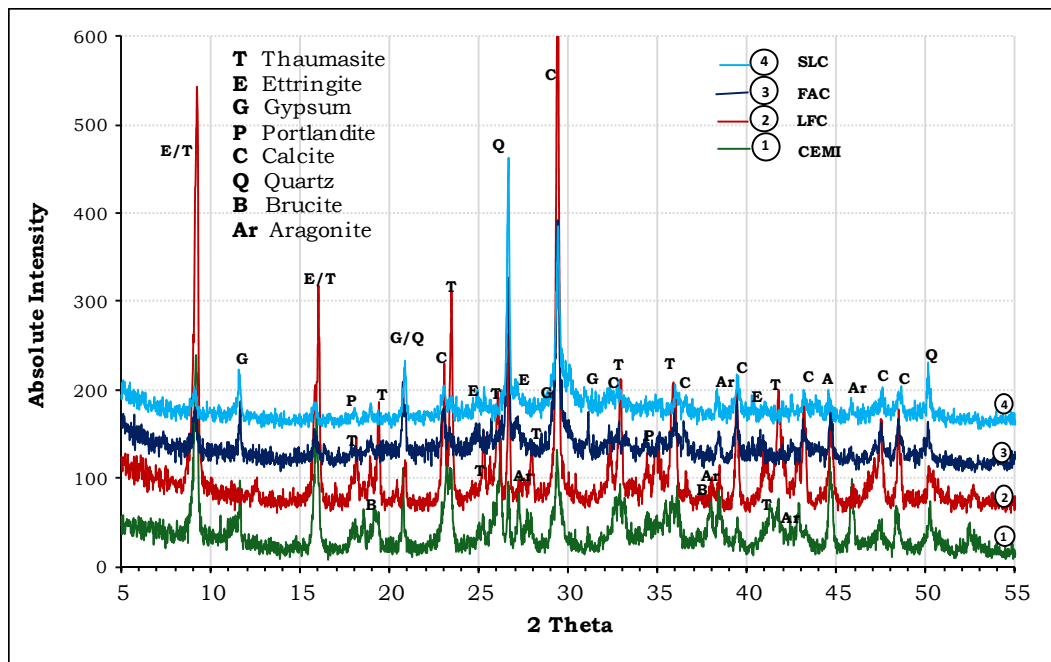
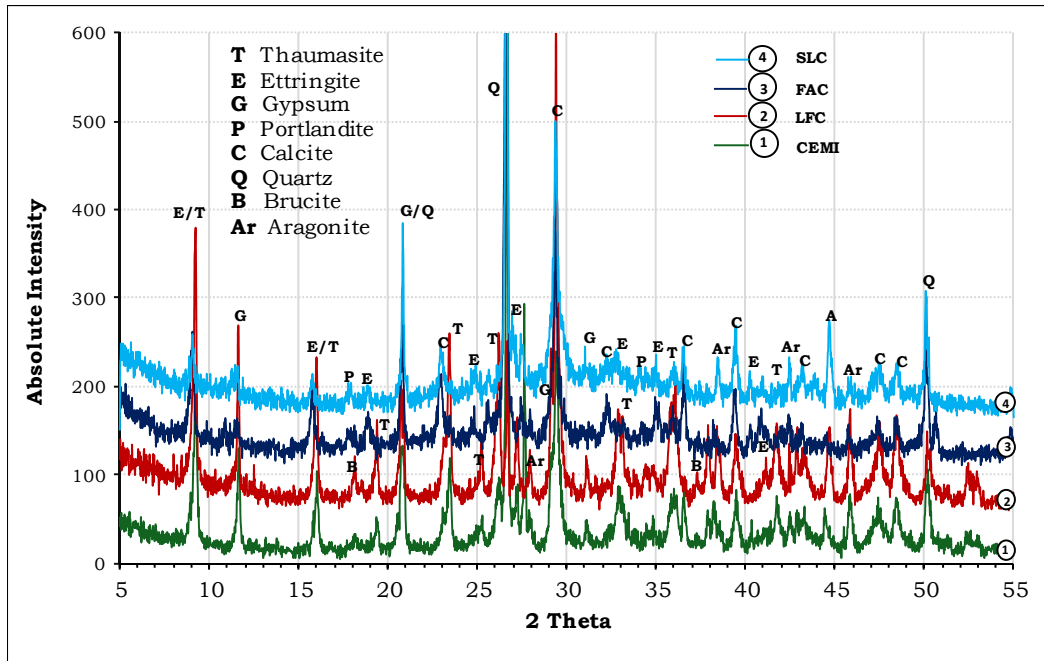


Figure 4.26 XRD patterns for samples in DS4 solutions at 5 °C (continuous immersion)

#### 4. Effect of wetting and drying cycles on thaumasite formation



**Figure 4.27 XRD patterns for samples in DS4 solutions at 5 °C(wetting and drying)**

At 20 °C the XRD patterns for samples immersed in DS3 sulfate solution continuously and under wetting and drying cycles are presented in Figure 4.28 and Figure 4.29. In these the peaks assigned to thaumasite/thaumasite solid solutions are very strong in CEMI continuously immersed in DS3 solution (this is the only sample which showed signs of deterioration, as shown in Figure 4.4). Ettringite is identified in FAC and SLC cements only in continuous immersed samples implying this storage regime could be worse than wetting and drying curing regime. Gypsum appeared in all wetting and drying samples while they can only be identified in plain and slag containing cement under continuous immersion. Calcite is also detectible in all samples and they are stronger in samples subjected to wetting and drying cycles. Portlandite can be observed strongly in LFC suggesting that due to its low stability in the presence of sulfate ions further

#### 4. Effect of wetting and drying cycles on thaumasite formation

reactions may occur (Torres 2004). These peaks are again weaker in case of samples kept under the wetting and drying regime. Brucite is only detected as a weak peak in the deteriorated sample of CEMI in continuous immersion. As mentioned before calcite peaks are identified in all samples with stronger peaks in the cyclic wetting and drying samples. Aragonite peaks seem to be stronger in the continuously immersed samples, especially for CEMI sample.

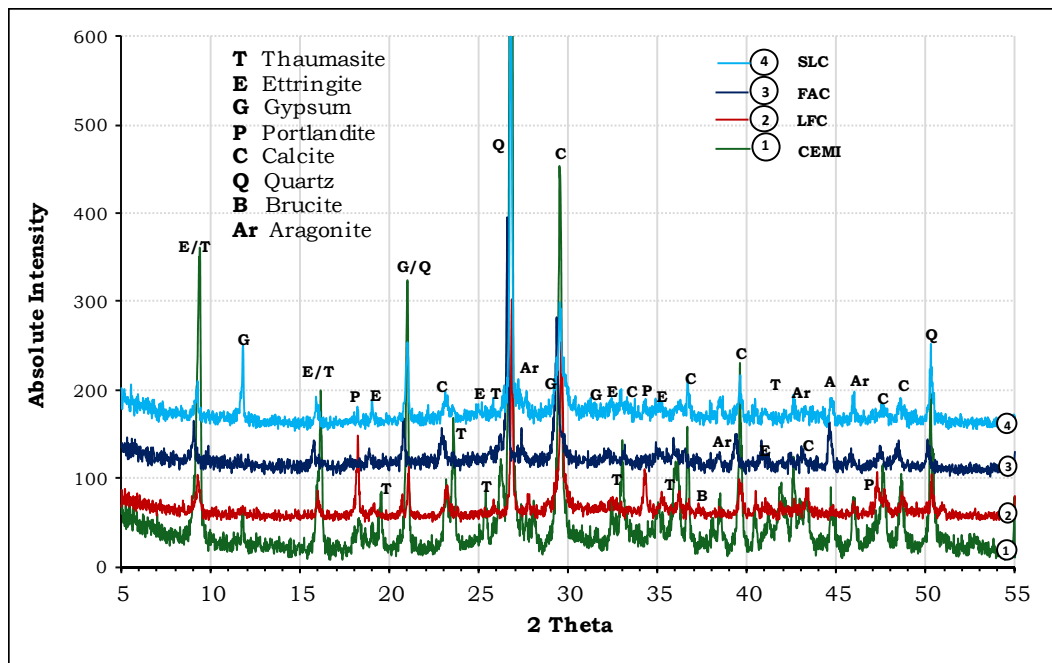
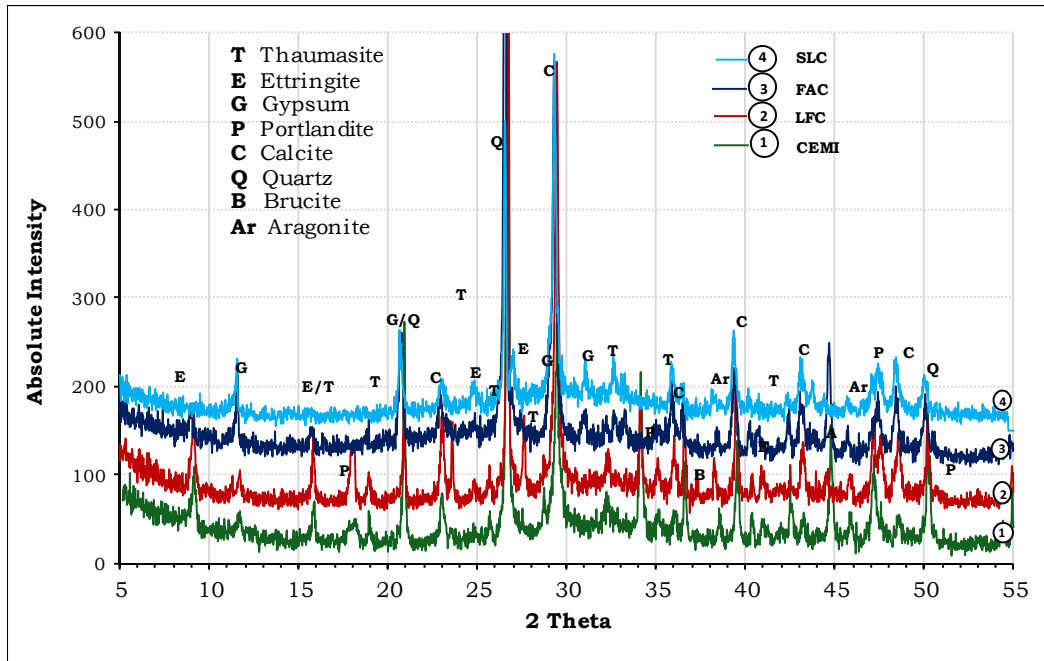


Figure 4.28 XRD patterns for samples in DS3 solutions at 20 °C (continuous immersion)

#### 4. Effect of wetting and drying cycles on thaumasite formation



**Figure 4.29 XRD patterns for samples in DS3 solutions at 20 °C (wetting and drying)**

Concerning samples kept in DS4 at 20 °C, the XRD patterns for the two storage regimes are illustrated in Figure 4.30 and Figure 4.31 respectively. It can be noted from these Figures that the peaks attributed to either thaumasite or thaumasite-ettringite solid solutions are more intense in continuous immersion samples compared to cyclic wetting and drying. This is very clear in both samples that showed physical signs of deterioration in Figure 4.5, and this agrees with the observations that CEMI samples are showing higher peak intensities than limestone blended cement. However these peaks are weaker than those observed at lower temperature for the same solutions as in Figure 4.26 and Figure 4.27, which confirms the effect of temperature on thaumasite formation. Gypsum peaks were identified in all samples apart from the limestone containing cyclical wetting and drying sample and were stronger than those observed for DS3, and the continuously immersed samples. Portlandite peaks were absent from FAC and SLC cements while

#### 4. Effect of wetting and drying cycles on thaumasite formation

higher gypsum peaks were observed in these samples, suggesting that portlandite reacts with sulfate ions to form gypsum instead of thaumasite or ettringite.

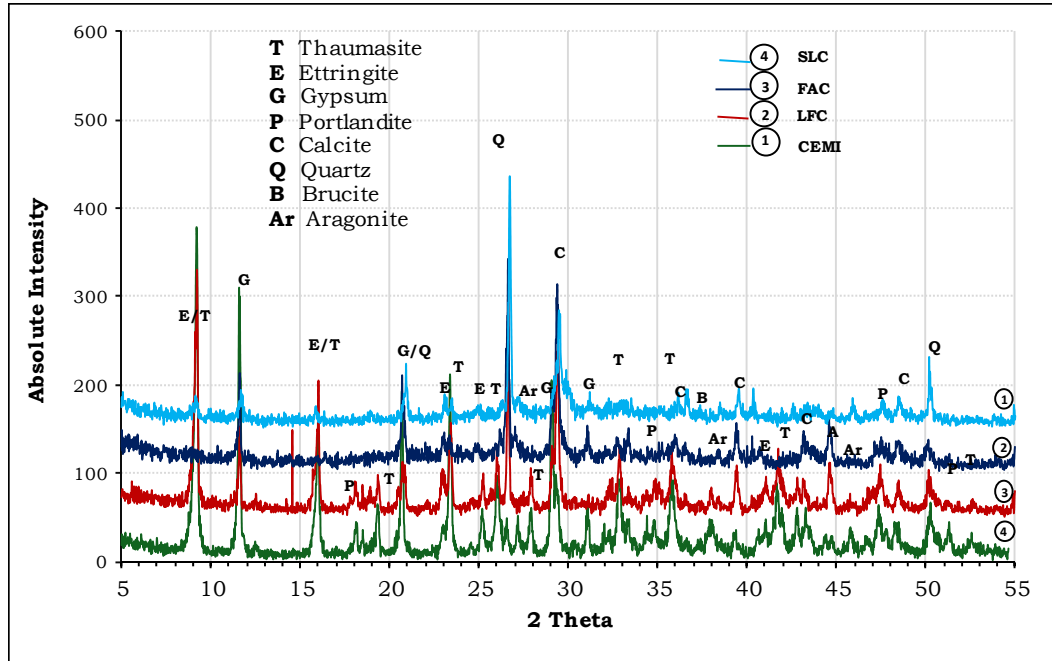


**Figure 4.30 XRD patterns for samples in DS4 solutions at 20 °C (continuous immersion)**

Calcite peaks are present in all samples with higher intensities for wetting and drying samples, whereas aragonite peaks are detectable only in wetting and drying samples and continuously immersion of CEMI and SLC samples.

#### 4. Effect of wetting and drying cycles on thaumasite formation

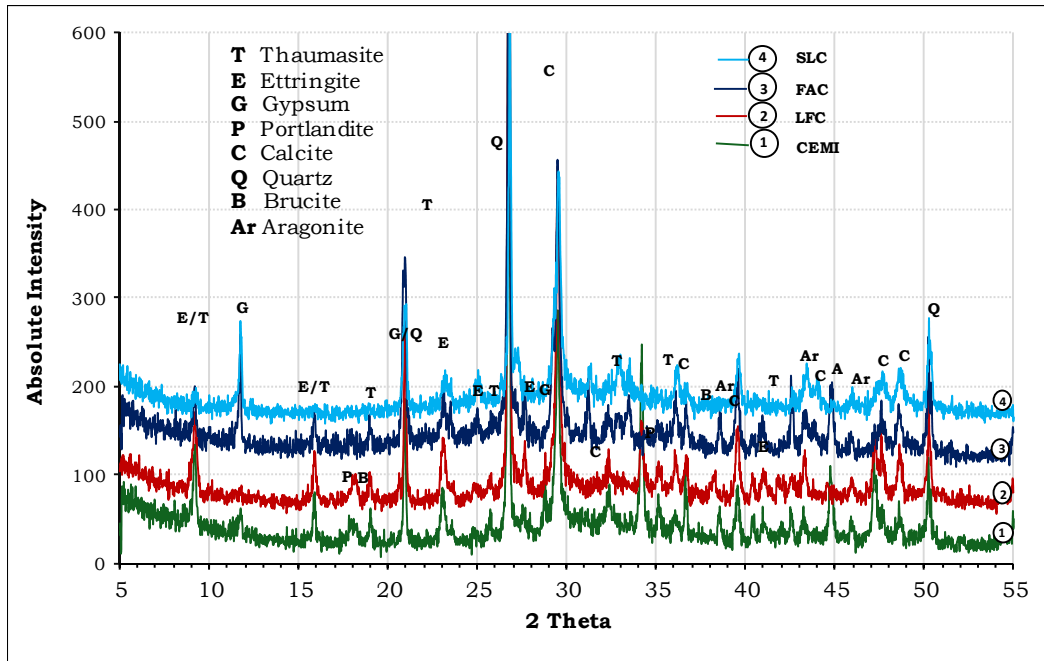


**Figure 4.31 XRD patterns for samples in DS4 solutions at 20 °C (wetting and drying)**

A summary of XRD analysis results based on relative intensities is shown in Table 4.3. as this table shows, the intensities of thaumasite is higher in LFC than other cements, it can be also noted that these intensities are higher in case of continuous immersion samples compared to wetting and drying samples, this agrees well with the rate of deterioration observed visually and with mass change results. The presence of gypsum is in relation with the sulfate concentration where higher concentration of solutions led to more gypsum to form. Calcium carbonate products (calcite and aragonite) are more obvious in wetting and drying samples as a result of carbonation reactions.

4. Effect of wetting and drying cycles on thaumasite formation

**Table 4.3 Relative intensities of phase assemblage as identified by XRD analysis**

Exposure condition	Sample	Exposure solution	Temperature											
			5 °C						20 °C					
			Th	Ett	Gyp	Port	Cal	Arag	Th	Ett	Gyp	Port	Cal	Arag
continuous immersion	CEMI	DS3	xxxx	xxx	–	xx	xxx	xxx	xxxx	xx	x	xx	xxx	xx
		<b>DS4</b>	xxxx	xxx	xx	xx	xxx	xxx	xxxx	xx	xxx	x	xx	x
	LFC	DS3	xxxxx	xx	–	xx	xxxx	xx	x	x	–	xxx	xx	–
		<b>DS4</b>	xxxxx	x	–	xx	xxxx	xx	xxx	xx	xx	x	xxx	
	FAC	DS3	xx	xx		x	xx	x	x	x	–	–	xx	xx
		<b>DS4</b>	xx	xx	xx		xx		–	–	xx		xx	
	SLC	DS3	xx	xx	x	x	xx	x	x	x	xxx	–	xx	x
		<b>DS4</b>	xx	xx	xx		xx	x	–	–	xx	–	xx	–
Wetting and drying	CEMI	DS3	xx	x	–	x	xxxx	xxx	xx	xx	x	x	xxx	xx
		<b>DS4</b>	xxx	xx	xx		xxx	xxx	xxx	xx	x	x	xxx	xx
	LFC	DS3	xxxx	xx	xx	x	xxxxx	xxx	xx	xx	x	xx	xxx	xx
		<b>DS4</b>	xxxx	x	xxx	x	xxxxx	xxxx	xxx	xx	–	x	xxx	x
	FAC	DS3	xx	xx	xx	–	xx	xx	–	–	xx	–	xxx	xx
		<b>DS4</b>	xx	xx	x	x	xx	x	x	x	xxx	x	xxx	x
	SLC	DS3	xx	xx	x	–	xx	x	–	–	xx	–	xxx	xx
		<b>DS4</b>	xx	xx	x	x	xx	xx	x	x	xxx	–	xxx	x

Th. =thaumasite  
 Ett. = Ettringite  
 Gyp. = Gypsum  
 Port. = Portlandite  
 Cal. = Calcite  
 Arag. = Aragonite

#### **4.7 Fourier Transform Infrared Spectroscopy (FTIR)**

Fourier Transform Infrared Spectroscopy FTIR is a very useful technique to differentiate between thaumasite and ettringite, due to the unique vibration of octahedral silicate  $\text{SiO}_6$  at around  $500\text{ cm}^{-1}$  which indicates the presence of thaumasite. The technique was used in this research particularly to distinguish between thaumasite and ettringite in the deteriorated samples.

FTIR testing was not performed on all samples, only deteriorated samples and samples immersed in DS4 sulfate solutions were tested as these were considered to be the most aggressive environments. Thus only CEMI or LFC samples in DS3 at  $5\text{ }^\circ\text{C}$  in both storage regimes were subjected to FTIR.

Figure 4.32 and Figure 4.33 show the IR spectra for both binders under different exposure regimes at  $5\text{ }^\circ\text{C}$ , where strong peaks at around  $500\text{ cm}^{-1}$  and  $760\text{ cm}^{-1}$  related to octahedral silicates ( $\text{SiO}_6$ ) in addition to  $\text{CO}_3$  and  $\text{SO}_4$  and hence indicate that thaumasite or thaumasite containing phases are present (Barnett et al. 2002, Torres et al. 2004). These peaks can be seen in both systems but they are stronger in continuously immersed samples, and strongest in limestone filler containing samples. Peaks assigned to calcite occurring at  $712\text{ cm}^{-1}$  and  $875\text{ cm}^{-1}$  also appeared in both cements in both exposure systems but unlike thaumasite, these peaks are stronger in the samples kept under wetting and drying cycles, which is probably due to more calcite being formed as a result of carbonation reactions. The presence of peaks at around  $850\text{ cm}^{-1}$  assigned to  $\text{AlO}_6$ , indicates ettringite, where the co-existence of these peaks with thaumasite peaks might be an indication of thaumasite-ettringite solid solutions. Indeed these bands are very weak in limestone containing samples in continuous immersion regime, suggesting that a thaumasite end-member is being approached. However

#### 4. Effect of wetting and drying cycles on thaumasite formation

these peaks are stronger in CEMI samples and in cyclic wetting and drying samples, suggesting that more thaumasite is formed at the expense of ettringite which suggests that ettringite is being consumed to form thaumasite.

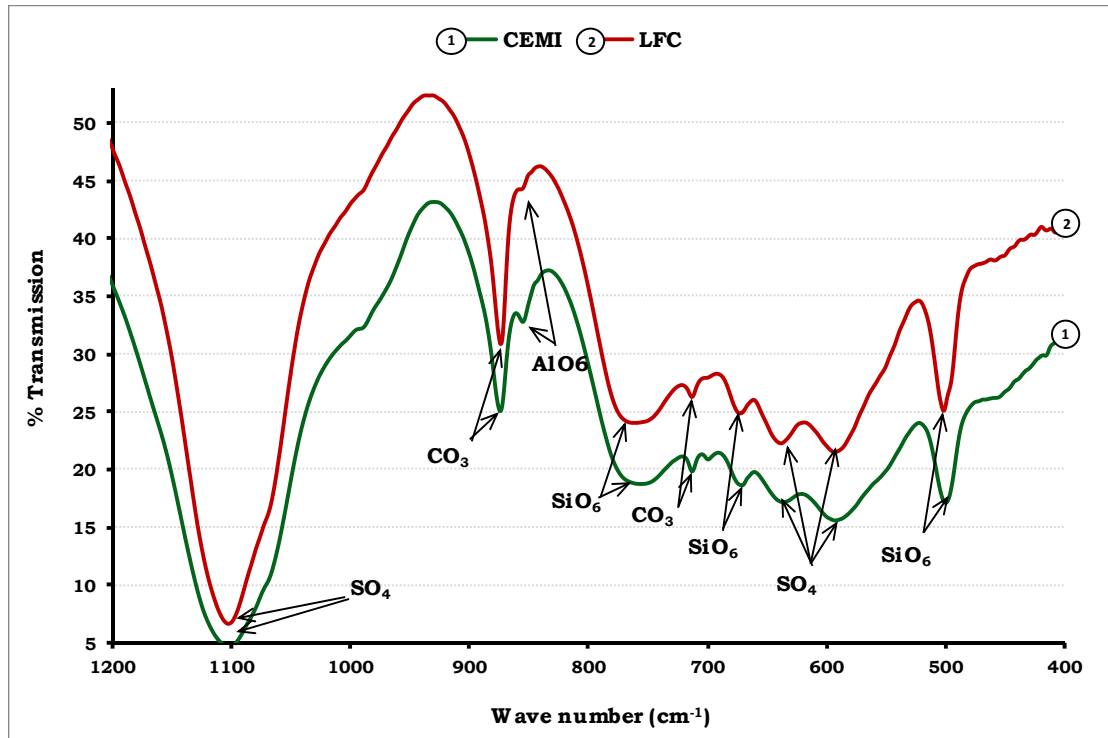
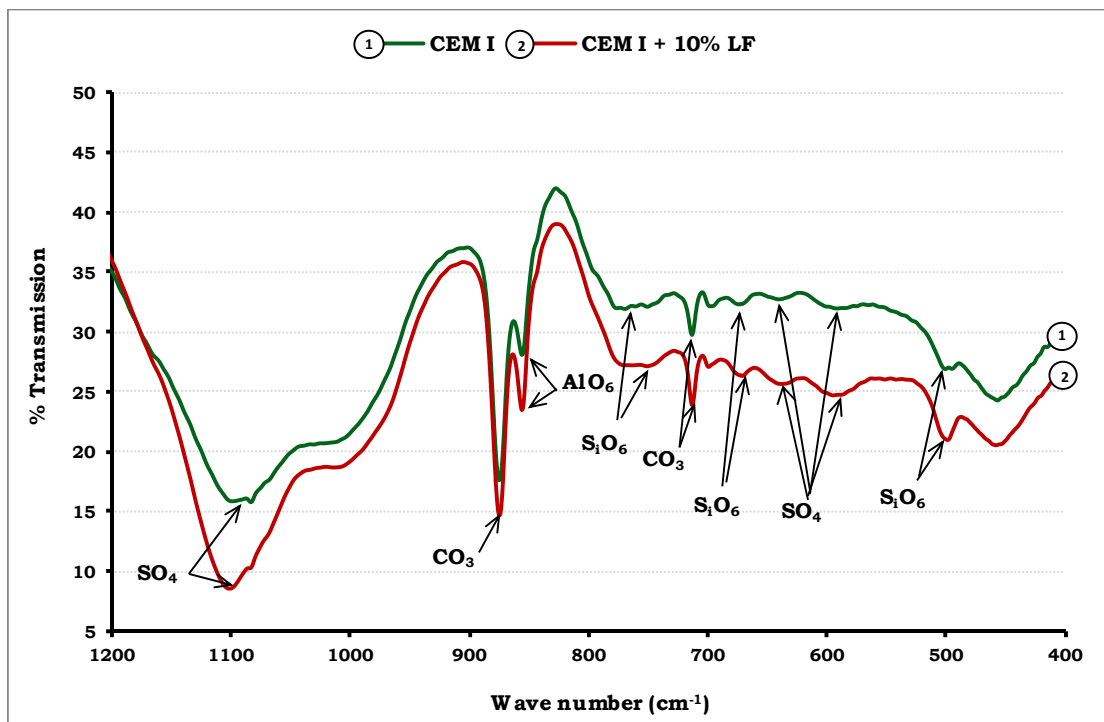


Figure 4.32 IR spectra for samples in DS3 solutions at 5 °C (continuous immersion)

The presence of SO<sub>4</sub> wave bands at around 600 cm<sup>-1</sup>, 650 cm<sup>-1</sup> and 1100 cm<sup>-1</sup> might be indicative of gypsum or sulfates incorporated in other minerals such as thaumasite and ettringite. The intensity is higher for continuously immersed samples. The peaks at around 1000 cm<sup>-1</sup> are due the presence of SiO<sub>4</sub> ions which may be due to the formation of C-S-H gel (Bensted and Varma 1974). However, these peaks are hardly noticeable in the continuous immersed samples, which suggest that C-S-H gel is almost completely decomposed and transformed into thaumasite. As these SiO<sub>4</sub> peaks can be clearly seen in samples subjected to wetting and

#### 4. Effect of wetting and drying cycles on thaumasite formation

drying cycles, some binding gel remains. The appearance of peaks at around  $700\text{ cm}^{-1}$ , in addition to those at  $712\text{ cm}^{-1}$ , are indicative of the aragonite form of calcium carbonate, and they can be observed in all samples although they are higher intensities in the wetting and drying samples and less obvious in samples containing limestone filler, where thaumasite is the dominant phase.



**Figure 4.33 IR spectra for samples in DS3 solutions at  $5\text{ }^{\circ}\text{C}$  (Wetting and drying cycles)**

The FTIR spectra for samples exposed to DS4 at  $5\text{ }^{\circ}\text{C}$  are presented in Figure 4.34 and Figure 4.35. As can be observed the spectra are similar to those exposed to DS3, where the FAC and SLC samples were tested as the exposure condition was severe. Again it is clear that the damage caused to these samples was due to the formation of thaumasite type of sulfate attack TSA. This is confirmed by the presence of sharp peaks at  $500\text{ cm}^{-1}$  and broad peaks at around  $760\text{ cm}^{-1}$  in all samples, in addition

#### 4. Effect of wetting and drying cycles on thaumasite formation

to carbonate peaks at  $712\text{ cm}^{-1}$  and  $875\text{ cm}^{-1}$  and sulfate group peaks at  $600\text{ cm}^{-1}$ . Once again these peaks are much stronger in samples exposed to sulfate solution continuously. Fly ash and slag samples did not show peaks at  $500\text{ cm}^{-1}$ , suggesting that thaumasite did not form in these samples. This is in agreement with the visual observations since these samples did not exhibit any damage. Notwithstanding, a clear peak assigned to  $\text{SiO}_6$  at  $760\text{ cm}^{-1}$  Zhou et al. (2006) can be seen in these two cements which may be because thaumasite had formed in these samples but this did not result in attack (TSA). Crammond (2003) refers to the possibility of non-damaging thaumasite formation in cracks and voids.

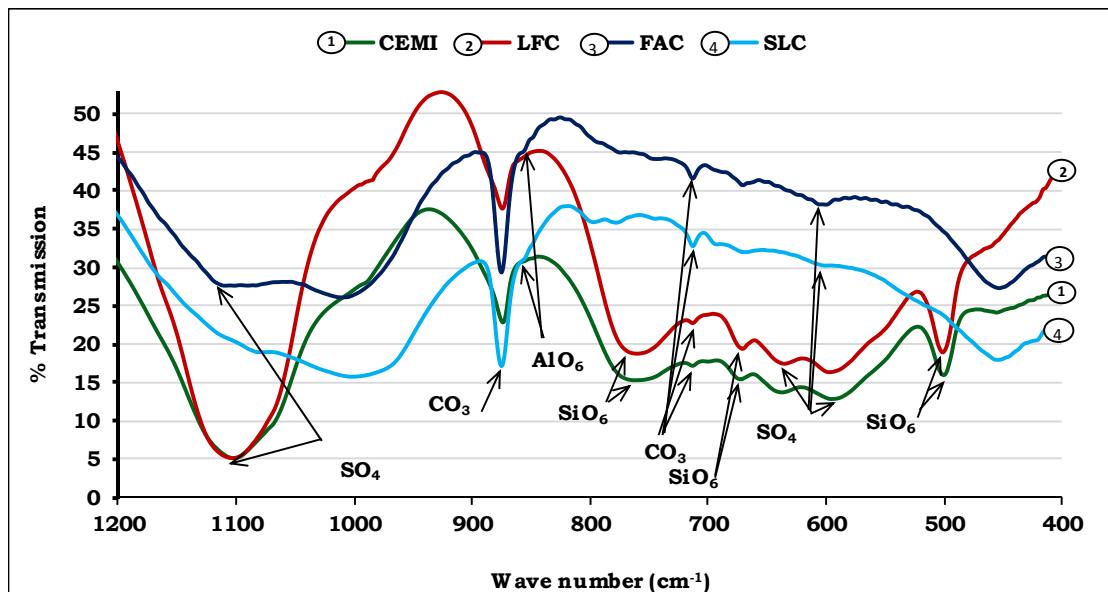


Figure 4.34 IR spectra for samples in DS4 solutions at  $5\text{ }^{\circ}\text{C}$  (continuous immersion)

Calcite peaks at  $875\text{ cm}^{-1}$  and  $712\text{ cm}^{-1}$  are present in all samples. However they are at higher intensities in samples subjected to wetting and drying cycles.

The presence of the peaks at  $850\text{ cm}^{-1}$  assigned to  $\text{AlO}_6$  group is indicative ettringite. These are very clear in samples exposed to wetting and drying cycles, but on the other hand these peaks are absent from

#### 4. Effect of wetting and drying cycles on thaumasite formation

samples continuously immersed in the sulfate solutions, indicating that thaumasite is becoming an end-product in the severe exposure conditions. Once more, peaks at  $1000\text{ cm}^{-1}$  representing CSH are hardly seen in samples under continuous immersion, but they are more obvious in samples subjected to wetting and drying, which suggests that more binding gel is converted to thaumasite. However samples made of cements blended with FAC and SLC show good broad peaks indicating that they are still sound and their binding capacity is still maintained. As noted in samples exposed to DS3 solutions, aragonite peaks at  $700\text{ cm}^{-1}$  and  $712\text{ cm}^{-1}$  can be seen in cyclic wetting and drying samples but they are absent from continuously immersed samples, which suggests that aragonite may serve as a reactant to form thaumasite.  $\text{SO}_4$  group peaks at  $600\text{ cm}^{-1}$  and  $650\text{ cm}^{-1}$  associate with sulfate bearing phases such as thaumasite, ettringite and gypsum can be seen in both systems and in all samples tested.

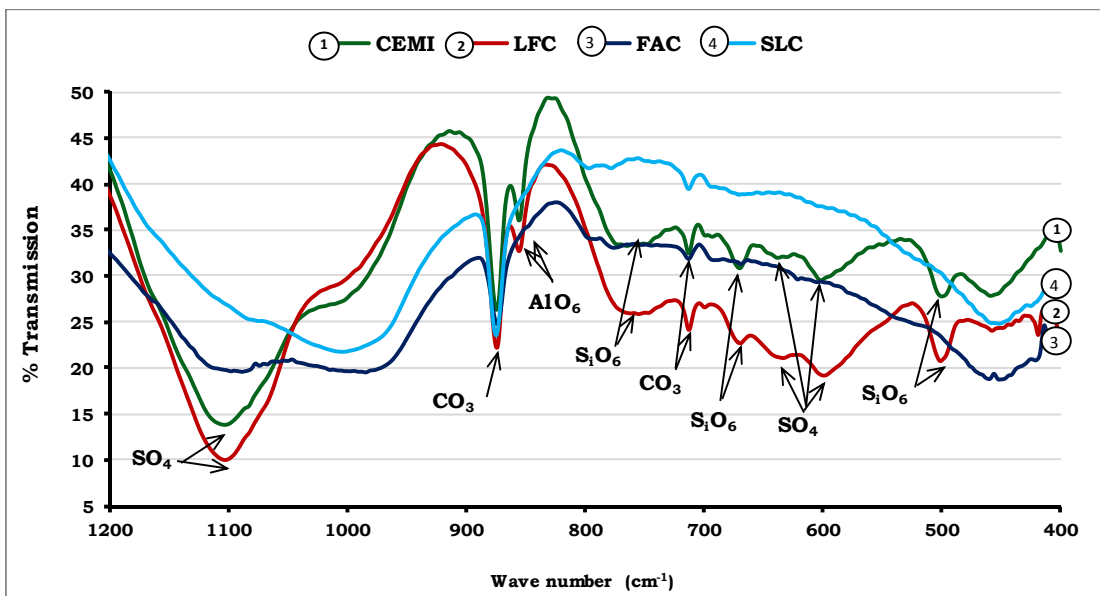


Figure 4.35 IR spectra for samples in DS4 solutions at  $5\text{ }^\circ\text{C}$  (Wetting and drying cycles)

#### 4. Effect of wetting and drying cycles on thaumasite formation

---

At 20 °C, for samples immersed in DS3 solutions, only CEMI and LFC samples were subjected to FTIR testing to compare them with samples showed signs of deterioration in the same solutions at 5 °C. These spectra are presented in Figure 4.36 and Figure 4.37. As these graphs show peaks at around 500 cm<sup>-1</sup> assigned to thaumasite can be easily identified in both cements in continuous immersed samples, although LFC sample did not show any outward signs of attack, which suggests that thaumasite had formed in this sample but it was not sufficient to cause physical deterioration but could well result in TSA. Samples subjected to wetting and drying cycles did not show any peaks around this wave number leading to the conclusion that thaumasite had not formed in these samples. These peaks are stronger in CEMI sample hence the more damage observed visually. Comparing these peaks with those observed at 5 °C shown in Figure 4.32, it is clear that the latter are stronger, confirming that thaumasite is favoured to form at lower temperatures. The strong bands at 850 cm<sup>-1</sup> in limestone blended cement indicates the formation of ettringite in this continuously immersed sample. On the contrary, CEMI sample showing weaker peak at this range, and taking into account that this sample showed signs of damage, it is suggested that ettringite is converted to form thaumasite, as was described by Bensted (2003) as the woodfordite route of thaumasite formation.

#### 4. Effect of wetting and drying cycles on thaumasite formation

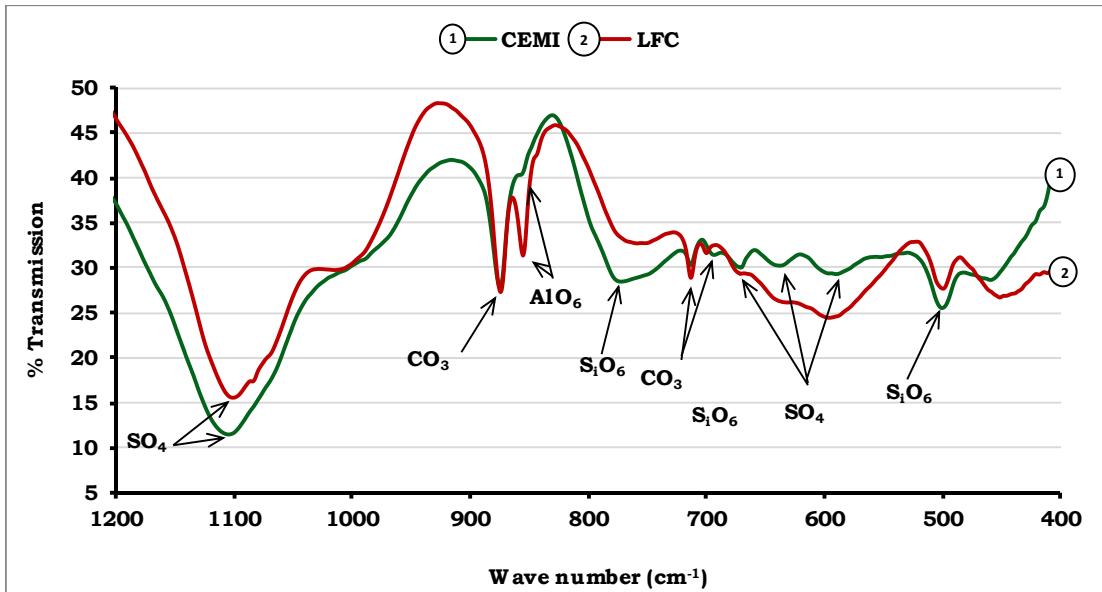


Figure 4.36 IR spectra for samples in DS3 solutions at 20 °C (continuous immersion)

However this band was very weak in the cyclic wetting and drying sample, where the slightly higher peaks in CEMI samples could be taken as an indication of greater susceptibility to thaumasite type of sulfate attack (TSA) at higher temperatures. Gypsum peaks are stronger in CEMI samples confirming what was observed by XRD in Figure 4.28, while calcite peaks are stronger in LFC samples in both systems. Peaks indicative for CSH are hardly seen in the continuously immersed CEMI sample, where this sample started to lose its binding capacity due to the sulfate attack. These peaks are more obvious in LFC and in cyclic wetting and drying samples.

#### 4. Effect of wetting and drying cycles on thaumasite formation

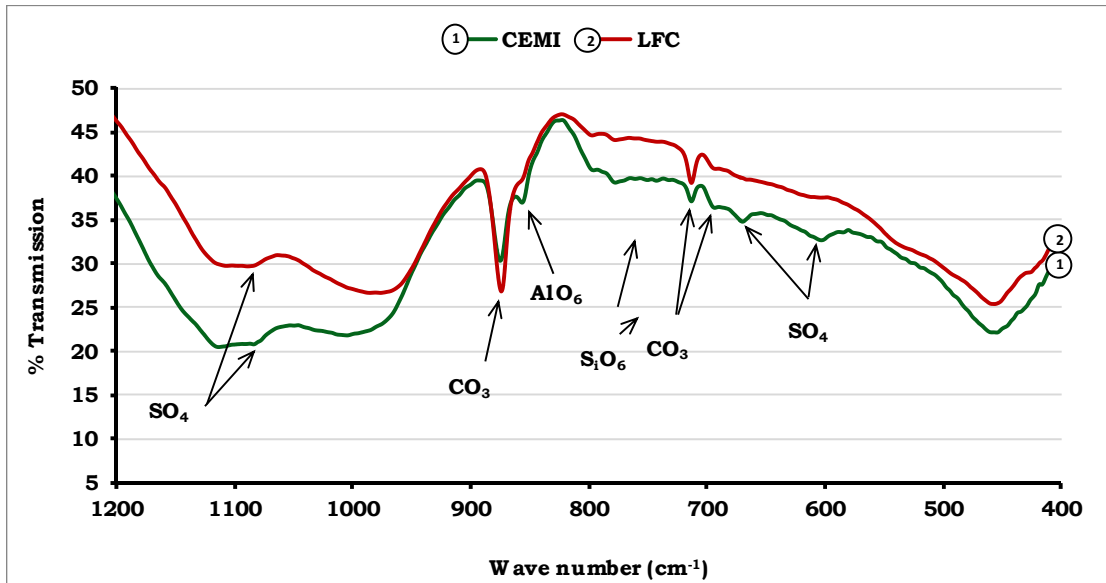


Figure 4.37 IR spectra for samples in DS3 solutions at 20 °C (Wetting and drying cycles)

FTIR spectra for all cement samples in DS4 sulfate solutions are shown in Figure 4.38 and Figure 4.39, from which it is clear that thaumasite attack was responsible for the damage that was observed visually in CEMI and LFC cements, hence the sharp peaks around 500  $\text{cm}^{-1}$  in both samples. These wave bands are absent from wetting and drying samples and from FAC and SLC cements, where no visual damage was observed. Moreover, these peaks are slightly higher in CEMI sample indicating a higher attack rate. Strong gypsum peaks can be observed in all samples immersed continuously in DS4 sulfate solution similar to what was seen in XRD analysis results. In samples subjected to wetting and drying cycles, these peaks can only be identified in flay ash and slag blended cement, instead, ettringite peaks were clearly observed in CEMI and LFC.

#### 4. Effect of wetting and drying cycles on thaumasite formation

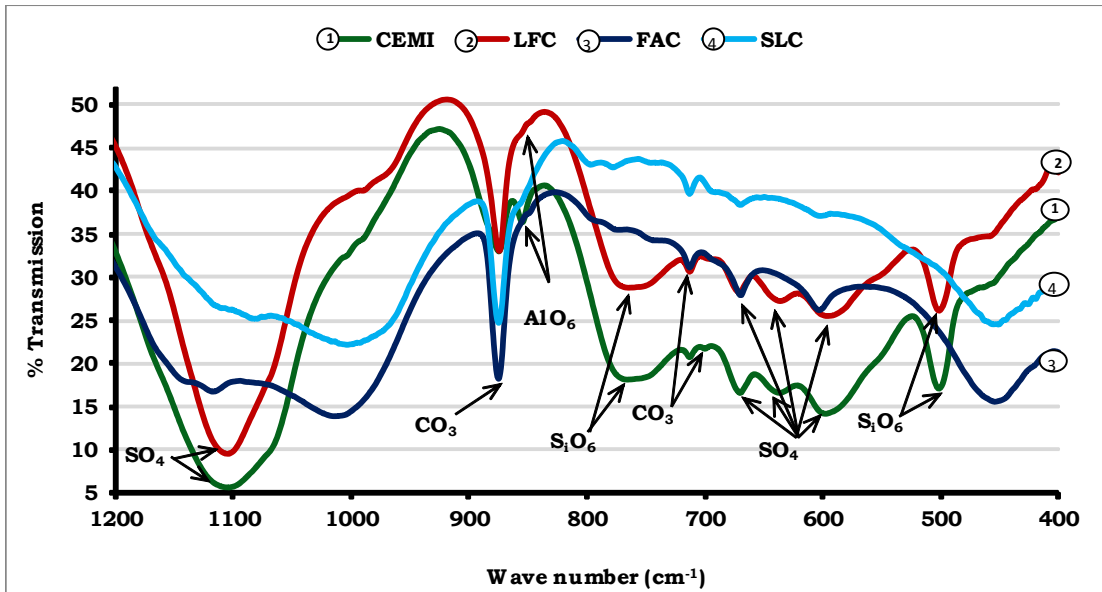


Figure 4.38 IR spectra for samples in DS4 solutions at 20 °C (continuous immersion)

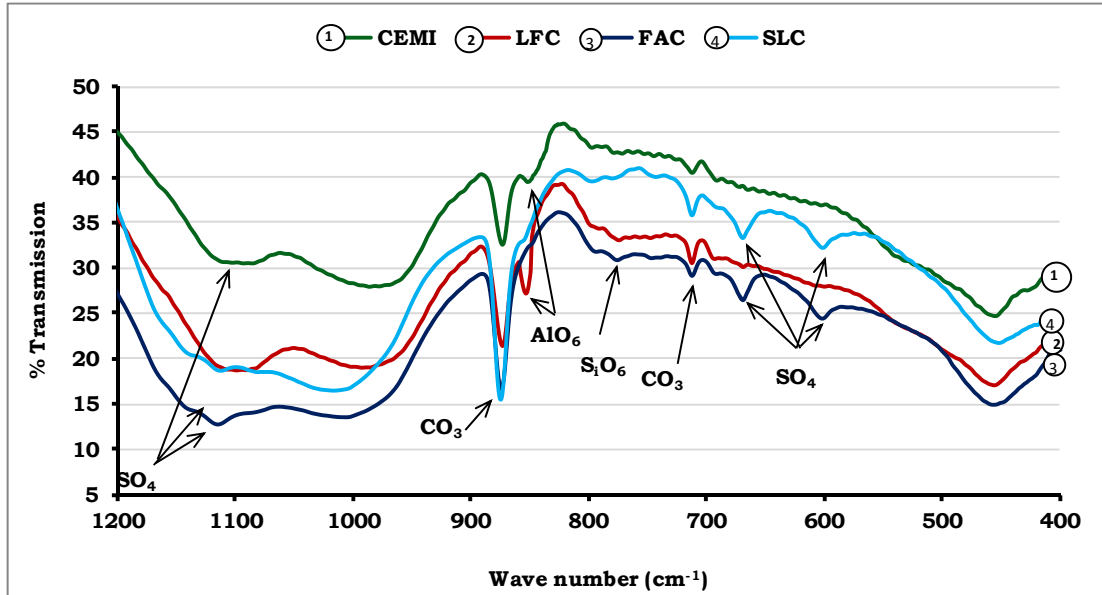


Figure 4.39 IR spectra for samples in DS4 solutions at 20 °C (Wetting and drying cycles)

### 4.8 PH measurements

The variations of pH values in the exposure solutions with time are presented in Figure 4.40 and Figure 4.41 which show the pH variations for samples exposed to DS3 sulfate solutions at 5 °C for continuous and cyclic wetting and drying immersion respectively. As these Figures illustrate, the pH trends are quite similar, where all samples show a dramatic increase in pH during the first 7 days of exposure to sulfate solutions, then the values drop. This reduction in pH values continued till after the change of the solutions which occurred at 90 and 180 days after which the pH values started to rise again. However the increment of pH values were vary dependent on the cement type and the exposure condition. LFC showed the highest pH values followed by CEMI then FAC and SLC cements.

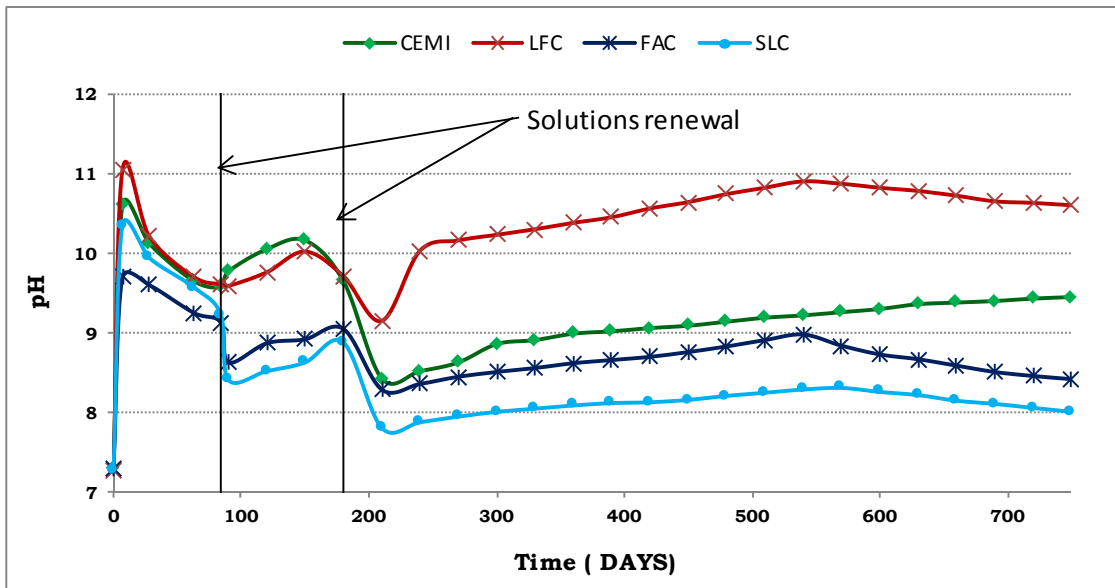


Figure 4.40 pH values for samples in DS3 solutions at 5 °C (continuous immersion)

#### 4. Effect of wetting and drying cycles on thaumasite formation

---

The increase in pH during the first period of exposure can be attributed to the leaching of alkaline species, mainly calcium hydroxide into the solution in order to maintain equilibrium between mortar and surrounding medium, soon after calcium hydroxide reacts with sulfates, a magnesium hydroxide mineral known as brucite ( $\text{Mg}(\text{OH})_2$ ) is formed which as this is insoluble causes pH values to drop (Gaze and Crammond 2000, Liu et al. 2013).

By the time thaumasite was formed in these samples at around 110 days, the pH values were about 9.8 for CEMI and LFC cement and 8.7 in the cyclic wetting and drying exposure samples which was when they started to show signs of attack or thaumasite formation at around 300 days. It is obvious that the pH values for the wetting and drying samples is much lower than for continuous immersion. This could be related to the carbonation of the samples ( Chapter 5 gives further details regarding the effect of carbonation on thaumasite formation) which decrease the alkalinity of mortars and results in depletion of portlandite and lowering in pH values to 8.3 or below (Papadakis et al. 1992).

The formation of calcium carbonate as a result of the carbonation reactions and filling the pores and making physical barrier against portlandite leaching could be another reason to cause drop in pH level. The pH values for the PFA and GGBS blended cements are lower than those of CEMI and LFC, which could be the result of pozzolanic reactions, which tend to consume portlandite and produce more calcium silicate hydrate CSH (Veiga and Gastaldini 2012, Neville 2002).

#### 4. Effect of wetting and drying cycles on thaumasite formation

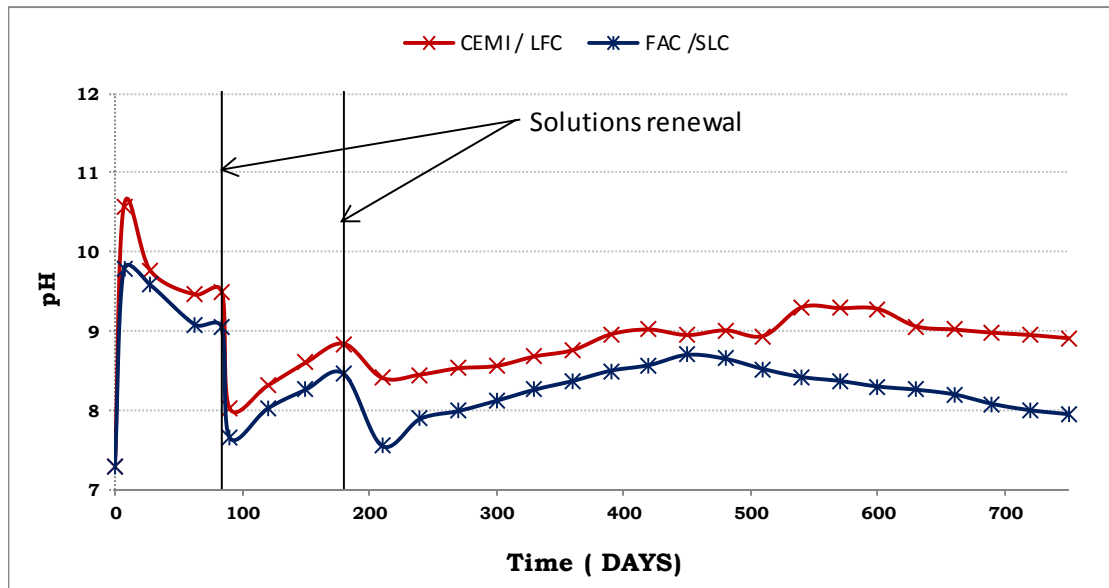


**Figure 4.41 pH values for samples in DS3 solutions at 5 °C (wetting and drying cycles)**

These effects could also be related to the low permeability for these two cements and their dense pore structure which may reduce the amount of calcium hydroxide leached from samples. As it can be also noted that there is an agreement between the greater pH values and higher rate of deterioration observed visually

#### 4. Effect of wetting and drying cycles on thaumasite formation

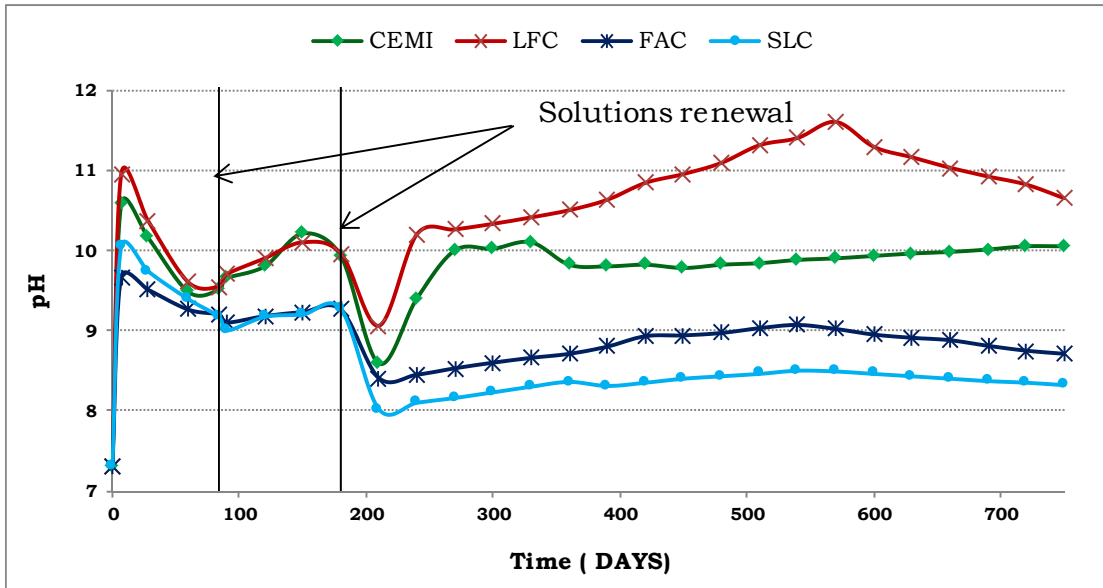


**Figure 4.42 pH values for samples in DS4 solutions at 5 °C (continuous immersion)**

For samples exposed to DS4 at 5 °C, the pH graphs are presented in Figure 4.42 and Figure 4.43. The trends are similar to those observed for samples exposed to DS3 sulfate solutions; however the values of pH are higher. It was reported by Irassar et al. (2005) that mortars exposed to strong magnesium sulfate solution suffer destructive attack resulting from CSH decomposition. This is due to the formation of gypsum and magnesium hydroxide which are known for their stability in lower pH values. CSH gel is not stable in low pH media possible  $\text{pH} < 11.00$  Liu et al. (2013), which leads to exposure to sulfates of more mortar surfaces. Thus more portlandite is released into the solution in order to maintain the stability of CSH by keeping the pH values high enough to preserve it.

For the most deteriorated sample it was noted that pH reached a maximum of about 11.60 at around 570 days after which this value started to decrease and ended up at 10.65 after 750 days of exposure. This suggests that thaumasite has started to decompose or carbonate. Jallad et al. (2003) reported that calcium carbonate results from the

#### 4. Effect of wetting and drying cycles on thaumasite formation

reaction between thaumasite and ions available in the solutions, which was tested to happen at  $\text{pH} > 11.00$

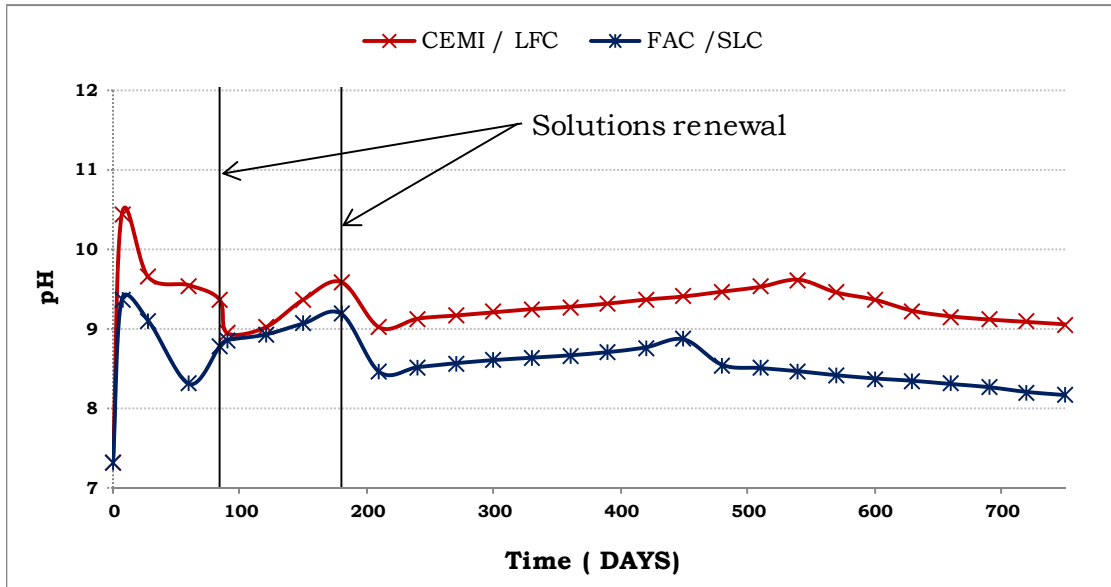


**Figure 4.43 pH values for samples in DS4 solutions at 5 °C (wetting and drying cycles)**

The pH values plotted against exposure time in sulfate solutions at 20 °C are presented in Figure 4.44 to 4.47. In general, the trends are similar to, but much lower than, the results presented earlier for samples kept at 5 °C. However the values are much lower, which is possibly as a result of less damage being caused to these samples so that the inner part of the samples was not exposed to the solutions. However the low pH values in these cements may lead to gypsum formation rather than thaumasite, as was observed in XRD graphs, since gypsum is more likely to form in low pH solutions.

#### 4. Effect of wetting and drying cycles on thaumasite formation

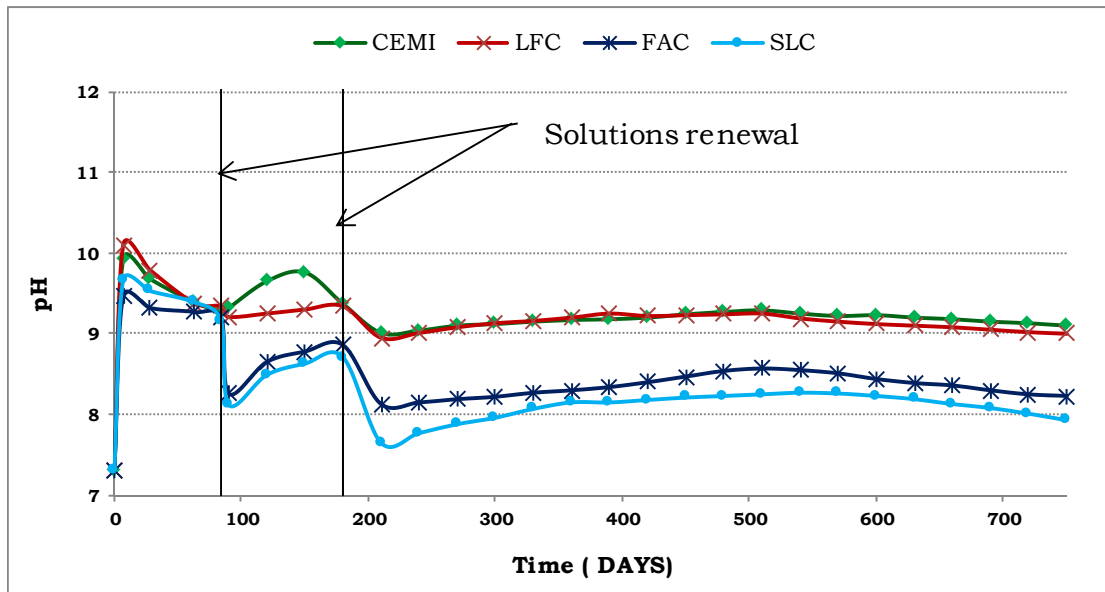


Figure 4.44 pH values for samples in DS3 solutions at 20 °C (continuous immersion)

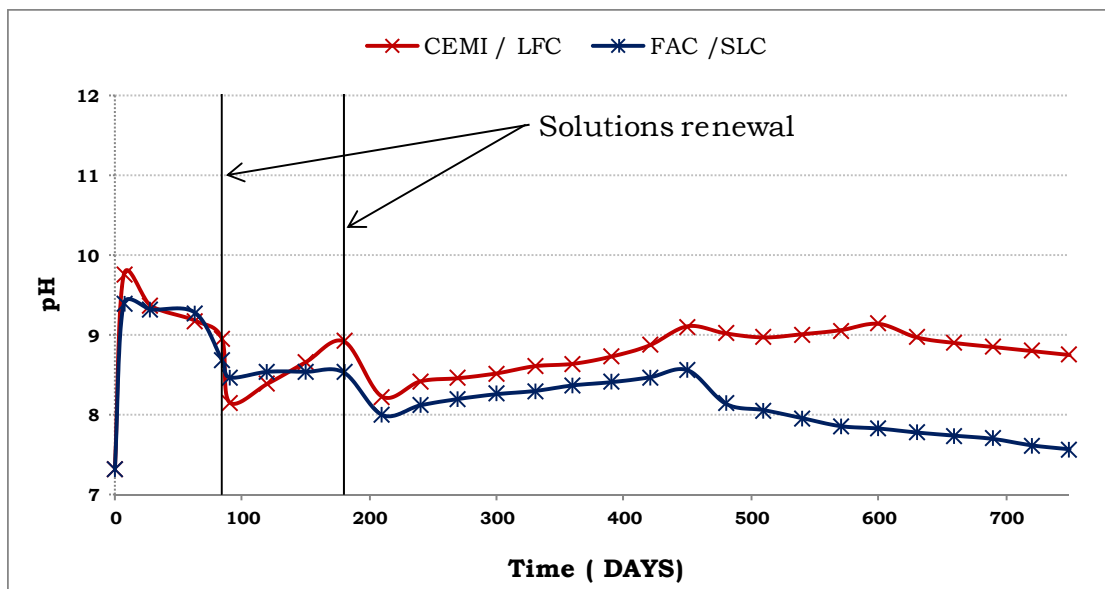


Figure 4.45 pH values for samples in DS3 solutions at 20 °C (wetting and drying cycles)

#### 4. Effect of wetting and drying cycles on thaumasite formation

Looking to the pH variation in all graphs, it can be seen that, after each renewal of sulfate solutions, pH recovery to near to its values before replenishment occurs. Yet the time needed for recovery was longer each time. This increase is possibly was due to the release of more calcium hydroxide from the inner parts of the mortars. Indeed, this is more obvious in samples that suffered from great attack such as limestone blended samples in DS4 at 5 °C, where the recovery time was quicker and the increment was higher compared to the non-deteriorated samples.

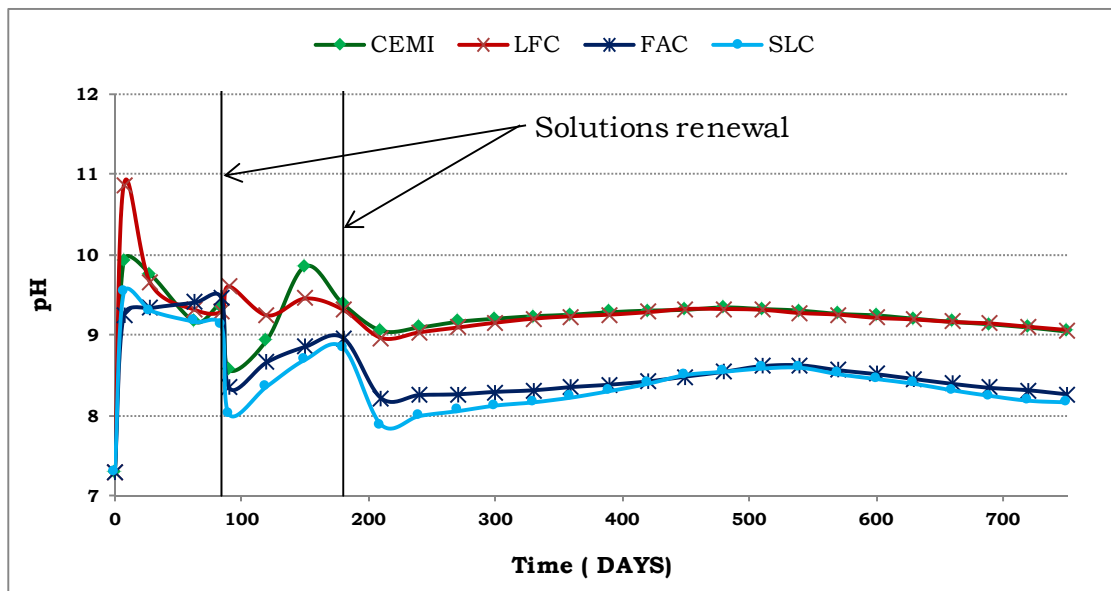


Figure 4.46 pH values for samples in DS4 solutions at 20 °C (continuous immersion)

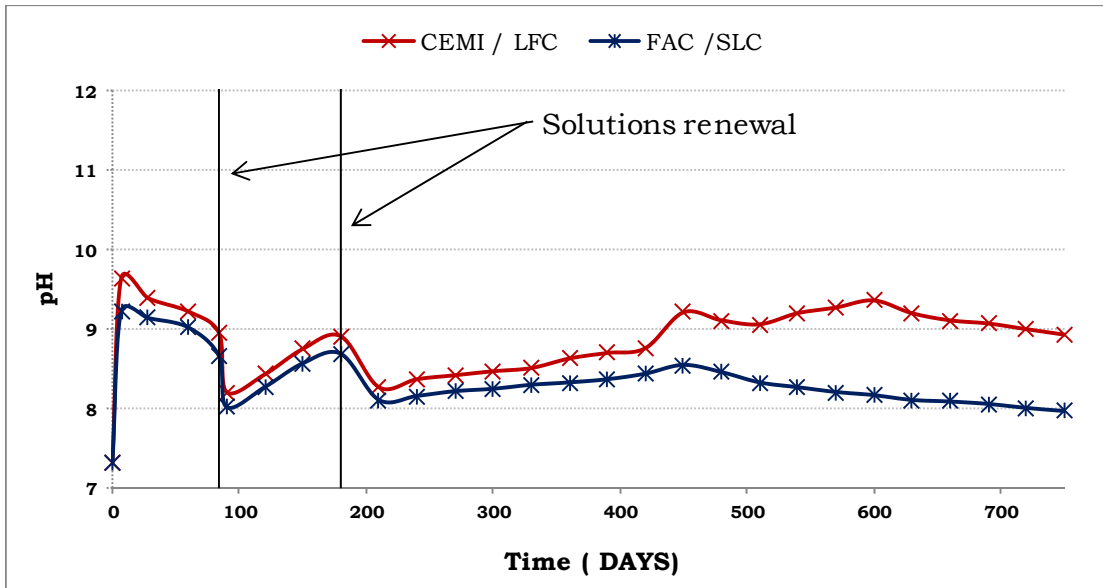


Figure 4.47 pH values for samples in DS4 solutions at 20 °C (wetting and drying cycles)

#### 4.9 Microstructure of thaumasite and other deterioration products.

In this section, the results of scanning electron microscopy for the TSA and other deterioration products in selected cement samples are presented. The deterioration products and fractions from the surfaces of non-deteriorated samples were investigated by means of scanning electron microscopy. In addition, backscattered electron images (BSE) are used with EDX microanalysis to assist the identification of the phases present.

Figure 4.48 shows a micrograph of deteriorated CEMI sample exposed continuously to DS4 at 5 °C. As shown the majority of the sample is converted to thaumasite (the dark grey areas). A network of cracks is clearly observed in the matrix and around the aggregate particles and the sample is losing its integrity while CSH gel is being decalcified. The EDX microanalysis for spot A is shown in Figure 4.49, from which it may be

#### 4. Effect of wetting and drying cycles on thaumasite formation

noted that spot A consists of Ca, S, Si, in addition to O, and C. This is indicative of thaumasite sulfate attack, which was responsible for the damage caused to these regions.

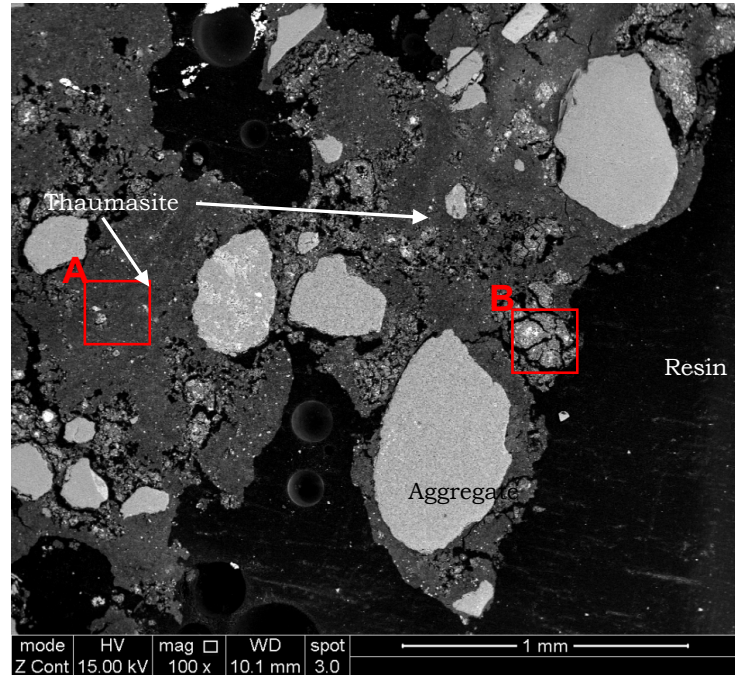


Figure 4.48 BSE of CEM I sample in DS4 at 5 °C in continuous immersion

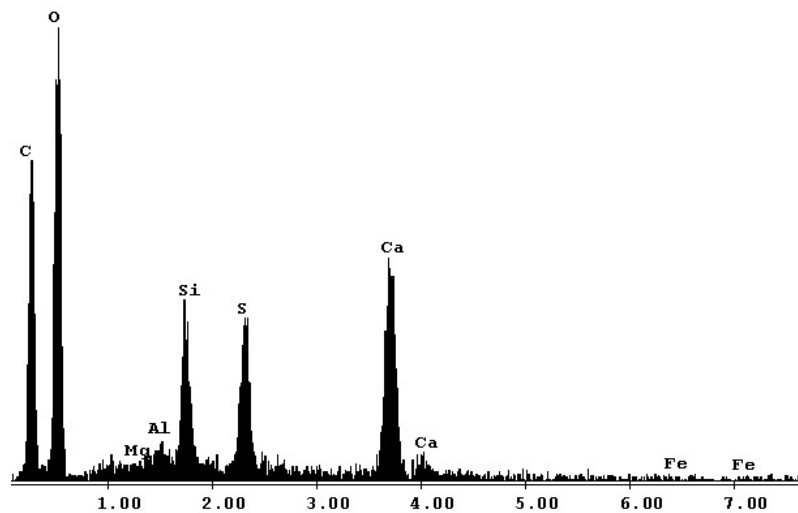
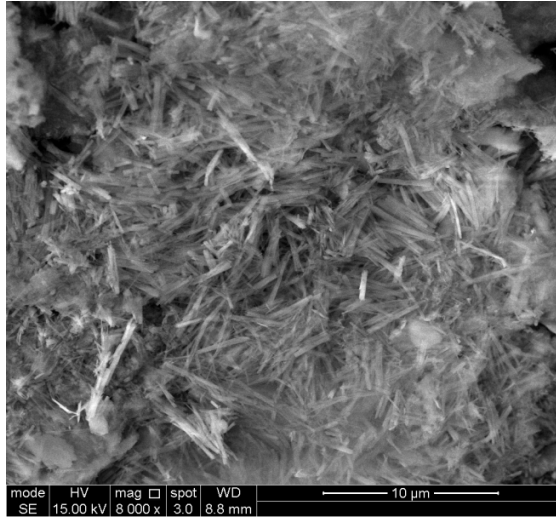


Figure 4.49 EDX microanalysis for spot A in Figure 4.48 showing thaumasite elements

#### 4. Effect of wetting and drying cycles on thaumasite formation

---

However, the presence of small aluminium peaks compared with silicon indicates the possible presence of ettringite in the corroded regions either as an end product of in a thaumasite ettringite solid solution. A high magnified BSE image for spot A is presented in Figure 4.50 where needle-like thaumasite crystals can be seen.



**Figure 4.50 Magnified BSE image for thaumasite crystals in CEM I sample**

A magnified image for spot B is shown in Figure 4.51 and the accompanying EDX analysis is shown in Figure 4.52, where these figures show the remains of calcium silicate hydrate gel CSH (the white regions) where only a few spots can be seen throughout the sample indicating the severe attack caused by thaumasite formation.

#### 4. Effect of wetting and drying cycles on thaumasite formation

---

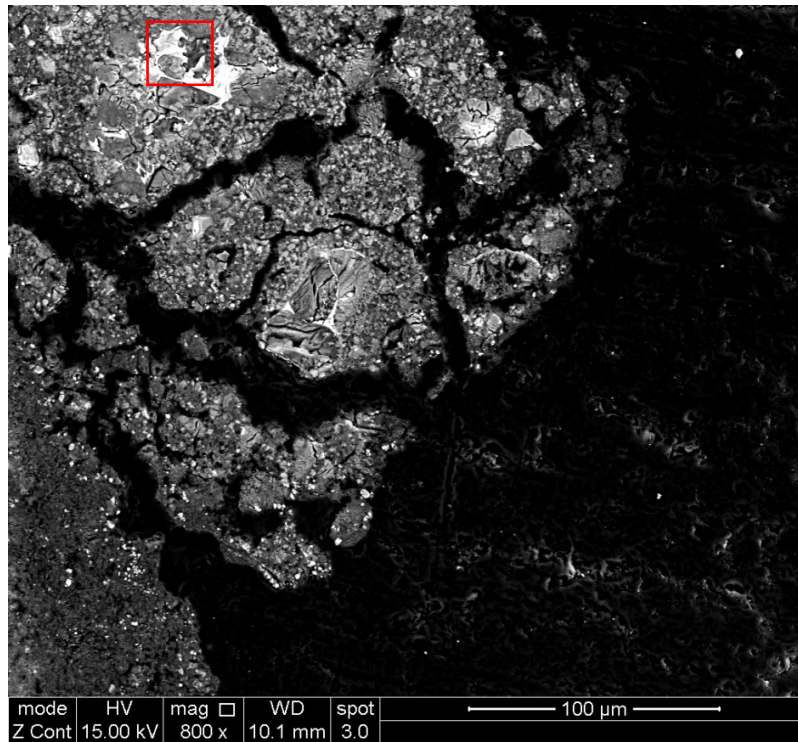


**Figure 4.51 Magnified BSE image for spot B in Figure 4.48**

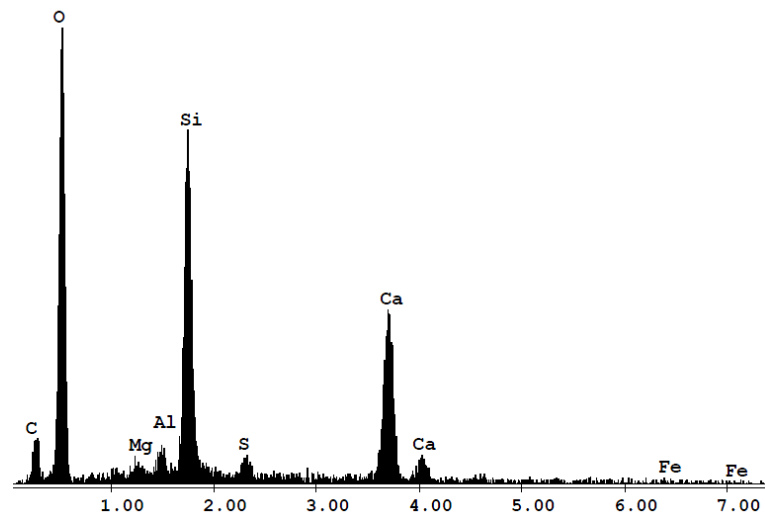


**Figure 4.52 EDX microanalysis for spot A in Figure 4.48 showing CSH gel**

#### 4. Effect of wetting and drying cycles on thaumasite formation

---

The SEM results for LFC are shown in Figure 4.53, in which cracks are seen to be developed in the sample and around the aggregate particles, and much of the sample is converted to thaumasite and badly deteriorated.

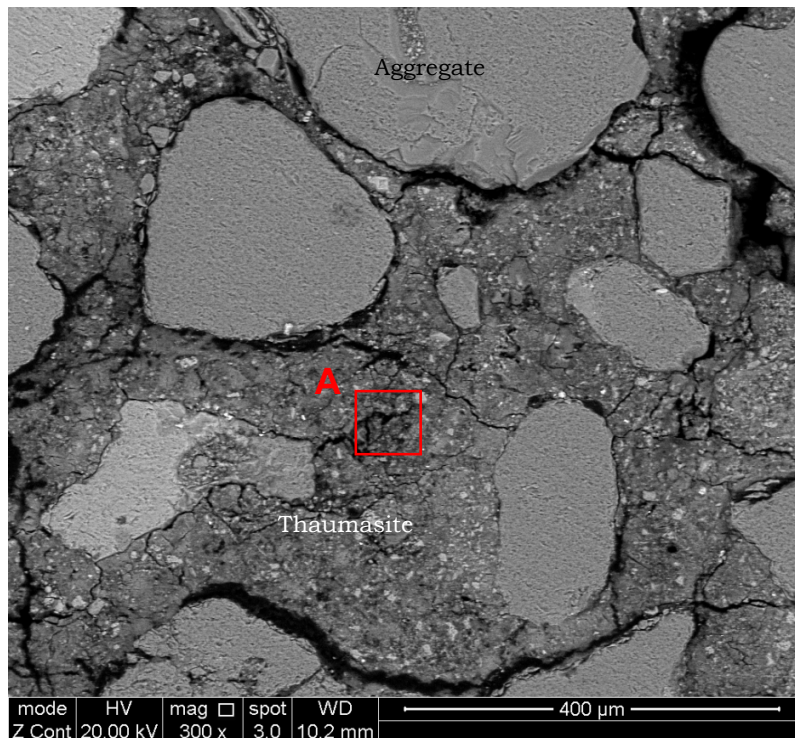


**Figure 4.53 BSE of LFC sample in DS4 at 5 °C in continuous immersion**

A magnified image for spot A is shown in Figure 4.54 where the needle-like thaumasite crystals are distributed through the sample. The microanalysis for this spot is illustrated in Figure 4.55, where Ca, S, Si, C, and O indicate the presence of thaumasite in the sample. However, the absence of Al peaks may indicate that there is no ettringite in the sample and thaumasite alone is the end product of the deterioration materials.

#### 4. Effect of wetting and drying cycles on thaumasite formation

---

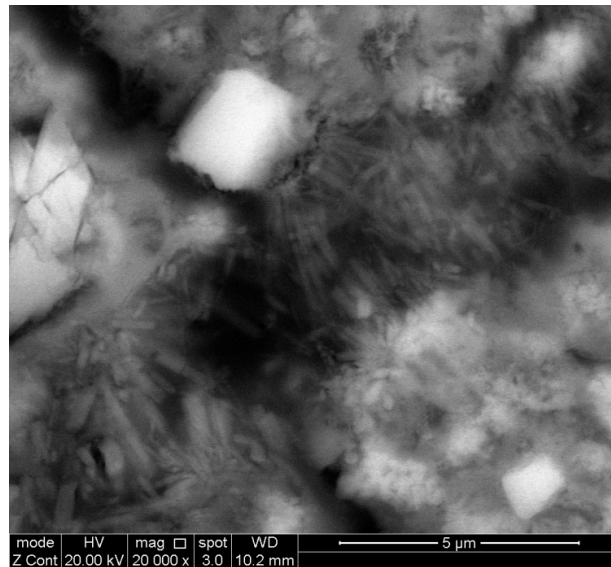


**Figure 4.54 Magnified BSE image for spot A in Figure 4.53**

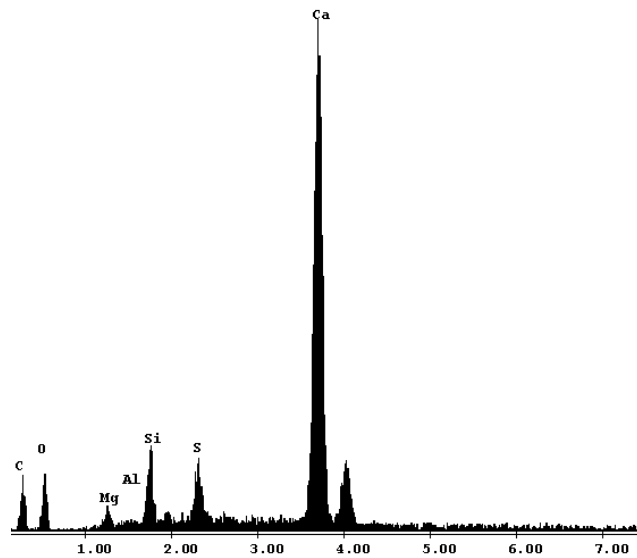


**Figure 4.55 EDX microanalysis for spot A in Figure 4.53 showing thaumasite elements**

For samples subjected to wetting and drying cycles the analysis where done for the outer layer and the results are presented in Chapter 5 where more attention is paid to the role of carbonation on the formation of thaumasite.

#### **4.10 Summary**

In this chapter, the results of the effect of wetting and drying cycles on the formation of thaumasite in cement mortars were presented and compared to each other. The summary of this chapter shall be presented in the next following points.

Thaumasite type of sulfate attack was responsible for causing severe deterioration to cement mortar made with CEMI and LFC exposed to BRE class DS3 and DS4 solutions stored at 5 °C, where it was found that serious damage could occur in a time as short as 3 months.

Samples subjected to wetting and drying cycles also showed signs of deterioration, but it was much lower than for continuously immersed samples, and it took a much longer time for the attack to happen. The time needed to cause damage to the samples was almost 3 times as that needed for continuously immersed samples.

The delay in thaumasite formation in samples subjected to wetting and drying cycles can be possibly attributed to different causes:

- Formation of carbonation layer as a result of the reaction between CO<sub>2</sub> available in the air during the drying time and portlandite in cement mortars. The resulting dense calcite layer would work as a physical barrier to slow the diffusion of sulfate ions and delay their ingress to the underlying cement paste.
- The formation of the carbonation layer could have consumed the portlandite, thus reducing one of the reaction elements necessary for thaumasite formation.
- It is likely that reactions would cease during the dry cycle as the moisture available for ion transfer and chemical interaction becomes more restricted. There is good agreement between the

#### 4. Effect of wetting and drying cycles on thaumasite formation

---

time needed for the thaumasite to form in the wetting and drying exposed samples and that needed in case of continuously immersed samples and the cycle length. The ratio was found to be 1 to 3 in both cases.

- The carbonation reaction lowers the pH of the mortar to around 8.3, the value at which is thaumasite is not favoured to form. (the effect of carbonation on thaumasite formation is studied in more details in Chapter 5)

Thaumasite is readily formed in temperatures as high as 20 °C once the other requirements for its formation are met. However the time needed for this formation is much longer and the quantities are less compared to its formation in temperatures as low as 5 °C.

Formation of thaumasite in sulfate concentration as low as 3 g/l  $\text{SO}_4^{2-}$  is very possible at low temperatures. However the extent of thaumasite formation at higher temperature at these low concentrations is not clear.

Cements containing more limestone filler are more susceptible to thaumasite formation in all cases at low temperature. On the other hand samples containing limestone filler performed a little better than plain cements at 20 °C.

Fly ash (PFA) and blast furnace slag (GGBS) blended cements performed very well in resisting thaumasite type of sulfate attack and showed no signs of deterioration after two years of exposure to sulfate solutions in both exposure regimes. On the other hand plain cement CEM I performed better than limestone filler blended cement. However, despite the fact that they did not show any physical damage after 2 years of exposure in DS4 sulfate solutions, the XRD and SEM results showed that cement blended with fly ash and blast furnace slag are susceptible to thaumasite formation TF, hence thaumasite is formed in the pores and voids and not causing any deterioration. However this stage could

#### 4. Effect of wetting and drying cycles on thaumasite formation

---

possibly precede the thaumasite sulfate attack TSA if the other conditions for thaumasite continue to occur.

It was reported by Mulenga et al. (2003) that cements containing fly ash are susceptible to thaumasite sulfate attack. However in this study, the initial air curing had possibly improved the performance of this cement type to resist thaumasite sulfate attack for up to two years.

A gradual increase in mass in both exposure conditions occurred during immersion in solutions. This continued until spalling led to a reduction in mass of the samples. However the onset of mass loss was earlier and the magnitude was higher in the continuous immersion regime. Moreover, samples suffered from thaumasite sulfate attack TSA showed great mass loss, where samples made of LFC lost more than 25% its original weight after 2 years of exposure.

Length change measurements did not show any significant changes in length for the mortars at the time when thaumasite started to form, this implies that measuring length change is not useful tool to assess the deterioration caused by thaumasite type of sulfate attack. In addition this also confirms that, the formation of thaumasite does not causing any significant length change. However an overall expansion was recorded for the deteriorated samples by the end of the study.

Thaumasite can readily form in media with pH values of as low as 8.7 as happened in wetting and drying samples. In continuous immersion samples the thaumasite started to form when the pH was 9.7. This value is near but less than 10.5 the value stated by Crammond (2003) as an optimum value for thaumasite formation. However the differences in pH values could be referred to different reasons such as:

#### 4. Effect of wetting and drying cycles on thaumasite formation

---

- The samples used for this study were air cured for 21 days before immersion in sulfate solution and this had probably led to reduction in pH values.
- The ratio of the volume of solution to the volume of solids in the samples was 4:1, which could cause pH values to drop by processes: first, the leaching resulting from the samples will have little impact on the composition of the solutions. Secondly: the high volume of solution led to high CO<sub>2</sub> availability in the water which could then react with samples and form a thicker carbonation layer that would cause more restriction on leaching, thereby reducing the values of pH.

The suggested mechanism of thaumasite formation in this study is the woodfordite route where thaumasite is formed from ettringite by replacing Al ions in the ettringite system with Si ions to form thaumasite.

The gypsum could serve as a source of sulfate during the later stages of thaumasite sulfate attack to form more thaumasite.

# 5

## Effect of Carbonation

### 5.1 Introduction

The results presented in Chapter 4 indicated that carbonation may have delayed thaumasite sulfate attack to samples subjected to wetting and drying storage regime. In order to investigate the effect of carbonation and carbonated layer of the formation of thaumasite in cement mortars, further investigation was made on the this role, where sample from all cement were tested for carbonation depth and powder samples where made from these samples and exposed to sulfate solution DS4 for 3 months at 5 °C. This chapter presents the results regarding the effect which the carbonation may have on the formation of thaumasite.

### 5.2 Carbonation depth

Figure 5.1 shows the depth of carbonation layer in each of these cements. Where the pink areas indicate high pH zones due to presence of portlandite, while the gray areas around the edges indicate low pH zones at which portlandite has involved in the carbonation reaction to form calcite. Figure 5.2 shows the carbonation depth for these samples in mm. As it can be noted from the graph, CEMI and LFC samples have similar carbonation depth of about 6 mm, these two cements showed the worst performance regarding thaumasite sulfate attack as shown in

Chapter 4. FAC sample has the highest carbonation depth of 14 mm while SLC has a carbonation depth of 7.5 mm.

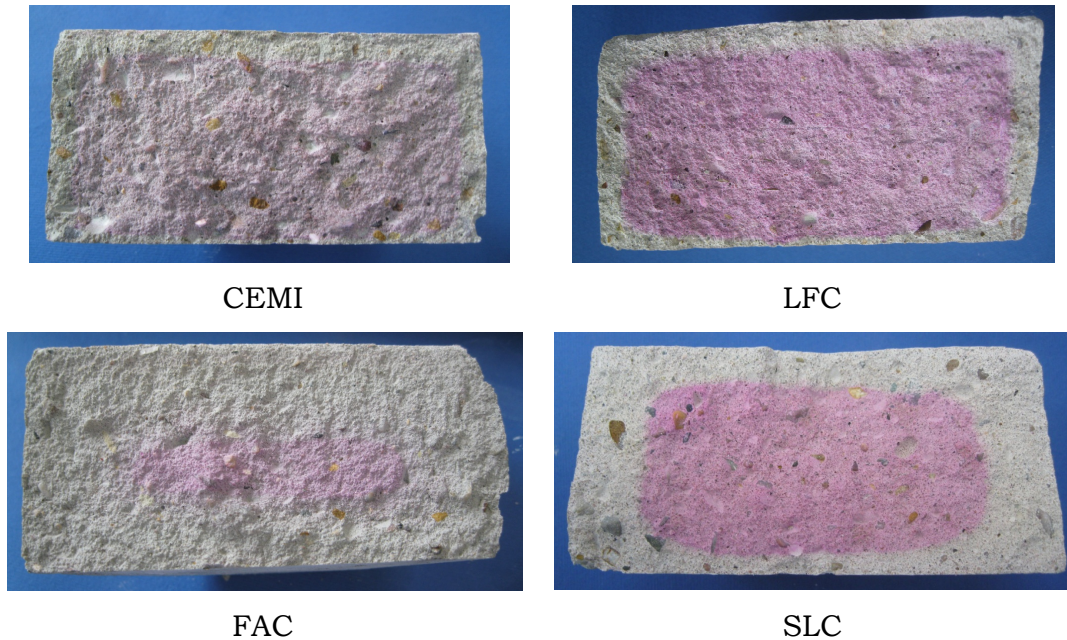


Figure 5.1 Carbonation results for different samples

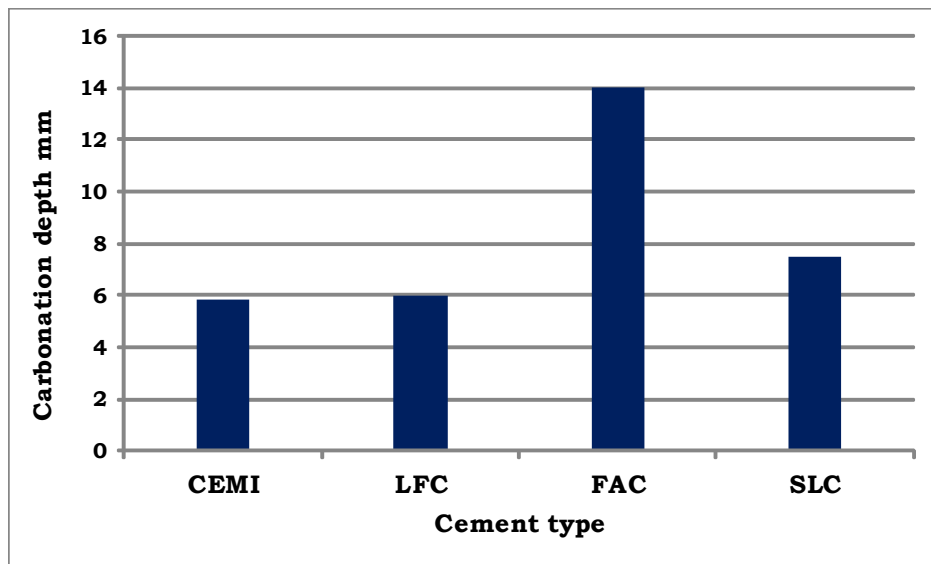


Figure 5.2 carbonation depth for different samples

As it can be observed there is a good agreement between the depth of carbonation and the visual deterioration of samples shown in Chapter 4

section 4.2. The wetting and drying cycles may have played a significant role in making the carbonation layer deeper during the drying cycle.

The effect of blended cement on carbonation depth of cement mortars or concrete has been studied in the literature by many authors, including Khan and Lynsdale (2002) who studied the effect of PFA on the thickness of the carbonated layer. They found that, increasing PFA level had led to an increase in the carbonation depth. Similar finding was reported by Byfors (1985) where he found that incorporation of PFA increased the rate of carbonation for test samples. Maage (1985) tested OPC samples blended with PFA and slag and concluded that the rate of carbonation was faster in blended cements concrete than those made with OPC. In another study Borges et al. (2012) compared the carbonation rates for OPC blended with different levels of PFA and GGBS and found that the carbonation rate is much faster in PFA samples compared to GGBS samples with same replacement level. The reason behind the FAC and SLC cement having the highest carbonation depth is coming from their higher replacement level which dilute cement content and from the pozzolanic reaction which involve consuming portlandite in order to form CSH phase.

### **5.3 pH measurements**

Figure 5.3 shows the pH values for the carbonated and core samples shown in Figure 5.1. As can be seen in this graph, there is a good correlation between the thicknesses of carbonation layers in Figure 5.1 and the pH values. Although the pH on non-carbonated layer was above the threshold pH value for thaumasite formation for all samples, the pH is significantly dropped to values where thaumasite is reported to be unstable for FAC and SLC. The pH of carbonated layers for CEMI and LFC was still high enough for thaumasite to form.

The relation between thaumasite formation and pH levels was explained by Crammond (2003) as follows: For ettringite and thaumasite to form, an extra calcium is required which can be obtained from portlandite and de-calcified CSH phase. As a result of this de-calcification, the pH of pore fluids will drop from around 13 towards 7. When the de-calcification is delayed as a result of magnesium ions on CSH, the pH will drop below 10.5, eventually this will stop thaumasite formation. A further fall of pH value towards 7 will make thaumasite unstable, and calcite will be the only calcium bearing stable phase.

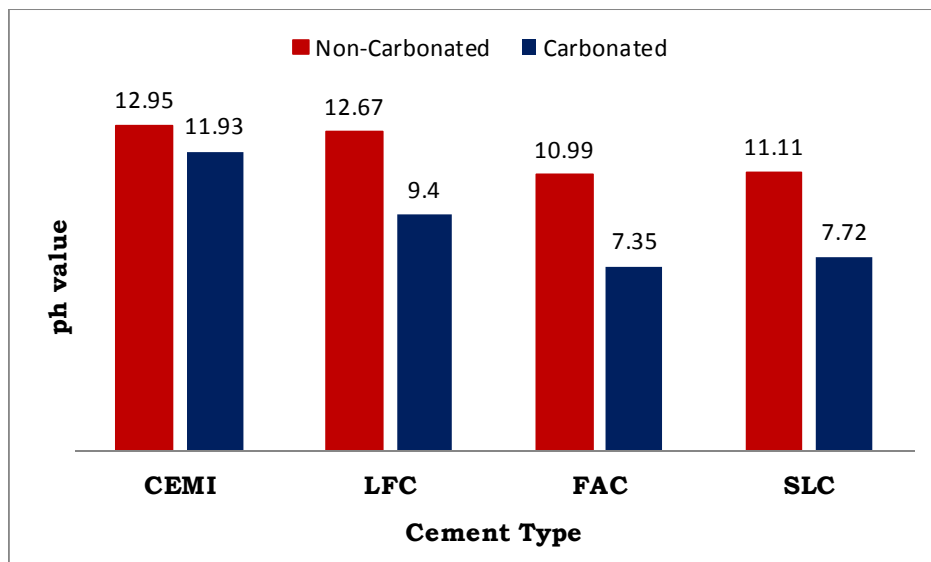


**Figure 5.3 pH values of carbonated and non-carbonated samples**

The low pH value also explains why less thaumasite was formed in wetting and drying samples, despite more calcium carbonate being present in the system when the latter is required to form thaumasite

#### 5.4 XRD analysis

The XRD results for the non-carbonated samples (core) are presented in Figure 5.4, as these show, the strong peaks at around (9.2 2 $\theta$ ) are attributed to either thaumasite or ettringite\thaumasite solid solutions.

## 5. Effect of Carbonation

These peaks can be seen in all samples with good strength indicating the formation of thaumasite in these samples. Gypsum can only be seen in FAC sample with peak at around (11.59 2θ) which is relatively stronger than thaumasite, the absence of gypsum from the other samples could be due to its consumption to serve as a source of sulfate to form more thaumasite or it may not been formed at all. Portlandite peaks at around (18.11 2θ) can be observed in all samples also but with different intensities, CEMI and LFC with the strongest peaks duo to the high amount of cement in them followed by SLC while only small portlandite peaks can be seen in FAC sample where portlandite possibly involved in the pozzolanic reaction to form more CSH gel. Calcite can be seen in all samples mainly at (29.5 2θ) and aragonite also present with small peaks in all samples. A strong peaks related to quartz in all samples come from crashed sand during sample preparation.

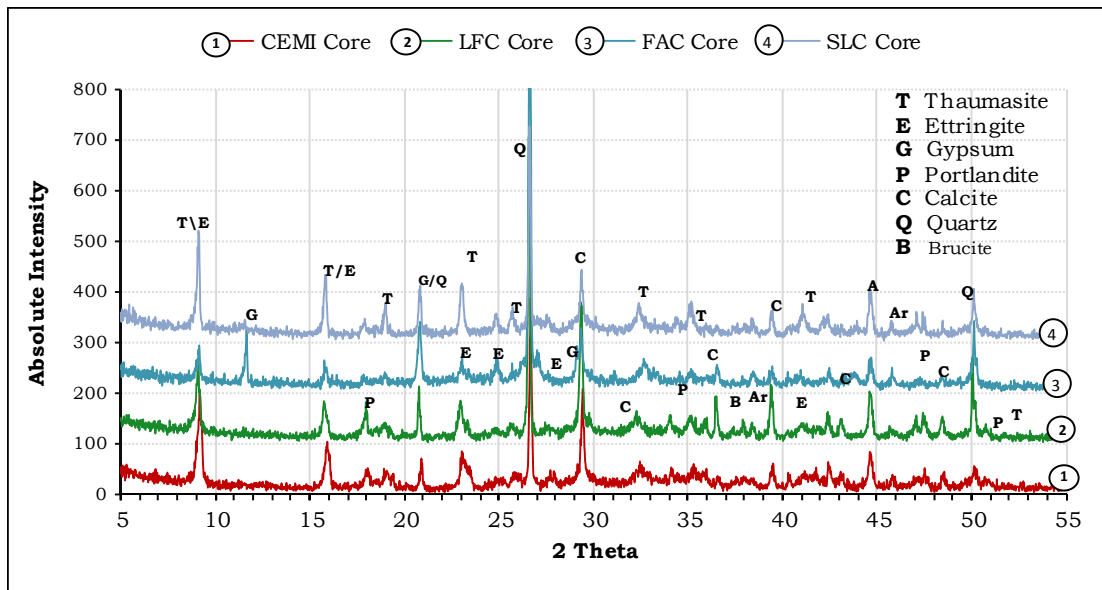


Figure 5.4 XRD patterns for core samples in DS4 at 5 °C

For the carbonated samples (surface), the XRD patterns are shown in Figure 5.5. As these indicate the presence of thaumasite, thaumasite containing phases only in CEMI and LFC samples and it is absent from FAC and SLC cements, this could be related to the low pH of these samples as shown in Figure 5.3 where these samples having pH of 7.35 and 7.72 respectively, these relatively low values make thaumasite unstable and prevent its formation (Jallad et al. 2003, Crammond 2003). This low pH value is more favour for gypsum formation which is available in all samples with strong peaks. Portlandite can still be seen with a strong peak in CEMI sample due to it is high cement content and with less intensity in LFC and it is absent from FAC and SLC samples due to the higher level of cement replacement materials and its involvement in the pozzolanic and carbonation reactions. Calcite peaks in these samples are relatively higher than the core samples due to more calcite formation as a result of carbonation reaction, and same observation could be applied for aragonite.

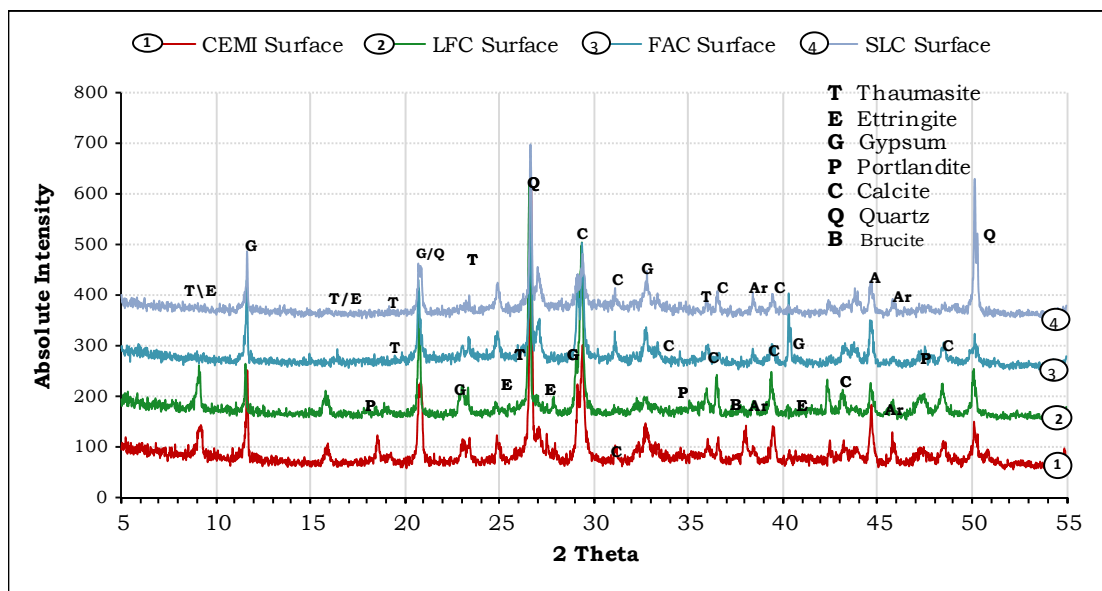
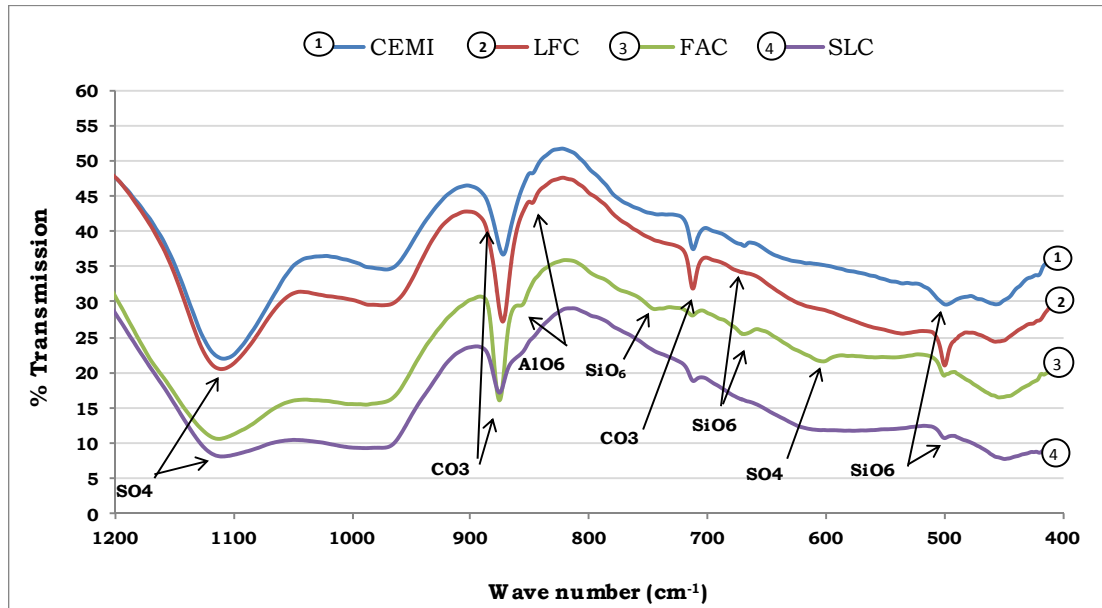


Figure 5.5 XRD patterns for surface samples in DS4 at 5 °C

### **5.5 Fourier Transform Infrared Spectroscopy (FTIR)**

The results of FTIR analysis for none-carbonated samples (core) are presented in Figure 5.6 . A presence of peak at  $500\text{ cm}^{-1}$  which is an indicative for thaumasite (Bensted and Varma 1973, Torres et al. 2004), these peaks can be seen in all samples with higher intensity in limestone containing sample LFC. Peak at around  $611\text{cm}^{-1}$  assigned to gypsum is only present in FAC in agreement to what was observed in XRD analysis for the same sample. Calcite peaks around  $712\text{ cm}^{-1}$  and  $875\text{ cm}^{-1}$  can be seen in all samples, they are more notable in CEMI and LFC probably due to more cement content and portlandite in these cements, while aragonite peaks at around  $700\text{ cm}^{-1}$  are absent from all samples. Ettringite peaks at around  $855\text{ cm}^{-1}$  are detectable in all samples with small intensities. However, the presence of these peaks indicates the co-existence of thaumasite and ettringite in these samples either as a two separate minerals or as a solid solution between the two. Peaks at around  $980\text{ cm}^{-1}$  are indicative for the presence of CSH gel in these samples, this suggests that this phase is still present in these samples and it is not converted to thaumasite yet. Sulfate peaks at around  $1100\text{ cm}^{-1}$  are attributed to sulfate in thaumasite structure and they are present in all samples.



**Figure 5.6 FTIR spectra for core samples in DS4 at 5 °C SiO<sub>6</sub> indicating Thaumasite, AlO<sub>6</sub> indicating Ettringite**

For the carbonated samples (surface), the FTIR spectra are shown in Figure 5.7. As these spectra represent, thaumasite peaks at 500 cm<sup>-1</sup> can only be seen in CEMI and LFC confirming the XRD results about the formation of thaumasite in these cements, however, peaks around 750 cm<sup>-1</sup> which is also attributed to SiO<sub>6</sub> (Bensted and Varma 1973) are present in all samples, this could be taken as an indication that thaumasite will be formed soon in these samples. Gypsum is present with strong intensity peaks in all samples but CEMI sample where it can be hardly seen. Gypsum peaks are stronger in fly ash and GGBS containing cements, which is possibly due to their low pH values as shown in Figure 5.3 which increase the stability of gypsum. Peaks attributed to ettringite at 855 cm<sup>-1</sup> are observed in all samples with small intensities. However these peaks were not detectable by XRD analysis Figure 5.5. Calcite is present in all samples and its peaks seem to be stronger than those observed for core samples, this is due more calcite

formation from carbonation reactions. Aragonite is hardly seen at around 700  $\text{cm}^{-1}$  in CEMI and LFC samples but it is absent from FAC and SLC cement samples.

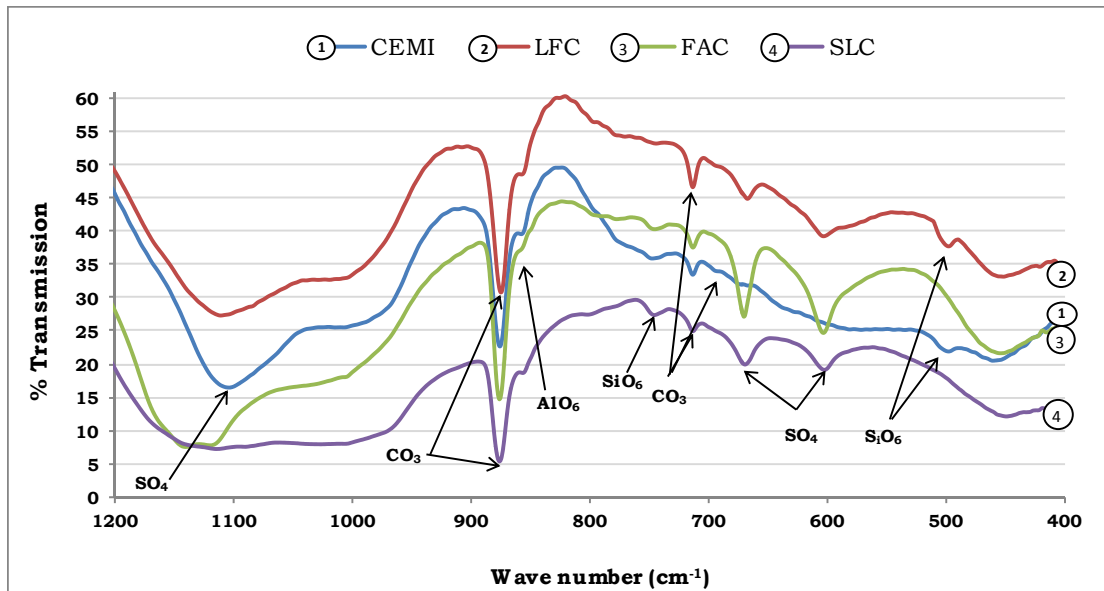


**Figure 5.7 FTIR spectra for surface samples in DS4 at 5 °C (SiO<sub>6</sub> indicating Thaumassite, AlO<sub>6</sub> indicating Ettringite)**

## 5.6 SEM analysis

The results presented in this section are for samples subjected to wetting and drying regime from Chapter 4. Where the small carbonated layer shown in Figure 5.8 was prepared and tested under SEM analysis.



**Figure 5.8 the outer layer used for SEM analysis**

The micrograph for this sample is shown in Figure 5.9. The sample is around 1.5 mm thick. The sample was divided to different zones depends on different in colours, scanning from inward towards outward. The EDX microanalysis for the dark gray area (zone no. 1) is shown in Figure 5.10. As this indicates, this layer is almost pure thaumasite, moving one step towards the outer layer (zone 2), the EDX microanalysis for this zone is shown in Figure 5.11 where the co-existence of Al peak together with Si peak could be taken as an indication of thaumasite ettringite solid solution in this region.

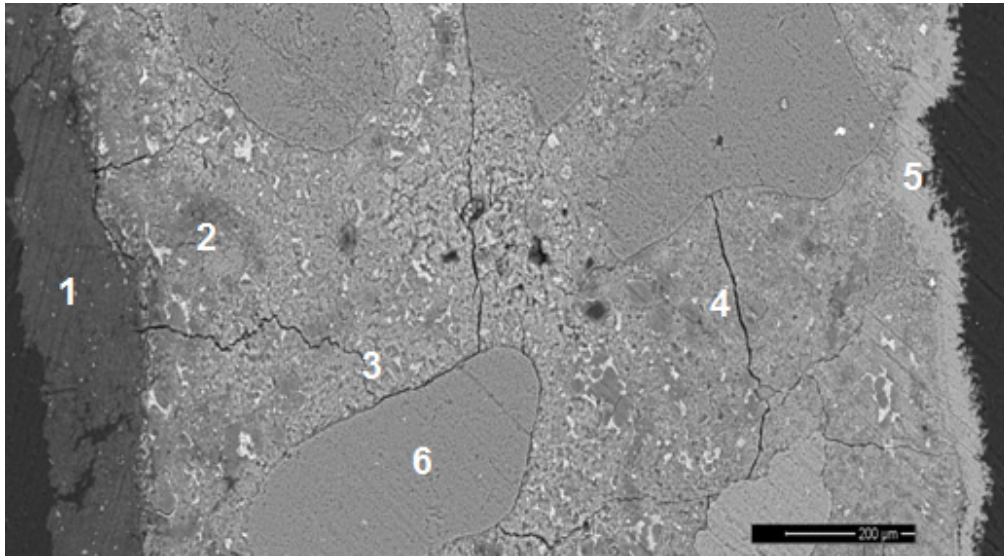


Figure 5.9 BSE of CEM I+ 10%LF sample in DS4 at 5 °C in under wetting and drying system

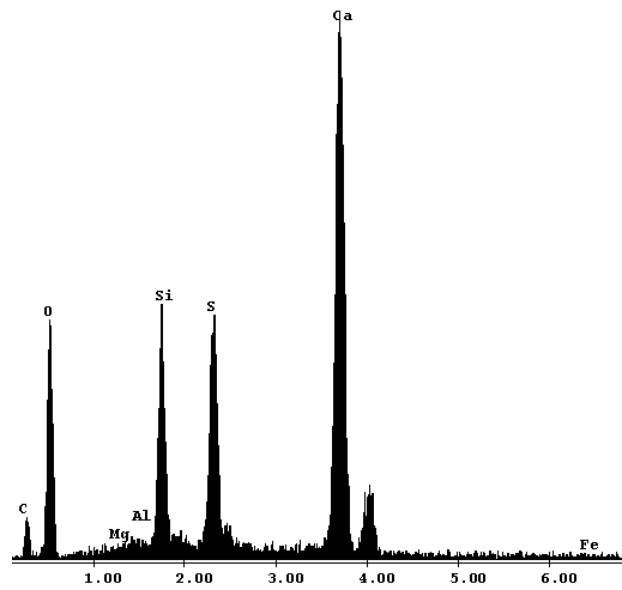
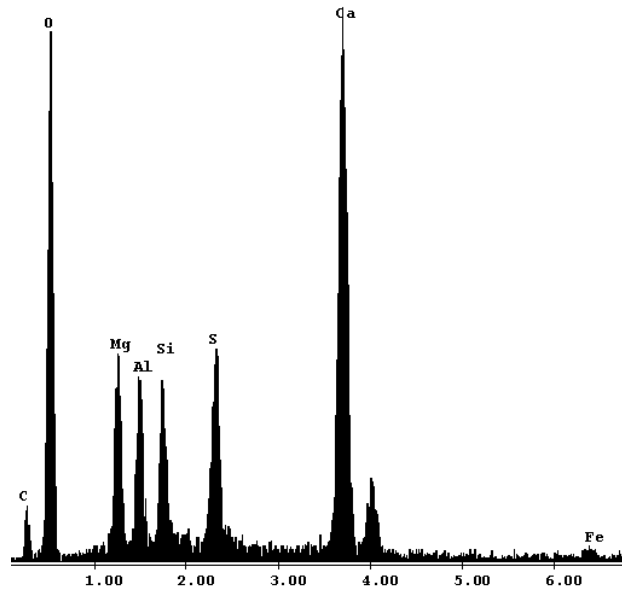
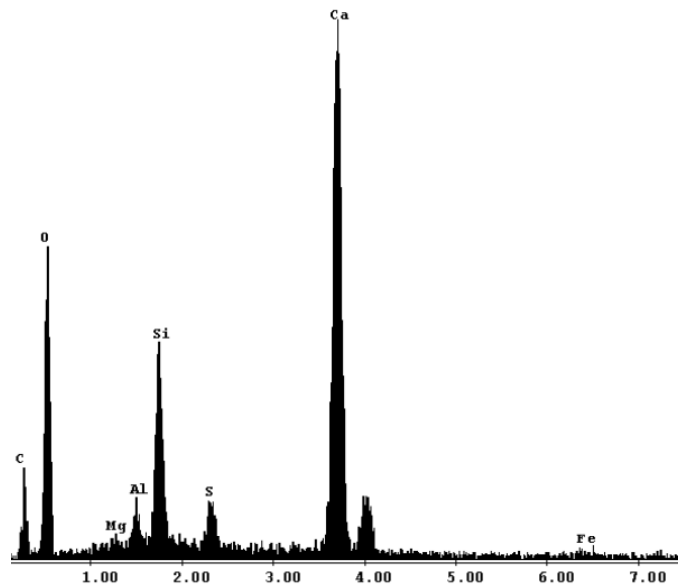


Figure 5.10 EDX microanalysis for zone 1 in Figure 5.9 showing thaumasite



**Figure 5.11 EDX microanalysis for zone 2 in Figure 5.9 showing thaumasite Ettringite solid solution**

It could also indicate that ettringite was formed first and then reacted again to form thaumasite; this layer could be a transition state between ettringite and thaumasite. Moving further towards the outer direction, another different layer can be identified (zone 3). The microanalysis of this layer revealed that it contains mainly Ca, Si and O peaks in addition to small peaks of Al and S which are attributed to calcium silicate hydrate gel CSH, this gives this layer the binding ability.



**Figure 5.12 EDX microanalysis for zone 3 in Figure 5.9 showing Calcium silicate hydrate**

The next layer is (zone 4) and as it can be seen from the DEX microanalysis in Figure 5.13, this layer mainly consists of O, Mg and Si peaks in addition to Ca, Al, and S in this zone magnesium is replacing Ca in the previous layer and forming what known as magnesium silicate hydrate, this layer probably formed as a result of the reaction between  $\text{MgSO}_4$  and cement paste (Prasad J et al. 2006).

The last layer (zone 5) is the layer in touch with solution. As Figure 5.14 shows this layer is a deposition of calcium carbonate resulting from the carbonation reaction. Zone 6 is indicating aggregate particles in the samples.

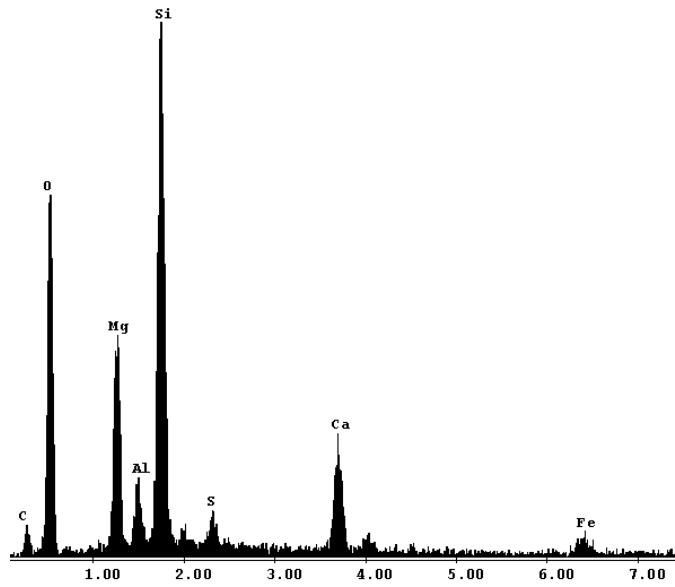


Figure 5.13 EDX microanalysis for zone 4 in Figure 5.9 showing magnesium silicate hydrate

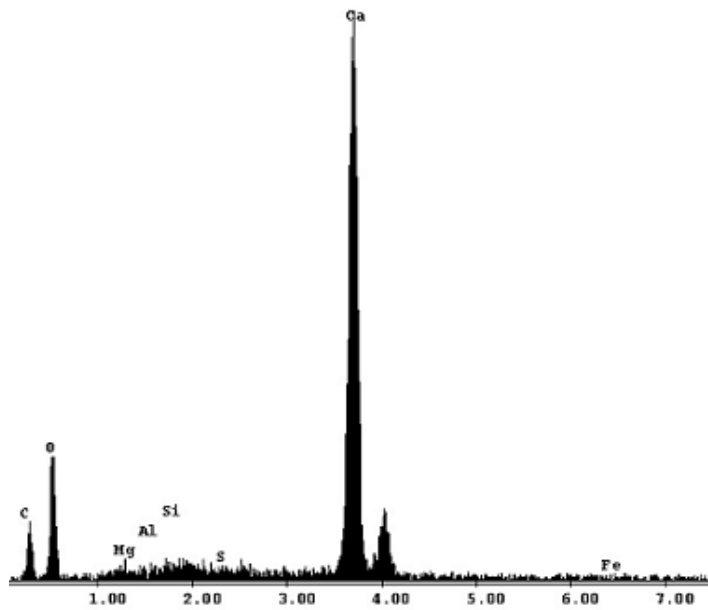


Figure 5.14 EDX microanalysis for zone 5 in Figure 5.9 showing calcium carbonate

## 5.7 Summary

The results presented in this chapter related to the effect of carbonation process on the formation of thaumasite in cement mortars. The summary of this chapter is presented in the next following points.

- The formation of thaumasite in carbonated zones can be retarded or prevented depending on the cement type.
- The Calcite layer formed during carbonation reaction may have worked as physical barrier to restrict more sulfate ingress to the mortar and improved the permeability by filling the pores.
- The low pH values of the carbonated layer may also retard the formation of thaumasite in these areas since thaumasite is not stable at low pH values (Jallad et al. 2003).
- Thaumasite was not formed in carbonated zones in samples made with fly ash and GGBS cements (FAC and SLC). However, gypsum was the dominant phase in these regions suggesting high susceptibility of these cements to classical type of sulfate attack at low temperatures.
- The carbonation depth in samples made with fly ash and GGBS cements (FAC and SLC) was deeper compared to CEMI and LFC samples, that may also gave these samples more resistance to thaumasite type of sulfate attack.
- Thaumasite may have formed through woodfordite route in which, ettringite is formed first as a result of sulfate attack and then it reacts with sulfate again to produce thaumasite.

# 6

## **Effect of water to cement ratio**

### **6.1 Introduction**

This chapter presents the effect of water to cement ratio, cement type, permeability and physical properties of concrete on the formation of thaumasite for up to 24 months, under various temperatures and sulfate solution concentrations. The results reported for 24 months exposure unless otherwise stated.

Four cement types were used in this study, as follows: 100% CEM I , 90% CEM I +10% LF, 50% CEM I + 50% PFA and 30% CEM I + 70% GGBS. For the first two cements three water to binder ratios were used: 0.45, 0.55 and 0.65 and for the latter two cements, ratios of 0.55 and 0.65 were used, as shown in Table 6.1. Following exposure to different environmental conditions, these results are compared with those for powders made of the same cements and exposed to the same conditions. This was to investigate the possible role of permeability on the good resistance to thaumasite sulfate attack reported in the literature (see Section 2.6.1.2) for GGBS containing cements.

**Table 6.1 Coding system for used cements**

Cement	Water: binder ratio		
	0.45	0.55	0.65
100% CEM I	CEMI-45	CEMI-55	CEMI-65
90% CEM I + 10% Limestone filler	LFC-45	LFC-55	LFC-65
50% CEM I + 50 % Fly Ash		FAC-55	FAC-65
30% CEM I + 70 % GGBS		SLC-55	SLC-65

Samples were exposed to DS3 and DS4 sulfate solution at 5 and 20 °C. Assessment was based on visual observations, mass and length change, XRD, FTIR, and SEM.

## 6.2 Visual observation assessment

Visual assessment of the samples was performed on a regular basis (two weeks). The results presented in this section compare the individual assessments within each cement to investigate the role of water to cement ratio on the visual appearance of samples after two years immersion in sulfate solutions.

### 6.2.1 CEMI cement samples

Figure 6.1 shows the appearance of CEMI samples after two years of exposure to sulfate solutions at different temperatures. Samples made with CEMI-65 exposed to DS4 at 5°C were the first samples to show signs of deterioration among this cement type. This took the form of small cracks appeared alongside the edges, which was recorded after around 100 days. The next set of samples to show signs of deterioration was CEMI-55 exposed to same solution at the same temperature at 115 days and the attack was similar to that seen in CEM-65.

6. Effect of water to cement ratio

Temperature	w/c	water	DS3	DS4
5 °C	0.45			
	0.55			
	0.65			
20 °C	0.45			
	0.55			
	0.65			

**Figure 6.1 Visual appearance of CEMI samples of various mixes under different exposure conditions and temperatures after 24 months.**

The CEMI-65 samples exposed to DS3 started to show signs of similar attack shortly after this at 120 days, followed by CEMI-55 in DS3 at 130 days.

The cracks appeared on CEMI-45 in DS4 at 250 days and the last samples to exhibit deterioration were CEMI-45 in DS3 and that was after around 270 days of exposure.

Samples exposed to sulfate solutions at 20 °C showed good resistance to attack and no signs of deterioration was recorded for up to 240 days, when samples made with CEMI-65 exposed to DS4 started to show small cracks around the corners. Samples made with the same cement exposed to DS3 showed similar cracking after about 30 days of exposure. A longer time was required for CEMI-55 exposed to DS4 to show first signs of deterioration which was at around 530 days of exposure while samples exposed to DS3 showed only small blistering after 24 months of exposure. None of the samples made with CEMI-45 cement showed any signs of deterioration and remained intact after 720 days of exposure to both sulfate solutions at this temperature.

### **6.2.2 LFC cement samples**

The visual appearance of LFC samples is shown in Figure 6.2. As it can be seen all samples kept at 5 °C suffered sulfate attack, although the intensity of the attack varies according to the sulfate concentration and water to cement ratio. The samples made with the highest w/c ratio namely LFC-65 samples which exposed to DS4 solutions were the first to show signs of attack after around 84 days of exposure followed by samples made with LFC-55 cement exposed to same solutions. Samples made with the lowest w/c ratio LFC-45 were the last to show signs of deterioration after around 120 days. The intensity of the attack increased rapidly as the w/c ratio increased.

6. Effect of water to cement ratio

Temperature	w/c	water	DS3	DS4
5 °C	0.45			
	0.55			
	0.65			
20 °C	0.45			
	0.55			
	0.65			

Figure 6.2 Visual appearance of LFC samples of various mixes under different exposure conditions and temperatures after 24 months.

It can be also noted that the samples exposed to DS3 solution suffered severe attack, but it was less than the deterioration caused by DS4 solutions in that samples were heavily damaged and lost their cubic shape, especially samples with 0.65 w/c ratio.

As Figure 6.2 shows, the performance of samples of LFC cements exposed to sulfate solutions at 20 °C was dramatically different, where all remained intact with a complete absence of signs of attack after 24 months of exposure to both sulfate solutions.

### **6.2.3 Visual observations of FAC cement samples**

The visual appearance of samples made with FAC after 24 months of exposing to sulfate solutions are shown in Figure 6.3. As this Figure illustrates, none of this type of cement (unlike the first two cements) showed any visual signs of deterioration as their edges remain sound and they kept their geometry. Neither the increase in concentration of the sulfate nor the increase in w/c ratio affected the visual appearance of the samples.

Temperature	w/c	water	DS3	DS4
5 °C	0.55			
	0.65			
20 °C	0.55			
	0.65			

**Figure 6.3 Visual appearance of FAC samples of various mixes under different exposure conditions and temperatures after 24 months.**

#### 6.2.4 Visual observations of SLC cement samples

Figure 6.4 shows the visual appearance of samples made with SLC cement at different temperatures in different solutions after 24 months of exposure. It can be clearly seen that the samples remained intact as the case of FAC, and showed high resistance to sulfate attack in both

6. Effect of water to cement ratio

temperatures and solutions. Again all corners and edges remained sound and no cracks could be visually observed.

Temperature	w/c	water	DS3	DS4
5 °C	0.55			
	0.65			
20 °C	0.55			
	0.65			

**Figure 6.4 Visual appearance of SLC samples of various mixes under different exposure conditions and temperatures after 24 months.**

### **6.2.5 Visual observations (overall comparison)**

Comparing the visual assessment results for all cements in different exposure conditions, it can be seen that the samples made with 10% limestone filler showed the worst performance among the other cements when compared to same conditions followed by CEMI while FAC and SLC did not show any signs of damage. However, a closer look to these results reveals that samples made with low w/c ratio with limestone filler addition performed better than samples made with no limestone addition and with higher w/c which may suggest that controlling the w/c ratio is more beneficial than controlling the limestone addition amount in order to retard thaumasite sulfate attack.

With regard to the sulfate concentration, it is clear that at 5 °C thaumasite can readily form in sulfate concentrations as low as 3 g/l SO<sub>4</sub>. However the higher the sulfate concentration the greater the damaged caused.

Concerning the exposing temperature it could be concluded from the results that the attack is more severe at lower temperature 5 °C, although samples made with CEMI and LFC showed significant signs of attack at 20 °C.

## **6.3 Mass Changes**

In this section the results of mass change for mortar samples exposed to sulfate solutions at different temperatures are presented. Results from all cements are compared to each other to investigate the effect of variation in water to cement ratio on the extent of the attack.

### **6.3.1 CEMI cement samples**

Figure 6.5 and Figure 6.6 show the mass change measurements for CEMI samples with different w/c ratios in different solutions at 5 °C and 20 °C respectively. As it can be seen, at 5 °C samples from all mixes

initially showed a gradual increase in their masses probably due to hydration products is being formed and filling the voids. It is also noted that as samples started to show signs of attack, their masses increased more rapidly. This is thought to be due to opening of cracks such that solutions are able to ingress further into the specimens which would cause samples to swell and gain more weight. In comparison, it can be seen that samples made with CEMI-65 showed the greatest level of mass loss (9% of initial mass) under immersion in DS4 solution. The same cement samples exposed to DS3 solutions shown a weight loss (3%) similar to CEMI-55 exposed to DS4. CEMI-55 samples exposed to DS3 showed a mass loss of around 1%, while both CEMI-45 samples did not show any significant mass loss after 24 months of exposure. The CEMI-45 sample exposed to DS4 showed the highest mass gain after the cracks started to appear and absorb more solutions, ending with about 2% increase. Sample exposed to DS3 maintained a constant mass in the last few months of exposure and showed no signs of mass loss.

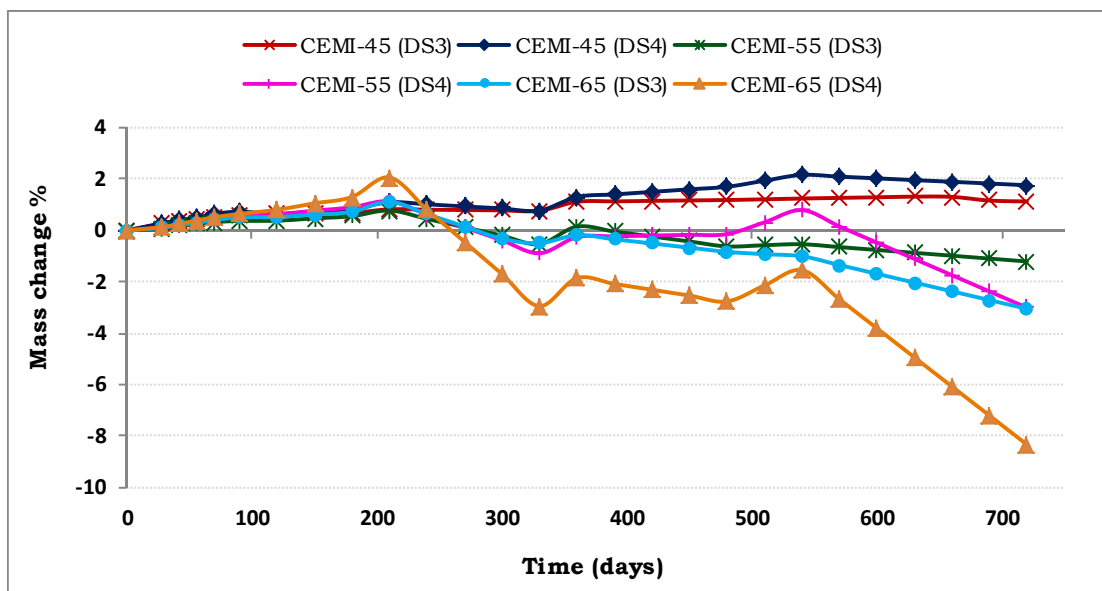


Figure 6.5 Mass change for CEMI samples in sulfate solutions at 5 °C .

Regarding samples exposed to sulfate solutions at 20 °C, as it can be seen in Figure 6.6, Samples made with high w/c ratio and exposed to DS4 showed the highest increase in mass of up to around 1.5% for CEMI-65 and 1.4% for CEMI-55 sample, where the former sample started to show some mass loss due to deterioration of the edges and corners while the latter did not show any signs of deterioration. CEMI-55 and CEMI-65 samples exposed to DS3 solutions behaved in a similar way to each other, where they both gained around 1.2% in mass and their rate of gaining weight increased, indicating that hair-line cracks started to form. Sample made with low w/c ratio such as CEMI-45 in DS3 and DS4 solution respectively continued uniform mass gain of almost 1%, indicating they were still sound, and without any hair-line cracks.

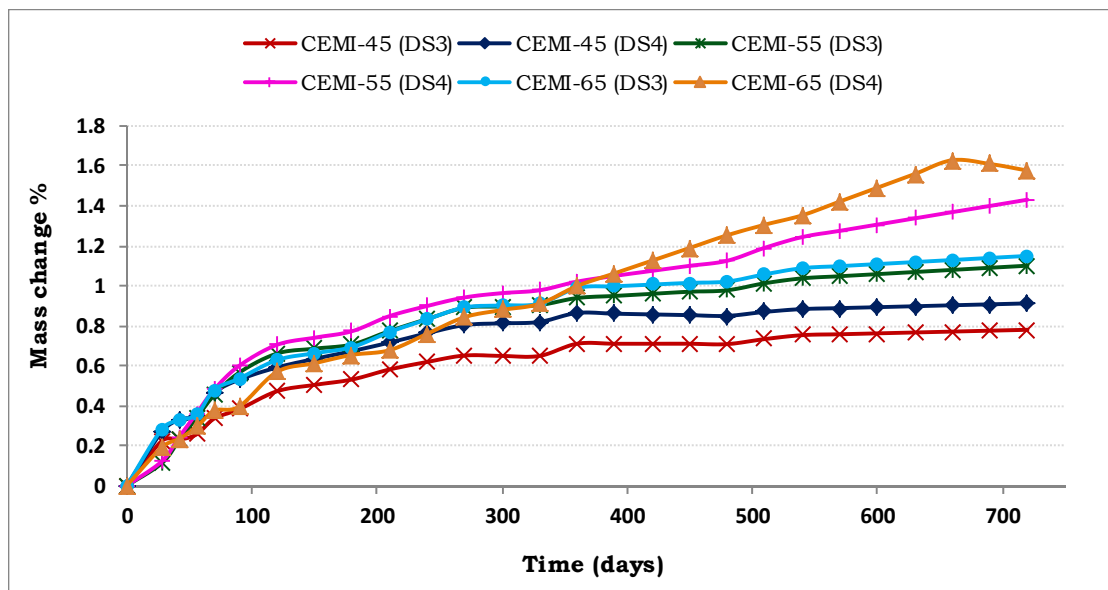


Figure 6.6 Mass change for CEMI samples in sulfate solutions at 20 °C .

### 6.3.2 LFC cement samples

The measurements for mass change plotted against time exposure for LFC are presented in Figure 6.7 and Figure 6.8. As observed visually in

section 6.2.3 all these samples showed visual deterioration, and in accordance with this, the mass change measurements, as it can be seen in Figure 6.7, demonstrate that all samples experienced mass loss. However, the degree of loss varies depending on w/c ratio and exposure solution. Sample made with LFC-65 exposed to DS4 solution showed the greatest mass loss of around 26%, followed by LFC-55 which lost around 20%. Interestingly, and as observed for CEMI samples, samples made with LFC-55 and LSC-65 in DS3 showed similar trends to each other ending up around 15% lost. Samples made with low w/c ratio LFC-45 showed the lowest levels of mass loss, where samples exposed to DS4 lost about 5% and samples exposed to DS3 lost less than 1% of its mass.

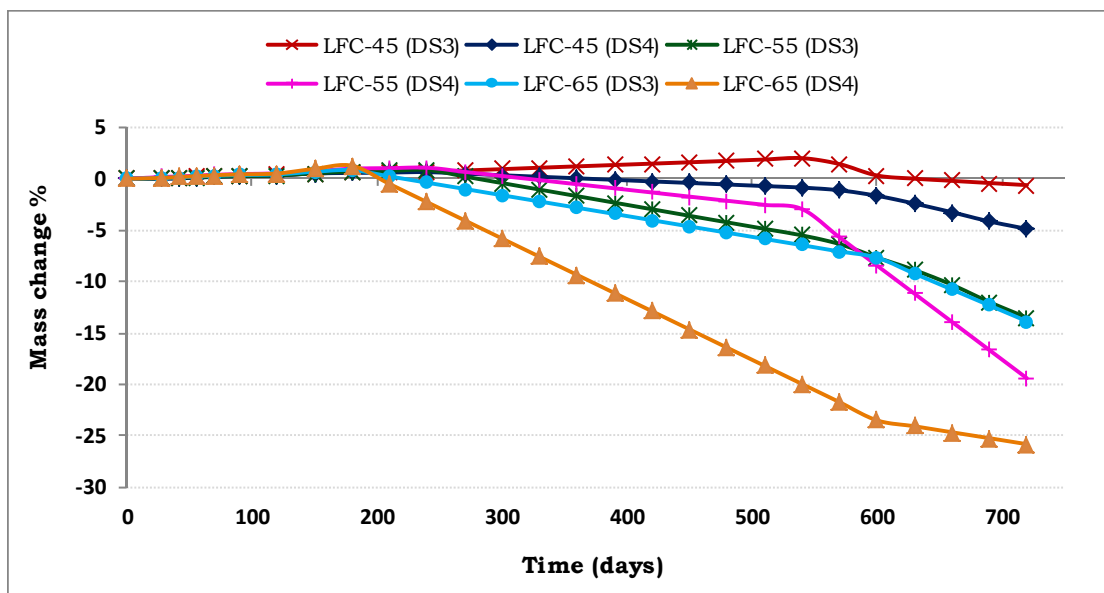


Figure 6.7 Mass change for LFC samples in sulfate solutions at 5 °C .

The results for LFC samples exposed to sulfate solutions at 20 °C are shown in Figure 6.8. As explained in section 5.2.2, there were no visual signs of deterioration but all samples showed a gradual increase in their masses that were greatest for higher w/c ratios and more severe

exposure solutions. The sample which showed the greatest mass gain was LFC-65 exposed to DS4 with about 0.9% followed with same cement samples immersed in DS3 with an increment of more than 0.8%. The samples made with low w/c ratio did not show any significant mass change and gained around 0.5% after 720 days of exposure to sulfate solutions.

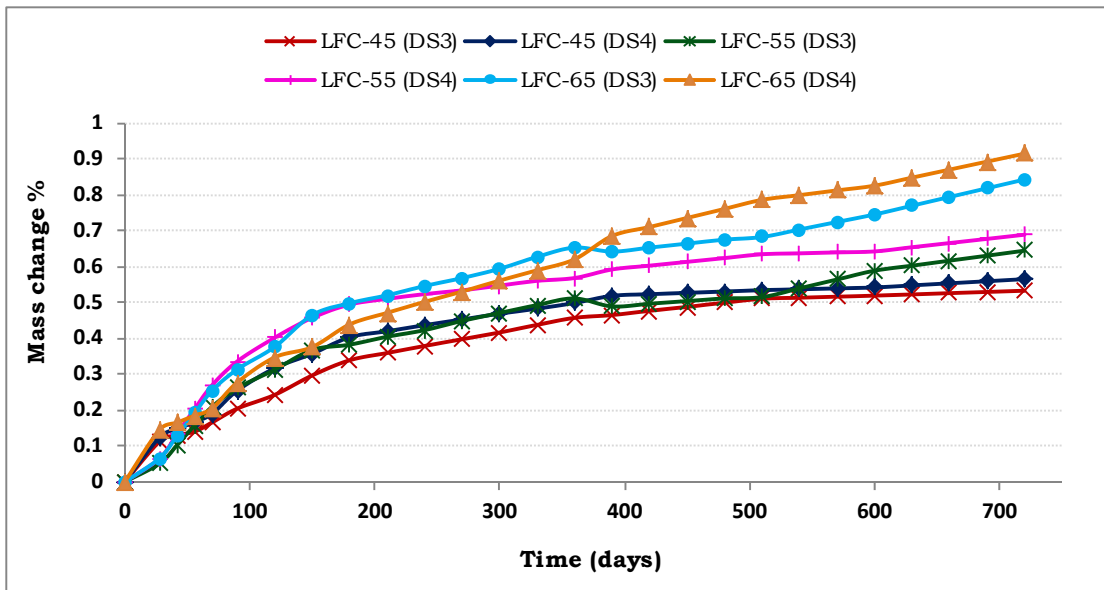
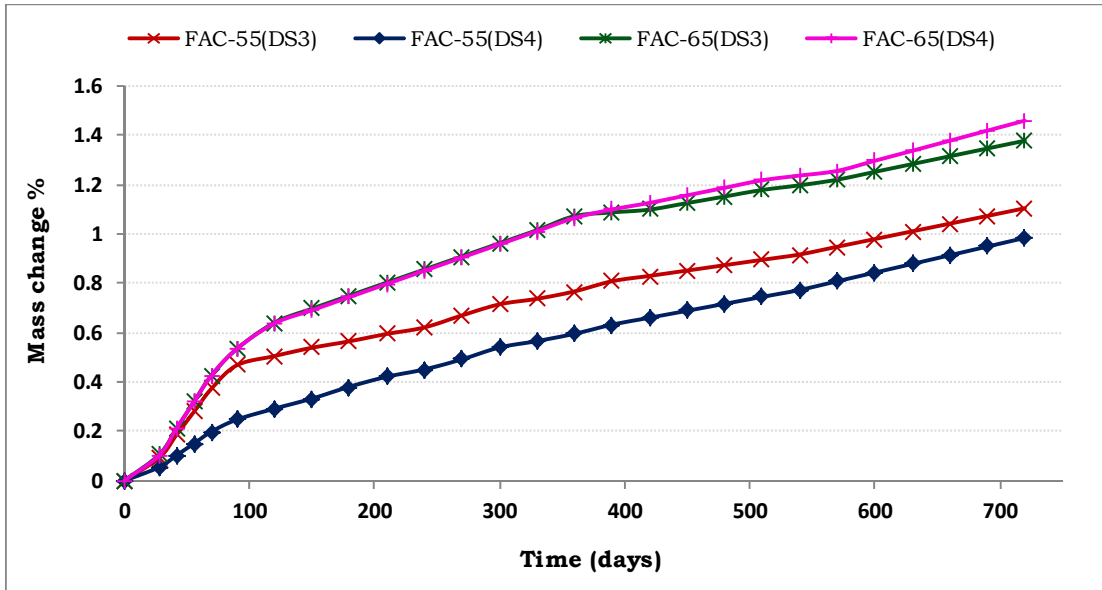


Figure 6.8 Mass change for LFC samples in sulfate solutions at 20 °C .

### 6.3.3 Mass changes for FAC cement samples

The results for mass change measurements for LFC samples are presented in Figure 6.9 and 5.10. As these samples did not show any visual damage (Section 5.3.3), they were not expected to show significant mass change. Indeed all samples at 5 °C show a continuous increase in their mass as a result of them absorbing solution and the formation of hydration products which would occur in these cements that undergo slow hydration reactions. However, FAC-65 cement samples showed a higher rate of mass increase of about 1.4%, probably due to their more porous structure regardless of the exposure solution, which seems not to

affect the performance of this cement. Samples with lower w/c ratio FAC-55 showed lower rate of mass increase and ended up with an increase of 0.9% in DS4 and 1.1% in DS3.



**Figure 6.9 Mass change for FAC samples in sulfate solutions at 5 °C.**

FAC cement samples kept at 20 °C showed similar trends regarding their mass change as shown in Figure 6.9. All samples showed an increase in their masses of around 1.1%. The differences in w/c ratios and concentrations of sulfate solutions had no significant influence on the performance of this cement at this temperature.

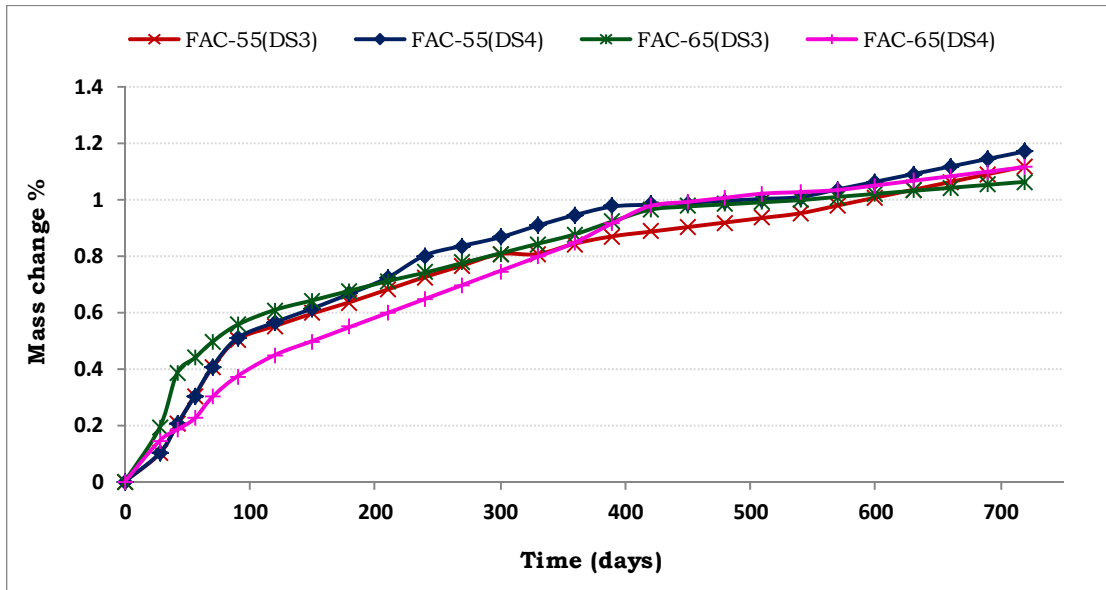


Figure 6.10 Mass change for FAC samples in sulfate solutions at 20 °C.

#### 6.3.4 Mass changes for SLC cement samples

Figure 6.11 and Figure 6.12 show the measurements of mass change for SLC samples. As it can be seen from these graphs, all samples followed similar trends which was they all showed a gradual increase in their masses throughout the monitoring time. It does not seem that these samples were influenced by the w/c ratio values, the concentration of sulfate solution or even the temperature.

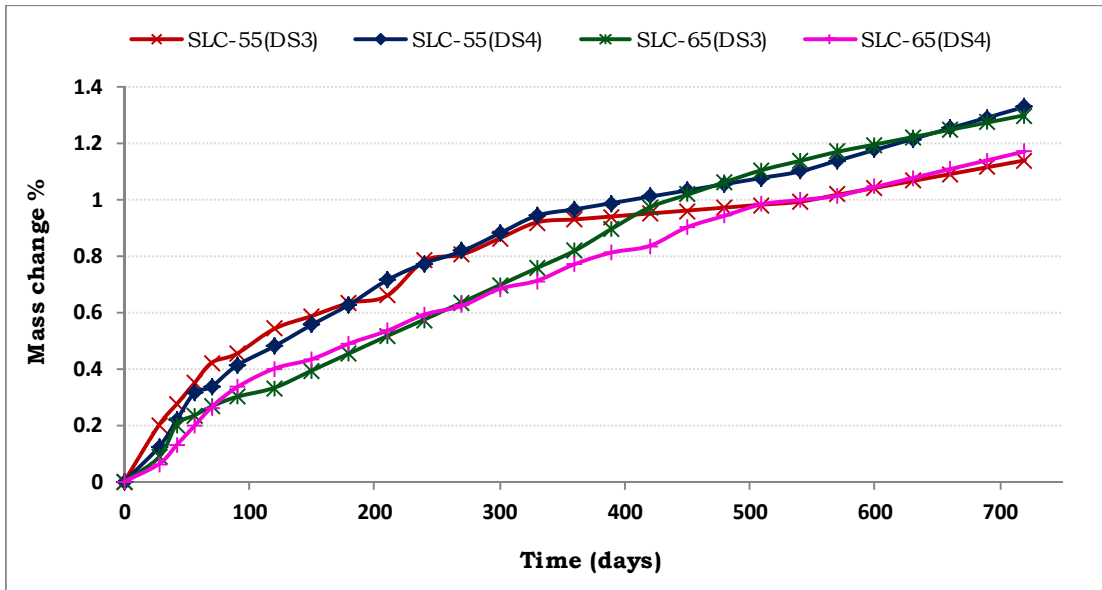


Figure 6.11 Mass change for SLC samples in sulfate solutions at 5 °C.

Samples recorded an increase in their mass of around 1.2%, which was expected since as explained in Section 5.3.4 these samples displayed no visual signs of attack or damage.

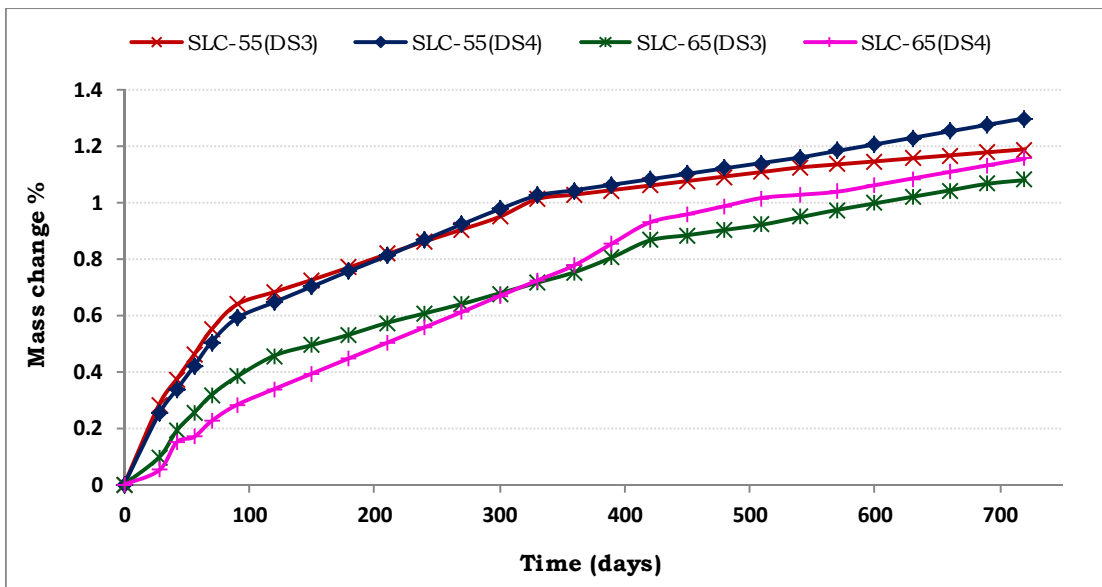


Figure 6.12 Mass change for SLC samples in sulfate solutions at 20 °C.

### **6.3.5 Overall comparison of mass changes**

The overall summary of the intensity of the attack based on the values obtained from mass change measurements for different cements is presented in Table 6.2. It could be concluded that the intensity of the attack is linked to the w/c ratio values, where samples with higher w/c ratios showed the greatest damaged. This may suggest that increasing w/c ratio from 0.45 to 0.55 had significantly affected the performance of cements to sulfate attack while increasing them again from 0.55 to 0.65 did not reflect the same amount of effect and the concentration of sulfate solutions was the dominant factor at the high level of w/c ratios of the samples in terms of their resistance to the sulfate attack. As the table shows, most of the mass losses were recorded for 5 °C, which is the temperature that would favour thaumasite formation rather than conventional sulfate attack.

**Table 6.2 Summary of the intensity of the attack based on mass loss for different samples.**

order	Cement type	Temperature	solution	Mass change %
1	LFC-65	5 °C	DS4	-25.81
2	LFC-55	5 °C	DS4	-19.39
3	LFC-65	5 °C	DS3	-13.86
4	LFC-55	5 °C	DS3	-13.50
5	CEMI-65	5 °C	DS4	-8.33
6	LFC-45	5 °C	DS4	-4.88
7	CEMI-65	5 °C	DS3	-3.05
8	CEMI-55	5 °C	DS4	-3.01
9	CEMI-55	5 °C	DS3	-1.21
10	LFC-45	5 °C	DS3	-0.62

## 6.4 Length change

In this section the measurements of length change are presented in order to investigate the possible relationship between thaumasite formation and any expansion that may have occurred in the samples.

### 6.4.1 CEMI cement samples

Figure 6.13 and Figure 6.14 present the change in length for CEMI samples with different w/c ratios and under different sulfate concentrations at 5 and 20 °C respectively. As Figure 6.13 illustrates, at 5 °C it can be noted that the change in length was small during the first year of exposure where all samples apart from CEMI-65 in DS3 solution

showed expansion of less than 0.1%. As attack was observed in some samples (CEMI-65 in DS4) after around 100 days, this may suggest that the attack did not cause any significant change in length up to the time when samples started to show significant signs of damage, here after one year of exposure in sulfate solutions. As far as the different water to cement ratios is concerned, it can be seen that CEMI-45 samples, with the lowest value, showed the least expansion despite showing visual signs

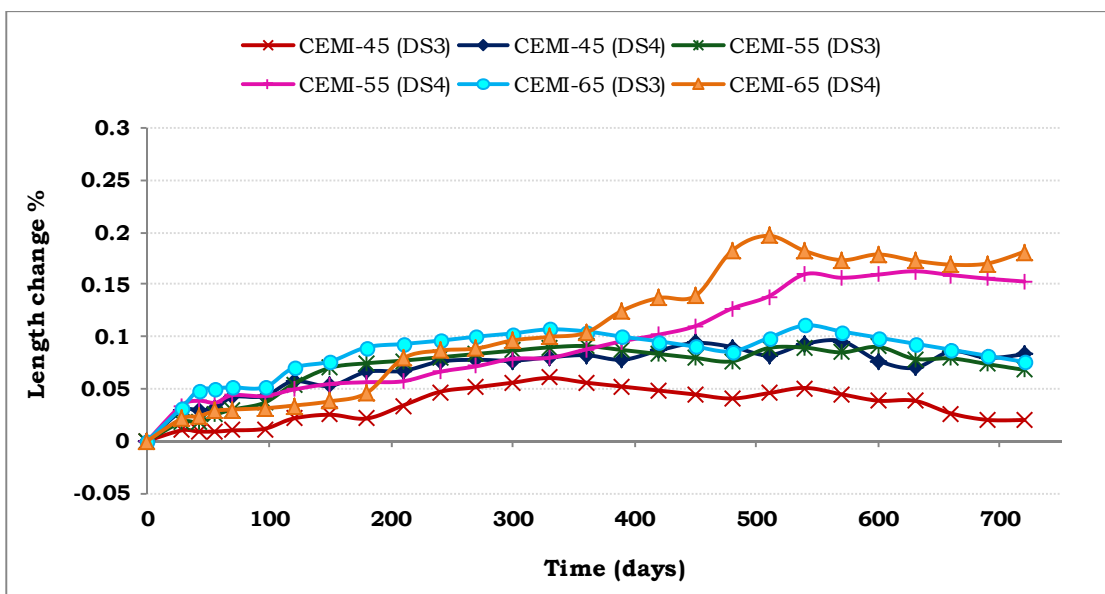


**Figure 6.13 Length change for CEMI samples in sulfate solutions at 5 °C**

of attack. CEMI-65 sample in DS4 showed the highest expansion value with about 0.2% after two years of exposure, which was in agreement with what was visually observations and loss of mass. Sample made with CEMI-55 cement exposed to DS4 was the one to follow with expansion value of 0.15%. Samples exposed to DS3 solutions showed expansion values less than 0.10% at the end of exposure, although these samples have shown mass loss and clear signs of visual attack.

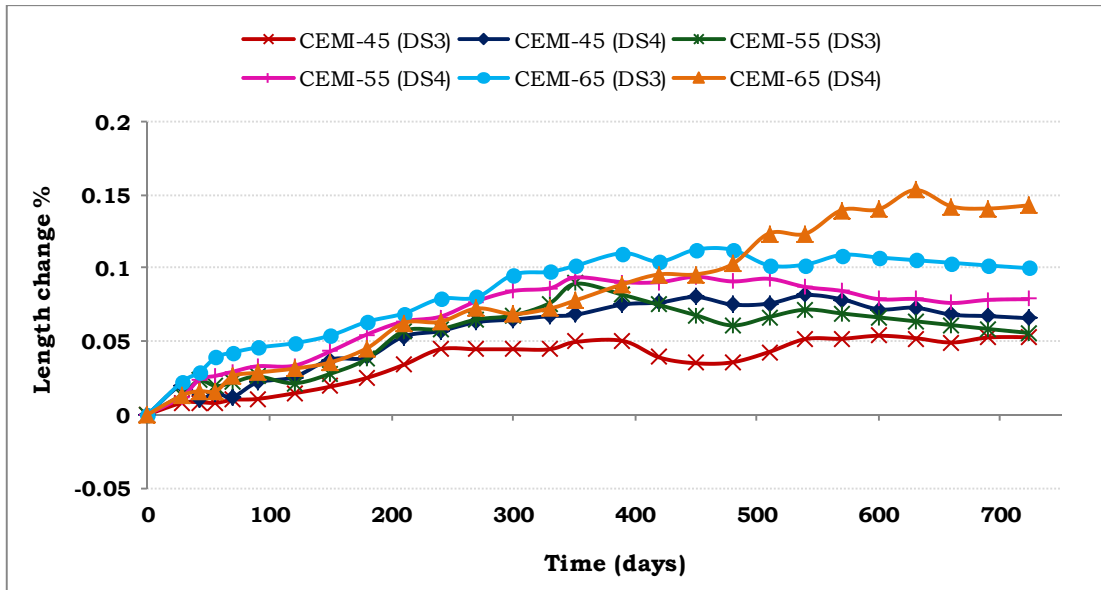


Figure 6.14 Length change for CEMI samples in sulfate solutions at 20 °C

At 20 °C, as shown in Figure 6.14, again samples made with the highest w/c ratio showed the highest level of expansion in both sulfate solutions with about 0.15% and 0.10% in DS4 and DS3 respectively. Samples made with 0.45 and 0.55 w/c ratios showed expansion values less than 0.10% throughout the whole period of exposure. In both temperatures, the rate of expansion was increased after the first year of exposure particularly in the deteriorated samples and the expansion in samples exposed to sulfate solutions at 5 °C was higher than those kept at 20 °C.

#### 6.4.2 LFC cement samples

Figure 6.15 and Figure 6.16 show the expansion values for LFC plotted against time at 5 and 20 °C. As noted for CEMI samples, no significant change in length was recorded during the first year of exposure. As Figure 6.15 shows, LFC-65 sample in DS4 showed expansion of about 0.35% followed by LFC-55 sample in same solution with about 0.27%, the later sample behaved in a similar way to LFC-65 in DS3 solution

which showed an expansion of about 0.26% at the end of exposure. Samples made with lower w/c ratio of LFC-45 showed the least expansion among all LFC samples with values around 0.10%. It is worth mentioning that these samples displayed obvious visual signs of attack in both solutions. Sample made with LFC-55 exposed to DS3 showed expansion of 0.18%.

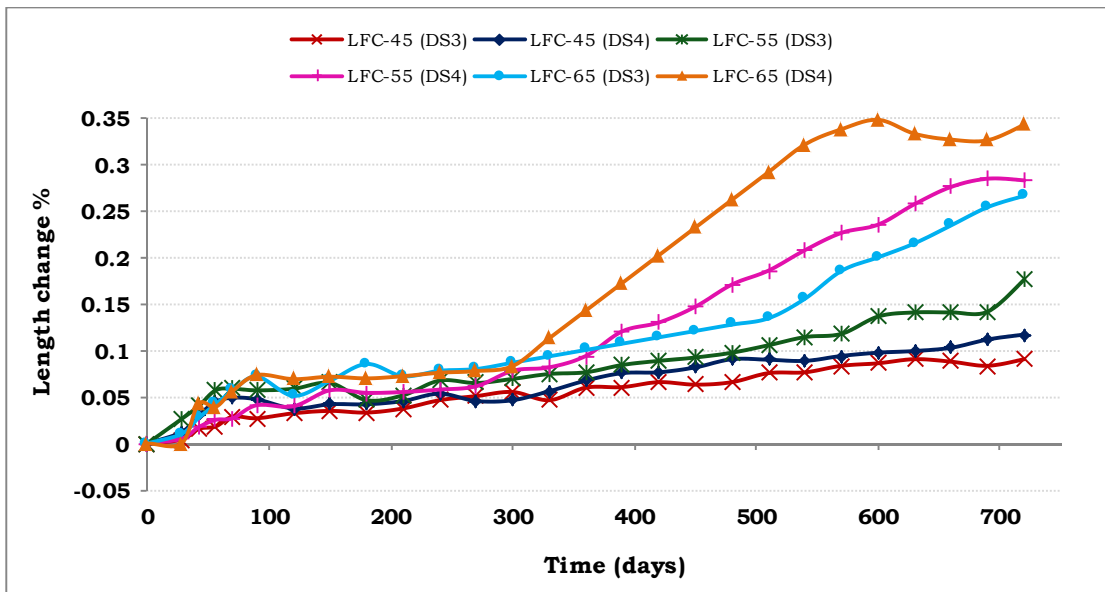


Figure 6.15 Length change for LFC samples in sulfate solutions at 5 °C

Samples exposed to solutions at 20 °C are shown in Figure 6.16. As mentioned in Section 5.2.2 none of these samples showed any signs of visual attack, and in accordance with this, the length change measurements also revealed that the expansion of these samples was small with some samples showing shrinkage rather than expansion. As per mass change, sample made with LFC-65 in DS4 showed the highest expansion value of about 0.07%. Although this value is still below the limit of 0.10%, it may indicate that this sample will be the first to suffer from attack.

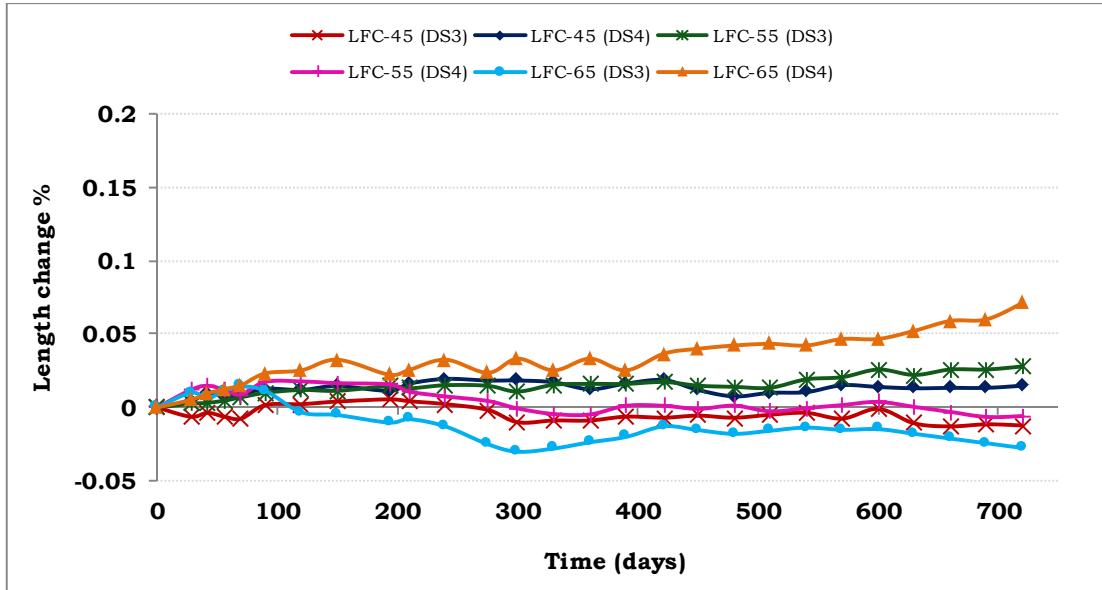


Figure 6.16 Length change for LFC samples in sulfate solutions at 20 °C

#### 6.4.3 FAC cement samples

The results of length change for FAC cement samples exposed to sulfate solutions at different temperatures are presented in Figure 6.17 and Figure 6.18. As these show, no significant change in length was recorded. This was expected since neither visual deterioration nor mass loss was recorded. Concerning the effect of w/c ratio on the expansion, it can be seen that samples with the lower w/c ratio FAC-55 are less affected and showed almost no expansion or shrinkage during the exposure time, while samples made with higher w/c ratio showed shrinkage of about 0.05% at both temperatures. It seems here that concentration of solutions had no impact on the performance of the samples which is probably due to the low permeability of these samples and the resulting in reduction in sulfate ingress in to the samples.

6. Effect of water to cement ratio

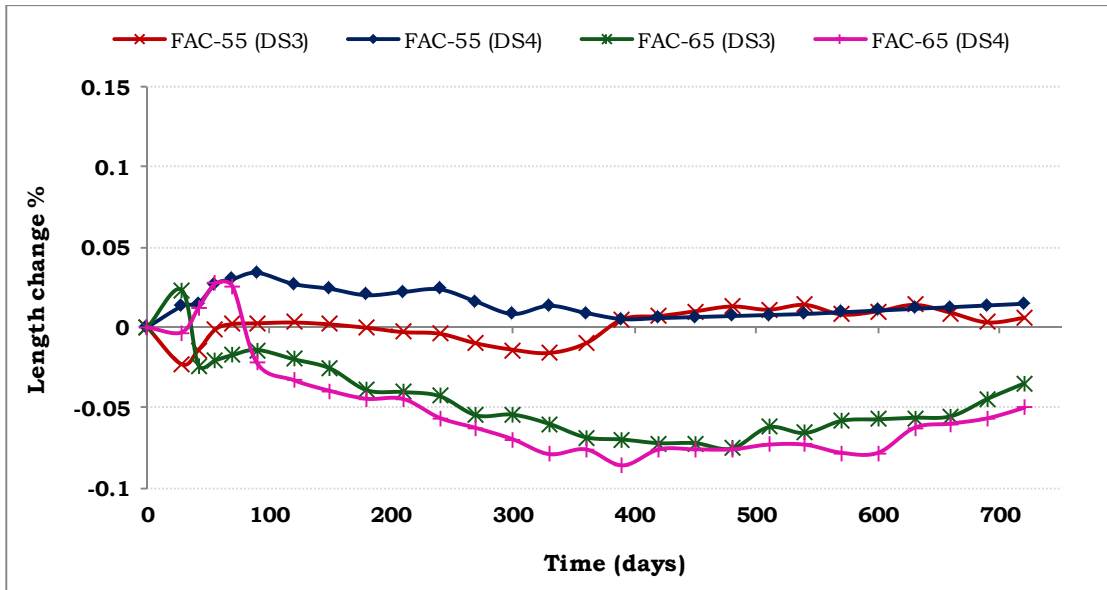


Figure 6.17 Length change for FAC samples in sulfate solutions at 5 °C

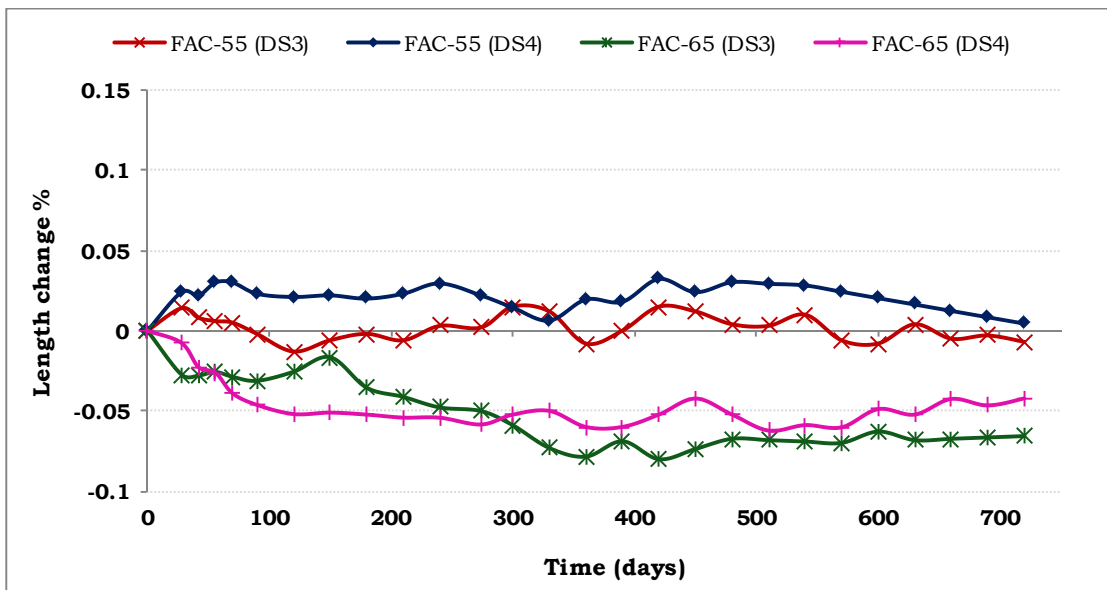


Figure 6.18 Length change for FAC samples in sulfate solutions at 20 °C

#### 6.4.4 SLC cement samples

Figure 6.19 and Figure 6.20 show the length change measurement results for SLC samples after two years of exposure to sulfate solutions at 5 and 20 °C. None of these samples showed any visual signs of deterioration after two years of exposure to sulfate solutions in both temperatures which is reflected in the very low length change measurements obtained for these samples. However, the variation in length in samples with low w/c ratio SLC-55 was very small for samples kept at 5 °C. Samples made with higher w/c ratio SLC-65 which showed a little shrinkage during the exposure period.

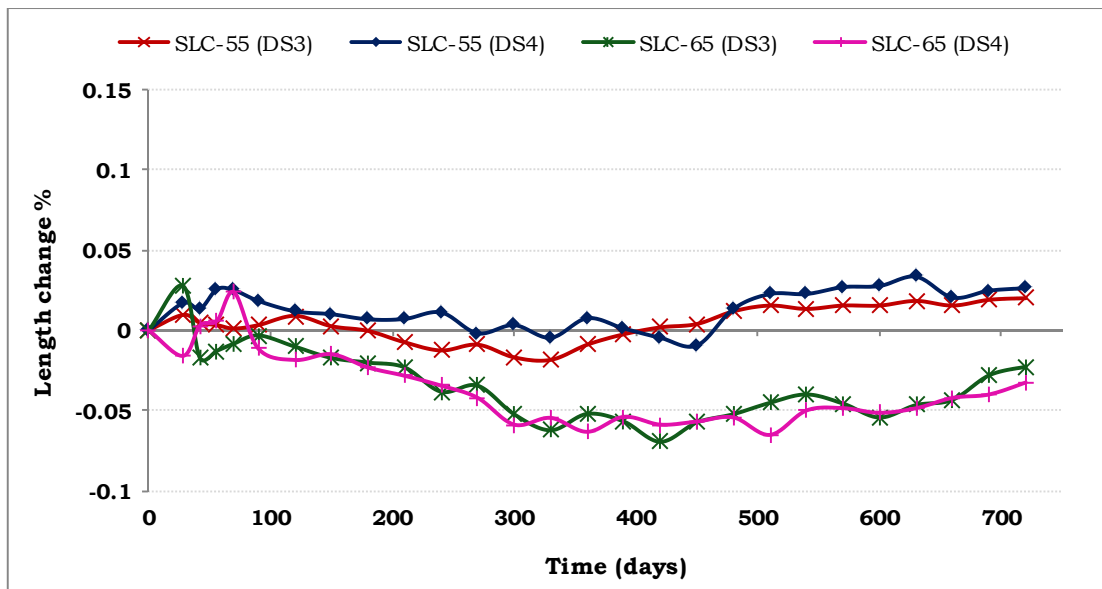


Figure 6.19 Length change for SLC samples in sulfate solutions at 5 °C

At 20 °C and as shown in Figure 6.20, all samples followed the same trends and showed a small shrinkage. As for FAC cement samples, the concentration of the sulfate solutions did not seem to affect the performance of these samples possibly for the same reason where the low

permeability and improved the microstructure of these samples protected them from the ingress of external sulfates.

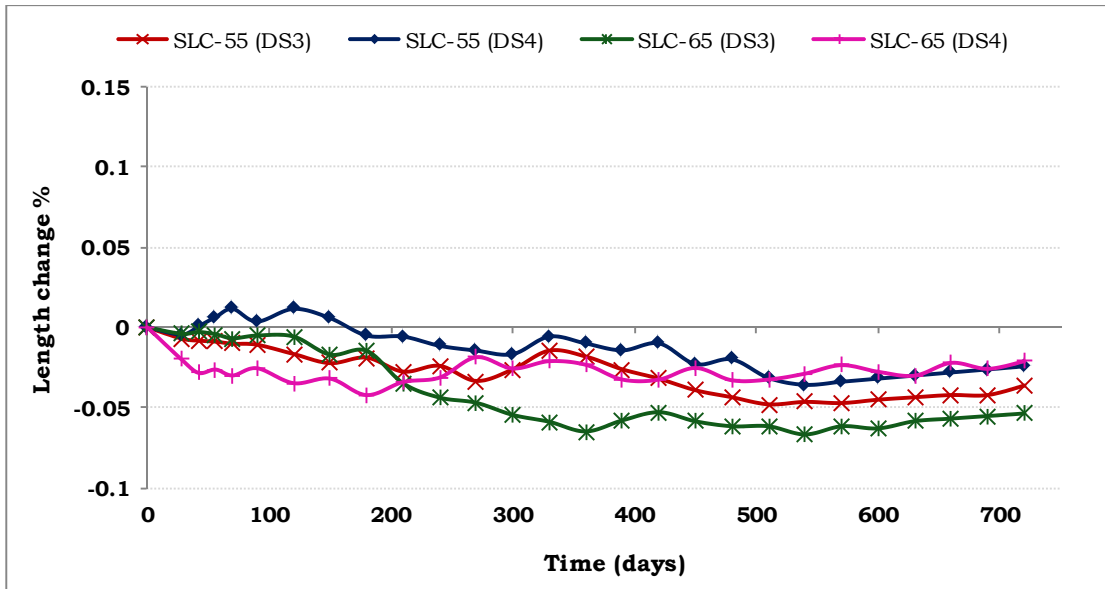


Figure 6.20 Length change for SLC samples in sulfate solutions at 20 °C

#### 6.4.5 Length change (overall comparison)

The summary of the length change results for the deteriorated samples from different cement is presented in Table 6.3 whereby it can be noted that samples that suffered from severe damage showed the highest expansion values. The higher expansions were also recorded for the higher w/c samples especially in strong sulfate solution DS4, while in lower w/c ratio samples, the expansion was below the limit set by ASTM C1012 standard which is 0.10%.

**Table 6.3 Summary of Length change results for the most deteriorated samples**

order	Cement type	Temperature	solution	Expansion %
1	LFC-65	5	DS4	0.34
2	LFC-55	5	DS4	0.28
3	LFC-65	5	DS3	0.27
4	CEMI-65	5	DS4	0.18
5	LFC-55	5	DS3	0.17
6	CEMI-55	5	DS4	0.15
7	CEMI-65	20	DS4	0.14
8	LFC-45	5	DS4	0.11
9	CEMI-65	20	DS3	0.1
10	LFC-45	5	DS3	0.09
11	CEMI-45	5	DS4	0.08
12	CEMI-55	20	DS4	0.08
13	CEMI-65	5	DS3	0.06
14	LFC-65	20	DS4	0.071
15	CEMI-55	5	DS3	0.07
16	CEMI-45	20	DS4	0.06
17	CEMI-55	20	DS3	0.05
18	CEMI-45	20	DS3	0.05

## 6.5 X-Ray Diffraction

This section presents the XRD results for two types of samples: 1) Solid Samples: deterioration products collected from the samples described in pervious sections, where in cases that samples that did not show signs of attack, small fractured pieces (about 1mm thick) were taken from the surface of the specimen and 2) , Powder Samples: sub-samples of the crushed concrete (See Section 3.4.2) from samples made with the same cements that were exposed to the same conditions as the solid samples, The results from both types of samples are compared with each other in order to investigate the effect of concrete permeability and microstructure on the formation of thaumasite. By eliminating the effect of permeability in the latter powder samples it would be possible to determine whether the main control on the performance of the concretes was due to chemical effects, or the impact of physical effects, particularly porosity and permeability. Powders were evaluated after exposure periods of 3 and 12 months.

### 6.5.1 XRD for CEMI cement samples

The XRD results for samples collected form CEMI solid samples at 5 °C in different solutions are shown in Figure 6.25. As the figure shows, the trends are similar for all samples, with High intensity peaks observed at  $2\theta$  around 9.2, 16 and 23.5° signify thaumasite, ettringite, or thaumasite-ettringite solid solution, since both minerals have very similar crystal structures. This also confirms that the visual damage observed (See Section 6.2.1) in these samples is due either to thaumasite formation or a thaumasite containing phase. Gypsum was clearly identified (at 11.59°  $2\theta$ ) in all samples exposed to DS4 solutions, but not in any of the samples which kept in the lower sulfate concentration DS3 solutions. Portlandite was also seen (at 18.11°  $2\theta$ ) in all samples at similar intensity. Brucite was also detectable (at 37.98 and 50.88°  $2\theta$ ) in

all samples, however these peaks seemed to be sharper in DS4 exposed samples, where more magnesium was available to produce more brucite. Quartz can be seen in all samples as well as calcite, where the peaks for the latter are not quite strong due to the low level of carbonate in this cement. Aragonite is also notable in all samples.

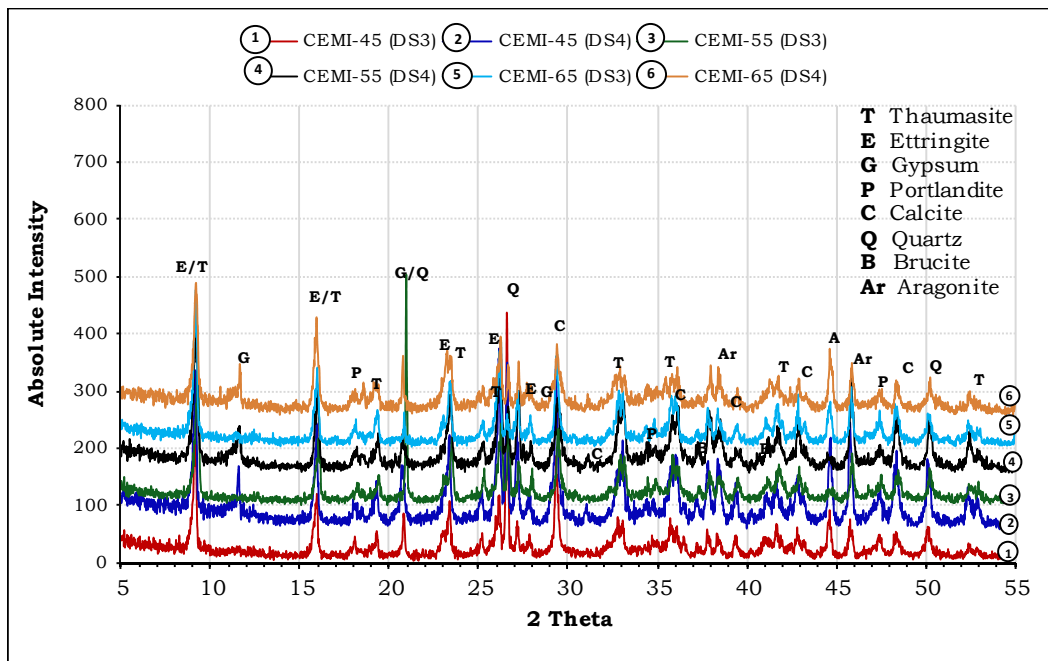


Figure 6.21 XRD patterns for CEMI solid samples at 5 °C

The XRD results for the Powder Samples are presented in Figure 6.22 whereby it can be seen that clear peaks indicating thaumasite/thaumasite containing phases could be observed in all samples. This can be taken as an indication that thaumasite was readily formed in all the cements in less than three months. No gypsum could be identified in any samples, even those kept in high sulfate concentration solutions, which is probably due to gypsum acting as a source of sulfate in the formation of thaumasite, as explained in Chapter 4, Section 4.6.

Portlandite is present in all samples, but in greater quantities at 3 months than at 12 months. This suggests that, portlandite was consumed in the formation of thaumasite in these older samples. Quartz peaks are very strong in all samples; relatively higher than for the Solid Samples. The most likely source of this quartz is the fine aggregate which would be present as a higher proportion of the Powdered Sample than the Solid Sample. Calcite could be clearly seen in all samples with similar intensities, while aragonite was almost absent from these samples.

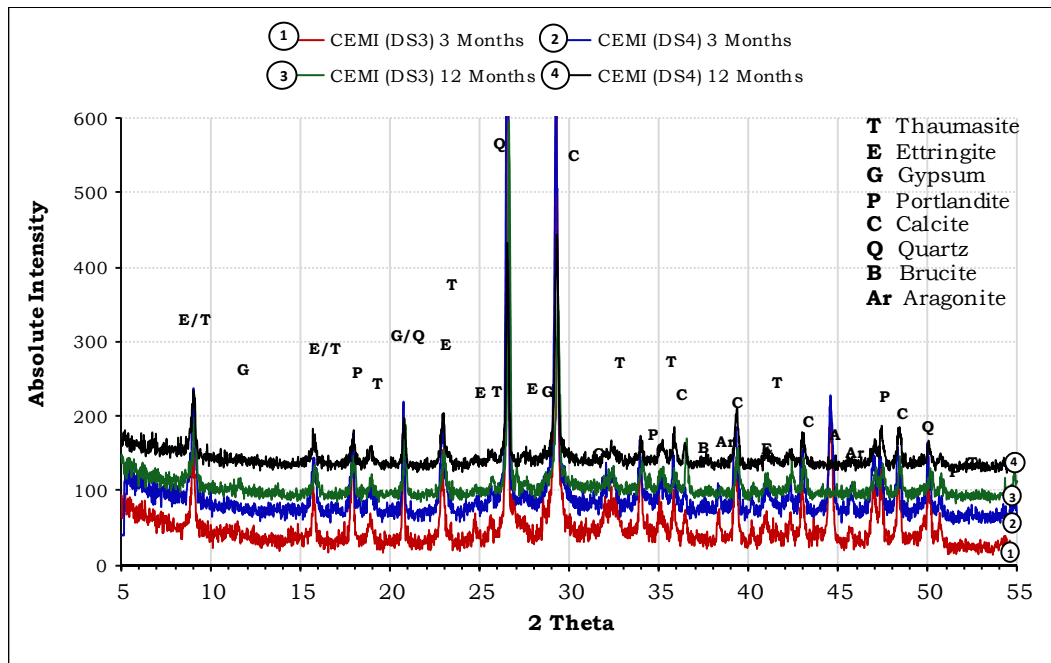


Figure 6.22 XRD patterns for CEMI Powder samples at 5 °C

XRD results for Solid CEMI samples kept at 20 °C are shown in Figure 6.23 from which the effect of w/c ratio can be clearly observed. Samples with low w/c ratio (eg CEMI-45) showed small peaks assigned to thaumasite\ thaumasite containing phases. However, these peaks became stronger as the w/c increased to reach maximum intensity in

CEMI-65 samples. Gypsum was detectable in all samples with weak peaks in CEMI-45 samples and in the CEMI-55 sample exposed to DS3 solution. CEMI-55 and CEMI-65 samples that were immersed in DS4 solution showed high intensity of gypsum peaks and compared to 5 °C samples, it can be noted that, gypsum peaks are much stronger at higher temperature, presumably because less or no thaumasite was formed. The portlandite levels seem to have gone in the opposite to the deterioration rate, where again, samples that made with CEMI-45 showed the strongest portlandite peaks while the most deteriorated samples which were made from CEMI-65 showed the least. This confirms the finding from the literature (Hartshorn et al. 1999, Q. Zhou et al. 2007, Torres et al. 2003, Collett et al. 2004); which proposes that, portlandite serves as a reactant in thaumasite formation. Quartz, calcite and aragonite were also identified in all samples.

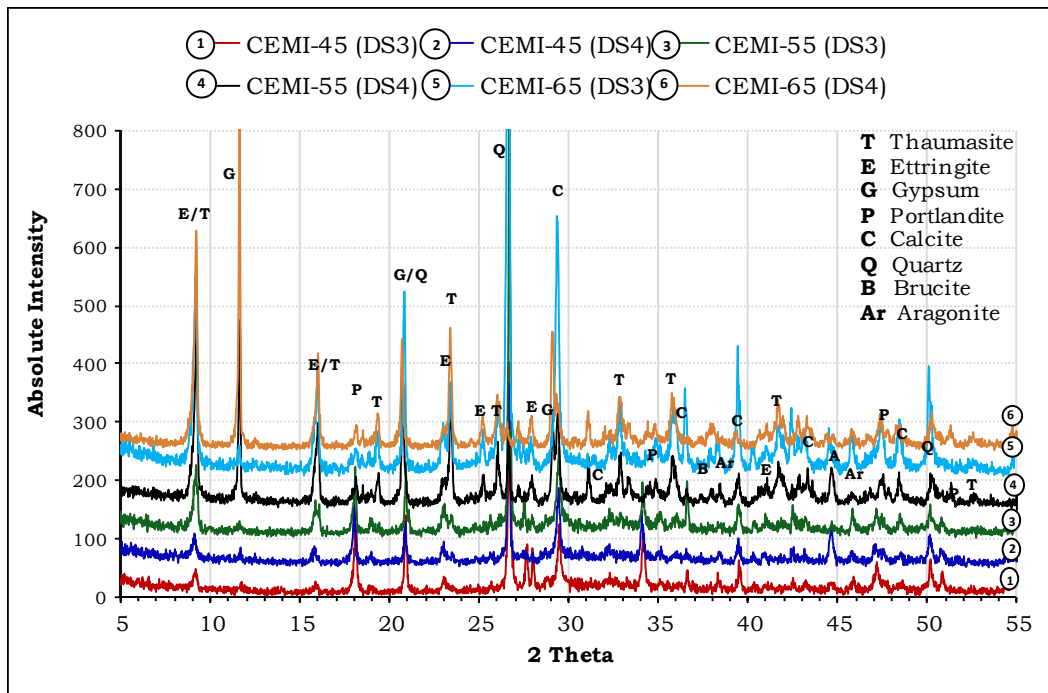


Figure 6.23 XRD patterns for CEMI solid samples at 20 °C

The XRD results for CEMI powder samples exposed to sulfates at 20 °C are shown in Figure 6.24. As this shows, thaumasite\thaumasite containing phases were clearly seen in all samples, including at 3 months samples, thus confirming that, thaumasite was readily formed in as little as 3 months even at 20 °C and in a sulfate concentration as low as 3g/l SO<sub>4</sub>, providing that the system is open. Similar Solid Samples (See Section 6.2.1) resisted the attack and remained intact for up to 9 months of exposure. Gypsum was not detectable in any of the samples, while portlandite peaks were getting weaker as time passed. Quartz, calcite and aragonite were also detected in all samples.

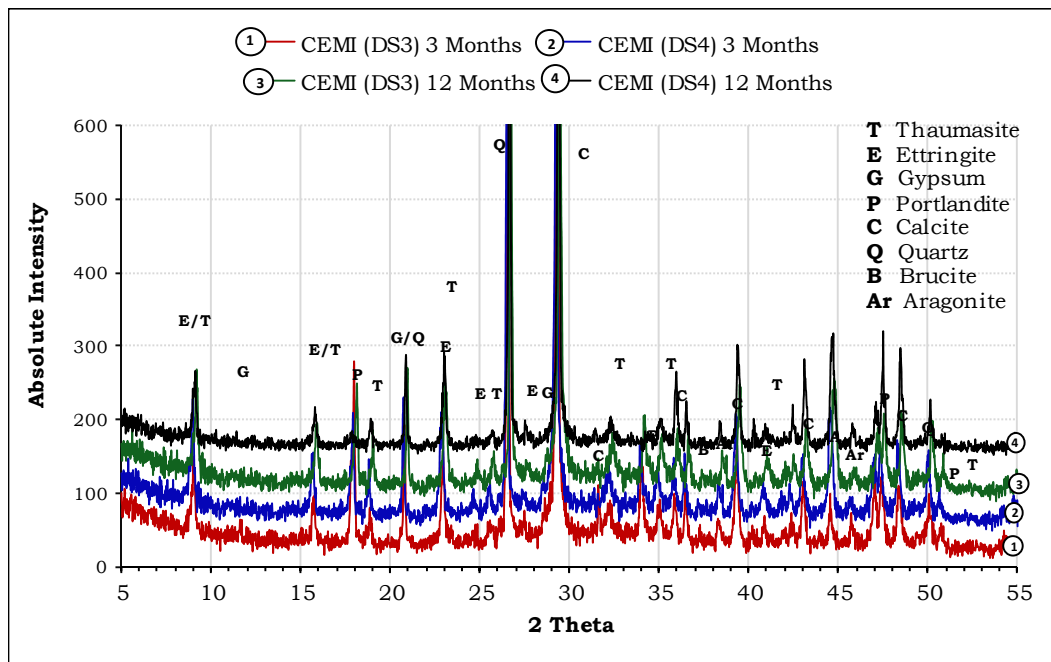


Figure 6.24 XRD patterns for CEMI Powder samples at 20 °C

### 6.5.2 XRD for LFC cement samples

Figure 6.25 shows the XRD patterns for different solid LFC samples after exposure to sulfate solutions for 24 months at 5 °C. It can be seen that peaks relevant to thaumasite\thaumasite containing phases are

detectable in all samples. However, these peaks were relatively stronger in samples made with high w/c ratios, for example LFC-65 and LFC-55. They are also stronger for samples exposed to DS4 compared to DS3 solutions. Gypsum is abundant in high w/c samples notably those exposed to DS4 solutions. The intensity of portlandite decreased as w/c and sulfate concentration increased, which would be due to more porous microstructures in these samples such that a higher consumption of portlandite would form other phases. Brucite is more noticeable in LFC-55 and LFC-65 in DS4 solutions, whereas both calcite and quartz are present, with strong peaks in all cements.

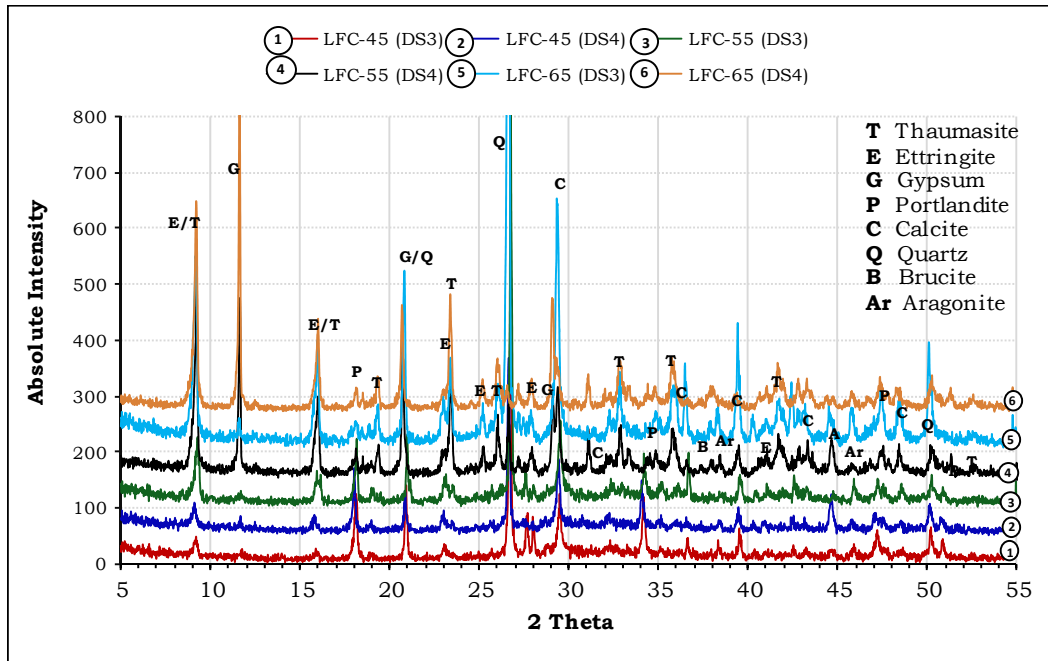


Figure 6.25 XRD patterns for LFC solid samples at 5 °C

Figure 6.26 shows the XRD results for LFC Powder Samples at different ages and solutions which were kept at 5 °C. The patterns are similar to those described in Sections 6.5.1. Thaumasite was detected with strong peaks at early ages in both solutions, whereas no gypsum was observed

in any samples and the amount of portlandite decreased with both time and sulfate concentration.

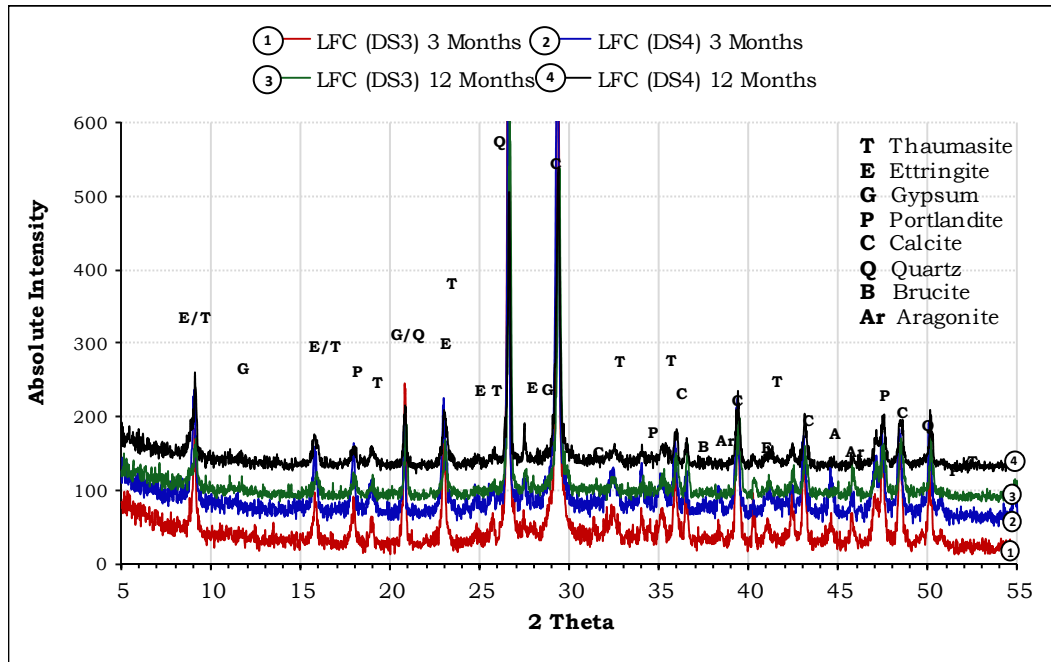
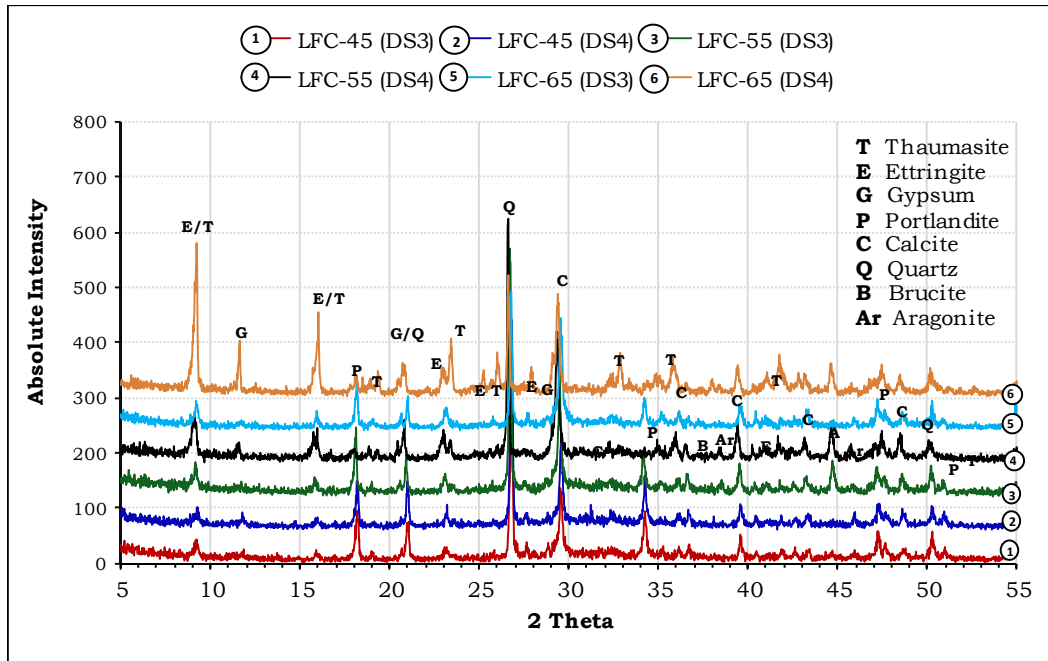


Figure 6.26 XRD patterns for LFC powder samples at 5 °C

At 20 °C, AS shown in Figure 6.27, the XRD patterns show an intensive peak attributed to thaumasite\thaumasite containing phases in sample LFC-65 exposed to DS4. Gypsum is also clearly identified in the same sample. As none of these samples at this temperature showed signs of deterioration, this could suggest that LFC-65 exposed to DS4 suffered non-damaging thaumasite formation, which might be a pre-cursor to TSA.

## 6. Effect of water to cement ratio



**Figure 6.27 XRD patterns for LFC solid samples at 20 °C**

The XRD results for LFC Powder Samples, are shown in Figure 6.28. The patterns are very similar to those obtained from samples stored at 5 °C. Thaumasite was formed in these samples at age of less than 3 months while the same Solid Samples at same temperature remained intact for up to 24 months.

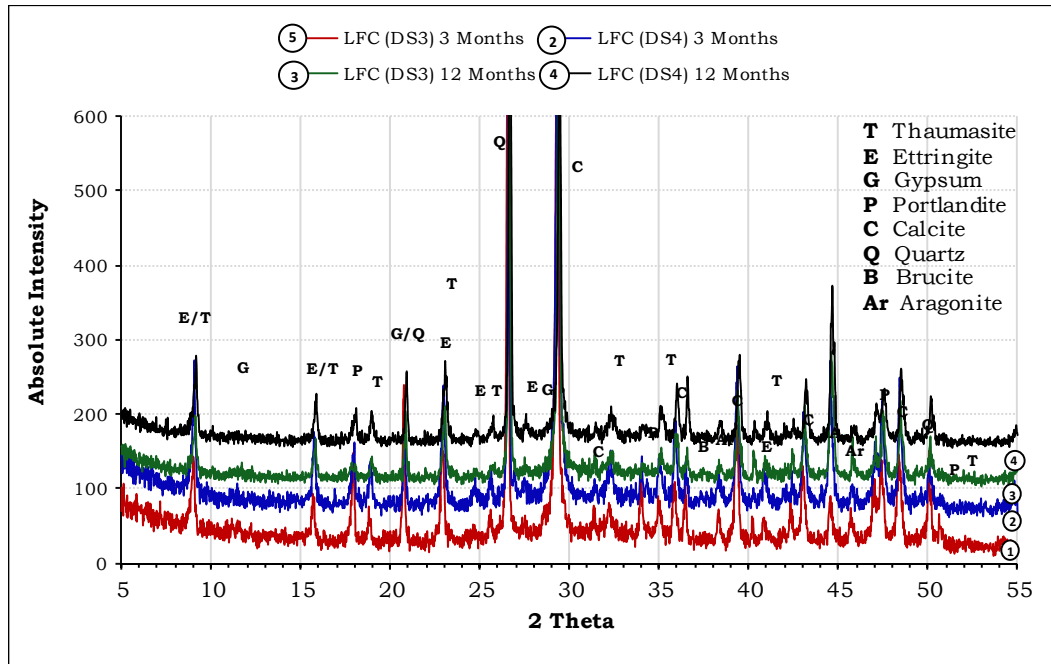


Figure 6.28 XRD patterns for LFC powder samples at 20 °C

### 6.5.3 XRD for FAC cement samples

Figure 6.29 shows the XRD patterns for FAC cement Solid Samples exposed to different solutions at 5 °C after 24 months. From this graph, it can be noted that, peaks (at around 9.2 2 $\theta$ ) due either thaumasite or ettringite are obvious in all samples. Gypsum is only observed in samples exposed to higher concentration sulfate solution DS4, and portlandite is hardly notable in any sample. This near absence of portlandite is possibly due to the lower cement content which would result in reduction in portlandite formation during hydration. Any existing portlandite would be also consumed to form other products, including calcite and thaumasite. Strong quartz and calcite peaks were indicated in all samples, whereas brucite was absent from all samples. The lack of brucite could be again related to less portlandite formed in the system. Aragonite is also detectible with weak peaks in all samples.

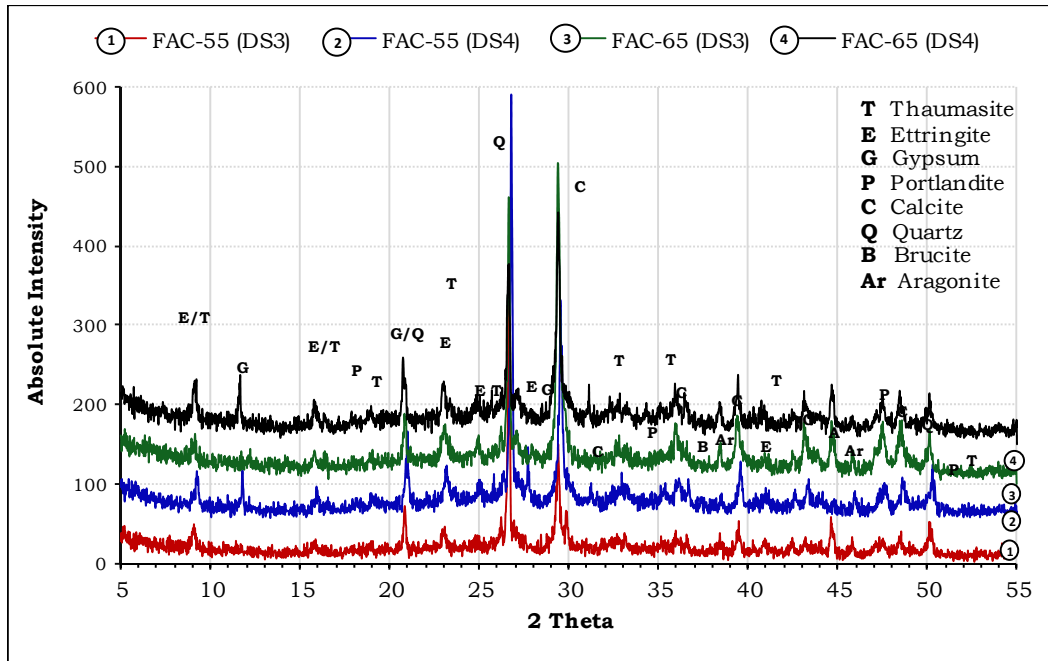


Figure 6.29 XRD patterns for FAC solid samples at 5 °C

For the XRD results of FAC Powder Samples, the results are shown in Figure 6.30. As this indicates, strong thaumasite peaks which would imply formation of thaumasite in these samples at age of 3 months. This applied to both sulfate solutions, although the intensity of the peak was higher for samples exposed to DS4 solutions. These peaks were also much stronger after 12 months of exposure. Again, no gypsum was detected in these samples and portlandite peaks are very weak. Quartz and calcite were identified with strong peaks present, while only weak peaks for aragonite were detected, as was the case for the solid samples.

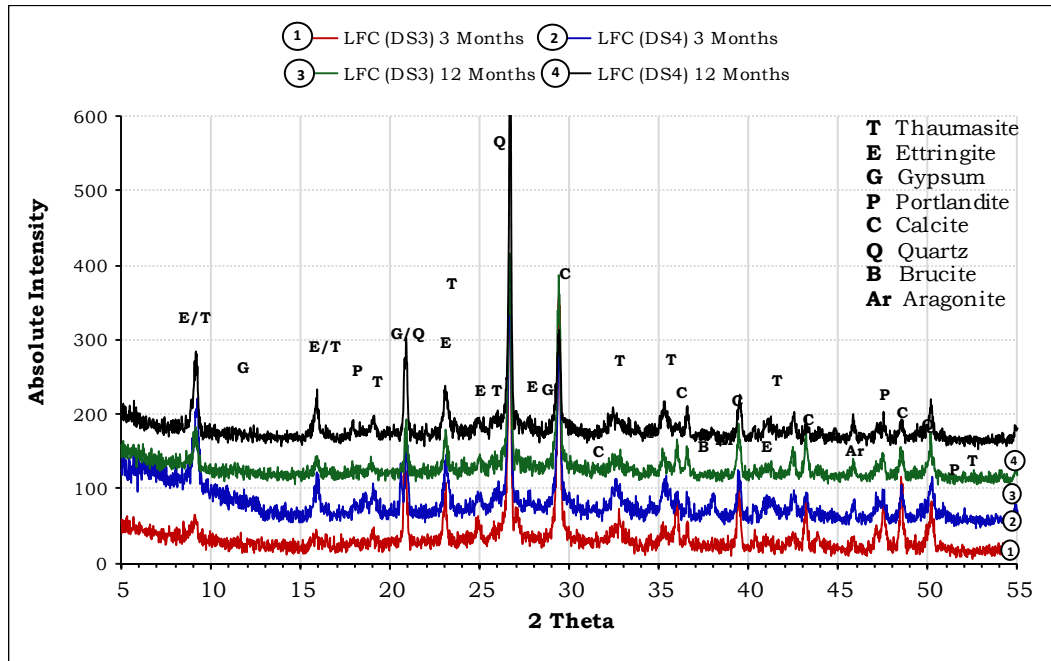


Figure 6.30 XRD patterns for FAC powder samples at 5 °C

Solid FAC cement samples kept at 20 °C showed XRD patterns similar to those stored at 5 °C and exposed to DS4 sulfate solution where the only differences were the absence of thaumasite from FAC-65 and presence of stronger gypsum peaks instead, as seen in Figure 6.31, this would suggest that FAC cements are more likely to be attacked by classical sulfate attack at higher temperatures.

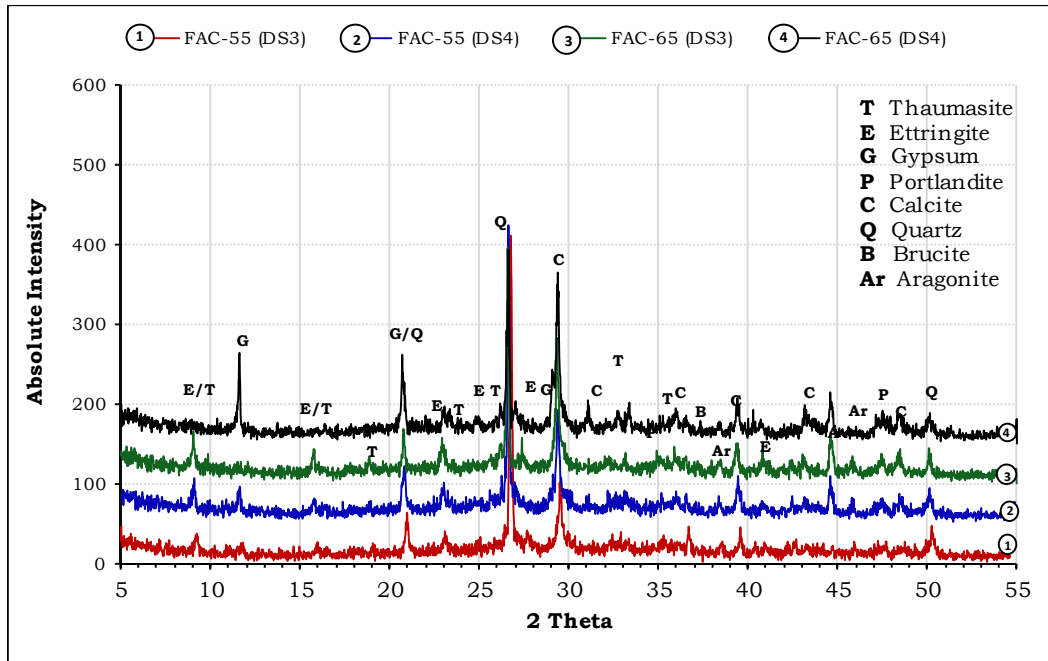


Figure 6.31 XRD patterns for FAC solid samples at 20 °C

XRD results for FAC powder samples are shown in Figure 6.32. In these samples, no thaumasite or ettringite was detected at age of 3 months in both exposure solutions. However, strong peaks could be seen in these samples after 12 months of exposure in both solutions with more intensity in DS4 samples. Gypsum was detectable only at an age of 3 months in FAC-55 exposed to DS4 solution. Other phases were similar to those observed in powder samples kept at 5 °C.

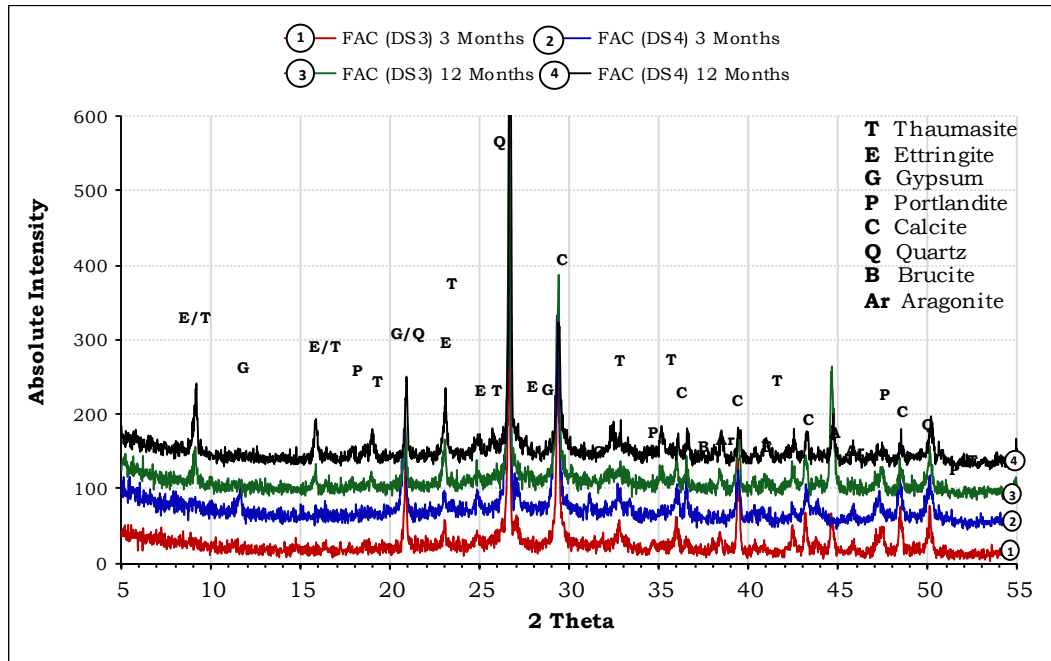


Figure 6.32 XRD patterns for FAC powder samples at 20 °C

#### 6.5.4 XRD for SLC cement samples

The XRD results for SLC cement Solid samples are presented in Figure 6.33. Despite no visual attack signs (see Section 6.2.3) in any of these samples, it can be seen in the patterns there were good intensity peaks (at around 9 and 16° 2θ) indicating presence of thaumasite\thaumasite solid solution phases in these cements in both solutions and w/c ratios. Strong gypsum peaks were also seen in all samples with higher intensities in samples exposed to DS4, following same trends as in all cements. Traces of portlandite were also observed in all cements with higher intensities in lower w/c ratio SLC-55 samples, with these peaks becoming weaker as thaumasite, and gypsum peaks became stronger. Other phases such as quartz, calcite and aragonite were detectable in all samples and traces of brucite were seen in samples immersed in DS4 solutions.

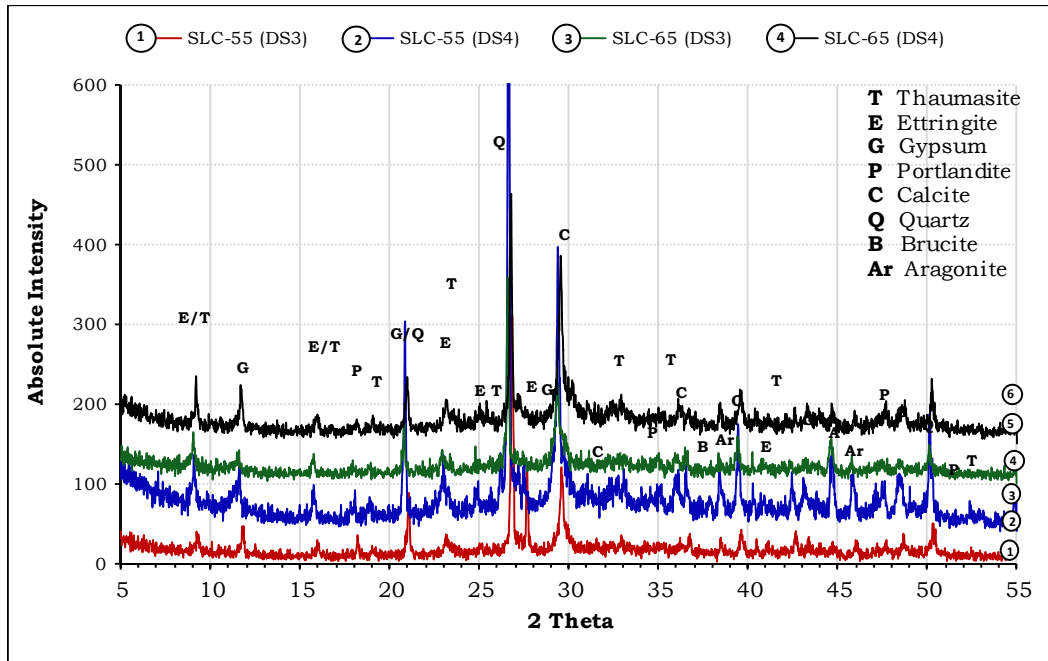


Figure 6.33 XRD patterns for SLC solid samples at 5 °C

The XRD patterns for SLC cement Powder Samples are presented in Figure 6.34. Thaumasite\thaumasite ettringite solid solution peaks was clearly present at both test ages, indicating the formation of thaumasite in these samples in a time as short as less than 3 months. However, these peaks became stronger in samples tested at 12 months of exposure. Gypsum was present in all samples with higher intensities in samples exposed to DS4 solutions, as usual. Portlandite was more obvious in samples tested at 3 months compared to one year and other phases were similar to what was noted for Solid Samples of the same cements.

The XRD results for SLC cement samples exposed to sulfate solutions at 20 °C are presented in Figure 6.35. These patterns were very similar to those for samples stored in sulfate solutions at 5 °C that are presented in Figure 6.33 and same description would apply to both.

6. Effect of water to cement ratio

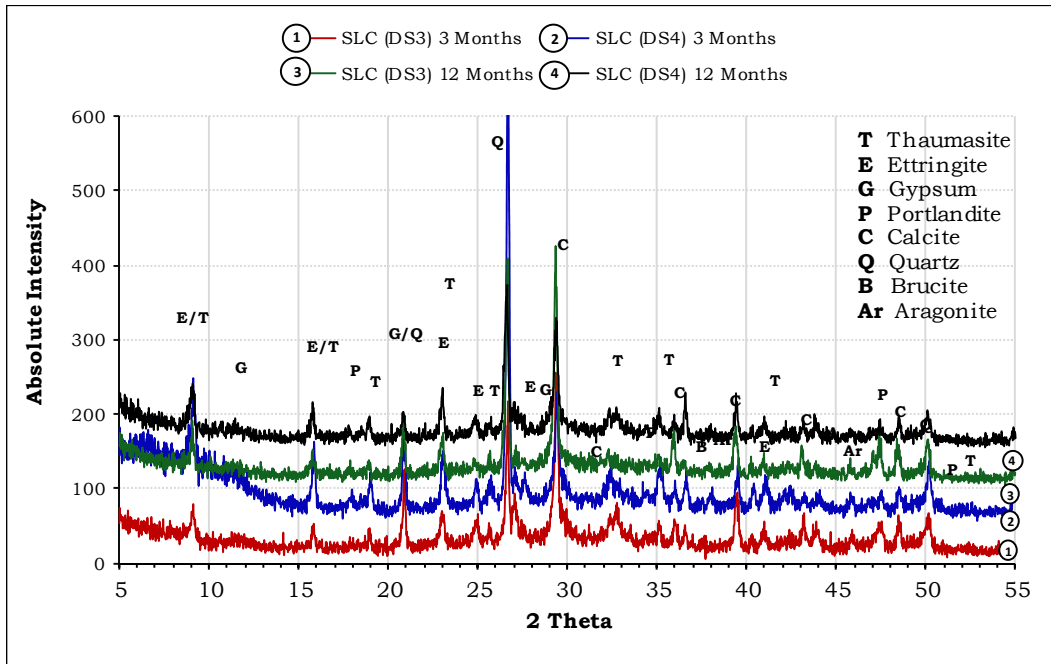


Figure 6.34 XRD patterns for SLC powder samples at 5 °C

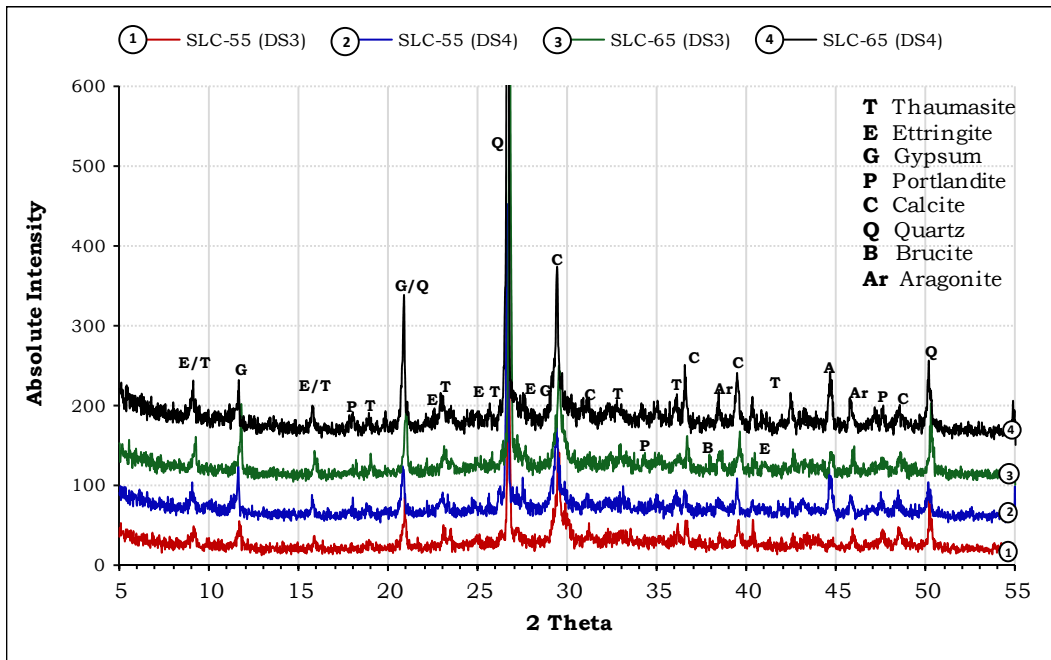


Figure 6.35 XRD patterns for SLC solid samples at 20 °C

Figure 6.36 shows the XRD patterns for SLC cement Powder Samples exposed to sulfate solutions at 20 °C. As shown there were no peaks attributed to thaumasite or phases containing thaumasite at the age of 3 months. On the other hand, portlandite peaks were quite intense at this age, which might be an indication of slow reactions at this temperature. At the age of 12 months the patterns showed clear peaks indicating formation of thaumasite\thaumasite containing phases in these samples in both exposure solutions. Traces of gypsum could be identified in all samples and the other phases detected in all samples were similar to those for samples kept at 5 °C.

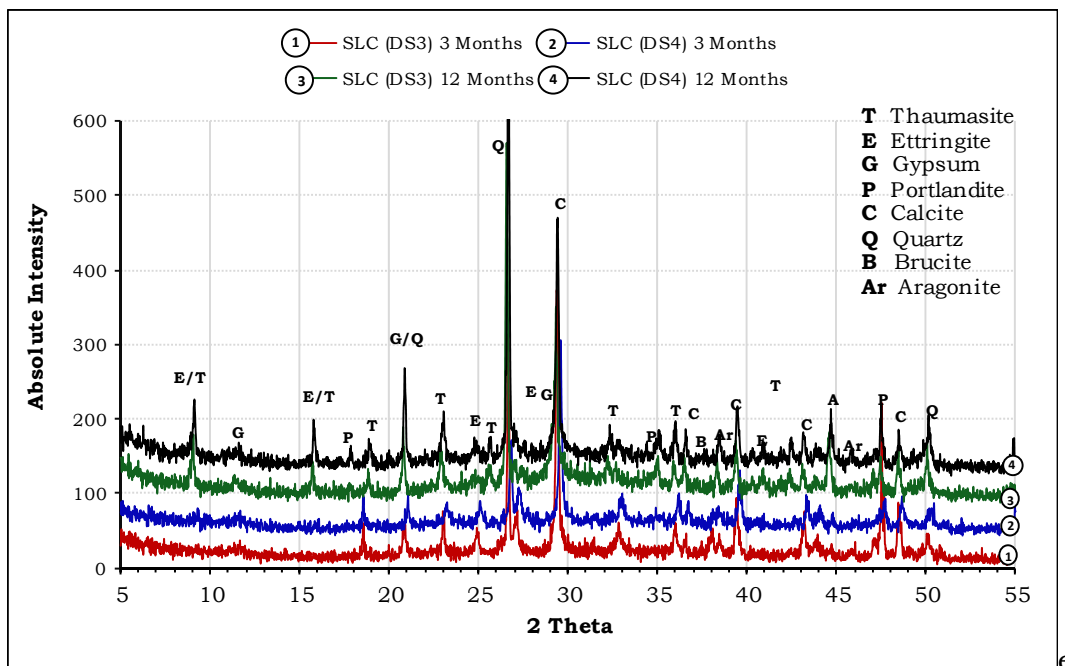


Figure 6.36 XRD patterns for SLC powder samples at 20 °C

## 6.6 Fourier Transform Infrared Spectroscopy (FTIR)

Infrared spectroscopy is a very powerful tool for distinguishing between thaumasite and ettringite, as described in Chapter 4, Section 4.7. In this section, this technique is used to differentiate between thaumasite and

ettringite and to clarify whether XRD peaks denote thaumasite or ettringite.

Since the results obtained from XRD were similar to each other in the patterns tested, only selected samples were subjected to IR analysis. None of the samples exposed to DS3 are presented in this section, the comparison is based on the different in w/c ratio and temperatures. Powder Samples were tested at 3 and 12 months as was done for XRD and these results were compared with those for Solid Samples for the same cements and temperature. The focus was only on the deteriorated samples and samples kept in the most aggressive environments.

#### **6.6.1 FTIR for CEMI cement samples**

Figure 6.37 presents the IR spectra for different CEMI samples exposed to sulfate solutions at 5 °C respectively. As can be seen from these spectra, strong peaks observed in Solid Samples at 500 cm<sup>-1</sup> and 760 cm<sup>-1</sup> related to octahedral silicates (SiO<sub>6</sub>) in addition to CO<sub>3</sub> and SO<sub>4</sub>, and hence these indicate that thaumasite or thaumasite containing phases were present (Barnett et al. 2002, Torres et al. 2004). Although this test is not quantitative, the intensities of the peaks can be taken as a good indication to compare the presence of different phases in the system. It can be seen that these peaks were stronger as the w/c becomes higher. Peaks related to ettringite at around 850 cm<sup>-1</sup> can be seen only in cements with low w/c ratio, but not in the fully deteriorated sample. This may suggest that the conversion of ettringite to thaumasite at later stages of the attack, where thaumasite become the end product of the reactions.

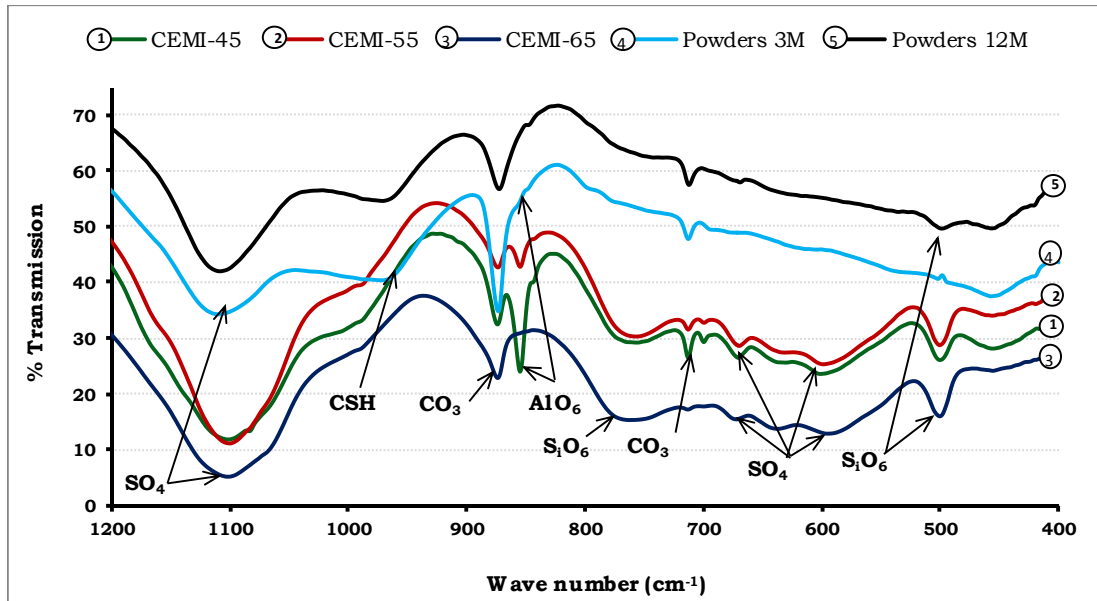
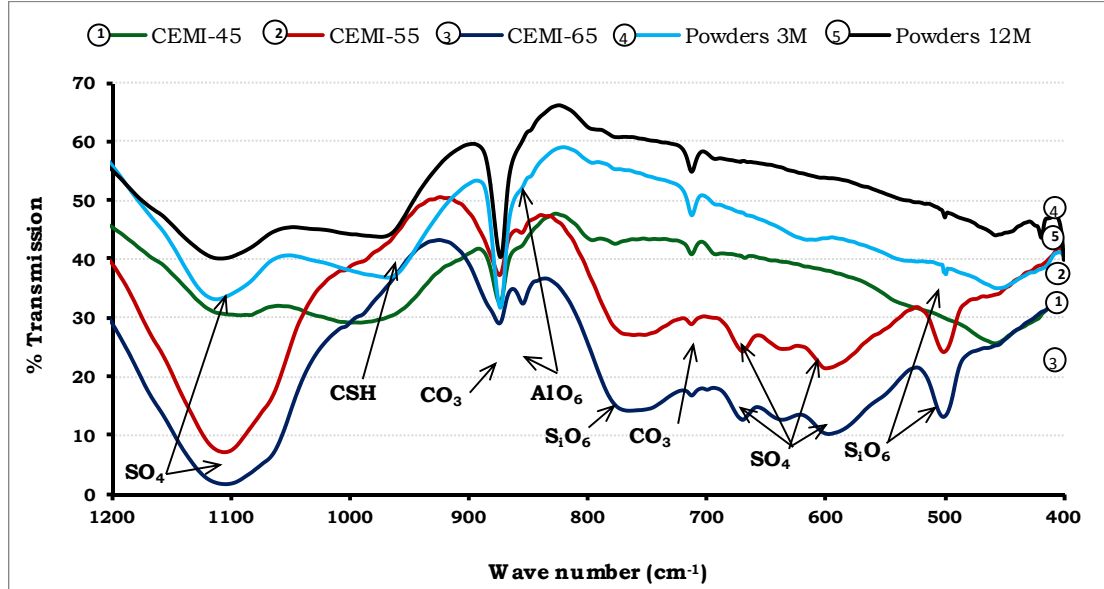


Figure 6.37 IR spectra for CEMI samples in DS4 solutions at 5 °C

Gypsum peaks at around  $600\text{ cm}^{-1}$ ,  $650\text{ cm}^{-1}$  and  $1100\text{ cm}^{-1}$  can be seen more obviously in Solid Samples which confirms the XRD observations. Aragonite peaks at around  $700\text{ cm}^{-1}$ , in addition to those at  $712\text{ cm}^{-1}$ , were stronger in Solid Samples lower w/c ratio cements, but they were hardly detectable in the Powder Samples or in the high w/c ratio samples. The presence of peaks at around  $1000\text{ cm}^{-1}$  is an indication to the presence of the binding CSH gel (Bensted and Varma 1974). These are stronger in Powder Samples and they became weaker as the degree of attack became worse. The presence of thaumasite peaks at the age of 3 months in the Powder Samples indicated that the thaumasite was formed in these samples before this age.

It is worth mentioning here that, the relative weak peaks of Powder Samples resulted from the samples being from a homogeneous mixture of crushed concrete and deterioration products, while in the Solid

Samples the deteriorated materials were carefully collected for analysis from the samples.



**Figure 6.38** IR spectra for CEMI samples in DS4 solutions at 20 °C

Figure 6.38 shows the IR spectra for CEMI samples at 20 °C. The absence of a peak at 500  $\text{cm}^{-1}$  in the CEMI-45 spectra indicated the absence of thaumasite in this sample, even after two years immersion in DS4 solution. This would explain the good visual appearance of this sample as described in Section 6.2.1. The other two Solid Samples: CEMI-55 and CEMI-65 both showed strong thaumasite peaks at 500  $\text{cm}^{-1}$  co-existing with ettringite which would indicate that attack is still in its early stages. Confirming the XRD results, gypsum was detectable only in the CEMI-55 and CEMI-65 samples, but not in the other Solid Sample or in Powder Samples. CSH peaks were stronger in the low w/c ratio sample and powders, but they were very weak in deteriorated samples indicating that the samples lost their binding capacity due to thaumasite sulfate attack. Again the presence of peaks at 500  $\text{cm}^{-1}$  for Powder

Samples suggests that thaumasite formed at this temperature at this early age in the open system.

### 6.6.2 FTIR for LFC cement samples

For LFC cements, the IR spectra are shown in Figure 6.39 for samples stored at 5 °C. Since all Solid Samples containing this cement had shown considerable visual deterioration (see Section 6.2.2), the presence of thaumasite peaks confirmed that this deterioration is due to thaumasite type of sulfate attack (TSA). Ettringite was present in the low w/c ratio sample indicating the early stage of attack. Calcite was identified in all samples while aragonite was only observed in the less deteriorated sample. Small thaumasite peaks in the Powder Samples indicated the formation of thaumasite in these samples as early as at three months.

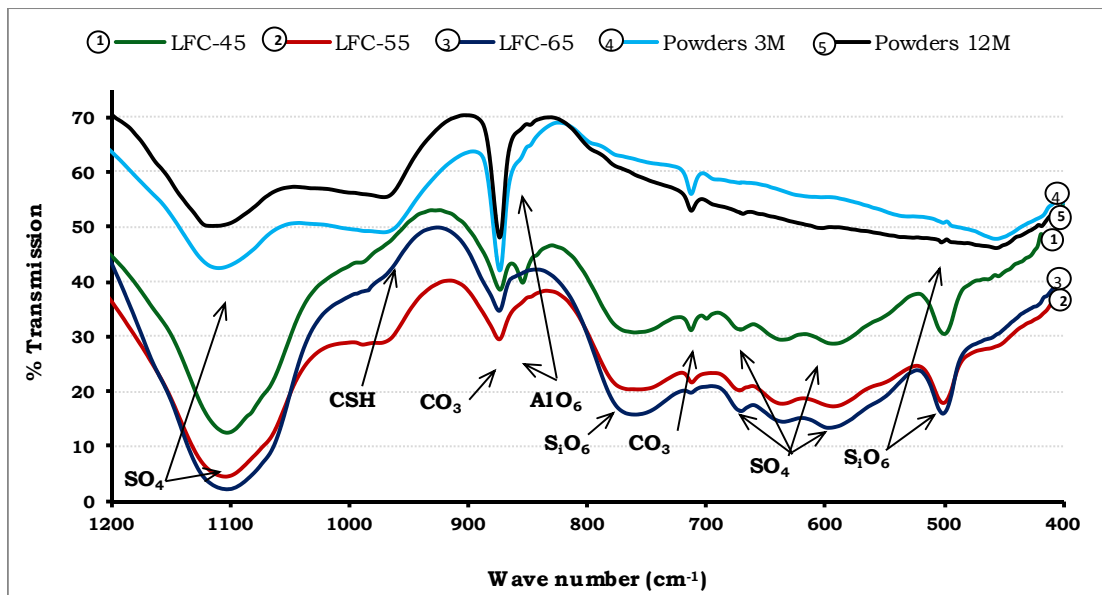


Figure 6.39 IR spectra for LFC samples in DS4 solutions at 5 °C

Figure 6.40 presents the IR spectra for LFC exposed to sulfate solutions at 20 °C. None of these samples had shown visual deterioration as illustrated in Figure 6.2, and described in Section 6.2.2. However, by

looking at their IR spectra it can be seen that intensive thaumasite peak were detected in LFC-65 followed a by weaker peak in LFC-55, but these were not noticeable in LFC-65. This suggests that, the former two samples have suffered thaumasite formation and it is likely that this will develop into TSA. The presence of a C-S-H peak reflected the soundness of these samples up to this age. Gypsum was detectable only in LFC-65, as noted in the XRD results. Gypsum peaks were very obvious in LFC-65 and they appeared in a board peak in Powder Samples after 12 months, which was possibly the result of the sulfate phase in the thaumasite structure rather than in gypsum. Moreover, there was no peak around  $650\text{ cm}^{-1}$  that would be indicative of gypsum in this spectrum.

For Powder Samples, a thaumasite peak at  $500\text{ cm}^{-1}$  was absent in the 3 months sample. This is possibly because no thaumasite had formed in this sample or the quantity was too small to be detected by IR, which is likely in view of the XRD that results showed peaks for thaumasite\ettringite phases that were not detected with IR. Samples tested after 12 months immersion showed small thaumasite peaks, indicating its formation in this sample within 12 months.

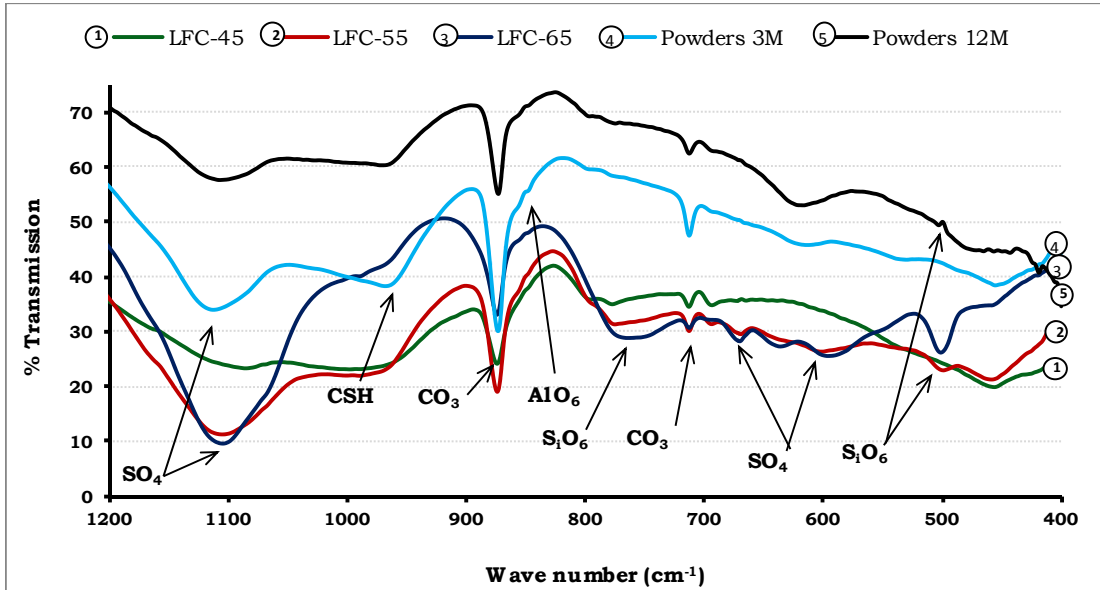


Figure 6.40 IR spectra for LFC samples in DS4 solutions at 20 °C

### 6.6.3 FTIR for FAC cement samples

IR spectra for FAC cements samples at 5 °C are presented in Figure 6.41 for the Solid Samples. No peaks indicating the presence of thaumasite at 500  $\text{cm}^{-1}$  can be observed, however small peaks also assigned to  $\text{SiO}_6$  at 760  $\text{cm}^{-1}$  may be taken as an indication of thaumasite formation were seen in both samples together with small peaks at 850  $\text{cm}^{-1}$  which would indicate ettringite. These observations collaborate the XRD results described in Section 6.2.3. Gypsum peaks were also seen in both samples, along with CSH and calcite in all samples. Powder Samples showed small peaks indicating thaumasite formation in these samples at both testing ages.

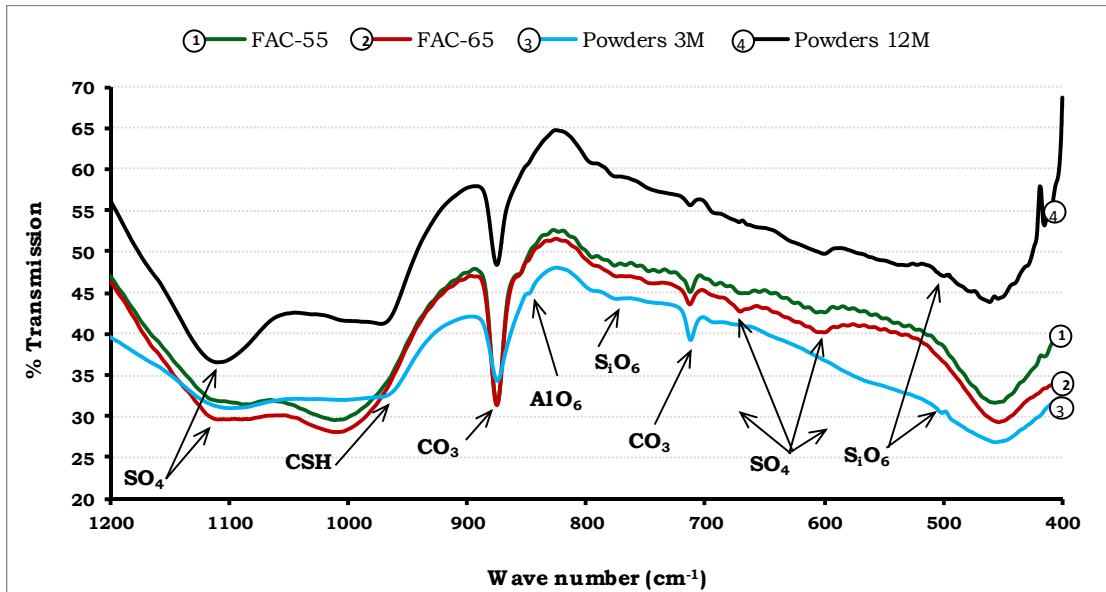


Figure 6.41 IR spectra for FAC samples in DS4 solutions at 5 °C

From the IR spectra shown in Figure 6.42 for the samples exposed to sulfate solutions at 20 °C. It can be seen that in the Solid Sample the dominant phase was gypsum, although small peaks at 760 cm<sup>-1</sup> 850cm<sup>-1</sup> may indicate the formation of thaumasite, thaumasite\ettringite solid solutions. Thaumasite\ettringite were absent from XRD results for this sample. Peaks indicating thaumasite were absent in Powder Samples at age of 3 months, while a small peak was present at 12 months, indicating that the slow process of thaumasite formation at higher temperatures.

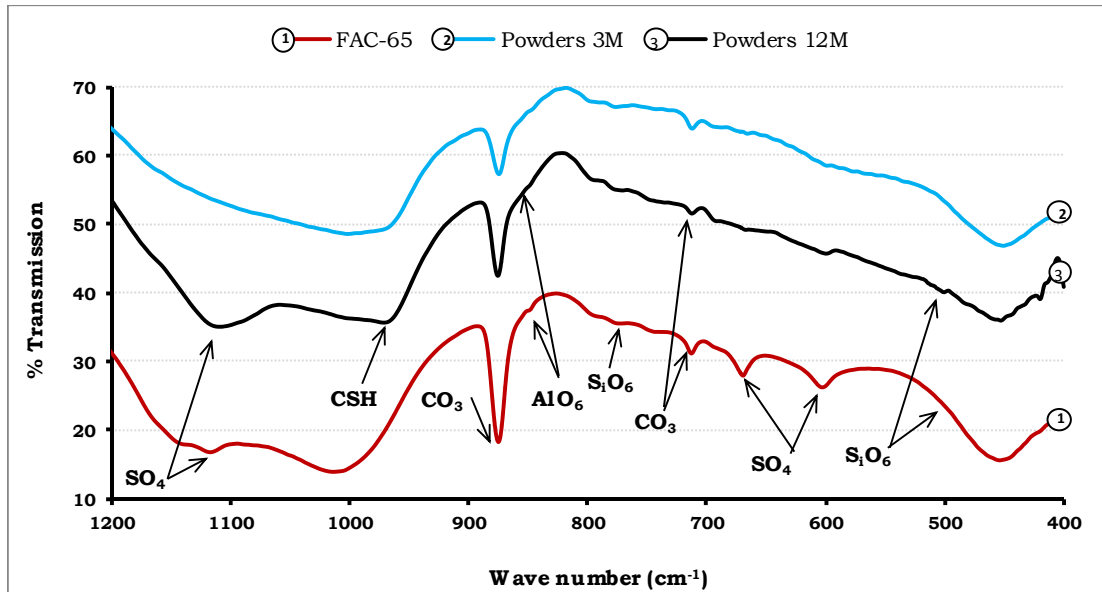


Figure 6.42 IR spectra for FAC samples in DS4 solutions at 20 °C

#### 6.6.4 FTIR for SLC cement samples

Figure 6.43 presents IR spectra for SLC cement samples exposed to sulfate solutions at 5 °C. As it can be noted from these, for Solid Samples, no peaks were observed at around 500  $\text{cm}^{-1}$ . However, small peaks at 760  $\text{cm}^{-1}$  could indicate thaumasite formation in these samples. An obvious peak indicating ettringite was seen in SLC-55 cement sample, indicating the co-existence of both minerals in this sample. Gypsum was also detected in both Solid Samples. Calcite was also present in all samples. The Powder Samples clearly showed the presence of thaumasite in both samples after 3 months of exposure.

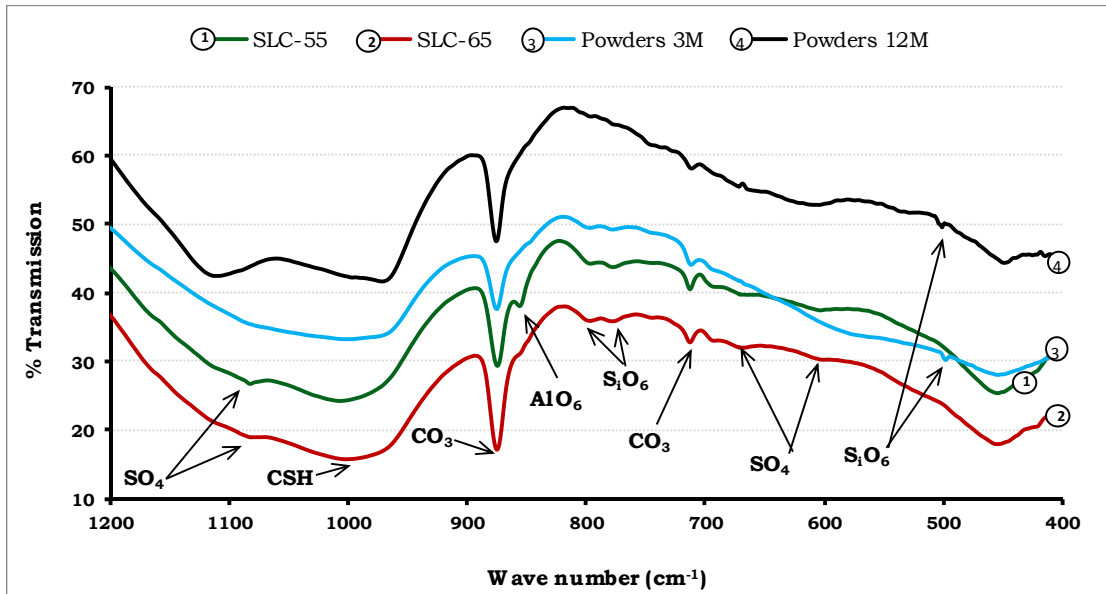


Figure 6.43 IR spectra for SLC samples in DS4 solutions at 5 °C

IR spectra for SLC that kept at 20 °C are shown in Figure 6.44. None of these samples showed peaks at 500  $\text{cm}^{-1}$  or at 850  $\text{cm}^{-1}$ . However, peaks at 760  $\text{cm}^{-1}$  may explain the presence of peaks in XRD traces at 9.2  $2\theta$  that would indicate thaumasite formation in these samples. Peaks attributed to CSH at around 1000  $\text{cm}^{-1}$  were present in all samples indicating the existence of binding CSH gel, which would be consistent with the high soundness of the Solid Sample and explain its high resistance to sulfate attack even after 24 months of exposure to sulfate solutions. Gypsum peaks at 670  $\text{cm}^{-1}$  were present in both Solid and Powder Samples at 12 months.

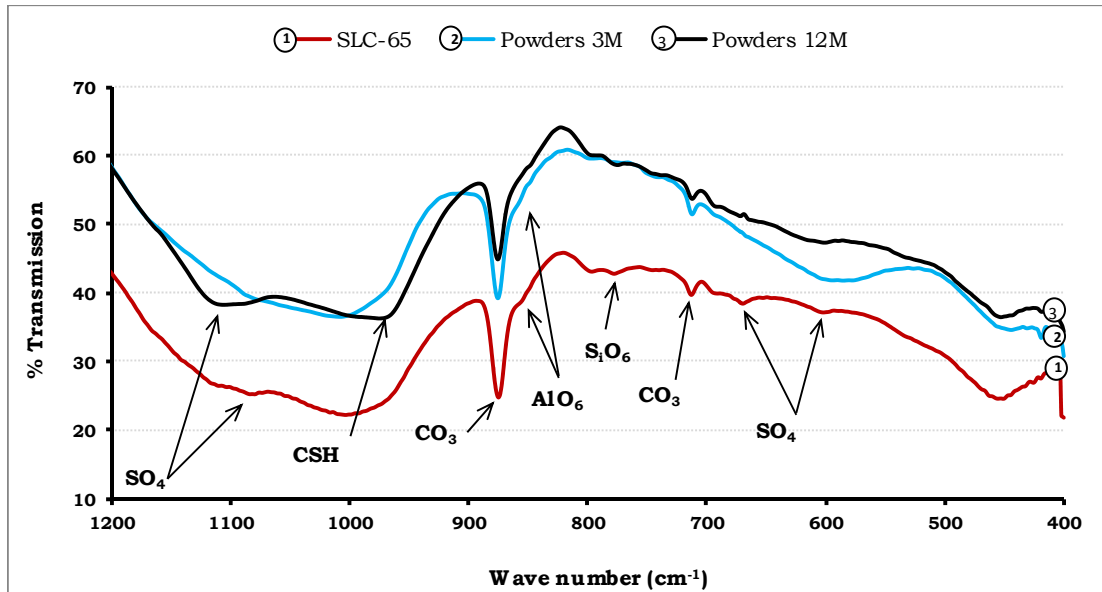


Figure 6.44 IR spectra for SLC samples in DS4 solutions at 20 °C

## 6.7 Microstructure of deterioration products.

As for FTIR, only selected samples were chosen to be examined using secondary electron microscopy SEM and EDX. The SEM results for CEMI-65 and LFC-65 samples are presented in Chapter 4. All results presented in this section are for samples exposed to DS4 sulfate solution as this was believed to be the most aggressive solution. For CEMI and LFC the focus was on the none-deteriorated samples to investigate thaumasite formation TF in these cements. More attention was given to FAC and SLC cements with respect to thaumasite formation, especially the latter which is known for its good resistance to thaumasite type of sulfate attack (see Section 2.6.1.2).

### 6.7.1 CEMI cement samples

Figure 6.45 shows a backscattered image for CEMI-45 cement sample at 20 °C. This sample did not show any visual deterioration after 24 months of exposure to sulfate solutions (see Section 6.2.1), however, a

network of cracks is developed in the mortar and around the sand particles.

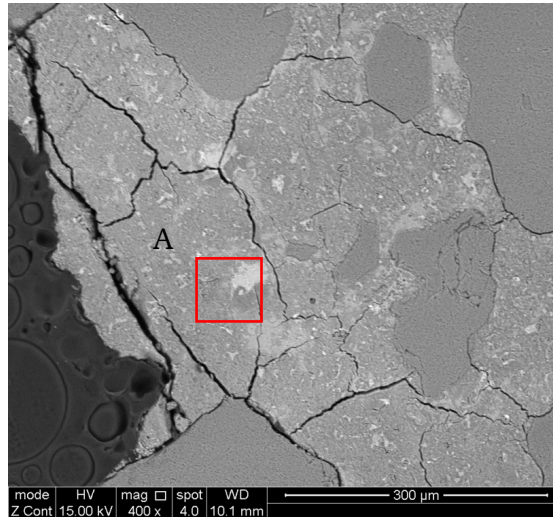
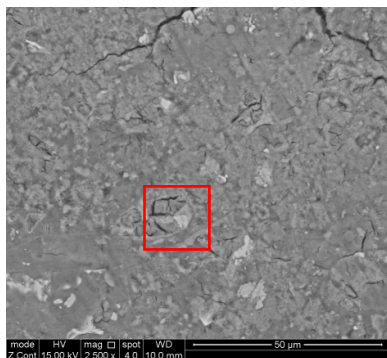
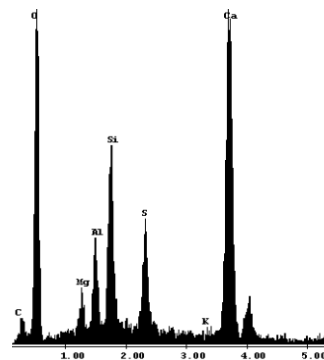


**Figure 6.45 BSE of CEMI-45 sample at 20 °C**

A magnified image for spot A is presented in Figure 6.46 with its microanalysis details. The image shows that the matrix is full of hair cracks while the EDX reveals the presence of Al, Si together with Ca, S, O and C which is consistent with the formation of thaumasite-ettringite solid solutions in this region. No gypsum was detected in this sample.



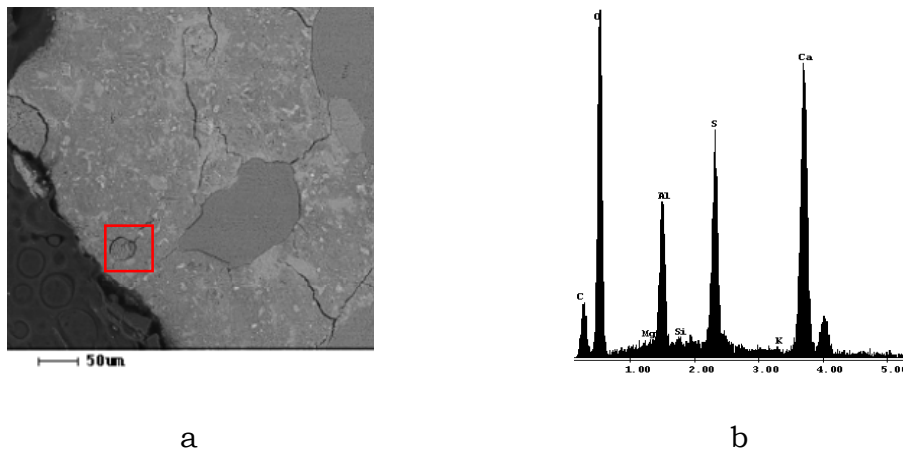
a



b

**Figure 6.46 Magnified image for spot A in Figure 6.45 a) microstructure of the matrix. b) EDX microanalysis showing thaumasite\ettringite solid solution**

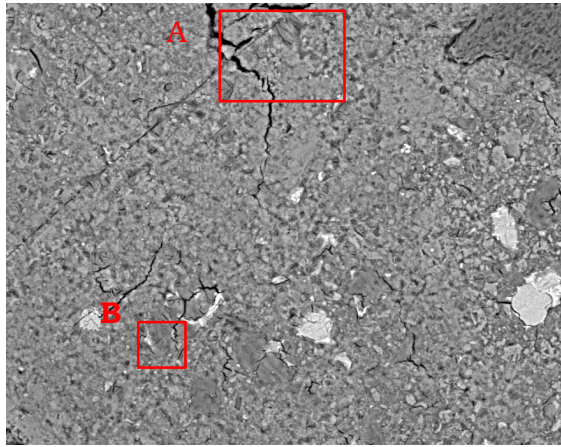
In another area from the same sample the image implied the formation of ettringite in an air void, as Figure 6.47 shows.



**Figure 6.47 a) BS image and b) EDX analysis for ettringite formed in air void**

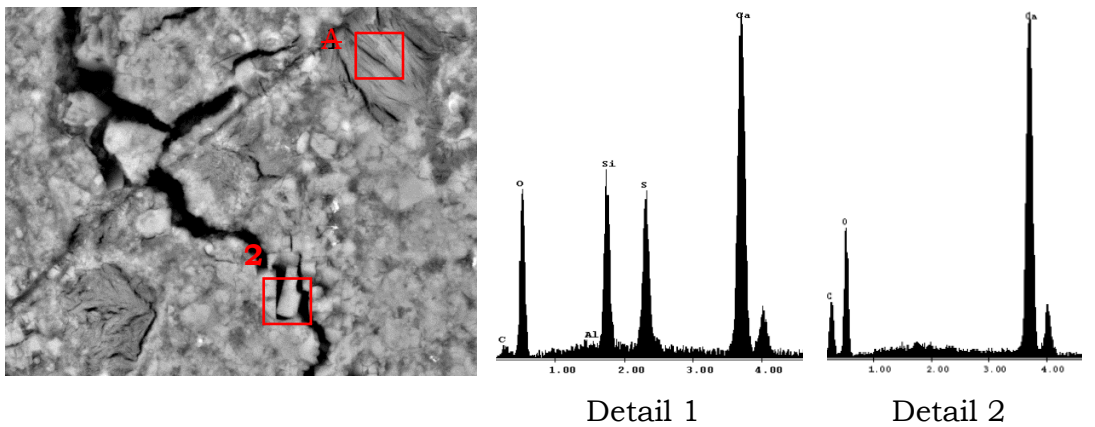
### 6.7.2 SEM for LFC cement samples

The SEM image for LFC-45 is shown in Figure 6.48, which shows that the cracks had started to appear in locations such as spots A and B, while other regions were still intact. This suggests that attack was in its early stages, and the cracking was insufficiently extensive for visual damage to the sample after 2 years of immersion in sulfate solutions to be described in Section 6.2.2. Gypsum was not seen in this sample and nor was it detectable.



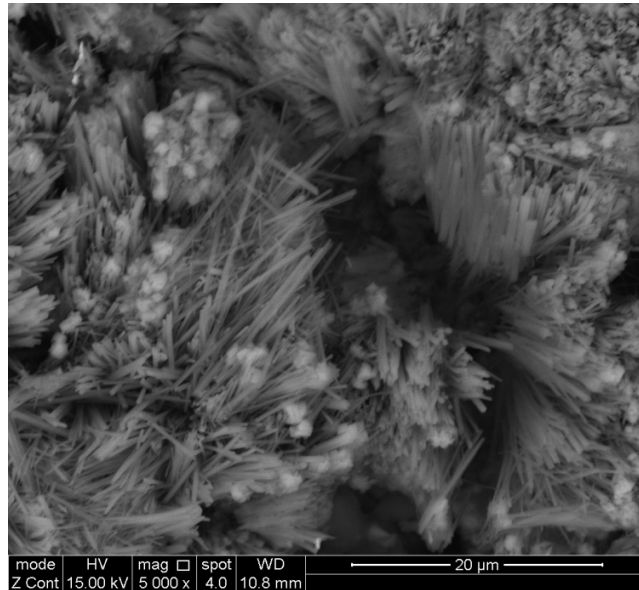
**Figure 6.48 BSE of LFC-45 sample at 20 °C**

A higher magnified image for spot A in Figure 6.48 is shown in Figure 6.49, in which it can be deduced that the cracks are filled with thaumasite and calcite.



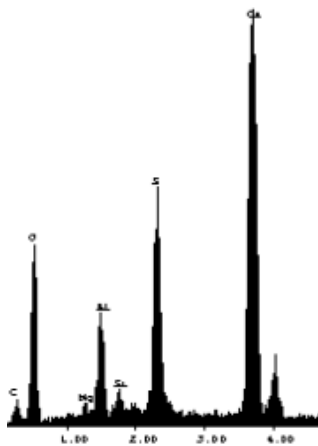
**Figure 6.49 Magnified image for spot A in Figure 6.48 and micro EDX analysis**

A further higher magnified image for detail 1 in Figure 6.49 is shown in Figure 6.50, which show thaumasite crystals growing in one of the cracks developed in the matrix. EDX analysis in Figure 6.49 detail 2 indicated that these crystals were nearly pure thaumasite



**Figure 6.50 A needle like thaumasite crystals filling the cracks in LFC-45 sample**

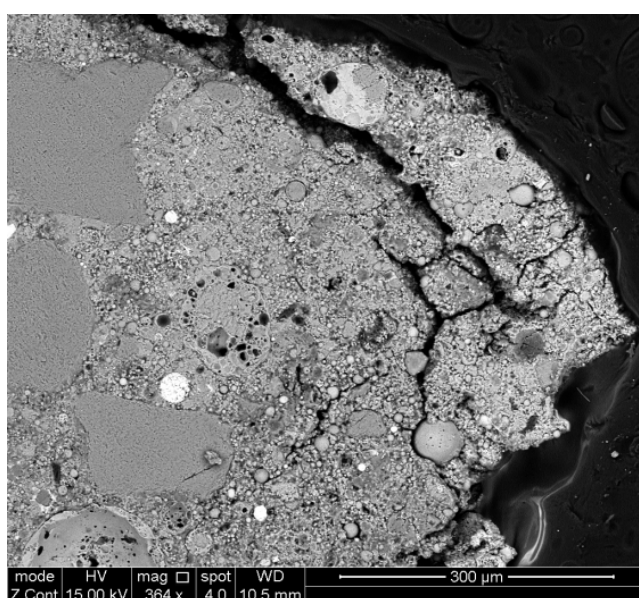
Spot B, in Figure 6.48 proved ettringite formation in another crack in the sample. Indeed, the small Si peaks in the micrograph may indicate the start of transformation stage for ettringite to be converted to thaumasite, where the EDX microanalysis for this spot is shown in Figure 6.51.



**Figure 6.51 EDX microanalysis for spot B in Figure 6.48 showing ettringite elements in additions to small Si peak**

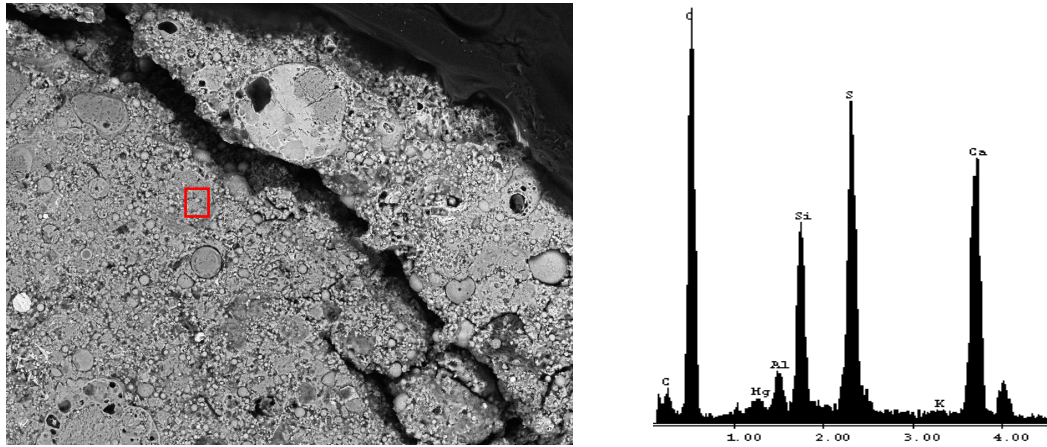
### 6.7.3 FAC cement samples

Figure 6.52 shows the microstructure for FAC-65 sample exposed to DS4 solution for 24 months at 5 °C. This sample did not show any visual signs of deterioration (See Section 6.2.3). However the SEM image revealed that cracks were clearly present near the surface of this sample. Fly ash particles can also be seen in the sample in form of spheres, while the white region indicates the presence of non reacted aluminate phases.



**Figure 6.52 BSE of FAC-65 sample at 5 °C**

A higher magnification image proved the presence of thaumasite near the cracks as shown in Figure 6.53. However, the presence of Al peak in the EDX analysis indicated presence of ettringite in the phase or thaumasite solid solution. This suggests that fly ash cements are not immune from thaumasite formation.



**Figure 6.53 Magnified image and EDX analysis for thaumasite ettringite solid solution in FAC-65 sample at 5 °C**

Another image from the same sample confirms the presence of gypsum as, Figure 6.54 shows, where gypsum crystals have filled an air void. Gypsum peaks were also observed in the XRD analysis for this sample (Section 6.5.3), promoting the possibility of gypsum formation in this cement at low temperature.

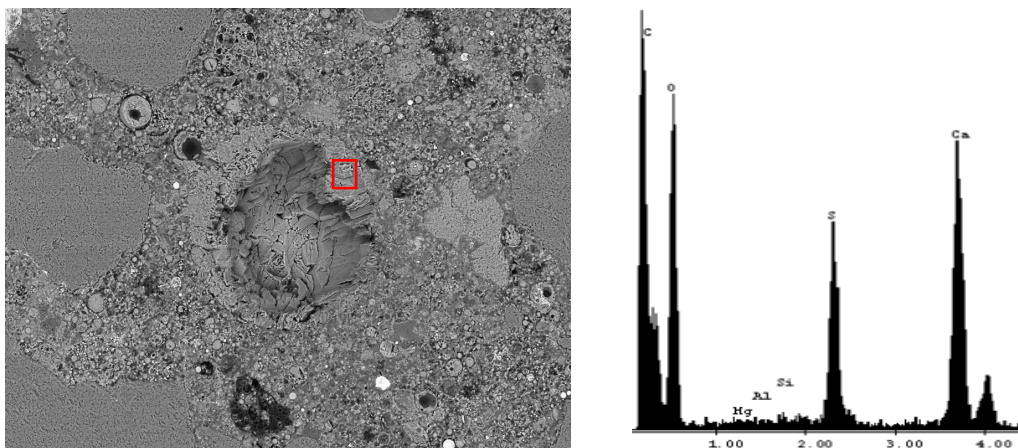


**Figure 6.54 Magnified image and EDX analysis for gypsum phase in FAC-65 sample at 5 °C**

Ettringite alone could not be identified in this sample via SEM analysis.

#### 6.7.4 SEM for SLC cement samples

The microstructure of SLC-65 sample exposed to DS4 sulfate solutions for 24 months at 5 °C is shown in Figure 6.55. Although this sample did not exhibit any visual damage (see section 6.2.4), it can be noted from the image that, the cracks were widely spread over the sample and around sand particles. The white phases indicate GGBS particles.

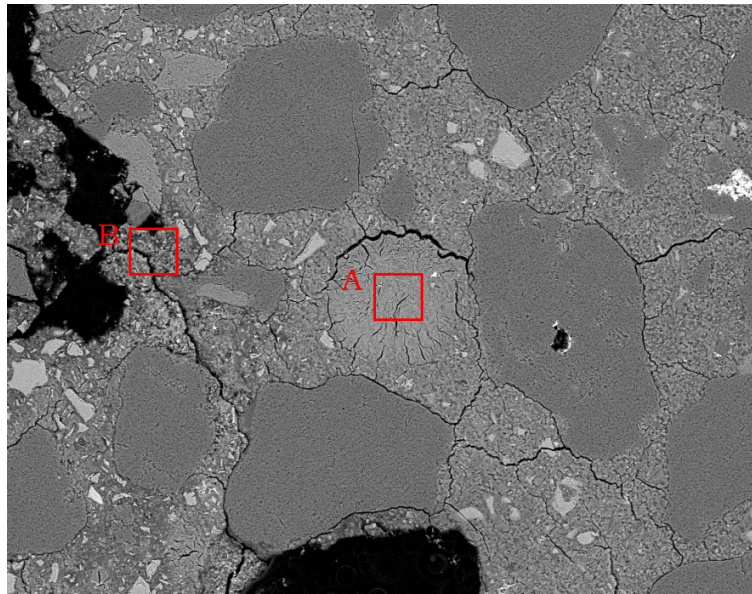


Figure 6.55 BSE of SLC-65 sample at 5 °C

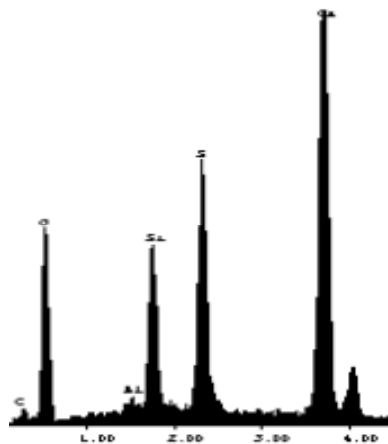
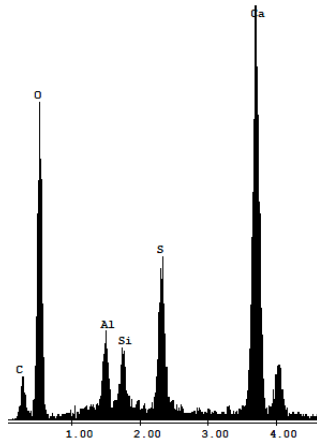


Figure 6.56 EDX microanalysis for spot A in Figure 6.55 showing thaumasite elements

The EDX micrograph for spot A in Figure 6.55 is shown in Figure 6.56. As this graph shows, thaumasite was present as an almost pure end product in this sample, suggesting the possibility of thaumasite formation in mortars with up to 70 % GGBS at 5 °C. The EDX microanalysis for spot B in Figure 6.55 is presented in Figure 6.57. The analysis showed the existence of both thaumasite and ettringite in the same region, which is an indication that a solid-solution phase was present in the near surface mortar.



**Figure 6.57 EDX microanalysis for spot B in Figure 5.55 showing thaumasite ettringite solid solution elements**

As it was observed from XRD results described in Section 6.5.4 that gypsum was present and the clearly seem almost pure crystals of gypsum confirmed this in Figure 6.58. This indicates that GGBS containing mortars are susceptible to sulfate attack with gypsum formation at low temperatures.

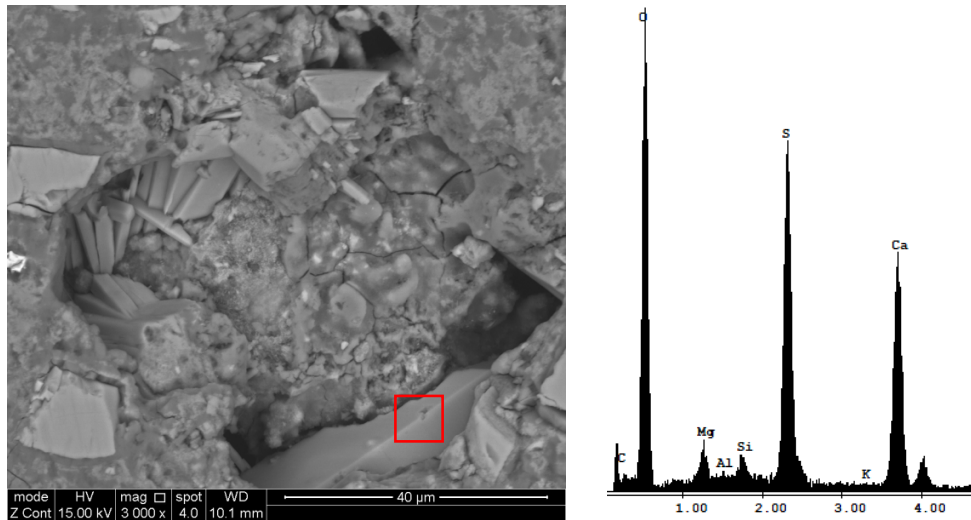


**Figure 6.58** Magnified image and EDX analysis for gypsum phase in SLC-65 sample at 5 °C

## 6.8 Thermodynamic modelling

### 6.8.1 CEMI cement samples

The thermodynamic modelling results of the interaction between CEMI samples and magnesium sulfate solutions are presented in Figure 6.59 and Figure 6.60 for DS3 and DS4 respectively at 5 °C. As it can be noted from these graphs the predicted phase assemblage are very similar and the only difference between them is the amount of solution needed to form sulfate bearing phases such as gypsum, and thaumasite is smaller for DS4 than DS3. CSH and portlandite phases are predicted to be stable at low sulfate concentration and started to dissolve at near surface regions where sulfates are available with higher quantities. The modelling also expected the stability of ettringite in regions where gypsum and thaumasite started to form (Kunther et al. 2013), however, as more quantities of these phases were formed, the ettringite dissolved to work probably as a source of sulfate to form more thaumasite and

## 6. Effect of water to cement ratio

gypsum. Only small amount of calcite was predicted according to thermodynamic calculations.

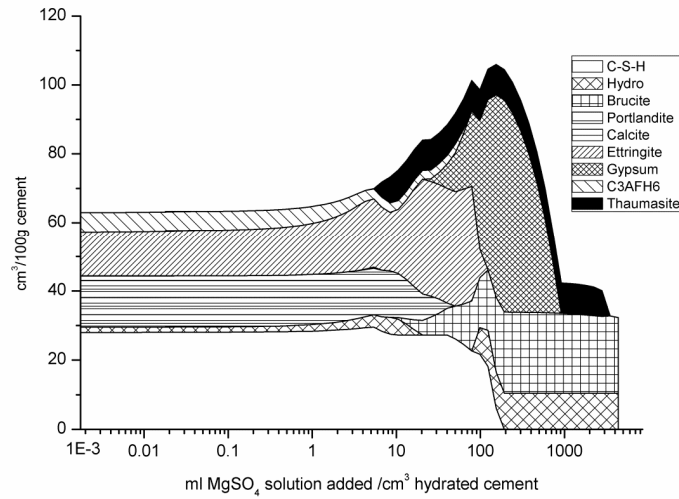


**Figure 6.59 Phase assemblage for CEMI in DS3 at 5 °C**

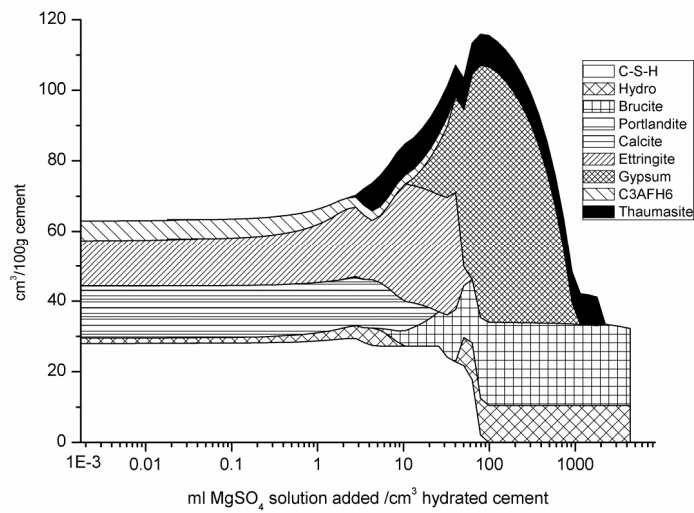


**Figure 6.60 Phase assemblage for CEMI in DS4 at 5 °C**

Magnesium containing phase's brucite and hydrotalcite are predicted to be the dominant phases close to the surface, which is expected due to the high sulfate concentration in this zone.

### 6.8.2 LFC cement samples

Figure 6.61 and Figure 6.62 show the predicted phases for LFC in DS3 and DS4 at 5 °C respectively. As it can be seen in these graphs, high quantities of thaumasite are predicted to be formed near the surface after the dissolve of gypsum and ettringite and due to limestone addition to the cement. The co-existence of thaumasite and ettringite can be clearly seen when thaumasite started to form representing the solid solution phase between these two minerals before thaumasite becomes the only end reaction member near surface. Calcite was calculated to be stable only near the core but it dissolves to form sulfate phases in regions close to surface. Portlandite and CSH phases are in abundance at near core zone and reacted to form other deterioration phase near the surface.

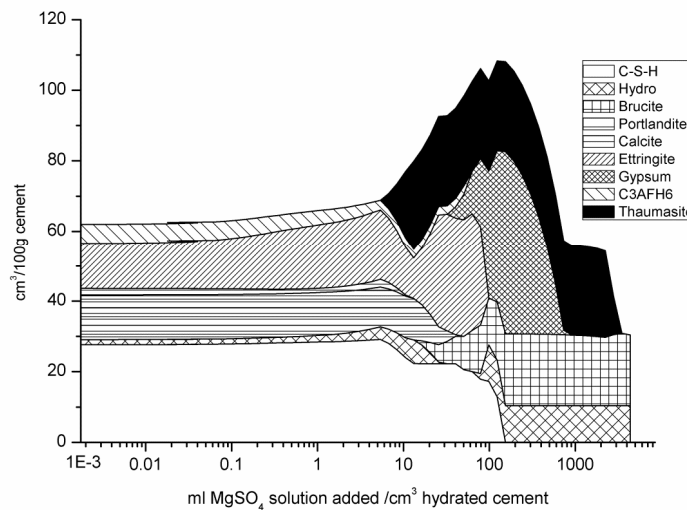


**Figure 6.61 Phase assemblage for LFC in DS3 at 5 °C**

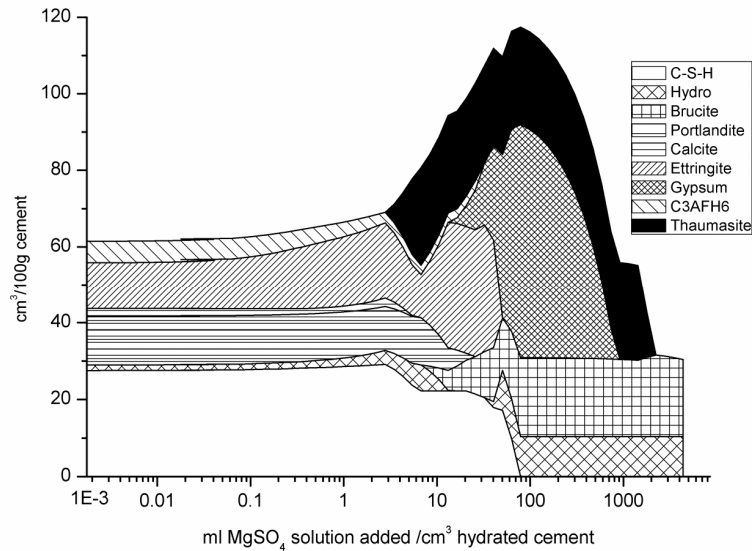


**Figure 6.62 Phase assemblage for LFC in DS4 at 5 °C**

### 6.8.3 FAC cement samples

Thermodynamic modelling calculations as a function of sulfate addition to hydrated cement for FAC are presented in Figure 6.63 and Figure 6.64 For DS3 and DS4 respectively. As it is shown in graphs, the calculated phase assemblages at small sulfate concentrations are; CSH and ettringite, thaumasite was predicted to form even at low sulfate amounts with small quantities. Gypsum only started to form at higher sulfate quantities where ettringite become unstable and started to dissolve. Neither calcite nor portlandite was predicted in this cement, this may suggest their early consumption to form another phases and involving in the pozzolanic reaction.

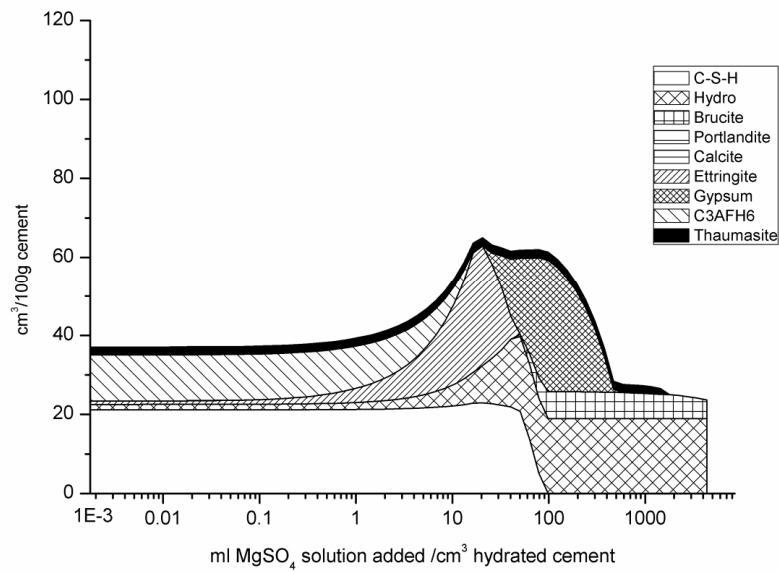


**Figure 6.63 Phase assemblages for FAC in DS3 at 5 °C**

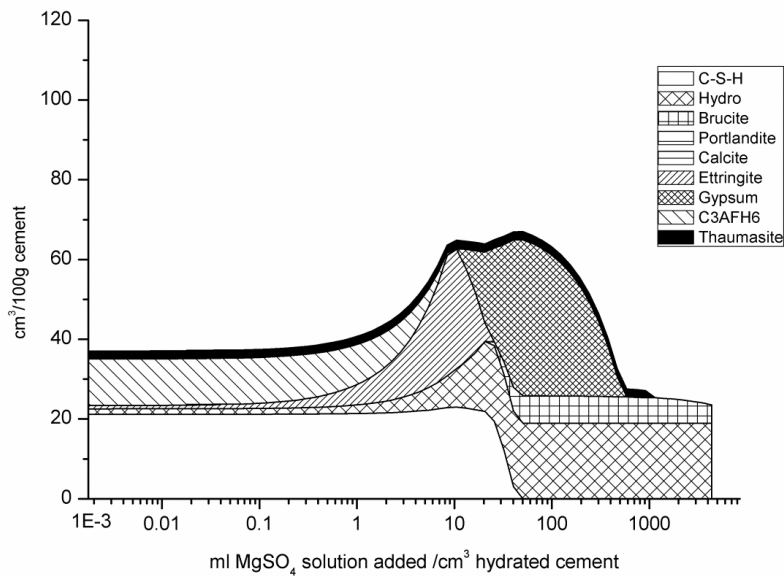


**Figure 6.64 Phase assemblages for FAC in DS4 at 5 °C**

#### 6.8.4 SLC cement samples

Figure 6.65 and Figure 6.66 show the predict phase assemblage calculated based on thermodynamic modelling for SLC cement exposed

## 6. Effect of water to cement ratio

from both graphs are very similar. Near core, CSH, ettringite and C3AFH6 in addition to hydrotalcite are the main phases, as the concentration of sulfate increased; the modelling predicted the conversion of ettringite to thaumasite (through solid solution and gypsum), however the gypsum consumed to form more thaumasite in near surface regions. Brucite can be clearly seen in outer layers while neither calcite nor portlandite were predicted to be available in the system.

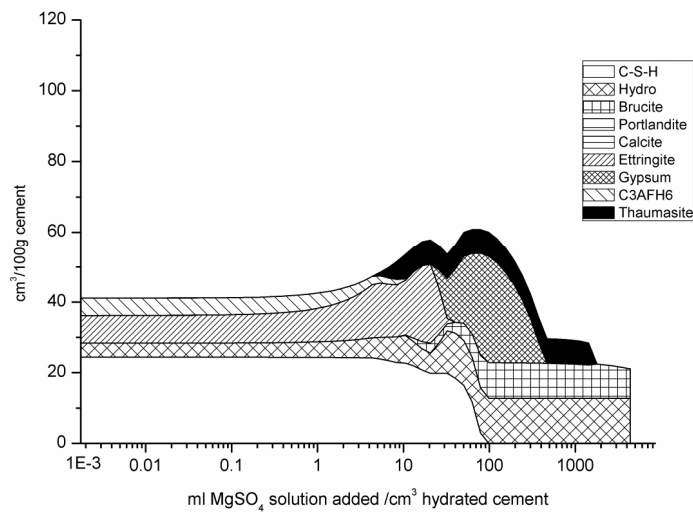


**Figure 6.65 Phase assemblages for SLC in DS3 at 5 °C**

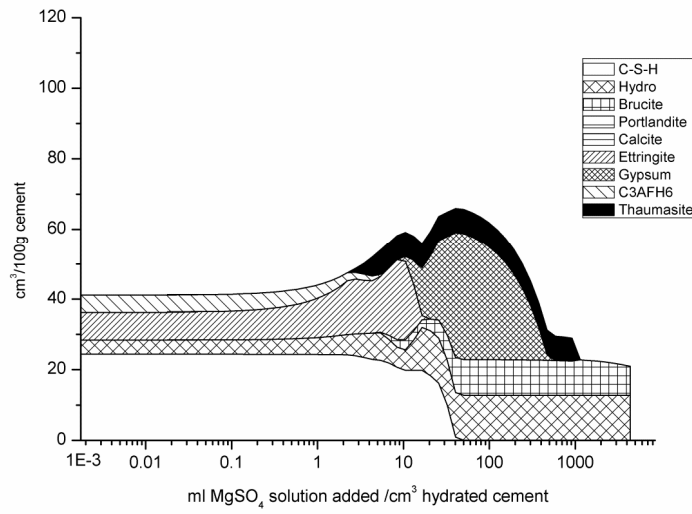


**Figure 6.66 Phase assemblage for SLC in DS4 at 5 °C**

Thermodynamic modelling for samples made with 0.45 and 0.55 w/c ratios exposed to DS4 sulfate solutions at 5 °C are shown in appendix B.

### **6.8.5 Thermodynamic modelling (overall quantitative comparison)**

The calculated volume of different phases for different cements exposed to DS3 and DS4 solutions at 5 °C are presented in Figure 6.67 and Figure 6.68 respectively. These results are qualitatively in good agreement with the experimental results obtained from XRD and FTIR presented in sections 6.5 and 6.6. By comparing the sulfate bearing phases, it can be seen from these two graphs that thaumasite is present in all cements in both solutions and its quantity is much higher in limestone containing cement LFC. More ettringite is calculated in samples exposed to DS3 than those of DS4 this may suggest the transforming of ettringite to thaumasite (woodfordite route). More gypsum was calculated to form under DS4 exposure due to high sulfate concentrations.

According to thermodynamic calculations, no portlandite was expected to form in fly ash (FLC) and GGBS (SLC) containing cements, this is possibly due to less cement content was used in these mixes which resulted in less portlandite formed. This portlandite would also be consumed to form deterioration products such as thaumasite.

The CSH phase are calculated to be more in DS3 samples, while the modelling expected its dissolving under higher sulfate concentrations where it was replaced with sulfate and magnesium containing phases.

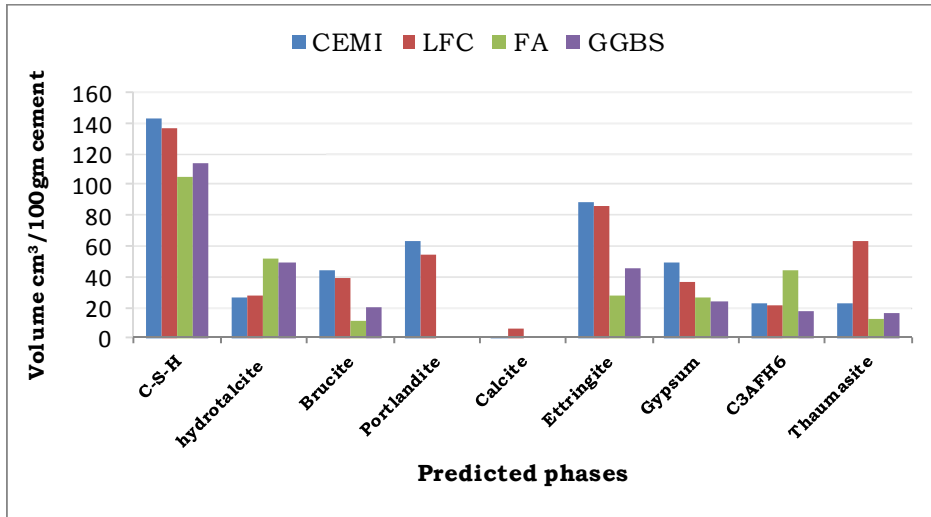


Figure 6.67 Volume of resulted phases for different cements in DS3

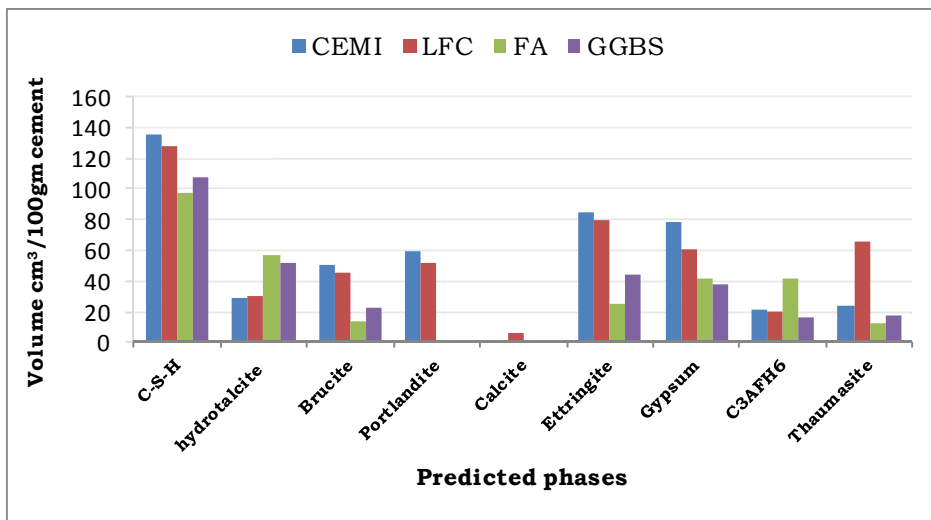


Figure 6.68 Volume of resulted phases for different cements in DS4

## 6.9 Summary

The investigation of the effect of variation in cement ratio on the formation of thaumasite in mortars made from different cements and exposed to two types of solutions BRE class (DS3 and DS4) at 5 and 20 °C has produced some interesting results. The variation in permeability due to differences of w:c ratio, would cause differences in resistance to chemical attack, but this effect was eliminated by grinding the samples to a fine powder, thus any differences would be due solely to chemical interaction effects. The following points shall present the main findings of this Chapter.

- Thaumasite is readily formed in mortar samples made with CEMI and LFC with w/c ratio as low as 0.45 and kept at 5 °C and in sulfate concentration as low as 3g/l SO<sub>4</sub>. However the intensity of attack is different from one cement to another.
- The intensity of the attack is very dependent on the value of w/c ratio, where, increasing the w/c ratio from 0.45 to 0.55 had significantly affected the performance of these cements against thaumasite type of sulfate attack. Nonetheless, increasing this ratio again to 0.65 did not affect the performance in a linear fashion. This suggests that there is a threshold water to cement ratio beyond which the performance of mortars will not be affected.
- CEMI samples exposed to sulfate solutions at 20 °C showed good resistance to thaumasite sulfate attack for up to 9 months after which samples made with 0.65 w/c ratio started to show signs of attack under DS4 solution immersion.
- CEMI mortar samples made with 0.45 w/c ratio resisted attack at 20 °C for the whole period of study (24 months) in both sulfate solutions.

- LFC mortar samples kept at 20 °C resisted attack for up to two years for all w/c ratios and both solutions.
- The intensity of the attack at 5 °C was greater in LFC samples while at 20 °C CEMI samples showed the worst behaviour. This suggests that limestone blended cements performed better against sulfate attack at higher temperatures at which the classical type of sulfate attack resulted in ettringite and gypsum formation that is more likely to happen or precede the thaumasite of sulfate attack.
- Although, it is known that the amount of thaumasite formed was increased by increasing the carbonate level in the mix, it was observed here that LFC samples performed better than CEMI samples that were made from higher water to cement ratio. This might lead to conclude that:
- The physical pore structure of the mortar is the dominant factor controlling the deterioration behaviour. This suggests that lowering the water to cement ratio and controlling the permeability are more beneficial than changing chemical compositions of cement in terms of resistance to thaumasite sulfate attack.
- The concentration of the sulfate seems to play a major role in affecting the performance of mortars against sulfate attack for samples with high w/c ratio. This effect is less noticeable in cases where the w/c ratio is low, and the physical properties of mortars delay the ingress of sulfates and other harmful species into the mortars.
- FAC and SLC mortar samples which were made from fly ash and GGBS blended cements showed superior resistance to the attack for up to 24 months and remained intact without showing any visual signs of deterioration. This can be generalised for all samples in all solutions and temperatures.

- The results from XRD, FTIR and SEM confirmed the possibility of thaumasite formation in FAC and SLC cements mortar powders in a time as short as 3 months at low temperatures, where the effect of pore structure and diffusion/permeability were eliminated and sulfates could readily access cement reacting phases. This can occur despite the low level of portlandite of these cements.
- The beneficial effect of GGBS in improving the resistance to TSA seems to stem from its effect in reducing the permeability of mortar or concrete rather than due to a chemical effect.
- Gypsum is detectable by all testing techniques in FAC and SLC mortar cements at 5 °C, suggesting the susceptibility of these cements to conventional type of sulfate attack. This gypsum could also serve as a source of sulfate to form more thaumasite.
- Monitoring mass change for immersed samples regularly can help in predicting the time at which the samples will start to show signs of deterioration, as the opening of unseen hair cracks in mortar matrix led to an increase in sample's mass.
- Again, similar to what was observed in Chapter 4 (Section 4.5), measuring length change is not a good tool to evaluate thaumasite sulfate attack, where samples only shown considerable amount of expansion after long time from shown first signs of visual deterioration.
- Ettringite seems to form before thaumasite as a first product in sulfate attack reactions, but with the progression of the attack ettringite is converted to thaumasite, this is in agreement with Brown and Hooton (2002).
- Thermodynamic modelling predicted the formation of thaumasite in GGBS containing cements. This confirmed the experimental results obtained from cement powders samples with this regard. In

general, there was a good agreement between calculated and observed phases in terms of qualitative measures.

# 7

## Overall Discussions

### 7.1 Introduction

The focus of this research was on the effect of wetting and drying cycles and carbonation on thaumasite formation in different cement mortars stored in conditions conducive to thaumasite formation. Another objective was to investigate the effect of physical properties of cement mortars on thaumasite formation, thus clarifying whether the superior resistance to TSA displayed by PFA and GGBS replacements of ordinary Portland cement is due to physical or chemical factors, or a combination of these controls. To do this mortar samples of the same types as the cube specimens were ground to fine powders and exposed to same conditions as the solid samples, which would eliminate the effect of permeability of the mortar and allow interaction between the mortar components and the solutions in systems having the same total chemistry.

Besides the type of cement, the amount of sulfate in solution and the temperature conditions were also varied.

This chapter presents the overall discussion of the results of these studies.

## **7.2 The effect of wetting and drying cycles on the formation of thaumasite in cement mortars.**

### **Visual observations:**

Samples that showed signs of visual deterioration followed almost the same patterns of attack:

Starting with small cracks developed around the corners and alongside the edges Figure 4.6a, these presumably the weakest points in samples where they are exposed to sulfate solutions from two or three directions. Once these cracks opened up, they are soon filled with a white substance (thaumasite) this material is soft and easily detachable. With passage of time, thaumasite will spread further beneath the skin of the samples which remains intact pushing it away from the sample. Thaumasite then, converts the mortar matrix to a mushy un-cohesive material losing its rigidity and integrity. It was noted that the attack is not limited to one face of the mortar; it can develop on any of the four faces even the face which is in contact with the container. It was also noted that the cracks are starting with a distance of around *1mm* from the edge as shown in Figure 4.6.

For wetting and drying samples the time needed for the sample to start showing the first signs of attack was much longer than continuous immersion samples and the un-affected layer was thicker.

### **Mass Change**

All samples showed a gradual increase in their masses in the first period of exposure. Samples which showed signs of deterioration started to show more weight gain compared to intact samples, this could be as a result of the opening of the cracks which were filled with solutions and to the formation of other products such as ettringite, gypsum and

thaumasite, with time passage, affected samples started to lose weight when the outer layer started to peel off. The amount of mass loss was in a relation to the severity of the attack where LFC samples showed the worst mass loss in DS4 solutions at 5 °C (section 4.4). They lost around 26% of their original mass which is almost three times to what CEMI samples in same solutions had lost (9%). Samples exposed to wetting and drying samples lost around 6 and 2.5 % for LFC and CDMI respectively. FAC and SLC samples continued in their mass gain with small increment in both storage regimes without showing any signs of mass loss or deterioration, this may suggest that their physical properties did not allow solution to penetrate inside due to their low permeability.

### ***Length Change***

Although LFC samples started to show signs of attack at around 84 days of exposure (section 4.2), these samples did not show any significant mass change till about 9 months of exposure (Figure 4.16). CEMI samples took around a year to exceed the limit of 0.1% set by standards and ended up with around 0.2 % expansion. FAC and SLC did not show any significant expansion for the whole period of the study. The same observation are applied for the samples went under wetting and drying cycles, where despite showing cracks and signs of attack after nine months of exposure and loosing around 6% of their weight, their expansion was under 0.1% for almost the whole period of study. This may suggest that measuring length change is not a useful tool in order to assist the deterioration caused by thaumasite type of sulfate attack.

### ***XRD and FTIR***

The results of the mineralogy of deteriorated materials presented in sections 4.4 and 4.5 showed that the deterioration products are quite

similar for both storage regimes. However few differences could be pointed out.

- Thaumasite was observed as an end product or as a solid solution with ettringite, however, ettringite alone as an end product could not be identified, this may suggest that ettringite phases tend to form first and then with more reactions with sulfate the aluminates ions replaced with silicate to form thaumasite, this what is known as woodfordite route (Bensted 2003)
- More calcium carbonate in forms of calcite and ettringite was identified in cements subjected to wetting and drying samples where less portlandite was there. This suggests the depletion of portlandite to form calcium carbonate phases rather than thaumasite since this reaction is quicker than thaumasite formation reaction.

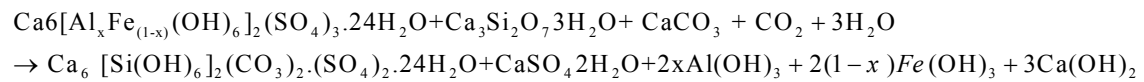
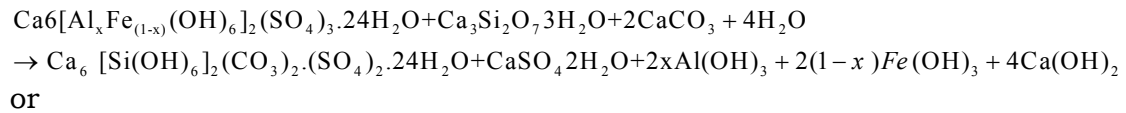
As for temperature, it was observed that the lower temperature of 5 °C is more favourable to thaumasite formation than 20 °C. This is also in agreement with the literature, and could be linked to the following points (Crammond 2003):

- The insolubility of thaumasite is much higher at lower temperatures.
- The stability of six co-ordinated  $\text{Si}(\text{OH})_6$  groups is higher at low temperatures.
- $\text{CO}_2$  which may work as a source of carbonate is more soluble at lower temperature.
- The solubility of portlandite is higher at low temperatures.

The mechanism by which thaumasite was formed in this research seems to be woodfordite route in which ettringite reacts with silicate from CSH and carbonate in presence of water to form thaumasite. The evidence for this suggestion is the presence of ettringite peaks both in XRD and FTIR

results particularly in the less deteriorated samples (i.e the early stages of the attack). This would indicate that the solid solution between these two minerals in the transition zone in which ettringite is becoming converted to thaumasite. This also can be seen in the SEM image and EDX microanalysis shown in Figures 4.57 and 4.59 where almost equal intensity peaks of both aluminates and silicates are present in the zone adjacent to thaumasite.

The woodfordite route reaction as described by Bensted (2003) is as follow:



Pulverised Fly ash (PFA) and blastfurnace slag (GGBS) blended cements performed very well in resisting thaumasite type of sulfate attack and showed no signs of deterioration after two years of exposure to sulfate solutions in both exposure regimes (See Figures 4.1-4.5). This high resistance to attack by slag containing cement was reported in literature (see section 2.6.1.2), but no clear explanation has given with this. It could be due to their low permeable structure or due to there being less portlandite available in the system. This is the result of a lower cement content which leads to most of the portlandite being consumed in the pozzolanic reactions. The high carbonation rate and low pH (as mentioned earlier) may also have played role in this high resistance. The same reasoning could be applied to PFA containing cements, although the susceptibility of PFA cement to TSA was reported in the literature (Mulenga et al. 2003). However, despite the fact that they did not show any physical damage after 2 years of exposure in DS4 sulfate solutions,

the XRD, FTIR and SEM results showed that cement blended with fly ash and blastfurnace slag are susceptible to thaumasite formation TF, involving thaumasite formation in the pores and cracks and not causing any deterioration. However this stage could possibly precede thaumasite sulfate attack TSA if the other conditions for thaumasite continue to occur.

### **Carbonation**

The carbonation process and the carbonated layer formed during the drying time have played a significant role in delaying thaumasite formation in wetting and drying samples as presented in chapter 5 where calcite formed in this layer filled the pores making a physical barrier to prevent more sulfate from ingression inside to react with CSH, the depletion of portlandite in this layer resulted in lower pH (section 5.3) to values at which thaumasite is not favoured to form. Figure 7.1 shows proposed phases changes after attacking with  $\text{MgSO}_4$  solution in the carbonated layer as it was observed by SEM analysis.

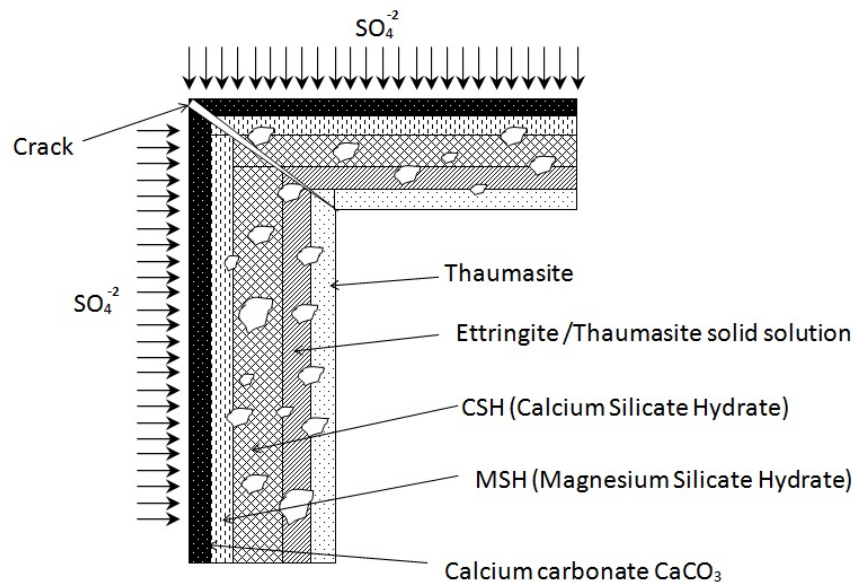


**Figure 7.1 Proposed phases in the carbonated layer based on SEM analysis**

### **7.3 The effect of water to cement ratio on thaumasite formation in cement mortars**

The results presented in Chapter 5 regarding the effect of variation in water to cement ratio on the formation of thaumasite in mortars made from different cements and exposed to two types of solutions BRE class (DS3 and DS4) at 5 and 20 °C has produced some interesting results. The variation in permeability due to differences of w:c ratio, would cause differences in resistance to chemical attack, but the effect on thaumasite formation of the physical structure was eliminated by grinding the samples to a fine powder, thus any differences would be due solely to chemical interaction effects.

Thaumasite was readily formed in mortars made with a water: cement ratio as low as 0.45, however, the intensity of the attack was dependant on the value of w/c ratio. Figure 7.2 shows the relation between the onset of attack for the different water to cement ratios, where only deteriorated samples are plotted, at 5 °C in both sulfate solutions. As it can be seen, samples with lower w/c ratios resisted attack for longer periods than those with higher w/c ratios. It is also observed that while increasing the w/c ratio from 0.45 to 0.55 had effect the onset of the deterioration, increasing the ratio again to 0.65 did not affect the deterioration by as much. Samples with limestone filler and low w/c ratio LFC-45, resisted attack for periods longer than sample with no limestone addition with higher w/c ratio CEMI-65. This suggests that in terms of resistance to thaumasite sulfate attack, controlling the permeability and improving the physical properties of the mortar are more beneficial than the changing chemical composition of the cement.

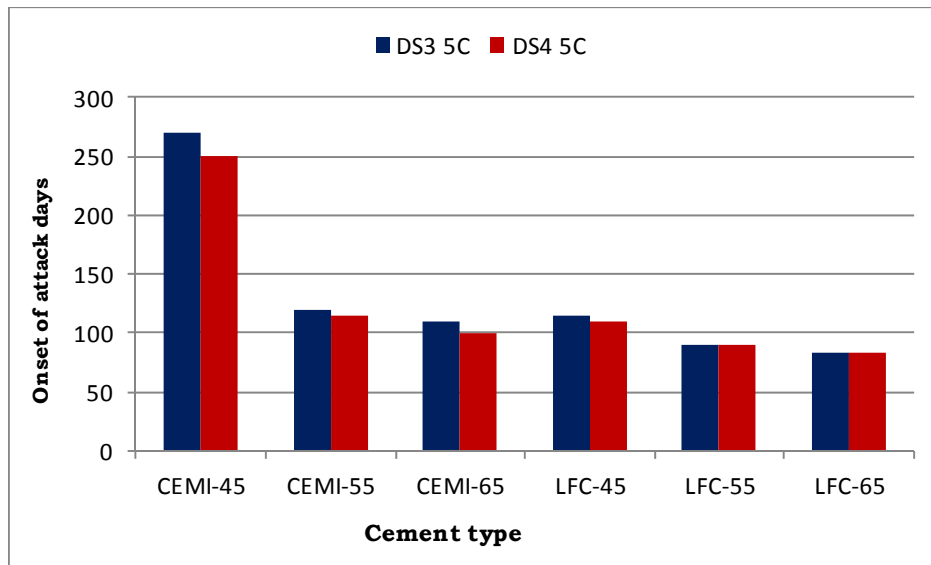


**Figure 7.2 Relationship between onset of attack and w/c ratio**

Regarding the rate of deterioration, it can be seen from Figure 7.3 that this is much faster in high w/c samples LFC samples. Although they started to deteriorate at a similar time (within 30 days) they ended up different losing weight according to their w/c ratios. It seems that the concentration of sulfate plays a more obvious role at higher w/c ratios. Again the LFC-45 sample performed better than CEMI-65 in terms of weight loss as an indication for sulfate attack.

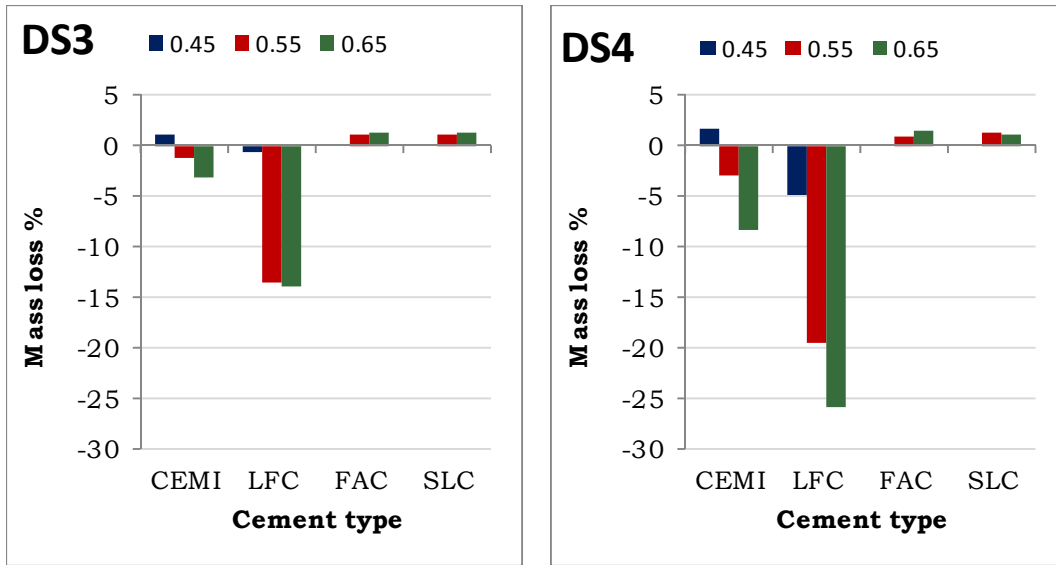


Figure 7.3 Relationship between mass change and different w/c ratios

The same trends were observed for length change measurements as shown in Figure 7.4 where samples with higher w/c ratio showed expansion values more than those with lower w/c ratios.

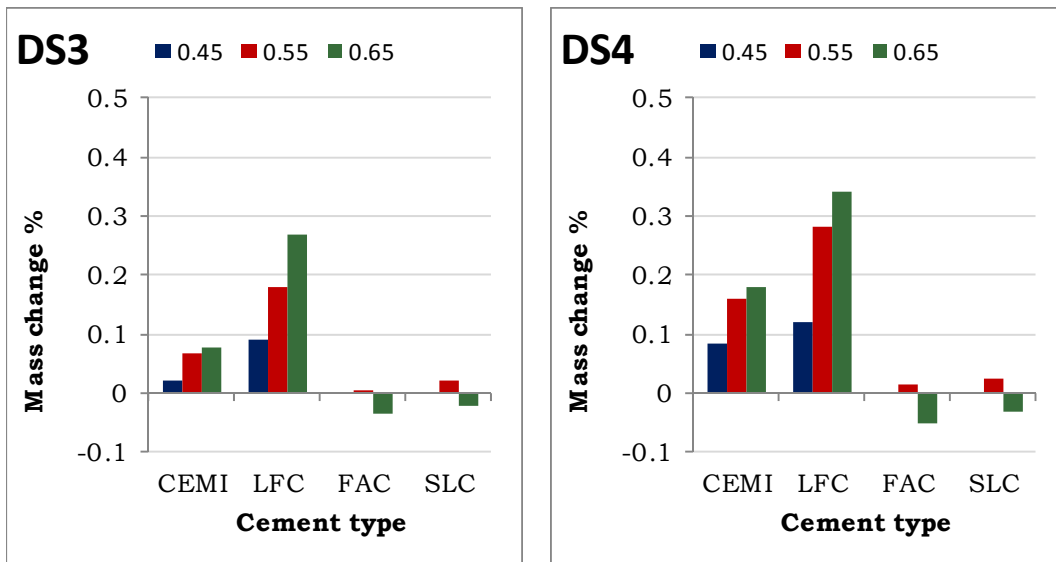


Figure 7.4 Relationship between length change and different w/c ratios

Despite showing no visual deterioration in solid samples, SEM images for PFA and Slag blended cements confirmed their susceptibility to Thaumaside formation TF. This is in spite of thaumasite peaks being observed in XRD and FTIR results for Powder Samples for both cements in as short a time as 3 months. This suggesting that the chemistry of these cements and less portlandite availability in the system does not prevent thaumasite formation; rather it is the low permeability which delays the attack on these cements. According to (Thaumasite Expert Group 1999) thaumasite formation TF could be the onset of thaumasite sulfate attack TSA.

### ***Thermodynamic modelling***

The thermodynamic modelling for powder samples confirmed the results obtained from the experimental work. The modelling showed that thaumasite is very possible to form in cements containing GGBS and PFA despite no or little portlandite available in the system, it also predict the dissolution of CSH phases at high sulfate concentration near the surface and its replacement with gypsum brucite and thaumasite. The co-existence of thaumasite and ettringite in the modelling calculations can be taken as an indication for the presence of thaumasite ettringite solid solutions and as evidence for woodfordite route as a way of thaumasite formation.

# 8

## **Overall conclusions and recommendations**

### **8.1 Overall conclusions**

This research investigated the effect of wetting and drying cycles, carbonation and physical properties of cement mortars on the thaumasite formation and thaumasite sulfate attack. The main conclusions which can be drawn from this study are as follow:

- Thaumasite type of sulfate attack TSA was responsible for the deterioration of CEMI and LFC cement mortars exposed to DS3 and DS4 sulfate solutions either continuously or under wetting and drying cycles at 5 °C, while samples made with FAC and SLC did not show any signs of visual deterioration after two years of exposure under same conditions and all cements performed better at 20 °C.
- Cyclic wetting and drying storage regime in which samples were kept in solution for 10 days at 5 and 20°C then followed by 20 days either at laboratory temperature of about 20±2 °C or in fridge at 5±1 °C delayed the formation of thaumasite in CEMI and LFC samples for up to 6 months compared to continuous immersion

samples at 5 °C. In other words the rate of attack was equivalent to the time that the samples were denied access to the solution, and it would appear that the reaction ceased once the sulfate in the remaining pore water had been consumed. (objective 1)

- In this study, good agreement was found between the length of wetting and drying cycles and the time needed for thaumasite to form which was 1:3 in both cases.
- The reduction in the rate of attack appears to be due to two complementary processes: carbonation effect as explained in Chapter 5 during the drying time seems to have caused this delaying effect by the surface calcite layer making a physical barrier which restricts sulfate ingress and by consumption considerable amount of portlandite which is main reactant in thaumasite formation reaction and finally by lowering the pH in the carbonated zones to levels which are not favour for thaumasite formation (see Figure 5.2). (Objective 2)
- The high resistance of GGBS and PFA blended cements to thaumasite type of sulfate attack seems to be derived from their low permeability rather than their matrix composition, where by eliminating the effect of diffusion and permeability and making the interaction with sulfates easier, this resulted in the formation of thaumasite in these samples in a time as short as three months. This can occur despite the low level of portlandite of these cements, which was the reason suggested by Hill et al. (2003). (objective 3)
- Although, the well-known relation between thaumasite formation and carbonate level in the mix, it was observed here that LFC samples performed better than CEMI samples that were made from higher water to cement ratio. It is assumed that reducing the

## 8. Overall conclusions and recommendations

---

w:c of LFC by 0.1 % gave LFC and CEMI (which include up to 5% added limestone) the same resistance.

- The results with powders and the carbonation effect imply that the physical pore structure of the mortar is the dominant factor controlling the deterioration behaviour. This suggests that lowering the water to cement ratio and controlling the permeability are more beneficial than changing chemical compositions of cement in terms of resistance to thaumasite sulfate attack.
- Thaumasite can readily form in solutions with sulfate concentration as low as DS3 3g/l SO<sub>4</sub> at 5 °C. However the intensity of attack and its progress rate are slower than DS4.
- The suggested mechanism of thaumasite formation in this study is woodfordite route where thaumasite is formed from ettringite by replacing Al ions in the ettringite system with Si ions to form thaumasite. This is suggested because of the presence of aluminate peaks attributed to ettringite in both FTIR and SEM results in the less deteriorated samples, while at the most deteriorated samples thaumasite appeared to be the only end product of the deterioration products.
- The presence of gypsum in the deterioration materials at early ages of attack and its disappearance in later stages suggests that gypsum could serve as a source of sulfate during the later stages of thaumasite sulfate attack to form more thaumasite.
- Thaumasite can readily form in media with pH values of as low as 8.7 as happened in wetting and drying samples. In continuous immersion samples the thaumasite started to form when the pH was 9.7. This is in contrast to the findings of Gaze and Crammond (2000) who suggest thaumasite required a pH of more than 10.5 to form / remain stable.

- The low pH values of wetting and drying samples had led to less thaumasite was formed in these samples despite more carbonate was there, where thaumasite tend to be not stable in low pH values.
- The results of mass change experiments show that monitoring mass change of samples regularly can help in predicting the time at which the samples start to show signs of deterioration, as the opening of unseen hair-line cracks in mortar matrix leads to an increase in sample's mass.
- The relation between the length change and thaumasite formation is not clear, where at the time when thaumasite started to form the change in length was not significant, and deteriorated samples took quite long time to become significant. However, at the end of the study there was an agreement between length change measurements and amount of deterioration.
- The carbonated layer of about 1mm thick remained intact and did not exhibit thaumasite attack TSA. Figure 7.1 shows a schematic diagram for proposed phase's changes after attacking with MgSO<sub>4</sub> solution in the carbonated layer as it was observed by SEM analysis.
- Thermodynamic modelling was a useful tool in predicting the deterioration products and its results were in agreement with the experiments and confirmed the possibility of thaumasite formation in GGBS cements where full interaction with sulfate is enabled.

### **8.2 Implementations for engineering**

This study has provided new information about the formation of thaumasite under cyclic wetting and drying exposure conditions, and about the possibility of thaumasite formation in mortars blended with GGBS and PFA cements.

The following key findings are considered from an engineering point of view:

- Structures subjected to wetting and drying exposure conditions are susceptible to thaumasite type of sulfate attack, this vulnerability depends on the length of wetting to drying cycle and temperature, this could be useful in estimating the life expectancy for samples exposed to these cycles.
- Cements with up to 3.5% lime filler which is allowed by standards can be easily attacked by thaumasite type of sulfate attack at 5 and 20 °C.
- CEMI and LFC made with low water to cement ratio 0.45 cannot provide protection against thaumasite type of sulfate attack at 5 °C.
- GGBS and PFA containing cements are susceptible to thaumasite formation TF, which was proposed by the Thaumasite Expert Group (Thaumasite Expert Group 1999) as a sign precedes thaumasite sulfate attack TSA.
- While the role of permeability is important in preventing the ingress of harmful sulfate, surface coating could offer an effective way in preventing the damage due to thaumasite sulfate attack.
- Pre-carbonation for plain concrete blocks could be useful with regard to their resistance to sulfate attack.

### **8.3 Recommendation for further study**

The following areas could be recommended for further study:

- More than one wetting and drying cycles could be used to establish the relation between the cycle length and time needed for thaumasite formation. A cycle length of with 1:1 or 1:2 could be used

- The formation of thaumasite TF in GGBS containing cements was confirmed in this research. Should this be treated as an onset of thaumasite type of sulfate attack? This may need further investigation by using accelerated conditions such as high w/c ratio with high sulfate concentration
- The effect on thaumasite formation of the carbonated layer appears to be clear from this study. However, a study in which access to CO<sub>2</sub> is completely prevented compare the performance of fully carbonated samples will help establishing the relation between them.
- pH plays an important role regarding thaumasite formation, so the threshold at which thaumasite will start to form requires more investigation.
- Thermodynamic modelling of the chemical changes to the specimens and the solutions in the experimental results is a useful way to predict the possibilities of thaumasite to form under different conditions such as different water / cement ratios and in powders and the stability of thaumasite in different pH media. A transport modelling which can predict the phases as a function of time and distance would be a great tool to confirm the results obtained experimentally.

---

## References

- Aye, T. , Oguchi, C. T. & Takaya, Y. (2010). Evaluation of sulfate resistance of Portland and high alumina cement mortars using hardness test. *Construction And Building Materials*, 24, 1020-1026.
- Barker, A. P. & Hobbs, D. W. (1999). Performance of Portland limestone cements in mortar prisms immersed in sulfate solutions at 5 °C. *Cement and Concrete Composites*, 21, 129-137.
- Barnett, S. J. , Macphee, D. E. & Crammond, N. J. (2003). Extent of immiscibility in the ettringite-thaumasite system. *Cement and Concrete Composites*, 25, 851-855.
- Barnett, S. J. , Macphee, D. E. , Lachowski, E. E. & Crammond, N. J. (2002). XRD, EDX and IR analysis of solid solutions between thaumasite and ettringite. *Cement And Concrete Research*, 32, 719-730.
- Bellmann, E. (2004a). On the formation of thaumasite  $\text{CaSiO}_3 \cdot \text{CaSO}_4 \cdot \text{CaCO}_3 \cdot 15\text{H}_2\text{O}$  : Part II. *Advances In Cement Research*, 16, 89-94.
- Bellmann, F. (2004b). On the formation of thaumasite  $\text{CaSiO}_3 \cdot \text{CaSO}_4 \cdot \text{CaCO}_3 \cdot 15\text{H}_2\text{O}$ : Part I. *Advances In Cement Research*, 16, 55-60.
- Bensted, J. (1988). Thaumasite—a deterioration product of hardened cement structures. *Cemento II*, 3-10.
- Bensted, J. (1999). Thaumasite -- background and nature in deterioration of cements, mortars and concretes. *Cement and Concrete Composites*, 21, 117-121.
- Bensted, J. (2003). Thaumasite--direct, woodfordite and other possible formation routes. *Cement and Concrete Composites*, 25, 873-877.
- Bensted, J. & Satya Prakash, V. (1976). A discussion of the paper "Thaumasite formation: A cause of deterioration of portland cement and related substances in the presence of sulphates" by J. H. P. Van Aardt and S. Visser. *Cement And Concrete Research*, 6, 321-322.
- Bensted, J. & Varma, S. P. (1973). Studies of thaumasite. *Silicates Industriels*, 38, 29-32.

- Bensted, J. & Varma, S. P. (1974). Studies of thaumasite—Part II. *Silicates Industriels*, 39, 11-19.
- Blanco-Varela, M. T. , Aguilera, J. & Martínez-Ramírez, S. (2006). Effect of cement C<sub>3</sub>A content, temperature and storage medium on thaumasite formation in carbonated mortars. *Cement And Concrete Research*, 36, 707-715.
- Borges, P. R. , Milestone, N. , Costa, J. , Lynsdale, C. , Panzera, T. & Christophoro, A. (2012). Carbonation durability of blended cement pastes used for waste encapsulation. *Materials And Structures*, 45, 663-678.
- BRE SD1 2001. BRE Special Digest 1 Concrete in aggressive ground Part 1: Assessing the aggressive chemical environment. BRE Centre for Concrete Construction and Centre for Ground Engineering Remediation.
- Brown, P. & Hooton, R. D. (2002). Ettringite and thaumasite formation in laboratory concretes prepared using sulfate-resisting cements. *Cement & Concrete Composites*, 24, 361-370.
- BS EN 197-1:2011 2011. Cement—Part 1: composition, specifications and conformity criteria for common cements. London: British Standards Institution.
- Byfors, K. (1985). Carbonation of concrete with silica fume and fly ash. *Nordic concrete research*, 26-35.
- Colleparidi, M. (1999). Thaumasite formation and deterioration in historic buildings. *Cement & Concrete Composites*, 21, 147-154.
- Collett, G. , Crammond, N. J. , Swamy, R. N. & Sharp, J. H. (2004). The role of carbon dioxide in the formation of thaumasite. *Cement And Concrete Research*, 34, 1599-1612.
- Crammond, N. (2002). The occurrence of thaumasite in modern construction - a review. *Cement & Concrete Composites*, 24, 393-402.
- Crammond, N. J. (2003). The thaumasite form of sulfate attack in the UK. *Cement & Concrete Composites*, 25, 809-818.
- Crammond, N. J. , Collett, G. W. & Longworth, T. I. (2003). Thaumasite field trial at Shipston on Stour: three-year preliminary assessment of buried concretes. *Cement & Concrete Composites*, 25, 1035-1043.
- Diamond, S. (2003). Thaumasite in Orange County, Southern California: an inquiry into the effect of low temperature. *Cement & Concrete Composites*, 25, 1161-1164.

- Escadeillas, G. , Aubert, J.-E. , Segerer, M. & Prince, W. (2007). Some factors affecting delayed ettringite formation in heat-cured mortars. *Cement And Concrete Research*, 37, 1445-1452.
- Gaze, M. E. & Crammond, N. J. (2000). The formation of thaumasite in a cement : lime : sand mortar exposed to cold magnesium and potassium sulfate solutions. *Cement & Concrete Composites*, 22, 209-222.
- Halliwell, M. A. & Crammond, N. J. (1999). Avoiding the thaumasite form of sulfate attack. *Durability Of Building Materials And Components* 8, Vols 1-4, Proceedings, 139-148.
- Hartshorn, S. A. , Sharp, J. H. & Swamy, R. N. (1999). Thaumasite formation in Portland-limestone cement pastes. *Cement And Concrete Research*, 29, 1331-1340.
- Hartshorn, S. A. , Sharp, J. H. & Swamy, R. N. (2002). The thaumasite form of sulfate attack in Portland-limestone cement mortars stored in magnesium sulfate solution. *Cement & Concrete Composites*, 24, 351-359.
- Hartshorn, S. A. , Swamy, R. N. & Sharp, J. H. (2001). Engineering properties and structural implications of Portland limestone cement mortar exposed to magnesium sulphate attack. *Advances In Cement Research*, 13, 31-46.
- Hekal, E. E. , Kishar, E. & Mostafa, H. (2002). Magnesium sulfate attack on hardened blended cement pastes under different circumstances. *Cement And Concrete Research*, 32, 1421-1427.
- Higgins, D. D. & Crammond, N. J. (2003). Resistance of concrete containing ggbs to the thaumasite form of sulfate attack. *Cement & Concrete Composites*, 25, 921-929.
- Hill, J. , Byars, E. A. , Sharp, J. H. , Lynsdale, C. J. , Cripps, J. C. & Zhou, Q. (2003). An experimental study of combined acid and sulfate attack of concrete. *Cement & Concrete Composites*, 25, 997-1003.
- Hobbs, D. W. & Taylor, M. G. (2000). Nature of the thaumasite sulfate attack mechanism in field concrete. *Cement And Concrete Research*, 30, 529-533.
- Hong, K. & Hooton, R. D. (1999). Effects of cyclic chloride exposure on penetration of concrete cover. *Cement And Concrete Research*, 29, 1379-1386.
- Hooton, R. D. & Thomas, M. D. A. (2002). *The Use of Limestone In Cement: Effect on the Thaumasite Form of Sulfate Attack*. Portland Cement Association, SN2658, 9pp.

- Irassar, E. F. , Bonavetti, V. L. , Trezza, M. A. & González, M. A. (2005). Thaumasite formation in limestone filler cements exposed to sodium sulphate solution at 20 °C. *Cement and Concrete Composites*, 27, 77-84.
- Jallad, K. N. , Santhanam, M. & Cohen, M. D. (2003). Stability and reactivity of thaumasite at different pH levels. *Cement And Concrete Research*, 33, 433-437.
- Jan Skalny , Jacques Marchand & Ivan Odler (2003). *sulfate Attack on Concrete*, New York, Spon Press.
- Juel, I. , Herfort, D. , Gollop, R. , Konnerup-Madsen, J. , Jakobsen, H. J. & Skibsted, J. (2003). A thermodynamic model for predicting the stability of thaumasite. *Cement & Concrete Composites*, 25, 867-872.
- Justnes, H. (2003). Thaumasite formed by sulfate attack on mortar with limestone filler. *Cement and Concrete Composites*, 25, 955-959.
- Kakali, G. , Tsvivilis, S. , Skaropoulou, A. , Sharp, J. H. & Swamy, R. N. (2003). Parameters affecting thaumasite formation in limestone cement mortar. *Cement and Concrete Composites*, 25, 977-981.
- Khan, M. I. & Lynsdale, C. J. (2002). Strength, permeability, and carbonation of high-performance concrete. *Cement And Concrete Research*, 32, 123-131.
- Kulik, D. A. , Wagner, T. , Dmytrieva, S. V. , Kosakowski, G. , Hingerl, F. F. , Chudnenko, K. V. & Berner, U. R. (2013). GEM-Selektor geochemical modeling package: revised algorithm and GEMS3K numerical kernel for coupled simulation codes. *Computational Geosciences*, 17, 1-24.
- Kunther, W. , Lothenbach, B. & Scrivener, K. (2013). Influence of bicarbonate ions on the deterioration of mortar bars in sulfate solutions. *Cement And Concrete Research*, 44, 77-86.
- Lange, L. C. , Hills, C. D. & Poole, A. B. (1997). Effect of carbonation on properties of blended and non-blended cement solidified waste forms. *Journal of Hazardous Materials*, 52, 193-212.
- Lee, S. T. , Moon, H. Y. , Hooton, R. D. & Kim, J. P. (2005). Effect of solution concentrations and replacement levels of metakaolin on the resistance of mortars exposed to magnesium sulfate solutions. *Cement And Concrete Research*, 35, 1314-1323.
- Liu, Z. , Deng, D. , De Schutter, G. & Yu, Z. (2013). The effect of MgSO<sub>4</sub> on thaumasite formation. *Cement and Concrete Composites*, 35, 102-108.
- Lixiong, G. , Yan, Y. & Ling, W. (2005). Effects of thaumasite formation on the performance of Portland-limestone concrete stored in magnesium sulfate

- solution. *Journal of Wuhan University of Technology--Materials Science Edition*, 20, 113-115.
- Lothenbach, B. , Bary, B. , Le Bescop, P. , Schmidt, T. & Leterrier, N. (2010). Sulfate ingress in Portland cement. *Cement And Concrete Research*, 40, 1211-1225.
- Lothenbach, B. & Gruskovnjak, A. (2007). Hydration of alkali-activated slag: Thermodynamic modelling. *Advances In Cement Research*, 19, 81-92.
- Lothenbach, B. , Matschei, T. , Möschner, G. & Glasser, F. P. (2008). Thermodynamic modelling of the effect of temperature on the hydration and porosity of Portland cement. *Cement And Concrete Research*, 38, 1-18.
- Lothenbach, B. & Winnefeld, F. (2006). Thermodynamic modelling of the hydration of Portland cement. *Cement And Concrete Research*, 36, 209-226.
- M. Maage, (1986) Carbonation in concrete made of blended cements, in: G.J. McCarthy, M. Maage, F.P. Glasser, D.M. Roy (Eds.), *Symposium of Materials Research Society*, vol. 65, Boston, USA, pp. 193-197.
- Macphee, D. & Diamond, S. (2003). Thaumasite in cementitious materials. *Cement & Concrete Composites*, 25, 805-807.
- Mangat, P. S. & El-Khatib, J. M. (1992). Influence of initial curing on sulphate resistance of blended cement concrete. *Cement and Concrete Research*, 22, 1089-1100.
- Martinez-Ramirez, S. , Blanco-Varela, M. T. & Rapazote, J. (2011). Thaumasite formation in sugary solutions: Effect of temperature and sucrose concentration. *Construction And Building Materials*, 25, 21-29.
- Matschei, T. (2007). *Thermodynamics of Cement Hydration*. PhD thesis, University of Aberdeen.
- Moukwa, M. (1990). Deterioration of concrete in cold sea waters. *Cement And Concrete Research*, 20, 439-446.
- Mulenga, D. M. , Stark, J. & Nobst, P. (2003). Thaumasite formation in concrete and mortars containing fly ash. *Cement & Concrete Composites*, 25, 907-912.
- Neville, A. M. (2002). *Properties of concrete*, Longman.
- Newman, J. & Choo, B. S. (eds.) 2003. *Advanced Concrete Technology ( concrete properties)*, London: Elsevier.
- Nixon, P. J. , Longworth, T. I. & Matthews, J. D. (2003). New UK guidance on the use of concrete in aggressive ground. *Cement & Concrete Composites*, 25, 1177-1184.

- Nobst, P. & Stark, J. (2003). Investigations on the influence of cement type on thaumasite formation. *Cement & Concrete Composites*, 25, 899-906.
- Novak, G. A. & Colville, A. A. (1989). Efflorescent mineral assemblages associated with cracked and degraded residential concrete foundations in Southern California. *Cement And Concrete Research*, 19, 1-6.
- Osborne, G. J. (1990). The effectiveness of a carbonated outer layer to concrete in the prevention of sulfate attack.
- Pajares, I. , Martinez-Ramirez, S. & Blanco-Varela, M. T. (2003). Evolution of ettringite in presence of carbonate, and silicate ions. *Cement & Concrete Composites*, 25, 861-865.
- Papadakis, V. G. , Fardis, M. N. & Vayenas, C. G. (1992). Effect of composition, environmental factors and cement-lime mortar coating on concrete carbonation. *Materials And Structures*, 25, 293-304.
- Pipilikaki, P. , Papageorgiou, D. , Teas, C. , Chaniotakis, E. & Katsioti, M. (2008). The effect of temperature on thaumasite formation. *Cement and Concrete Composites*, 30, 964-969.
- Plowman, C. & Cabrera, J. G. (1996). The use of fly ash to improve the sulphate resistance of concrete. *Waste Management*, 16, 145-149.
- Poitevin, P. (1999). Limestone aggregate concrete, usefulness and durability. *Cement & Concrete Composites*, 21, 89-97.
- Prasad J , Jain D.K & Ahuja A. K (2006). Factors influencing the sulphate resistance of cement concrete and mortar. *Asian Journal of civil engineering (Building and housing)*, 7, 259-268.
- Q. Zhou , E.W. Byars , C.J. Lynsdale , J.C. Cripps , J. Hill & Sharp, J. H. (2007). Relative Resistance of Portland and Pozzolanic Cements to the Thaumasite Form of Sulfate Attack (TSA). In: 12th International congress on the chemistry of cement, M4-03.4.
- Ramachandran, V. S. , Paroli, R. M. , Beaudoin, J. J. & Delgado, A. H. (2002). Formation and Hydration of Cement and Cement Compounds. *Handbook of Thermal Analysis of Construction Materials*. Norwich, NY: William Andrew Publishing.
- Sabbioni, C. , Zappia, G. , Riontino, C. , Blanco, M. T. , Puertas, F. , Aguilera, J. , Palomo, A. , Van Balen, K. & Toumbakari, E. E. (1999). Environmental deterioration of ancient and modern hydraulic mortars. *Structural Studies, Repairs And Maintenance Of Historical Buildings* Vi, 6, 201-210.

- Sahmaran, M. , Erdem, T. K. & Yaman, I. O. (2007). Sulfate resistance of plain and blended cements exposed to wetting-drying and heating-cooling environments. *Construction And Building Materials*, 21, 1771-1778.
- Sahu, S. , Exline, D. L. & Nelson, M. P. (2002). Identification of thaumasite in concrete by Raman chemical imaging. *Cement & Concrete Composites*, 24, 347-350.
- Santhanam, M. , Cohen, M. D. & Olek, J. (2003). Effects of gypsum formation on the performance of cement mortars during external sulfate attack. *Cement And Concrete Research*, 33, 325-332.
- Schmidt, T. , Lothenbach, B. , Romer, M. , Neuenschwander, J. & Scrivener, K. (2009). Physical and microstructural aspects of sulfate attack on ordinary and limestone blended Portland cements. *Cement And Concrete Research*, 39, 1111-1121.
- Schmidt, T. , Lothenbach, B. , Romer, M. , Scrivener, K. , Rentsch, D. & Figi, R. (2008). A thermodynamic and experimental study of the conditions of thaumasite formation. *Cement And Concrete Research*, 38, 337-349.
- Sims, I. & Huntley, S. A. (2004). The thaumasite form of sulfate attack-breaking the rules. *Cement & Concrete Composites*, 26, 837-844.
- Skibsted, J. , Rasmussen, S. , Herfort, D. & Jakobsen, H. J. (2003). <sup>29</sup>Si cross-polarization magic-angle spinning NMR spectroscopy - an efficient tool for quantification of thaumasite in cement-based materials. *Cement & Concrete Composites*, 25, 823-829.
- Slater, D. , Floyd, M. & Wimpenny, D. E. (2003). A summary of the Highways Agency Thaumasite Investigation in Gloucestershire: the scope of work and main findings. *Cement & Concrete Composites*, 25, 1067-1076.
- Thaumasite Expert Group (1999). The thaumasite form of sulfate attack: Risks, diagnosis, remedial works and guidance on new construction, Department of the Environment. London.
- Thomas, M. D. A. & Matthews, J. D. (2004). Performance of pfa concrete in a marine environment--10-year results. *Cement and Concrete Composites*, 26, 5-20.
- Torii, K. , Taniguchi, K. & Kawamura, M. (1995). Sulfate resistance of high fly ash content concrete. *Cement And Concrete Research*, 25, 759-768.

- Torres, S. M. (2004). The Influence of Chloride on the thaumasite form of sulfate attack in mortars containing calcium carbonate. PhD thesis, University of Sheffield.
- Torres, S. M. , Kirk, C. A. , Lynsdale, C. J. , Swamy, R. N. & Sharp, J. H. (2004). Thaumasite-ettringite solid solutions in degraded mortars. *Cement And Concrete Research*, 34, 1297-1305.
- Torres, S. M. , Sharp, J. H. , Swamy, R. N. , Lynsdale, C. J. & Huntley, S. A. (2003). Long term durability of Portland-limestone cement mortars exposed to magnesium sulfate attack. *Cement & Concrete Composites*, 25, 947-954.
- Tsivilis, S. , Kakali, G. , Skaropoulou, A. , Sharp, J. H. & Swamy, R. N. (2003). Use of mineral admixtures to prevent thaumasite formation in limestone cement mortar. *Cement & Concrete Composites*, 25, 969-976.
- Veiga, K. K. & Gastaldini, A. L. G. (2012). Sulfate attack on a white Portland cement with activated slag. *Construction And Building Materials*, 34, 494-503.
- Wagner, T. , Kulik, D. A. , Hingerl, F. F. & Dmytrieva, S. V. (2012). GEM-Selektor geochemical modeling package: TSolMod library and data interface for multicomponent phase models. *Canadian Mineralogist*, 50, 1173-1195.
- Wang, K. , Nelsen, D. E. & Nixon, W. A. (2006). Damaging effects of deicing chemicals on concrete materials. *Cement and Concrete Composites*, 28, 173-188.
- Yang, R. & Buenfeld, N. R. (2000). Microstructural identification of thaumasite in concrete by backscattered electron imaging at low vacuum. *Cement And Concrete Research*, 30, 775-779.
- Yigiter, H. , Yazici, H. & Aydin, S. (2007). Effects of cement type, water/cement ratio and cement content on sea water resistance of concrete. *Building and Environment*, 42, 1770-1776.
- Zelic, J. , Krstulovic, R. , Tkalcec, E. & Krolo, P. (1999). Durability of the hydrated limestone-silica fume Portland cement mortars under sulphate attack. *Cement And Concrete Research*, 29, 819-826.
- Zelic, J. , Krstulovic, R. , Tkalcec, E. & Krolo, P. (2000). The properties of Portland cement-limestone-silica fume mortars. *Cement And Concrete Research*, 30, 145-152.
- Zhou, Q. , Hill, J. , Byars, E. A. , Cripps, J. C. , Lynsdale, C. J. & Sharp, J. H. (2006). The role of pH in thaumasite sulfate attack. *Cement And Concrete Research*, 36, 160-170.

# Appendix A

Length change results for control samples (samples stored in water)

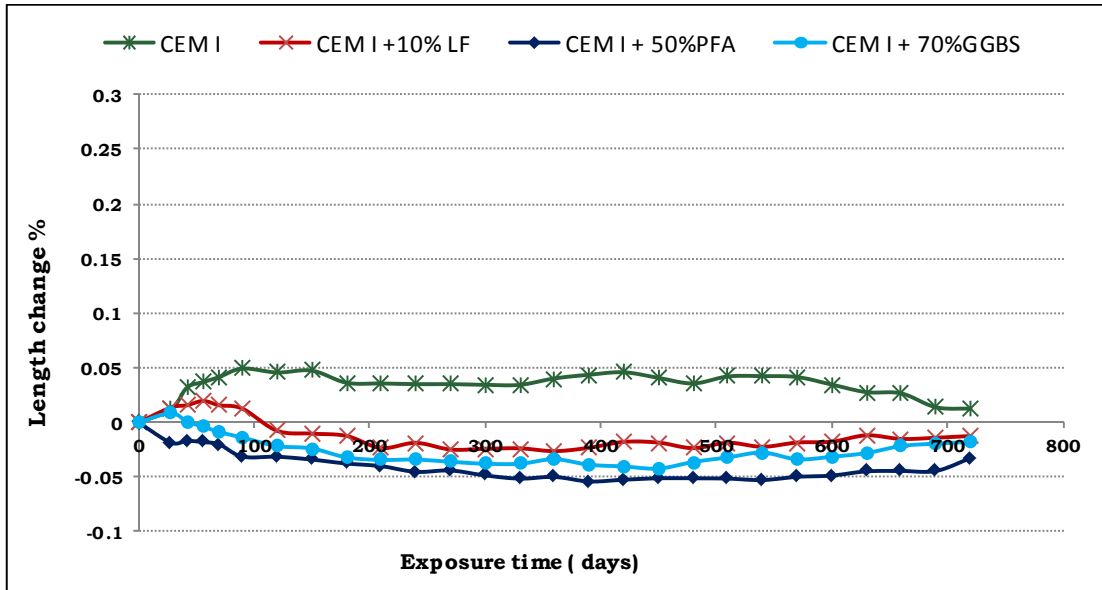


Figure A.1 Length change for samples in water at 5 °C. (Continuous immersion)

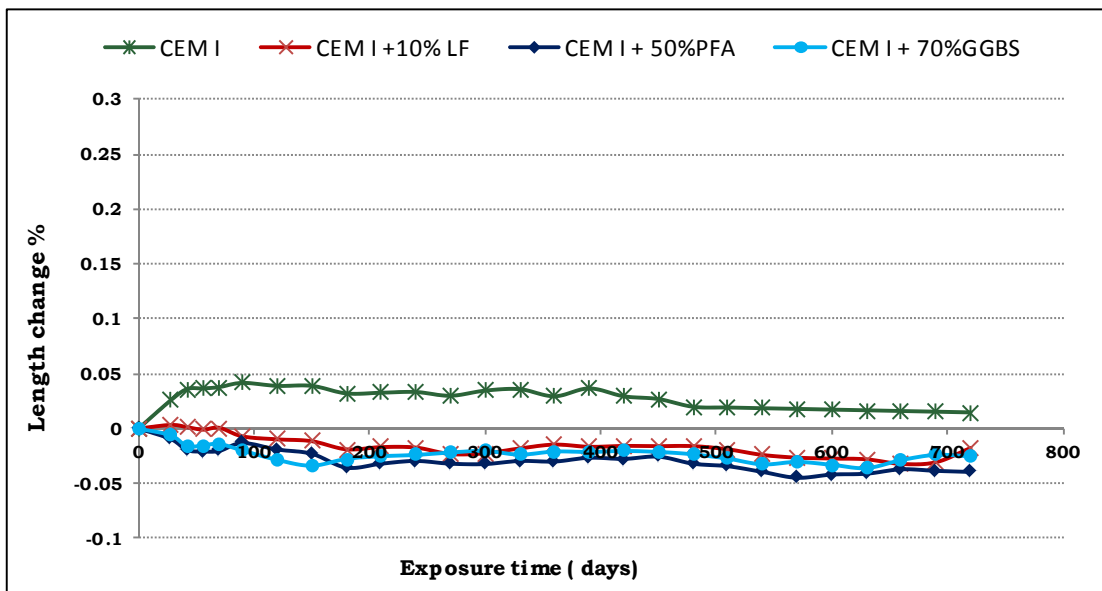


Figure A.2 Length change for samples in water at 20 °C. (Continuous immersion)

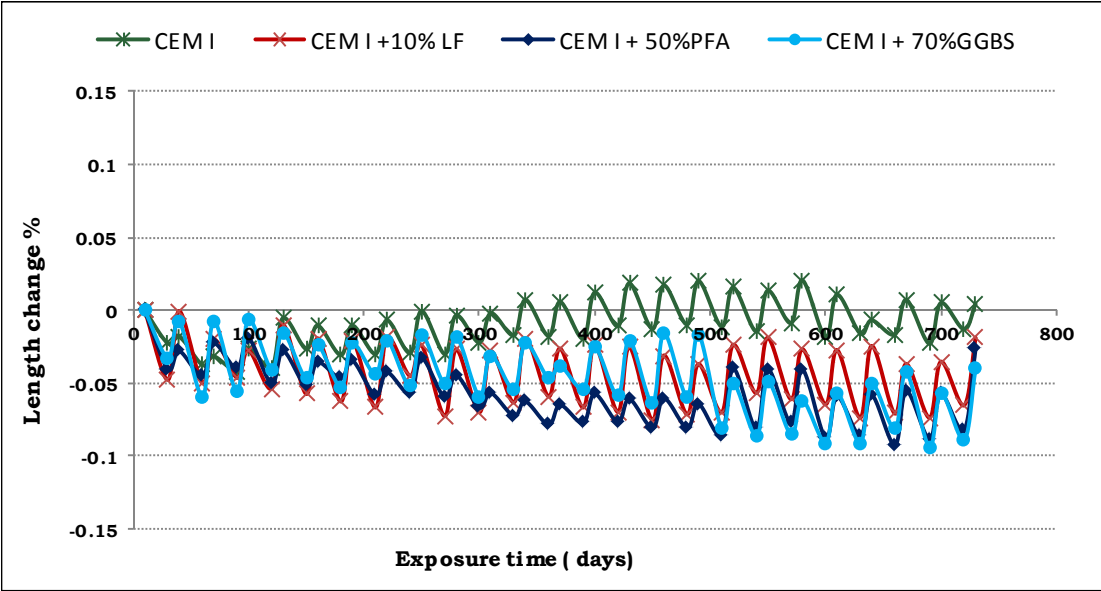
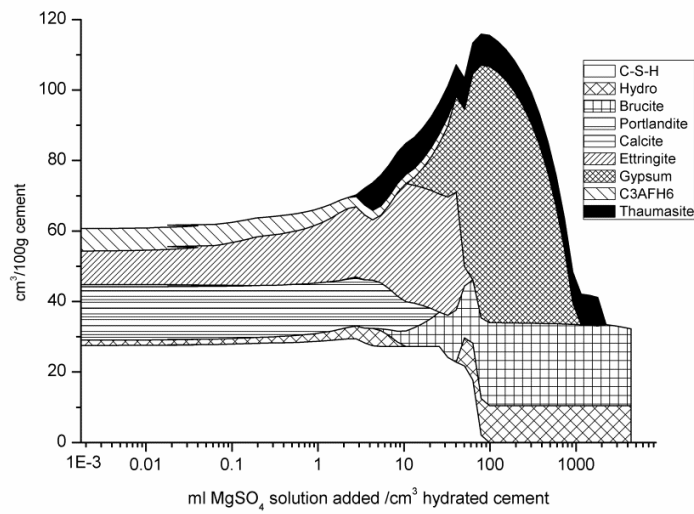


Figure A.3 Length change for samples in water at 20 °C. (wetting and drying)

# Appendix B

Thermodynamic results for samples made with 0.45 w/c ratio exposed to DS4



**Figure B.1 Phase assemblage for CEMI (w/c=0.45)**

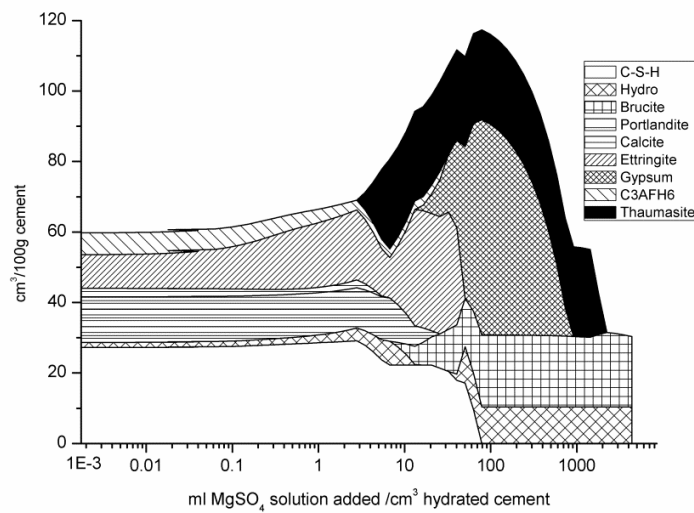


**Figure B.2 Phase assemblage for LFC (w/c=0.45)**

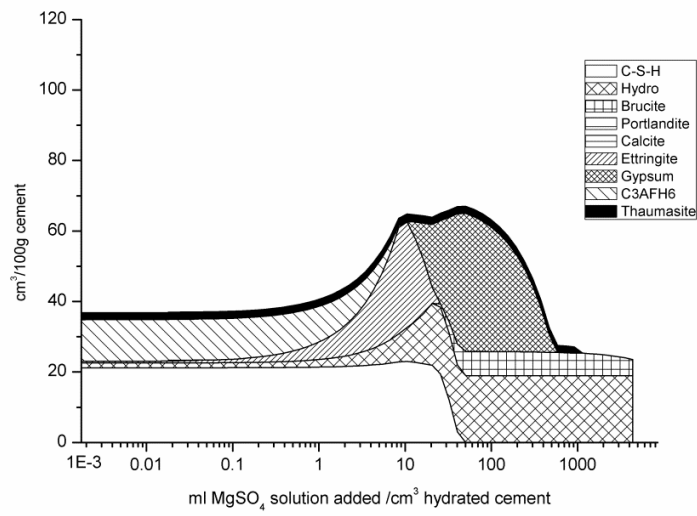


**Figure B.3 Phase assemblage for FAC (w/c=0.45)**

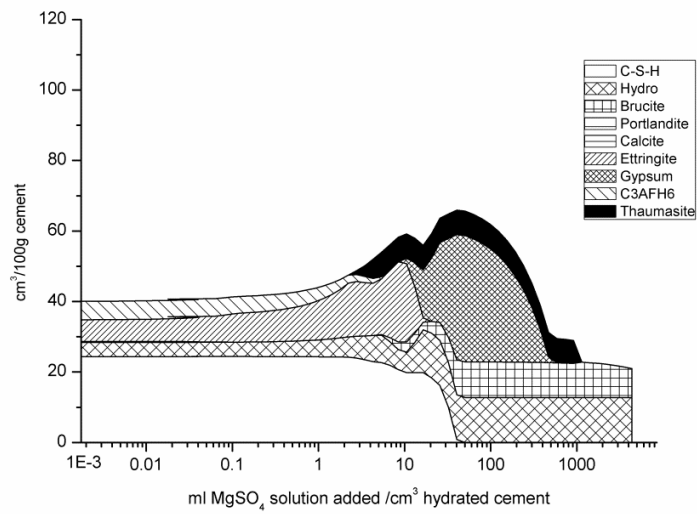


**Figure B.4 Phase assemblage for SLC (w/c=0.45)**

Thermodynamic results for samples made with 0.55 w/c ratio exposed to DS4

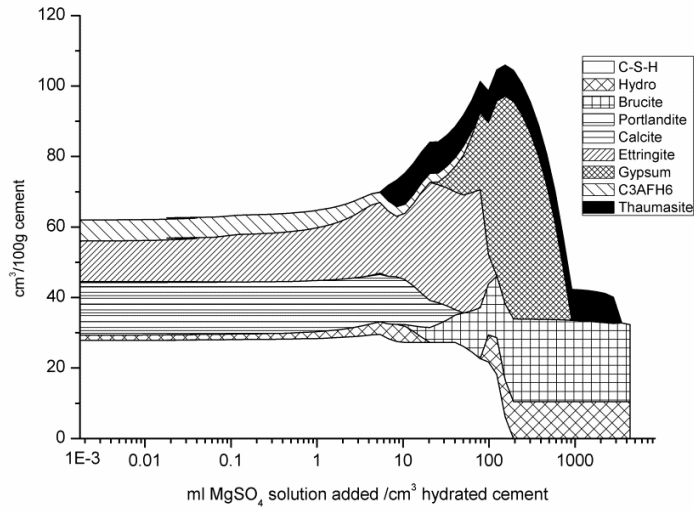


**Figure B.5 Phase assemblage for CEMI (w/c=0.55)**

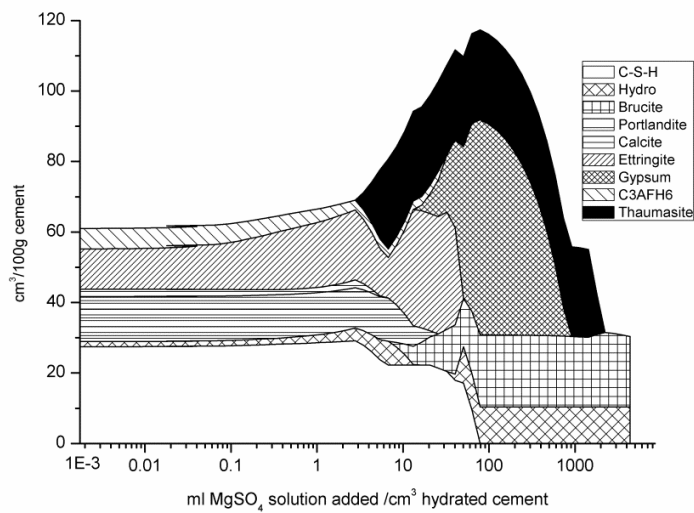


**Figure B.6 Phase assemblage for LFC (w/c=0.55)**

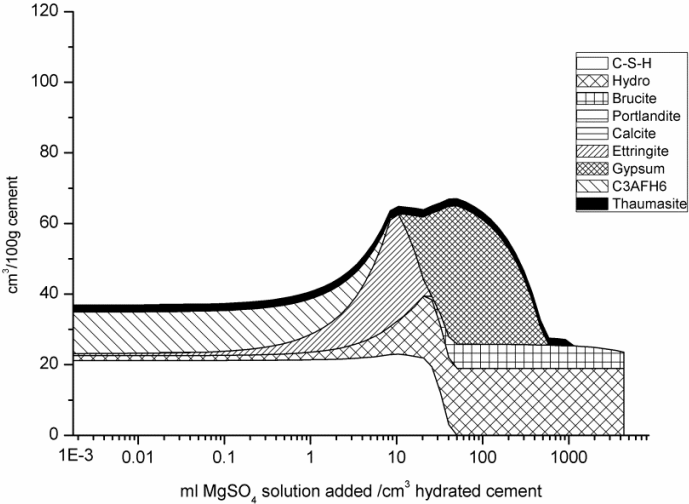


Figure B.7 Phase assemblage for FAC (w/c=0.55)

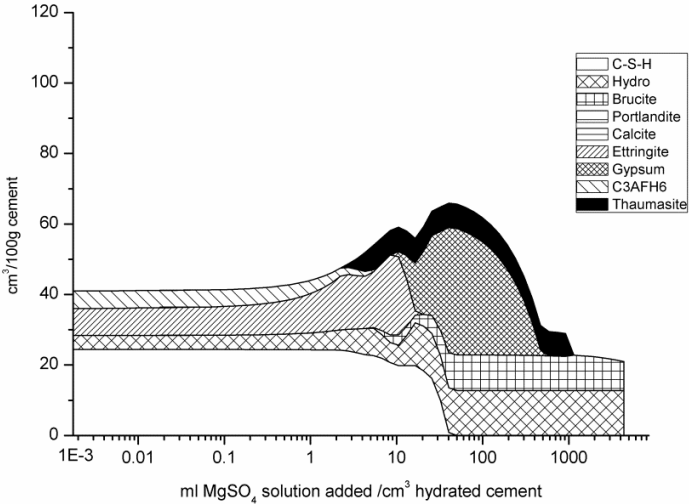


Figure B.8 Phase assemblage for SLC (w/c=0.55)